A Southern Hemisphere Record Of The Toarcian Oceanic Anoxic Event From The Neuquén Basin, Argentina

Aisha H. Al-Suwaidi

St. Peter's College

University of Oxford

A Thesis submitted for the degree of

Doctor of Philosophy

Michaelmas, 2011

Supervised by: Prof. Stephen Hesselbo and Dr. Hugh Jenkyns

EXTENDED ABSTRACT

The Toarcian, Early Jurassic, Oceanic Anoxic Event (T-OAE: ~183 Ma) was characterized by globally synchronous deposition of sediments rich in organic carbon (black shales), and is associated with an abrupt negative carbon isotope excursion, disrupting a positive carbon-isotope excursion during the *tenuicostatum–serpentinum* ammonite Zone boundary. The T-OAE is one of the largest carbon isotope excursions (CIE) in the Mesozoic and is characterized by a stepped negative-carbon isotope excursion, at the *tenuicostatum–falciferum* ammonite Zone. It is recorded in marine carbonates, bulk organic matter, biomarkers and fossil wood and is thought to record an injection of isotopically light carbon dioxide in to the atmosphere possibly from methane hydrate dissociation. Evidence for the T-OAE has mainly come from sediments located in northern and southern Europe, until recently when new data from Siberia, Morroco, Greece, Japan, Canada and Argentina has confirmed that the T-OAE is a global event. However the record of the T-OAE in the southern hemisphere is limited. Four stratigraphic succesions in the Neuquén Basin, Argentina, from Arroyo Lapa (North and South), Arroyo Chacay Melehue and Arroyo Serrucho, were examined to generate high resolution chemostratigraphic data ($\delta^{13}C$ from bulk sediment and fossil wood), biostratigraphy and sedimentology from the Pliensbachian–Toarcian of the Neuquén Basin, Argentina. Sedimentological data reveals marine transgression during the *tenuicostatum–hoelderi* Andean ammonite Zone boundary; equivalent to the *tenuicostatum–falciferum* North West European Province ammonite zone. $\delta^{13}C_{org}$ data reveals typical Toarcian values of ~-30– -32‰ in Arroyo Lapa (North and South side) and Arroyo Serrucho. The $\delta^{13}C_{org}$ data from Arroyo Lapa North and South can be correlated and shows a record of the complete negative excursion, including the steps leading up to the summit of the excursion and the recovery. This data can be compared with coeval data from the northern hemisphere specifically, UK, Greece, Italy and Canada and shows that the

Toarcian carbon isotope excursion is recorded in the southern hemisphere. The record of the Toarcian CIE in fossil wood also suggests that the release of isotopically light carbon during the Early Toarcian affected the whole ocean–atmosphere. Arroyo Chacay Melehue does not record the *tenuicostatum–hoelderi* boundary possibly as a result of a hiatus in deposition. However Arroyo Chacay Melehue and Arroyo Lapa South show evidence for the presence of the Pliensbachian–Toarcian carbon isotope excursion, showing a ~-2‰ excursion at the boundary, This data can be compared to data form Yorkshire, England and suggests that, this event has global expression. Bulk rock samples from Arroyo Lapa North and South were also analysed for $\delta^{98/95}$Mo; Biomarkers: Pristane/Phytane ratios; Sterane Index; Sterane/Hopane ratios; isorenieratane; hydrogen index; total organic carbon and pyrite framboid diameter distribution. The data generated reveals that the T-OAE can also be recognized in $\delta^{98/95}$Mo, with values falling to 0.7‰, , as well as in the presence of small syngenetic pyrite framboids, and Pristane/Phytane ratios of <0.8; which is indicative of anoxic marine settings. There is also an increase in total organic carbon burial (TOC = 12 %) during the excursion. Hydrogen Index data reveals a mixed signal of terrestrial and marine organic matter; though the abundance of each component varies through the sections and is dominated by marine organic matter during the summit of the negative excursion. This multiproxy data can be compared with coeval data from the Cleveland Basin, Yorkshire, England and from the Posidonia Shale, SW Germany, and reveals that while the T-OAE is recorded by the various proxies, local basin depositional settings, and sediment and organic matter types affect the absolute values of the proxy data.

ABSTRACT

The Toarcian, Early Jurassic, Oceanic Anoxic Event (T-OAE: ~183 Ma) was characterized by globally synchronous deposition of sediments rich in organic carbon (black shales), and is associated with an abrupt negative carbon isotope excursion, disrupting a positive carbon-isotope excursion during the *tenuicostatum–serpentinum* ammonite Zone boundary. The T-OAE has been extensively studied in northern and southern Europe, but evidence from the southern hemisphere is limited. New geochemical data from the *tenuicostatum–hoelderi* (*~serpentinum*) Andean ammonite Zone, from the Neuquén Basin, Argentina provides evidence for the global imprint of the event. The event is recorded in bulk-sediment from Arroyo Lapa (North and South) and Arroyo Serrucho with $\delta^{13}C_{org}$ values of -30‰ – -32.5‰ and $\delta^{13}C$ values from fossil wood fall to -30.7 ‰, isotopic ratios that are comparable to those identified in Europe for the T-OAE. Hydrogen Index (HI) data for the T-OAE in Argentina give values ranging from 12 to 425 mg HC/ g TOC, indicating a mixture of terrestrial and marine organic components. Pristane/Phytane ratios and pyrite framboid distribution data indicative of anoxic conditions occur at some levels, and new $\delta^{98/95}Mo$ data, with values ranging from ~ -0.2 to 0.78 ‰, which contrast with previously published molybdenum-isotope values from T-OAE black shales of northern Europe. Sedimentological data also reveals a marine transgression during the *tenuicostatum–hoelderi* Andean ammonite zone.

Acknowledgments:

Completion of my thesis would not have been possible without the help, endless support and love of my parents, Joanne and Hassan Al Suwaidi, my fiancée J. C. Walker and my friend Douglas Crockett. I must also thank Susana Damborenea, Miguel Manceñido and Alberto Riccardi for their help in the field, and with the very important task of biostratigraphy. As well as Steve Wyatt; Norman Charnley; Peter Ditchfield; Chris Siebert; François Baudin; Richard Pancost and everyone in the Organic Geochemistry Lab at Bristol University for their help with lab work and tolerance of my some times grumpy and mostly awkward disposition. Julie Retrum, Marina and Celina Suarez for their discussions, proof reading and company when times were bad. I would also like to thank my supervisors Stephen Hesselbo and Hugh Jenkyns for their excellent company in the field and endless discussions of Toarcian research. Finally I would also like to remember my friend Alec Waggoner who left us all too early.

The Scholarship Coordination Office, Abu Dhabi, UAE; the American Association of Petroleum Geologists Grants-In-Aid program; The Geological Society of London and the Jeremy Wilson Charitable Trust funded this research.

Epitaph On The World – Hendry David Thoreau

Here lies the body of this world,
Whose soul alas to hell is hurled.
This golden youth long since was past,
Its silver manhood went as fast,
An iron age drew on at last;
'Tis vain its character to tell,
The several fates which it befell,
What year it died, when 'twill arise,
We only know that here it lies.

"Bad times have a scientific value. These are occasions a good learner would not miss."

-Ralph Waldo Emerson

TABLE OF CONTENT

EXTENDED ABSTRACT II

ABSTRACT IV

ACKNOWLEDGMENTS V

TABLE OF CONTENT VII

LIST OF FIGURES IX

CHAPTER 1: INTRODUCTION 1

1.1 Introduction and Hypothesis 1
1.2.1 The Global Carbon Cycle 4
1.2.4 Oceanic Anoxic Events 11
1.2.5 The Toarcian Oceanic Anoxic Event (T-OAE) 14
1.3 The Early Jurassic World: An Overview of the geography and climate 15
1.3.1 Early Jurassic Palaeogeography 15
1.3.2 Early Jurassic Palaeoclimate 16
1.4 Analytical Methods 18
1.4.1 Total Organic Carbon 18
1.4.2 Organic Carbon Isotopes in bulk sediment 19
1.4.3 Organic Carbon Isotopes in fossil plant matter 20
1.4.4 Carbonate Carbon and Oxygen isotopes 21
1.4.5 Hydrogen Index 22
1.4.6 Biomarkers. 24
1.4.7 Molybdenum Isotopes 26
1.5 Summaries and Overview of Remaining Chapters 30
References: 31

CHAPTER 2: THE LATE PLIENSBACHIAN TO EARLY JURASSIC OF THE NEUQUÉN BASIN, ARGENTINA 50

Abstract 50
2.1 Introduction: 51
2.2 Palaeogeography and Tectonic Setting of the Neuquén Basin 52
2.3 Lithofacies and biostratigraphic framework of the Principal Localities 55
2.3.1 Arroyo Lapa North and South: Introduction 56
2.3.2 Lithostratigraphy: Arroyo Lapa South 2008 and 2010 57
2.3.4 Biostratigraphy: Arroyo Lapa South 61
2.3.5 Lithostratigraphy: Arroyo Lapa North 63
2.3.6 Biostratigraphy: Arroyo Lapa North 66
2.3.7 Arroyo Lapa, North and South Depositional setting 67
2.3.8 Chacay Melehue: Introduction 68
2.3.9 Lithostratigraphy: Chacay Melehue 71
2.3.10 Biostratigraphy: Chacay Melehue 72
2.3.11 Chacay Melehue Depositional Setting 73
2.3.12 Arroyo Serrucho: Introduction 74
2.3.13 Lithostratigraphy: Arroyo Serrucho 79

2.3.14 BIOSTRATIGRAPHY: ARROYO SERRUCHO 80
2.3.15 ARROYO SERRUCHO DEPOSITIONAL SETTING: 81
2.4 SUMMARY & CONCLUSION 82
REFERENCES 84

CHAPTER 3: EARLY JURASSIC (PLIENSBACHIAN-EARLY TOARCIAN) CARBON ISOTOPE CHEMOSTRATIGRAPHY, NEUQUÉN BASIN ARGENTINA 90

ABSTRACT 90
3.1 INTRODUCTION 91
3.2 METHODS 93
3.3 RESULTS 95
3.3.1 RESULTS: ARROYO LAPA SOUTH, 2008 AND 2010 95
3.3.2 RESULTS: ARROYO LAPA NORTH 98
3.3.3 RESULTS: CHACAY MELEHUE 101
3.3.4 RESULTS: ARROYO SERRUCH 103
3.4 DISCUSSION AND CHEMOSTRATIGRAPHIC CORRELATION 105
3.4.1 PLIENSBACHIAN–TOARCIAN BOUNDARY EXCURSION 105
3.4.1 TOARCIAN CARBON ISOTOPE EXCURSION **107**
3.5 CONCLUSION 111
REFERENCES 114

CHAPTER 4: A MULTIPROXY EXAMINATION OF THE TOARCIAN OCEANIC ANOXIC EVENT, ARROYO LAPA, (NORTH AND SOUTH) NEUQUÉN BASIN, ARGENTINA 118

ABSTRACT 118
4.1. INTRODUCTION 119
4.2. GEOLOGICAL AND PALEOGEOGRAPHICAL SETTING: ARROYO LAPA NORTH AND SOUTH. 120
4.3. MATERIALS AND METHODS: 123
4.4. RESULTS: 124
4.4.1. FOSSIL WOOD AND BULK SEDIMENT ORGANIC CARBON ISOTOPES AND TOTAL ORGANIC CARBON 125
4.4.2 HYDROGEN INDEX AND TOTAL ORGANIC CARBON 128
4.4.3. PYRITE FRAMBOID SIZE DISTRIBUTION RESULTS 133
4.4.4. BIOMARKERS RESULTS 136
4.4.5 MOLYBDENUM ISOTOPES RESULTS 141
4.5. DISCUSSION AND CONCLUSION 144
REFERENCES 149

CHAPTER 5: CONCLUSIONS 159

REFERENCES 162

APPENDIX A: DETAILED STRATIGRAPHIC LOGS WITH DATA 164

APPENDIX B: DATA 169

TABLE OF FIGURES

CHAPTER 1: INTRODUCTION

FIGURE 1: PALAEOGEOGRAPHIC MAP OF THE TOARCIAN 4
FIGURE 2: THE GLOBAL CARBON CYCLE 6
FIGURE 3: THE METHANE HYDRATE CAPACITOR 10
FIGURE 4: OCEAN ANOXIC EVENTS – GEOCHEMICAL PROCESSES 12
FIGURE 5: THE MOLYBDENUM CYCLE 28

CHAPTER 2: THE LATE PLIENSBACHIAN TO EARLY JURASSIC OF THE NEUQUÉN BASIN, ARGENTINA

FIGURE 1: A. PALAEOGEOGRAPHIC MAP OF THE TOARCIAN
B. GEOLOGICAL MAP OF THE NEUQUÉN BASIN 51
FIGURE 2: SCHEMATIC EVOLUTION OF THE NEUQUÉN BASIN 53
FIGURE 3: PLIENSBACHIAN–TOARCIAN DEPOSITIONAL TRACTS IN THE NEUQUÉN BASIN 54
FIGURE 4: GENERALIZED LITHOSTRATIGRAPHIC AND BIOSTRATIGRAPHIC COLOUMNS 55
FIGURE 5: SATELLITE IMAGE OF ARROYO LAPA 57
FIGURE 6: IMAGES FROM ARROYO LAPA SOUTH 58
FIGURE 7: STRATIGRAPHIC LOG ARROYO LAPA SOUTH, 2008 59
FIGURE 8: STRATIGRAPHIC LOG ARROYO LAPA SOUTH, 2010 60
FIGURE 9: IMAGES FROM ARROYO LAPA NORTH 64
FIGURE 10: STRATIGRAPHIC LOG ARROYO LAPA NORTH 65
FIGURE 11: IMAGES FROM CHACAY MELEHUE 69
FIGURE 12: STRATIGRAPHIC LOG CHACAY MELEHUE 70
FIGURE 13: GEOLOGICAL MAP ARROYO SERRUCHO 75
FIGURE 14: IMAGES FROM ARROYO SERRUCHO 76
FIGURE 15: STRATIGRAPHIC LOG ARROYO SERRUCHO MAIN SECTION 77
FIGURE 16: STRATIGRAPHIC LOG ARROYO SERRUCHO UNNAMED SECTIONS 78
FIGURE 17: COMPARATIVE STRATIGRAPHY 83

CHAPTER 3: EARLY JURASSIC (PLIENSBACHIAN-EARLY TOARCIAN) CARBON ISOTOPE CHEMOSTRATIGRAPHY, NEUQUÉN BASIN ARGENTINA

FIGURE 1: PALAEOGEOGRAPHIC MAP OF THE TOARCIAN 92
FIGURE 2: A. PALAEOGEOGRAPHIC MAP OF THE TOARCIAN
B. GEOLOGICAL MAP OF THE NEUQUÉN BASIN 93
FIGURE 3: SATELLITE IMAGE OF ARROYO LAPA 94
FIGURE 4: ARROYO LAPA SOUTH 2008, $\delta^{13}C_{ORG\&WOOD}$ CHEMOSTRATIGRAPHY 96
FIGURE 5: ARROYO LAPA SOUTH 2010, $\delta^{13}C_{ORG\&WOOD}$ CHEMOSTRATIGRAPHY 97
FIGURE 6: ARROYO LAPA NORTH, $\delta^{13}C_{ORG\&WOOD}$ CHEMOSTRATIGRAPHY 99
FIGURE 7: COMPARISON OF $\delta^{13}C_{ORG\&WOOD}$ CHEMOSTRATIGRAPHY FROM ARROYO LAPA SOUTH 2008 AND 2010 WITH ARROYO LAPA NORTH 100
FIGURE 8: CHACAY MELEHUE, $\delta^{13}C_{ORG}$ CHEMOSTRATIGRAPHY 102
FIGURE 9: GEOLOGICAL MAP OF ARROYO SERRUCHO AREA 103
FIGURE 10: ARROYO SERRUCHO, $\delta^{13}C_{ORG}$ CHEMOSTRATIGRAPHY 104
FIGURE 11: COMPARATIVE $\delta^{13}C_{ORG}$ AND TOTAL ORGANIC CARBON CHEMOSTRATIGRAPHY FOR THE PLIENSBACHIAN–TOARCIAN BOUNDARY 106
FIGURE 12: COMPARATIVE $\delta^{13}C_{ORG}$ CHEMOSTRATIGRAPHY FOR SECTIONS FROM ARGENTINA WITH DATA FROM EUROPE AND NORTH AMERICA. 110
FIGURE 13: COMPARATIVE $\delta^{13}C_{ORG}$ CHEMOSTRATIGRAPHY FOR ARROYO LAPA *VS.* YORKSHIRE, ENGLAND. 112

FIGURE 13: COMPARATIVE $\delta^{13}C_{ORG}$ CHEMOSTRATIGRAPHY FOR ARROYO SERRUCHO *VS.* DATA FROM MAZZINI ET AL., 2010. 113

CHAPTER 4: A MULTIPROXY EXAMINATION OF THE TOARCIAN OCEANIC ANOXIC EVENT, ARROYO LAPA, (NORTH AND SOUTH) NEUQUÉN BASIN, ARGENTINA

FIGURE 1: SATELLITE IMAGE OF ARROYO LAPA 121
FIGURE 2: COMPARISON OF $\delta^{13}C_{ORG\&WOOD}$ CHEMOSTRATIGRAPHY FROM ARROYO LAPA SOUTH 2008 AND 2010 WITH ARROYO LAPA NORTH. 126
FIGURE 3: HYDROGEN INDEX DATA FROM ARROYO LAPA SOUTH AND NORTH 129
FIGURE 4: TISSOT–WELTE DIAGRAM OF HYDROGEN INDEX DATA FOR ARROYO LAPA SOUTH AND NORTH. 132
FIGURE 5: BOX PLOT OF PYRITE FRAMBOID DIAMATER DATA FOR ARROYO LAPA SOUTH AND NORTH. 134
FIGURE 6: SCANNING ELECTRON MICROSCOPE IMAGES FOR ARROYO LAPA SOUTH AND NORTH. 135
FIGURE 7: ARROYO LAPA NORTH AND SOUTH, HYDROGEN INDEX, PRISTANE/PHYTANE RATIOS AND PYRITE FRAMBOID DIAMETER DATA. 137
FIGURE 8: COMPARISON OF $\delta^{13}C_{ORG}$, TOTAL ORGANIC CARBON, MOLYBDENUM CONCENTRATION (PPM) AND $\delta^{98/97}$MOCHEMOSTRATIGRAPHY FROM ARROYO LAPA SOUTH WITH ARROYO LAPA NORTH. 142
FIGURE 9: COMPARISON OF $\delta^{13}C_{ORG}$ AND $\delta^{98/97}$MO CHEMOSTRATIGRAPHY FROM ARROYO LAPA SOUTH AND NORTH. 143
FIGURE 10: CROSS-PLOT OF $\delta^{98/97}$MO *VS.* 1/[MO PPM] DATA FROM ARROYO LAPA NORTH AND SOUTH AND YORKSHIRE, ENGLAND (PEARCE ET AL., 2008) 144
FIGURE 11: COMPARISON OF $\delta^{13}C_{ORG}$ AND $\delta^{98/97}$MO CHEMOSTRATIGRAPHY FROM ARROYO LAPA SOUTH AND NORTH WITH DATA FORM YORKSHIRE, ENGLAND (KEMP ET AL., 2005 AND PEARCE ET AL., 2008). 145
FIGURE 12: COMPARISON OF TOTAL ORGANIC CARBON, HYDROGEN INDEX, PRISTANE/ PHYTANE AND STERANE/HOPANE DATA FROM ARROYO LAPA SOUTH WITH THE POSIDONIA SHALE SW GERMANY (FRIMMEL ET AL., 2004) 147

APPENDIX A

FIGURE 1: ARROYO LAPA SOUTH, 2008, DETAILED STRATIGRAPHIC LOG WITH DATA. 165
FIGURE 2: ARROYO LAPA SOUTH, 2010, DETAILED STRATIGRAPHIC LOG WITH DATA. 165
FIGURE 3: ARROYO LAPA NORTH, DETAILED STRATIGRAPHIC LOG WITH DATA. 166
FIGURE 4: CHACAY MELEHUE, DETAILED STRATIGRAPHIC LOG WITH DATA. 167
FIGURE 5: ARROYO SERRUCHO, DETAILED STRATIGRAPHIC LOGS WITH DATA. 168

Chapter 1

Introduction

1.1 Introduction and Hypothesis

Since the turn of the last century through the work of Arrhenius (1896), and Chamberlin (1899), scientists have been aware that variations in atmospheric carbon dioxide drives climatic change (Royer et al., 2004), and began to demonstrate this relationship through the study of ancient sediments, fossil plants, ice cores, and with monitoring stations to examine on-going variations in atmospheric composition. Studies of ice cores have demonstrated a strong coupling between carbon dioxide and temperature for the last 650,000 years (Revelle and Suess, 1957; Petit et al., 1999; Siegenthalaer et al., 2005), as well as indicating that present levels of atmospheric carbon dioxide are at their highest level for the last 800,000 years of Earth History, having risen from 172 ppmv to 390ppmv as a result of increased fossil fuel burning, due to industrialization (Rahmstorf et al., 2007; Lüthi et al., 2008). To understand the impact that this increase in carbon dioxide will have on global marine, atmospheric and terrestrial systems, and in particular the carbon-mediated biological pump and the global carbon cycle, it is important to identify and examine periods in the geological past with elevated atmospheric carbon dioxide levels, and understand how global systems respond and recover from massive influxes of this greenhouse gas.

It has been demonstrated that the Mesozoic Earth was a greenhouse world through various organic and inorganic proxies, such as oxygen-isotope ratios of skeletal calcite, the paleothermometer proxy; TEX_{86} (TetraEther indeX) values of organic matter, paleosols, palynology, stomatal index (e.g., Cerling, 1991; McElwain and Chaloner, 1995; Chaloner and McElwain, 1997; Retallack, 2001, 2002; Beerling and Royer, 2002a; Gröcke, 2002; Schouten et al., 2002, Jenkyns et al., 2004;Royer et al., 2004; Forster et al., 2007, Schouten et al., 2007) and geochemical models (i.e.,, Berner, 1991; Chandler et al., 1992; Berner and

Kothavala, 2001; Beerling and Royer, 2002b; Fletcher et al., 2005, 2008),with elevated concentrations of greenhouse gases (e.g., CO_2, CH_4, H_2O) and temperatures 5–10ºC warmer than at present, with interspersed episodes <1–3 m.y) of cooler temperatures.(e.g., Spicer et al., 1989; Chandler et al., 1992; Herman and Spicer, 1996; Price, 1999; Jenkyns, 2003; Royer et al., 2006).

Through examination of the carbon-isotope composition of certain geological material such as fossil plants, terrestrial and marine sediments, we know that the Mesozoic Era was punctuated by intervals with pronounced positive and negative shifts in carbon isotopes, suggesting abrupt disturbances to the carbon cycle. These disturbances are associated with extreme cases of global environmental change, including formation of Large Igneous Provinces (LIPs) such as the Central Atlantic Magmatic Province, (CAMP, Triassic–Jurassic); Karoo–Ferrar (Early Jurassic) and Ontong Java (Cretaceous); changes in seafloor-spreading rate, possible dissociation of methane hydrate, ocean acidification, and widespread deposition of marine black shales (e.g., Hesselbo et al., 2000; Pálfy and Smith, 2000; Jones and Jenkyns, 2001; McElwain et al., 2005; Coffin et al., 2006; Svenson et al., 2007; Kump et al., 2009). These organic-rich deposits have been linked to intervals of oxygen depletion in large volumes of ocean water and are referred to as Oceanic Anoxic Events (Schlanger and Jenkyns, 1976). Three major Oceanic Anoxic Events (OAE's) have been identified during the Mesozoic; Cenomanian/Turonian boundary (~ 93.5 Ma); Early Aptian (~ 120 Ma), and the Early Toarcian (~183 Ma) (Jenkyns, 2010). These OAE's have been identified in the geological record as events resulting in global deposition of organic rich black shales and are thought to be indicative of global anoxia. Carbon-isotope stratigraphy generally shows broad excursions to heavier $^{13}C/^{12}C$ ratios over these intervals, conventionally interpreted as due to increased global burial rates of organic matter in the oceans. However, large negative $d^{13}C$ excursions punctuate both the Toarcian and Aptian events, indicating fluxes of isotopically light carbon into the ocean and atmosphere, possibly initially as methane from gas hydrates or

thermal metamorphism of coals or black shales (e.g., Jenkyns, 1988, 2003, 2010; Hesselbo et al, 2000; Beerling et al., 2002; McElwain et al., 2005; Svenson et al., 2007). There is also an increase, during the Early Toarcian, in $^{187}Os/^{188}Os$ ratios, consistent with a major increase in continental weathering (e.g., Peucker-Ehrenbrink and Ravizza, 2000; Cohen, 2004; Cohen et al., 2007). Biomarkers from green sulphur bacteria indicate that euxinic conditions (i.e. H_2S-bearing) extended into the photic zone in some areas of the global ocean during all three OAEs (i.e.,, Pancost, et al., 2004; van de Schootbrugge, 2005a; van Breugel et al., 2006). Excursions have also been recorded in Molybdenum isotopes, $\delta^{98/95}Mo$, which may reflect the removal of Mo into euxinic sediments (Arnold et al., 2004; Pearce et al., 2008); and $\delta^{56}Fe$ which may record precipitation of framboidal pyrite in a sulphidic water column (e.g., Berner and Raisewell, 1983; Lyons et al., 2009; Anbar and Rouxel, 2007; Jenkyns, 2010).

While these tracers are broadly consistent with the development of extended global anoxic to euxinic water masses, detailed variations indicate more complex histories. Furthermore, there are also significant open questions as to how widespread these anoxic conditions were, the water depths over which anoxia/euxinia occurred, the redox potential of these regions or zones, and the environmental cycling of elements (e.g., Mo, Fe, Os) that took place.

This study primarily concerns the Toarcian Oceanic Anoxic Event, (T-OAE, ~ 183 Mya) which, as well as being characterized by remarkably widespread marine organic-rich sediment (Fig. 1), has one of the largest negative carbon isotopic excursions in the Mesozoic, values of $d^{13}C_{org}$ as low as -33‰ recorded in both fossil wood and marine sediments in both the Northern and Southern hemisphere (e.g., Hesselbo et al, 2000, 2007; Kemp et al., 2005; Sabatino et al., 2009; Al-Suwaidi et al., 2010; Hesselbo and Pieńkowski, 2010; Caruthers et al., 2011; Bodin et al., 2011; Gröcke et al., 2011; Kafousia et al., 2011; Suan et al., 2011).In recent years some researchers have questioned the global nature of the T-OAE, due to the perceived lack of, well-dated, organic rich sediment with an accompanying carbon-isotope

excursion, outside the Tethyan and Boreal domain. Some researchers have suggested that this event is a regional rather than a global phenomenon (van de Schootbrugge et al., 2005b; Wignall et al., 2005; McArthur et al., 2008). Confirmation of the global extent of the T-OAE could offer important information regarding its cause and effects. This study aims to produce a high-resolution multi-proxy records of sediments of Pliensbachian–Toarcian age from the southern hemisphere, specifically the Neuquén Basin, Argentina. Parameters investigated include sedimentology, biostratigraphy, organic carbon isotopes (bulk sediment and fossil wood), biomarkers, molybdenum isotopes, hydrogen indices, and total organic carbon.

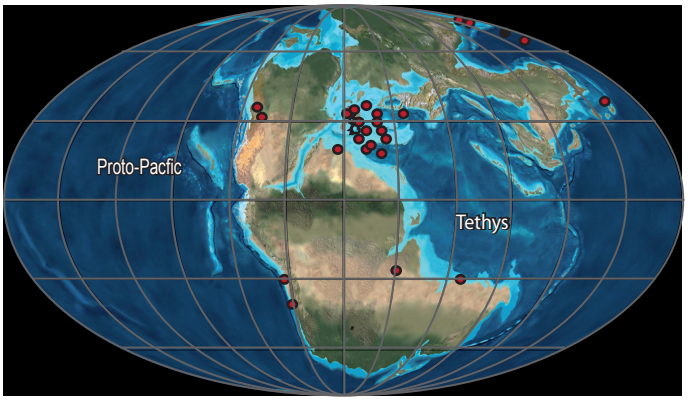


Figure 1. Paleogeographic map of the Toarcian ~183 Ma showing locationof organic rich black shales most of these localities are dated as *tenuicostatum-falcifurum* Ammonite Zones which corresponds with the Lower Toarcian stage (adapted from Jenkyns, 2001; Blakey, 2007).

The remainder of this chapter expands on some of the terms introduced, including carbon cycling, Oceanic Anoxic Events and molybdenum isotopes, and provides a discussion of Early Jurassic climate and geography. Summaries of the subsequent chapters within this thesis are provided in addition to details of the methods used to investigate the impact of the Toarcian Oceanic Anoxic Event in the southern hemisphere.

1.2.1 The Global Carbon Cycle

To understand the Toarcian Oceanic Anoxic Event it is necessary to examine the major sources and sinks of carbon, during the Early Jurassic. This can be explained through consideration of the global carbon cycle. This is concerned with natural perturbations to the carbon budget (Fig. 2), unaffected by human additions of carbon dioxide to the atmosphere,

through the burning of fossil fuels although the magma-related processes may closely mimic anthroprogenic carbon emission. The carbon cycle may be divided in to two sub-cycles, which are as follows:

1) The long-term carbon cycle, also known as the silicate–carbon sub-cycle, which acts over millions of years; the major process affecting atmospheric carbon dioxide in this sub-cycle is the exchange between carbon stored in rocks, carbon in the atmosphere, silicate weathering, metamorphism, tectonics and the distribution of land plants (Berner, 1999).

2) The short-term carbon cycle, which operates on a 0-1000 year time scale, and refers to exchange of carbon dioxide between the biosphere, oceans, soils and atmosphere and includes the biological pump, and the "methane capacitor" (Bolin, 1970; Berner and Lasaga, 1989; Berner, 1999; Dickens, 2003, 2011; Falkowski et al., 2000; Kvenvolden, 2002; Berner and Kothavala, 2001).

The long and short-term carbon cycle are intrinsically linked, but the processes involved in the long-term carbon cycle, which may have caused changes to atmospheric carbon dioxide are so slow that it is not useful in explaining events that disrupt the global carbon budget over 10-1000's of years. The short-term carbon cycle is likely to affect the atmospheric carbon budget on a daily to decadal scale and changes to it can be invoked to explain abrupt major disruptions to the carbon-isotope record through geological time (Bolin, 1980; Berner, 1990; Beerling and Royer, 2002b; Dickens, 2003, 2011). The key chemical processes associated with the short- and long-term carbon cycle, can be summarized as follows (Berner, 1990; Berner, 1999; Sarmiento and Bender, 1994; Dickens, 2003, 2011):

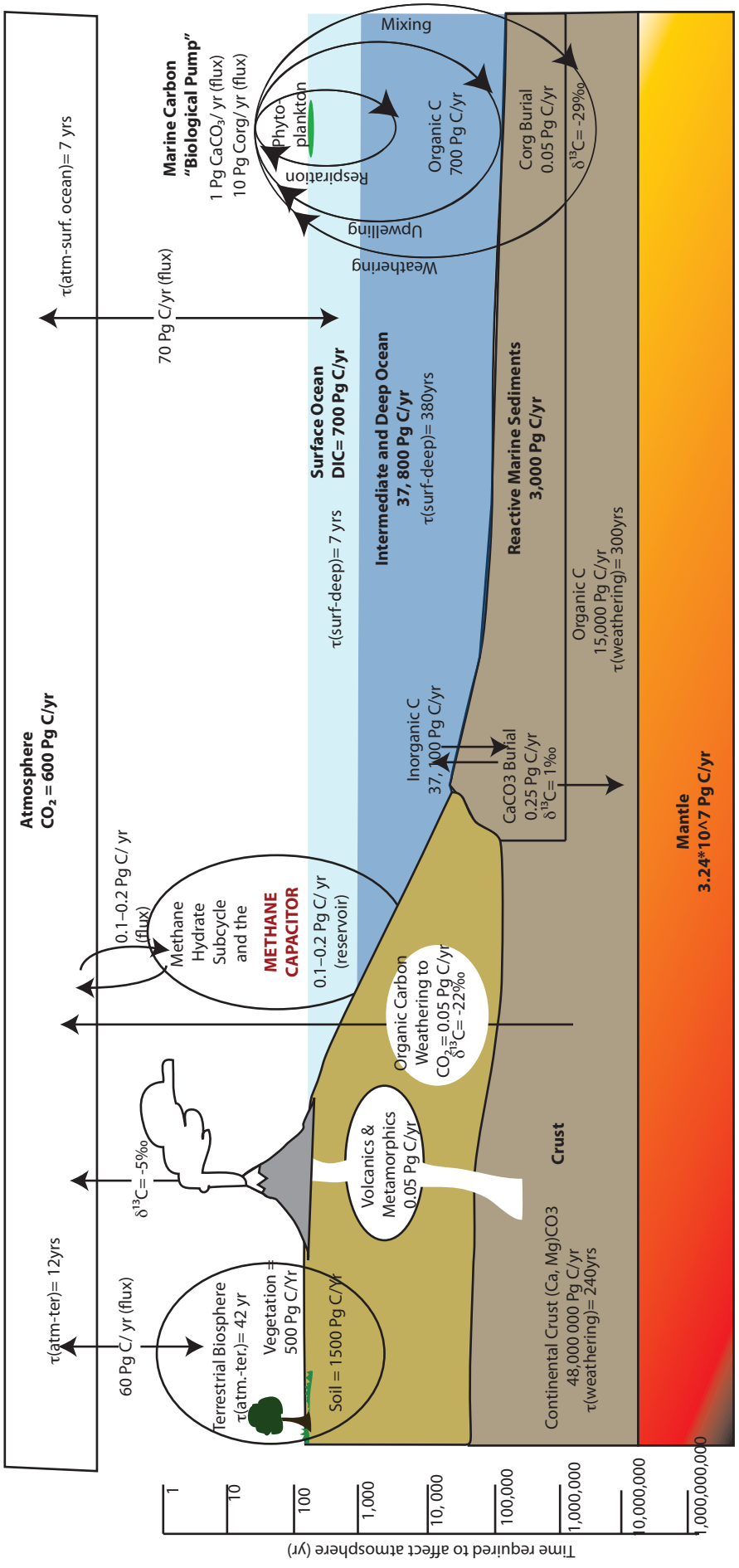


Figure 2. Cartoon depiction of the carbon cycle including a summary of the major process involved in the marine biological pump; reservoir sizes; major processes; chemical reactions, sources, sinks and typical δ13C values associated with the reservoirs, involved in the cycling of carbon in the marine and terrestrial realm (adapted from Berner & Lasaga, 1986; Berner, 1999; Sigman & Haug, 2003, P. 492–494.)

1) Long-term carbon cycle OR the silicate–carbonate subcycle;

A. This chemical reaction shows how atmospheric carbon dioxide is processed mostly by photosynthesis and respiration, to form soil carbon dioxide and organic acids, that are instrumental in the weathering of calcium and magnesium silicate minerals. The reaction is illustrated using calcium silicate minerals, but the reaction is the same for magnesium silicate minerals.

$$2CO_2 + H_2O + CaSiO_3 \rightarrow Ca^{2++} + 2HCO_3^- + SiO_2 \quad \text{(Equation 1)}$$

B. The dissolved calcium ions (Ca^{2++}) and bicarbonate ($2HCO_3^-$) are carried to rivers, and eventually to the sea where they are precipitated (mostly biologically) as calcium carbonate ($CaCO_3$) in sediment. If magnesium is also present it may be removed to form dolomite $CaMg(CO_3)_2$

$$Ca^{2++} + 2HCO_3 \rightarrow CaCO_3 + CO_2 + H_2O \quad \text{(Equation 2)}$$

C. The net overall reaction of the formation of calcium carbonate in marine sediments is as follows

$$CO_{2+} + CaSiO_3 \leftrightarrow CaCO_3 + SiO_2 \quad \text{(Equation 3)}$$

In this instance carbon dioxide is removed from the atmosphere through weathering processes and ultimately buried as carbonate sediment that lithifies to limestone, and is eventually metamorphosed and/or subducted. These processes occur on time scales

of millions of years but may be accelerated by an enhanced hydrological cycle and acidic rainfall.

2. Short-term carbon cycle

A. The “biological pump” or organic-matter subcycle:

This short-term cycle affects both atmospheric oxygen and carbon dioxide and is the result of marine and terrestrial photosynthesis. In this process plants take up carbon dioxide through photosynthesis and produce complex sugars, respiring oxygen. Once these organisms die and decompose this organic matter, if not oxidized, can be buried in sediments. In the reverse of the reaction, typically through thermal breakdown of organic matter, the CH_2O, releases carbon dioxide back in to the atmosphere. This subcycle occurs on the order of minutes, and can be easily disrupted.

$$CO_2 + H_2O + \text{energy} \leftrightarrow CH_2O + O_2 \quad \text{(Equation 4)}$$

This reaction represents the overall processes associated with the burial of the net excess of photosythnthetic production, on land and in marine and fresh water. One of the key components of the short-term carbon cycle is the uptake of carbon dioxide by phytoplanktonic marine organisms, which amounts to about 1-2% of the total global plant-consumed carbon. These organisms collectively fix between 30–50 x 10^9 metric tons of carbon per annum, which is nearly 40% of the global total of fixed carbon. This aspect of the short-term carbon cycle is referred to as the biological pump (Falkowski, 1994). As this is such a large sink of atmospheric carbon dioxide, any small change in either nutrient availability in surface water and in the atmospheric

carbon dioxide can result in major disturbances to this source of carbon. In a greenhouse world, with elevated runoff due to an enhanced hydrological cycle, warm temperatures and high contents of greenhouse gases, it is assumed that the biological pump will be very effective and organic-carbon burial will be elevated (Bolin, 1970; Falkowski, 1994; Berner, 1999).

B. The Methane Capacitor

Methane plays an important role when examining major perturbations to the carbon cycle, as methane hydrates store large amounts of isotopically light carbon.

Solid organic matter lands on the seafloor; during burial it undergoes several early diagenetic reactions including organoclastic sulfate reduction:

$$CH_2O + SO_4^{2-} \rightarrow 2HCO_3^- + H_2S \quad \text{(Equation 5)}$$

Methanogenesis then utilizes a fraction of the remaining solid carbon to form ^{13}C depleted CH_4 (typically with $\delta^{13}C < -60‰$) and ^{13}C-enriched HCO_3^- (often with $\delta^{13}C < +10‰$), in the upper few hundred meters of sediment. The ^{13}C depleted CH_4 can cycle between dissolved gas and gas hydrate within the sediment, while much of the enriched CH_4 slowly returns to the ocean. In shallow sediment ^{13}C depleted HCO_3^- slowly returns to the ocean when upward migrating CH_4 reacts with dissolved SO_4^{2-} through a process called anaerobic oxidation of methane (AOM).

$$CH_2O + SO_4^{2-} \rightarrow HCO_3^- + H_2O \quad \text{(Equation 6)}$$

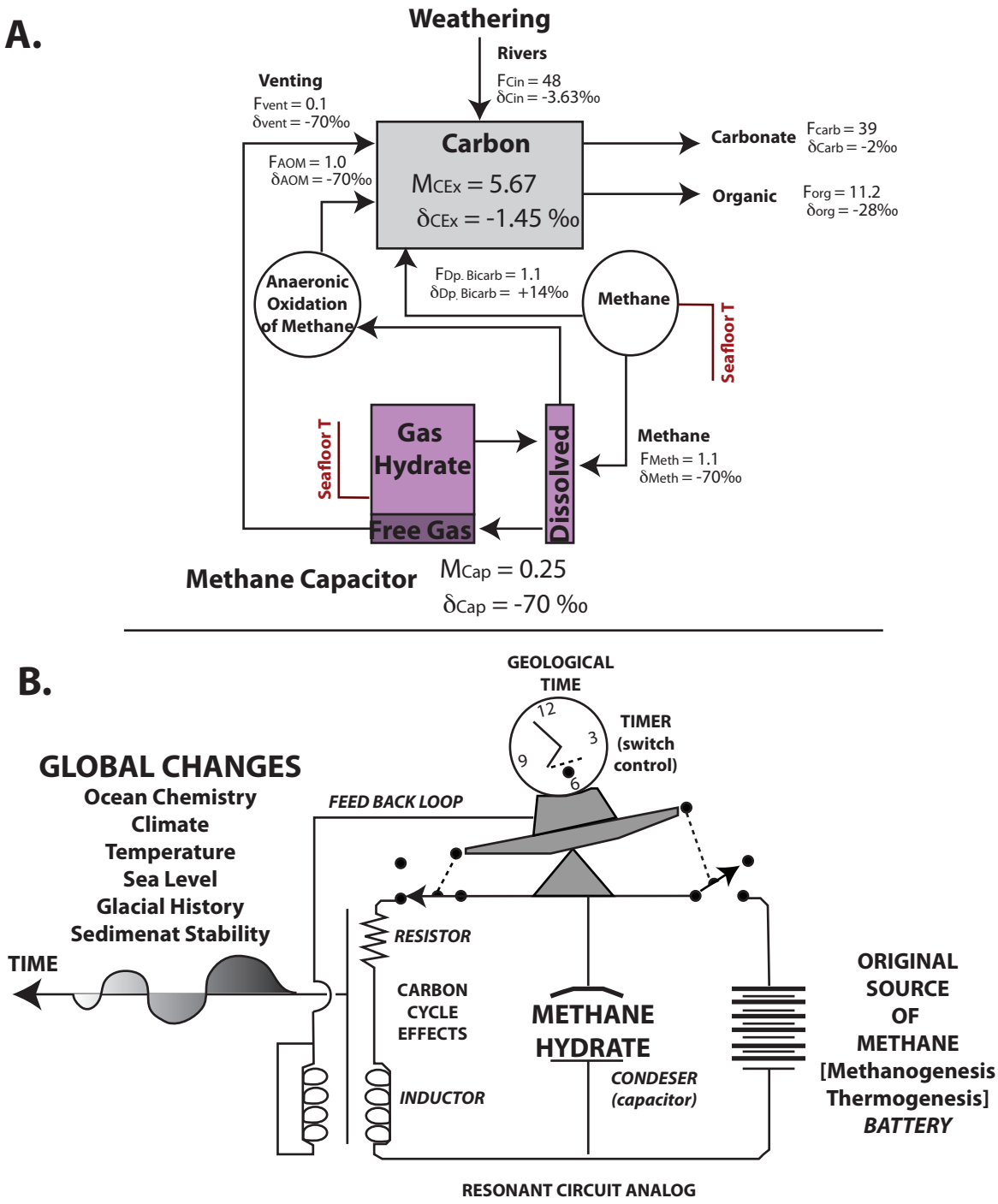


Figure 3. A. "Steady-state" model for Phanerozoic carbon cycle. M = Mass, 10 18 moles; F = Flux, 1012 moles/year; δ = delta. Postulated masses and fluxes are a composite (c.f. Kump and Arthur, 1999; Dickens, 2003; Kurtz et al., 2003. The exogenic carbon cycle is based on a world with nominally three times preindustrial atmospheric CO_2 (Dickens, 2011)

B. Cartoon depiction of the "Methane Hydrate Capacitor" illustrated as an electrical resonant circuit analogue for methane hydrate in the global organic carbon cycle. Illustrates the possible interrelated consequences resulting from methane hydrate formation and decomposition throughout geological time. The inductor, resistor and feedback circuit workings are analogous to the various global changes that may be influenced by methane hydrate (Kvenvolden, 2002).

Some amount of carbon also returns to the ocean through CH_4 venting and aerobic oxidation in the water column;

$$CH_4+2O_2 \rightarrow CO_2+ 2H_2O \text{ (Equation 7)}$$

Figure 3 illustrates the role of methane in the exogenic carbon cycle, as well as how the "methane capacitor works" (Dickens, 2011).

This thesis is concerned mainly with disruption of the carbon cycle reflected by the burial of organic carbon in marine sediments, as well as changes in the associated isotopic composition of this organic matter.

1.2.4 Oceanic Anoxic Events

The term Oceanic Anoxic Event was first coined by Schlanger and Jenkyns (1976), in an attempt to explain the presence of apparently coeval globally distributed marine organic-rich sediments, of Cretaceous age, specifically, Barremian–Aptian and Cenomanian–Turonian, from the South Central and Western North Atlantic, during legs 32 and 33 of the Deep Sea Drilling Project (DSDP). These authors suggested that these layers of organic-rich sediments maybe a record of some event related to poor oceanic mixing, which was a widespread, if not worldwide oceanographic phenomenon. They proposed that the stratigraphically restricted organic carbon-rich horizons were the result of widespread anoxia related to expansion of the oxygen minimum zone in the world ocean. This concept differed from the classic 'black shale model' which relied on water mass stratification and restricted basin geometry to explain the origin of organic-rich sediments.

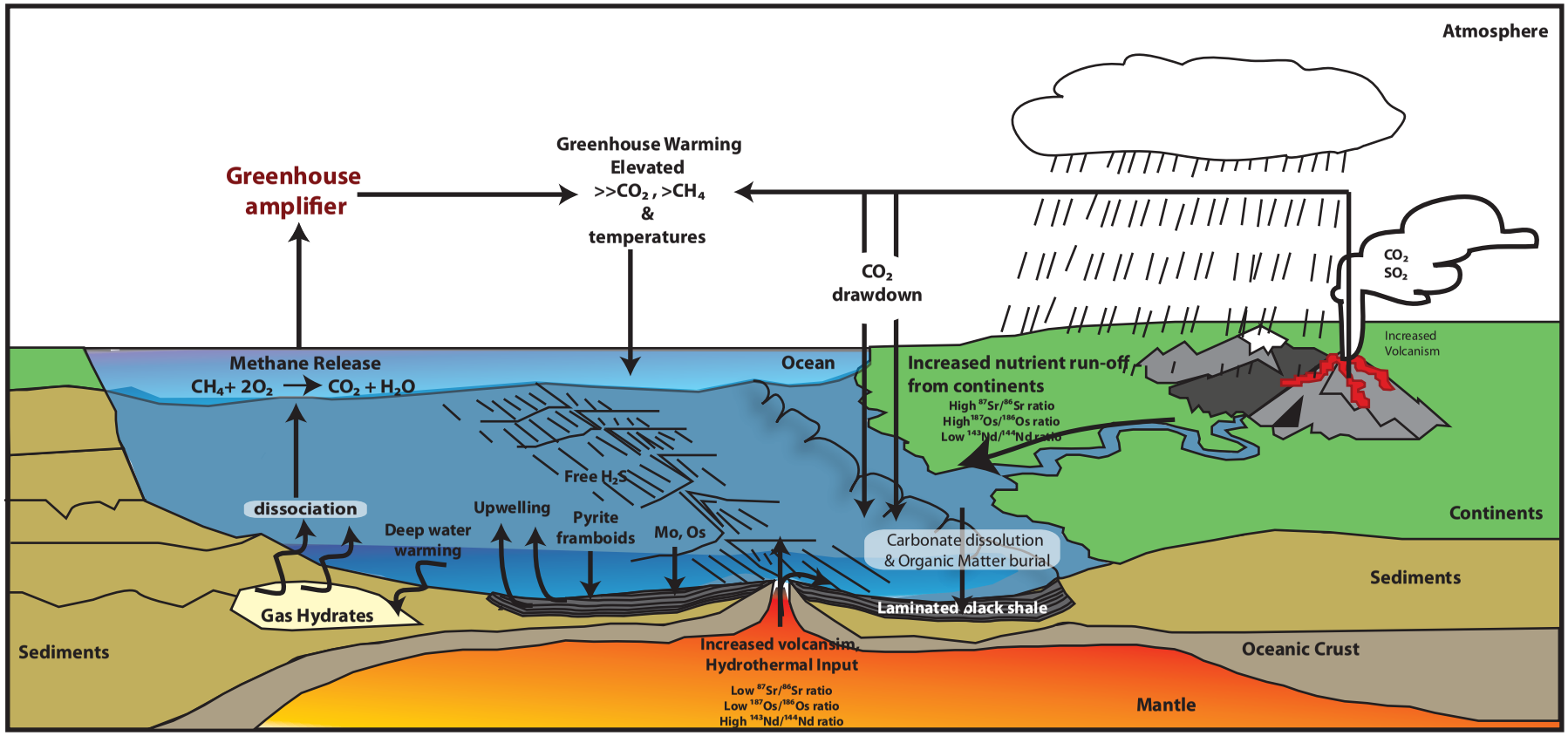


Figure 4. Cartoon illustrating some of the geochemical processes characteristics of OAEs. Volcanism results in the venting of greenhouse gasses, initiating global warming; increased acidification of the oceans from dissolution of CO_2 and SO_2 causes increased carbonate dissolution. Gas hydrates are destabilized as a result of either increased tectonic activity or deep water warming leading to dissociation of methane and the release of isotopically light carbon in to the atmosphere. The hydrological cycle accelerates with increased nutrient fluxes to the ocean; upwelling intensifies, as does organic productivity. Oxygen becomes limited and organic matter burial increases, resulting in the deposition of laminated black shales with no bioturbation, as benthos is excluded due to limited oxygen. As conditions become more euxinic large tracts of the water column have advanced sulfate reduction with free H_2S; and precipitation of pyrite framboids in the water column. Molybdenum and Osmium are drawn down into the organic-rich black shales, and the ratio of osmium, neodymium and strontium reflects the balance between fluvial input, related to the weathering of continental materials and fluxes from hydrothermal sources (adapted from Weissert, 2000; Erba, 2004 and Jenkyns, 2010).

Scholle and Arthur (1980) went on to demonstrate that carbon isotopic data from pelagic limestone could be successfully used not only to correlate sections of a similar age independent of biostratigraphic correlation, but also to identify Oceanic Anoxic Events. Scholle and Arthur (1980) suggested that these OAEs were a result of a complex combination of tectonic events, changes in climate, sea level fluctuations and variations in the rates of oceanic circulation and nutrient supply, and are characterized by a positive carbon-isotope excursion (CIE) associated with increased global sequestration of ^{12}C-rich organic matter, this lighter isotope is favourably incorporated into phytoplankton and bacteria during photosynthesis (Berner and Lasaga, 1989). These CIEs are recorded both in terrestrial (e.g., Hasegawa, 1997, 2003; Gröcke et al., 1999; Kuypers et al., 1999; Hesselbo et al., 2000, 2007; Ando et al., 2002, 2003), and in marine sediments (e.g., Jenkyns and Clayton, 1986; Arthur et al., 1988; Jenkyns et al., 1994; Menegatti et al., 1998; Tsikos et al., 2004) showing that the peturbations to the C-cyle affect the whole ocean-atmosphere.

Since the initial OAE hypothesis, scientists have begun to put together a more detailed carbon-isotope record of Earth History, recognizing that the Cretaceous OAEs are not isolated phenomena. Oceanic Anoxic Events have been suggested in the Devonian, Permian, Triassic, Jurassic, and Paleocene (e.g., Kump et al. 2009, Jenkyns 2010). Oceanic Anoxic Events are considered to be primarily forced by both increased carbon productivity and exceptional carbon preservation (Jenkyns, 2010). Complexities arise because, as well as being associated with positive carbon-isotope excursions due to the burial of isotopically light organic carbon (e.g., Jenkyns and Clayton, 1986; Dickens et al., 1997; Jenkyns and Clayton, 1997; Menegatti et al., 1998; Schouten et al., 2000; Weissert and Erba, 2004) negative excursions are recorded in some cases, and these must record injection of isotopically light ^{12}C-rich gases into the ocean–atmosphere system, possibly from methane hydrates (e.g., Hesselbo et al., 2000, 2007; Beerling et al., 2002; Arens and Jahren, 2000; Cohen et al, 2004, 2007; Kemp et al., 2005; Hesselbo and Pieńkowski, 2010). Each OAE has a slightly different

isotopic signature as a result in differences in the history of carbon cycle peturbations to the Earth systems (Fig.4).

1.2.5 The Toarcian Oceanic Anoxic Event (T-OAE)

The T-OAE is characterized by a broad positive excursion, punctuated by a stepped negative excursion across the *tenuicostatum–serpentinum* chronozone; approximately equivalent to the *tenuicostatum–falciferum* sub-boreal ammonite Zone; *the polymorphum–levisoni* mediterranean ammonite Zone and the *tennuicostatum–hoelderi* andean ammonite Zone. These regional ammonite zones can be used to correlate these sections chronostratigraphically (Page, 2003). The excursion is recorded in marine carbonates, bulk organic matter, organic biomarkers and fossil wood (e.g Jenkyns and Clayton, 1986, 1997; Jenkyns, 1988, 2003; Schouten et al. 2000; Jenkyns et al., 2002; van Breugal et al. 2006; Hesselbo et al., 2007). Organic-rich sediments of Early Toarcian age have been found in the Tethyan and Boreal region as well as in Japan, Canada, Russia, Argentina, and Madagascar (Fig. 1; e.g., Jenkyns, 2002; Al-Suwaidi et al., 2010; Caruthers et al., 2011; Gröcke et al., 2011) although the biostratigraphic constraints on Toarcian age sediments is highly variable, this event is also associated with a marine transgression with regional deepening (Hallam, 2001).

There are several hypotheses for the cause of the negative carbon-isotope excursion. The first hypothesis suggests that the isotope excursion, and elevated carbon burial rates are not related to a global event but instead reflect local recycling of re-mineralized carbon, which is incorporated into phytoplankton biomass. Support for this hypothesis was drawn from the apparent absence of the negative carbon-isotope excursion in the belemnite carbon-isotope record (e.g., Küspert , 1982; van de Schootbrugge et al., 2005b; Wignall et al., 2005, 2006). The second hypothesis invokes the liberation of massive amounts of isotopically light

carbon from Pangean coals by intrusive eruptions of magmatic sills, during the eruption of the Karroo–Ferrar Large Igneous Province (e.g., Jourdan et al., 2005; McElwain et al., 2005; Svenson et al, 2007). The third and final hypothesis suggests that massive volcanism coupled with intensified rift-related activity could have resulted in global warming, elevated bottom-water temperatures, and thermal dissociation of methane hydrates from continental-margin sediments, this destabilization would have injected isotopically light carbon into the atmosphere (e.g., Hesselbo et al., 2000; Cohen et al., 2004, 2007; Kemp et al., 2005; Hesselbo and Pieńkowski, 2010).

The first hypothesis is the least favoured and the evidence for the T-OAE and corresponding CIE in areas (1) outside of the Tethyan region and (2) in more open water settings, on continental margins, shelf seas, in fossil wood and the deep oceans supports the hypothesis that this is a global event (e.g., Hesselbo et al, 2000, 2007; Al-Suwaidi et al., 2010, Bodin et al., 2010; Hesselbo and Pieńkowski, 2010; Caruthers et al., 2011; Gröcke et al., 2011; Kafousia, et al., 2011; Suan et al., 2011).

1.3 The Early Jurassic World: An Overview of the geography and climate

1.3.1 Early Jurassic Palaeogeography

Continental configuration in the Jurassic was dominated by two large supercontinents, Pangea in the Southern hemisphere with Antarctica, Africa, Australasia, India and South America sutured together and Laurasia in the Northern Hemisphere with Europe and Central Asia sutured together (Fig. 1). Pangea was surrounded by a vast global ocean; Panthalassa, or the *Proto*-Pacific (Golonka and Ford, 2000; Veevers, 2004; Golonka, 2007). In the Northern Hemisphere during the Early to mid-Jurassic, the Alpine-mediterranean Tethys was beginning to open together with the Central Atlantic as Africa separated from North America (e.g., Steiner et al., 1998; Marzoli et al., 1999; Golonka, 2007).

A significant amount of volcanism took place during the Triassic–Jurassic, including emplacement of the Central Atlantic Magmatic Province and the Karoo–Ferrar basaltic eruptions that resulted from the breakup of Southern Pangea and is considered to be the most voluminous episode of continental volcanism in the Phanerozoic Era with some 2.5–3 x 10^6 km^3 of basalt erupted, most of which took place during a very short interval, around 183–184 Ma, coinciding with the Toarcian OAE (e.g., Pankhurst et al., 2000; Golonka, 2007; Svenson et al., 2007; Jourdan et al., 2008).

1.3.2 Early Jurassic Palaeoclimate

The Early Jurassic climate has been intensively examined through Global Circulation Models (GCM: e.g., Chandler et al., 1992; Valdes, 1993; Sellwood and Valdes, 2006, 2008); sedimentological proxies; e.g., bauxite distribution, palaeosol types, peat, evaporite and coral reef distribution, distribution of tillities, ice-rafted drop-stones, striated pavement and glendonite (e.g., Hallam, 1984; Frakes et al., 1992, p.76; Sellwood et al., 1997; Price et al., 1995, 1997, 1999; Rogov and Zakharov, 2010; Suan et al., 2011); biota (leaf physiognomy; global distribution of plant types and morphologies (e.g., Vakhrameev, 1991 p. 8–92; Ziegler et al., 1993; Rees et al., 2000; Beerling and Royer, 2002b;), and geochemical proxies (e.g., $\delta^{18}O$; $^{87}Sr/^{86}Sr$, Mg/Ca)(e.g., Gibbs et al, 1999; Bailey et al., 2003; Cohen and Coe, 2007), and is generally considered to have been warmer than present with limited climate zonality. Reconstructions of the Jurassic suggest seasonally dry low latitudes (subtropical), succeeded poleward in both hemispheres by desert, seasonally dry (winterwet), warm temperate and cool temperate biomes (e.g., Ziegler et al., 1993; Rees et al., 2000; Sellwood and Valdes, 2008). The large size of continental interiors means that they are likely to have been significantly drier then they are today, being remote from moisture sources. Trade winds that carry moisture to the centre of continents had less influence, allowing aridity to prevail during the

Triassic and Early Jurassic (Parrish et al, 1982; Hallam, 1984; Chandler et al., 1992; Parrish, 1993; Gibbs et al., 1999; Sellwood and Valdes, 2008). However, it is also important to note that, while there was a prevalence of arid zones in continental interiors, the Jurassic was considered to be generally less arid than today, due to increased water vapour in the warmer air and the lack of significant polar ice caps (Sellwood and Valdes, 2008).

Although plant biome reconstruction shows an absence of tundra or glacial biomes during the Early Jurassic there is evidence of glaciation events in the Late Pliensbachian and Aalenian–Bajocian based on the evidence for a relative sea level fall (Hallam, 1981, 2001); the presence of boreal species of phytoplankton in the Tethys (van de Schootbrugge et al., 2005a); the occurrence of ice-rafted drop stones, and the frequency of glendonite carbonate nodules at high latitudes (e.g., Crowley and North, 1991, p. 234; Frakes et al. 1992; Eyles, 1993; Price, 1999; Veizer et al., 2000; Price, 2010; Rogov and Zakharov, 2010; Suan et al., 2011). Glendonite nodules are stellate aggregates which have pseudomorphed the mineral ikaite, a low temperature polymorph of calcium carbonate which crystallises at temperatures close to 0ºC and are thought to reflect cold subaqueous depositional conditions (eg. Seuss et al., 1982; Frakes and Francis, 1988; Markwick and Rowley, 1998; Price, 1999).

Models suggest that the Pliensbachian cool period was modulated by a carbon dioxide decrease to a low of 500-600 ppm followed by an increase in carbon dioxide to 1500 ppm and a return to warmer climate, and higher sea levels in the Toarcian (McElwain et al., 2005; Royer, 2006). This increase in polar and subpolar temperatures during the Toarcian is also indicated by the presence of subtropical to tropical plants such as the cycadophyte; *Ptilophyllum* in central and NE Siberia; the presence of the thermophyllic pollen spore *Classopollis* in Toarcian age marine sediments from the arctic and the absence of glendonites or other sedimentological indicators of ice (e.g., Vakhrameev, 1991; Price, 1999; Dera et al., 2011; Suan et al., 2011).

1.4 Analytical Methods

In this study, a variety of analytical methods are utilized to examine the Toarcian-OAE, these methods are described below. Field methodology and details of fieldwork conducted and bulk sediment samples collected can be found in Chapters 2–4.

1.4.1 Total Organic Carbon

Total Organic Carbon (TOC) is a key measurement in the study of Oceanic Anoxic Events (OAE), as OAE's where initially identified by the presence of an increase in the burial of organic carbon during a given time interval (Schlanger and Jenkyns 1976). Total organic carbon is measured by total carbon combustion using a Strohlein Coulomat 702 SO/CS. This method analyses a pair of duplicate samples, each sample consisting of a homogenized powdered rock sample, weighed into ceramic boats, the pair of samples weigh 100 mg and 50 mg. The 100 mg sample is roasted at 420ºC overnight to remove all volatile organic carbon, while retaining carbonate; the 50 mg sample is not roasted, retaining both organic carbon and carbonate.

The samples are then combusted at 1220ºC in the Coulomat, to decompose all carbon (carbonate and organic) present. The combusted CO_2 is fed in to a 20% barium perchlorate solution, buffered to pH 10 by electrolysis. The addition of CO_2 from combustion of the sample alters the pH. This pH is then corrected through back titration; the quantity of electrical current required for the back titration is measured, as a count. The count can then be converted to absolute % total carbon (%TC) using the following equation:

$$\text{Total Carbon \%(released from Coloumat combustion)} = \frac{(\text{Electrical count} \times 0.2)}{(\text{Sample weight (mg)})}$$

The difference between the roasted (organic-carbon-free sample) and the unroasted sample is then taken:

$$T(\text{unroasted}) - T(\text{roasted}) = A \text{ (Equivalent } CaCO_3)$$

$$A(CaCO_3) \times 8.3333 = \% \text{ Total Organic Carbon}$$

The user then has two values, one of which is the total carbon concentration (organic and carbonate) from the unroasted sample and the other value is carbonate only and is organic-carbon free (from the roasted sample). The difference between the two samples can be calculated to give the total organic carbon content of the sample. These values can then be plotted in stratigraphic height to indicate how total organic carbon varies through the stratigraphic section and over time.

1.4.2 Organic Carbon Isotopes in bulk sediment

Stable carbon isotopes were measured in this study in both bulk sediment and in terrestrial plant remains . Bulk sediment records the carbon-isotope of a mixture of marine and terrestrial organic carbon ratios, depending on the composition of the organic matter in the sediment.

Bulk sediment samples were first hammered in aluminium foil to gravel size using a rock hammer and then placed in an acetone-cleaned agate ball mill to powder and homogenize the sample. About 1-2g of sample was treated with 30 ml of hot 3 M HCl for 24 hours to remove calcium carbonate and sulphur; the samples were shaken every few hours to increase the reaction surface area and prevent sediment settling. After 24 hours the samples were centrifuged and the HCl decanted, a second addition of HCl was made and the sample

was shaken. If any resulting effervescence was observed (suggesting the presence of surviving calcium carbonate) the sample was treated with HCl again until no more bubbling was observed. Clear, carbonate-free samples were rinsed with deionised water until clear and neutral and dried in an oven overnight at 60ºC. Dried samples were re-powdered and ~5–50 mg of sample was weighed into 8 x 6 mm tin capsules. The amount of sample weighed was dependent on the total organic carbon either assumed or measured for the sample. These samples were then analysed in the University of Oxford, Research Laboratory for Archaeology and Art History, School of Archaeology, using a Carlo Erba Elemental Analyser coupled to a Europa Scientific Limited CN biological sample converter connected to a Geo 20-20 stable-isotope gas-ratio mass spectromenter. Carbon-isotope and nitrogen-isotope ratios were measured against a laboratory standard, Alanine ($\delta^{13}C$ = -26.9 ± 0.2‰ and $\delta^{15}N$ =-1.6 ± 0.2‰, n=100, Appendix B, Table B25) and expressed relative to Vienna Pee Dee Belemnite (WPDB) and atmospheric nitrogen (air N_2). Although nitrogen-isotope values were measured they are not used in this study, but are available in Appendix B, Table B21–24. Organic-carbon isotope values are presented in the standard delta notation as given by:

$$\delta^{13}C_{org} = [[(^{13}C/^{12}C_{sample}) - (^{13}C/^{12}C_{standard})] / (^{13}C/^{12}C_{standard}) -1] \times 10^{3}.$$

1.4.3 Organic Carbon Isotopes in fossil plant matter

Fossil wood samples were either collected directly from outcrop in Argentina or extracted from the rock samples shipped back to the University of Oxford. Fossil wood samples collected directly from the section were typically large, >1cm long dimension, these samples were powdered and decarbonated in the same way as bulk sediment samples and did not need additional processing to remove sediment.

Samples extracted from bulk sediment were first broken up to gravel size and treated with hot 3M HF to further break up the matrix silicates and then rinsed with deionized water to remove any additional HF and neutralise the sample. Samples of charcoalified wood were then extracted using tweezers. Such samples were then powdered and decarbonated with hot HCl, as described in the previous section

All wood samples were powdered and < 1 mg of samples was weighed into 3 x 5 mm tin capsules. These samples were also analyzed in the University of Oxford, Research Laboratory for Archaeology and Art History, using the same instruments and delta notation as described above for bulk sediment. The $\delta^{13}C$ results from fossil wood were plotted stratigraphically for comparison with the $\delta^{13}C$ from bulk sediment.

1.4.4 Carbonate Carbon and Oxygen isotopes

Bulk rock samples were measured for carbonate stable carbon and oxygen isotopes. Bulk samples were drilled with a dental drill, to collect a few micrograms of samples in to metal thimbles and cleaned with acetone and dried at 60ºC. Samples were reacted with a purified orthophosphoric acid at 90ºC and analysed online, using a VG Isogas preparation system and Prism II mass spectrometer in the Stable Isotope Laboratory at the Department of Earth Sciences, University of Oxford. Normal corrections were applied and the results are reported as per mil deviation from the Vienna Pee Dee Belemnite (VPDB) standard, and results are presented in the standard delta ($\delta^{13}C$ and $\delta^{18}O$ ‰) notation:

$$\delta^{13}C_{carb} = [[(^{13}C/^{12}C_{sample}) - (^{13}C/^{12}C_{standard})] / (^{13}C/^{12}C_{standard}) -1] \times 10^{3}.$$

$$\delta^{18}O_{carb} = [[(^{18}O/^{16}O_{sample}) - (^{18}O/^{16}O_{standard})] / (^{18}O/^{16}O_{standard}) -1] \times 10^{3}.$$

Calibration to VPDB was performed via the satellite standards NBS19 and Oxford Carrara marble. Reproducibility of replicate analysis of standards is generally better than 0.1‰ (2σ) for both carbon- and oxygen-isotope ratios (Jenkyns et al., 1994).

1.4.5 Hydrogen Index

Hydrogen index is used to determine the source of organic matter (i.e.,, terrestrial *vs* marine) aiding interpretation of changes in $\delta^{13}C$ values through the stratigraphic section, which may in part be due to variability in the origins of bulk organic matter components. Characterization of this organic matter to determine its origin is essential to understanding the exact nature of the sedimentary record of the T-OAE in the southern hemisphere.

Rock-Eval Pyrolysis (Espitalié, et al., 1985; Peters, 1986) was undertaken to give Hydrogen Index (HI) from approximately ~150 samples from three different locations from the Neuquén Basin, Argentina. Samples were first hammered in aluminium foil to gravel size using a rock hammer and then placed in an acetone-cleaned agate ball mill to powder and homogenize the sample. One gram of sample was placed in an epindorf tube and sent to be analysed at the Institut des Sciences de la Terre de Paris, Université Pierre et Marie Curie, Paris, France, using a Rock-Eval III, Oil Show Analyzer (OSA).

Rock-Eval Pyrolysis takes a bulk-dried sample and heats it in an inert helium atmosphere, and then quantifies the hydrocarbons by flame-ionization detection. Organic compounds that occur as free gases and liquids in sediments are separated by temperature control from those that occur in bound form or as particulate matter. The amount of hydrocarbon generated during pyrolysis normalized to the amount of total organic carbon comprises the hydrogen index (HI) [mg Hydrocarbon/g Total Organic Carbon]. This index can then be used to differentiate between marine and terrestrial organic matter by plotting it on a Tissot–Welte diagram (based on the Van Krevelen diagram; Tissot and Welte, 1984, p.

152; Bordenave et al., 1993, p. 252). Other values/parameters that may also be obtained and are of use in Rock-Eval Pyrolysis include the S1 value, which is a measure of hydrocarbon in milligrams that can be thermally distilled from 1 gram of rock (i.e., mg HCtd/g rock), and S2, which gives the hydrocarbons generated by the pyrolysis, measured in milligrams of hydrocarbons per milligram of rock (i.e., mg HC/ mg Rock). The temperature at which the maximum amount of S2 hydrocarbon is generated is called the T_{max}. Strictly, the Hydrogen Index corresponds to the quantity of pyrolyzable organic compounds or "hydrocarbons" (HC) from S2 relative to organic carbon or total organic carbon (Peters, 1986; Langford and Blanc-Valleron, 1990; Cornford et al., 1998).

These HI values can be translated to organic matter or kerogen type, (kerogen is is the insoluble fraction of organic matter) based on the following scale (Pasley et al., 1991; Bordenave et al., 1993, p.260; Palliani et al., 2002; Peters et al., 2005, p. 76–79):

- Type I kerogen; dominated by lipinite macerals which is hydrocarbon rich material derived from pollen, leaf cuticles, spores and plant resin in coal, usually formed in an anoxic lacustrine setting: 80% hydrocarbon from pyrolysis, HI = > 600 mg HC/g TOC

- Type IIs and II kerogen; originates from mixed phytoplankton, zooplankton, and bacterial debris usually in marine sediments, also has a higher sulphur content than other forms of kerogen : 50-60% hydrocarbon from pyrolysis; HI = ~300–600 mg HC/g TOC

- Type III kerogen; terrestrial plant material, typically dominated by vitrinite (woody plant material), 15-30% hydrocarbons from pyrolysis; HI = 50–200 mg HC/g TOC

- Type IV kerogen: reworked and oxidized kerogen; “dead” carbon, often originates from other kerogen types that were reworked and oxidized; HI= <50 mg HC/g TOC

A Tissot–Welte diagram that plots Hydrogen Index against T_{max}, illustrates the thermal maturity of the sediments. T_{max} values of < 430ºC represent thermally immature/unaltered samples, T_{max} values of 430–470ºC represent samples that are thermally developing into oils. Samples with T_{max} values > 470ºC represent very thermally mature samples, whose organic matter is evolving in to gas or into a gas state (e.g., Pasley et al., 1991 and Bordenave et al., 1993 p.252)

1.4.6 Biomarkers.

Biomarkers are complex molecular fossils derived from biochemicals, particularly lipids in once-living organisms; they are complex organic compounds with a specific structure, comprising carbon, hydrogen and oxygen that can be related to a particular source organism. Biomarkers occur in sediment, rock and crude oil and show little or no change from their parent organic molecules in living organisms. A scan of biomarkers can be used to give important information about the redox state of the water column. For example, the presence of specific types of biomarkers indicates the occurrence, in the depositional environment, of organisms that can only exist in euxinic (i.e. sulphidic) water columns within the photic zone. In this case examination of such biomarkers through stratigraphic sections can indicate changes in the oxygenation of a given water column through geological time (Peters et al., 2005, p.3).

Bulk rock samples were analysed for biomarkers at the University of Bristol, School of Chemistry, Biogeochemistry Research Centre using a method developed by R.D. Pancost for analysis of whole-rock samples. Samples were collected in Argentina, in ethanol-cleaned

glass jars to limit contamination from polycarbonates and or other polymers from plastic sample bags. Samples were initially rinsed with ethanol and then dried at room temperature and then powdered using an ethanol-cleaned agate ball mill and returned to the glass jars and taken to the Biogeochemistry Research Centre, for preparation and analysis.

About 25–30 mg of sample was prepared using Soxhlet extraction using a 2:1 dichloromethane–methanol mixture (DCM:MeOH, 2:1 [vol/vol]), to remove the Total Lipid Extract (TLE) from the bulk sediments. Elemental sulphur was removed by the addition of activated copper turnings and allowed to react for 24 hours. Samples were then dried down to less than 7 ml using rotary evaporation, and transferred to weighed 7 ml glass vials using glass pipettes. The dried down sample in the glass vial was then weighed to establish the amount of TLE present in the sample. A 2 ml mixture of DCM:MeOH (2:1 [vol/vol]) was then added to the sample, 1ml of which was placed into a 7ml glass vile and dried under N_2 and frozen as an archive sample. The remaining sample was further processed for analysis and 10 μl of 5α-androstane/2-hexadecanol standard was added and the sample was dried down under N_2.

Polar and apolar fractions were separated using alumina column chromatography. Pre-extracted and activated alumina wool (Al_2O_3) was placed into furnaced short glass pipettes and the column was then rinsed with a n-hexane/dichloromethanol mixture (nhexane:DCM 9:1 [vol/vol]). The sample was then diluted in 1ml of dichloromethanol:isopropanol (DCM:iPA, 2:1[vol/vol]) and loaded on to the column and eluted into a 7ml glass vial. Four column volumes of nhexane:DCM were eluted: this is the apolar fraction. Three column volumes of DCM:MeOH (2:1[vol/vol]) were then eluted in to a new 7ml glass vial: this is the polar fraction. Samples were dried down using N_2, and the polar fraction was frozen for archive, as it was not used for this study.

Samples were dissolved in 100μl of ethyl acetate and 1μl of the product was analysed using a Carlo Erba High Resolution Gas Chromatography (GC) 5300 mega series

fitted with a fused capillary column (50m x 0.32 mm i.d.) coated with CPSil-5CB (dimethlpolysiloxane equivalent) stationary phase (0.12um film thickness) to establish the concentration of the apolar TLE. Components were eluted using H_2 carrier gas. Samples were injected at 70ºC, and then the temperature was programmed to increase at 20ºC/min to 130ºC, and at 4ºC/min to 300ºC and then held constant for 25 min. A Fatty Acid Methyl Ester standard (FAMEs) was injected in to the GC at the beginning of each run.

Once the concentration of the apolar fraction was determined, the correct dilution of the sample was analysed on a ThermoQuest Trace Mass Spectrometer, to establish the presence and quantity of individual biomarkers. Chromatograms were plotted as the sample eluted through the mass spectrometer, and samples were compared against a known quantity of a known standard (in this case 5α-androstane/2-hexadecanol) to establish concentration of specific biomarker compounds. One blank sample was created for every four samples; blanks were processed in the same way as sediment samples and underwent all of the chemical extraction techniques described above, and soxhalent extraction through column chromatography (method adapted from Pancost et al., 2000, Handley et al., 2008 and laboratory methodology from the University of Bristol, Biogeochemistry Research Group). Data were analysed for the presence of Pristane, Phytane, homohopanes, isorenieratane, and steranes.

1.4.7 Molybdenum Isotopes

Molybdenum (Mo) is readily transferred from the oceans and has a residence time of ~800,000 yrs (Morford and Emerson, 1999). The concentration of molybdenum in the oceans is fairly constant in oxygenated waters (~100 nM) and molybdenum speciation is dominated by the highly unreactive, soluble molybdate ion, MoO_4^{-2}. Isotopic analysis of modern seawater indicates a Mo isotope composition $\delta^{98}Mo_{sw}$= + 2.3‰, which is consistent with

seawater being a well-mixed reservoir. There are three major reservoirs of Mo in the marine environment: seawater, sediment and authigenically precipitated Mo (Barling, 2001; Siebert et al, 2003; Poulson et al., 2006). In oxic sediments, where aerobic respiration is the primary pathway for organic mater decomposition, Mo is sequestered through adsorption onto Mn oxyhydroxide (Bertine and Turkein, 1973; Calvert and Pederson, 1993). With increasingly reducing conditions, where anaerobic processes dominate electron transport, Mo is sequestered into sediment *via* Mo sulfide formation. Mo becomes highly reactive, particularly when dissolved hydrogen sulphide ($[H_2S]>11umol/kg^{-1}$) is present which acts as a "geochemical switch" and MoO_4^{-2} is transformed to reactive oxythiomolybdates ($MoO_{4-x}S_x^{2}$; Helz et al., 1996; Siebert et al., 2003; Anbar and Rouxel, 2007). Under these conditions Mo scavenging out of the water column and into sediments should be almost complete, resulting in deposits that contain Mo with an isotopic composition identical to or close to, the bulk dissolved Mo: so-called quantitative removal. The $\delta^{98/95}Mo_{seawater}$ should vary with the global extent of oxic seawater; and experimental studies show $\delta^{98/95}Mo$ values falling to -0.2 to +0.7‰ in anoxic to euxinic settings, recording a unique isotope signature of open-ocean anoxic sediments. This allows Mo to be used as a proxy for the determination of palaeoredox conditions by examining variability in, $\delta^{98/95}Mo_{seawater}$ - $\delta^{98/95}Mo_{sediment}$ (e.g., Emerson and Huested, 1991; Siebert et al., 2003; Poulson et al., 2006; Fig. 5).

Molybdenum enrichment in euxinic sediments and sedimentary rocks tracks: (1) the amount of organic matter and (2) the availability of molybdenum in the basin of deposition and (3) drawdown of the molybdenum inventory on an oceanic scale during times of widespread oxygen deficiency, for example Oceanic Anoxic Events (e.g., Anbar and Rouxel, 2007 and Lyons et al., 2009)

Samples for molybdenum analysis were prepared from whole-rock samples. Samples were hammered in aluminium foil to gravel size using a rock hammer and then placed in an acetone cleaned agate ball and mill to powder and homogenize the sample. A mass of 0.5 g of

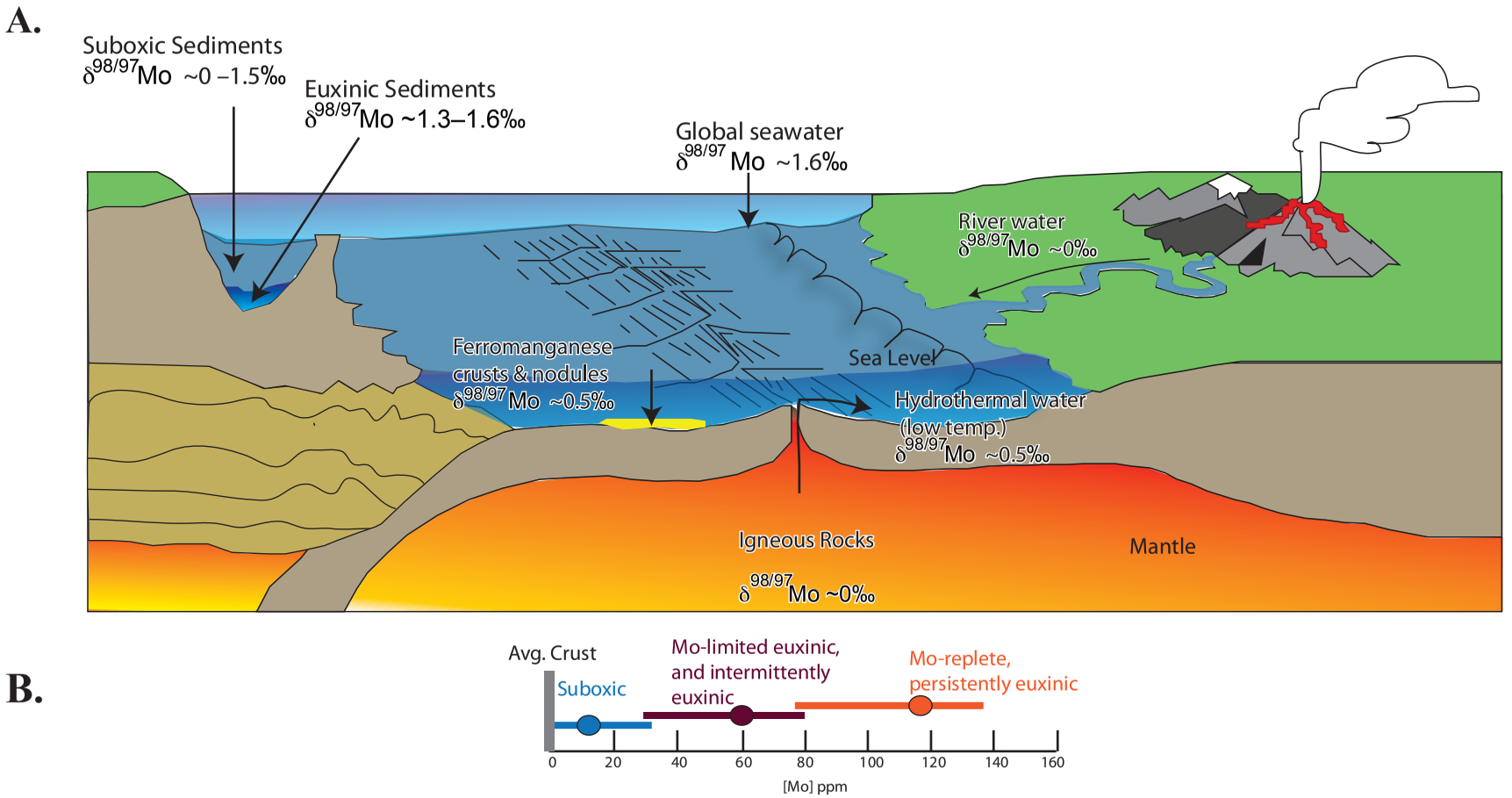


Figure 5. A.) Schematic depiction of molybdenum ocean isotope budget. Molybdenum enters the ocean primarily *via* rivers, probably with $\delta^{98}/^{97}Mo$ ~0‰. Light isotopes are preferentially removed from seawter into Fe-Mn oxides and suboxic sediments making $\delta^{98}/^{97}Mo_{seawater}$ heavy.There is relatively little fractionation during removal to euxinic sediments. Hence palaeo-$\delta^{98}/^{97}Mo_{seawater}$ may be recorded in black shales (adapted from Anbar & Rouxel, 2007).

B.) The mean and range of molybdenum concentrations observed at a large number of modern oxic, suboxic and euxinic environments. Euxinic settings are subdivided as a function of persistence of euxinia and Mo availability in the basin. Also included is the range for average crust (1–2ppm). Average crustal values are also seen at oxic marine sites with low total organic carbon (TOC) and a lack of appreciable enrichment in ferromanganese oxides (Lyons et al. 2007).

Samples for molybdenum analysis were prepared from whole-rock samples. Samples were hammered in aluminium foil to gravel size using a rock hammer and then placed in an acetone cleaned agate ball and mill to powder and homogenize the sample. A mass of 0.5 g of sample was ashed in a ceramic crucible at ~750ºC overnight to remove any volatile organics and then reweighed. Of the ashed sample100 mg was then placed in an acid-cleaned Teflon beaker with 3ml of 10 M hydrochloric acid (HCl) to decarbonate the sample. The sample was left in HCl overnight and dried down the following day. An additional 3 ml of 10M HCL was added to confirm the removal of all calcium carbonate (any effervescence suggesting the presence of calcium carbonate was treated until the sample no longer effervesced); the sample was then dried down on a hot plate.

The samples were then digested using 6 ml of hydroflouric acid (reagent grade), and 3 ml of distilled nitric acid was then added to the sample and the sample left overnight on a hot plate at 130ºC. The sample was then dried down on the hot plate, and 2 ml of distilled concentrated nitric acid was added. Peroxide was added in 20–30 μl amounts every 45 minutes over several hours until the sample ceased reacting. The sample was then heated at 130ºC overnight and then dried the following day.

The samples were then given to Dr. Chris Siebert, Dept. of Earth Sciences, University of Oxford, for anion and cation exchange based on molarity change in a HCl medium (detailed method in Siebert et al., 2001 and Wasylenki et al. 2008). Samples were spiked with a ^{97}Mo and ^{100}Mo double-isotope tracer (Siebert et al., 2001) and isotope measurements were made on a Nu MC-ICP-Mass spectrometer, at the University of Oxford. Isotope measurements were made relative to an external standard solution, Alfa Aesar Specpure solution (stock 35758, lot 011895D). All data are presented in the delta notation whereby:

1.5 Summaries and Overview of Remaining Chapters

While much work has already been done in furthering our understanding of Oceanic Anoxic Events, specifically with regard to those in the Cretaceous, the exact nature and extent of the Toarcian Oceanic Anoxic Event is still under significant scrutiny. In this thesis I aim to use the concepts and methodology discussed in this chapter to examine the Toarcian OAE as expressed in sediments deposited in the southern hemisphere, specifically the Neuquén Basin, Argentina.

Chapter 2 provides a detailed sedimentological and biostratigraphical overview of three localities, four stratigraphic sections in the Neuquén Basin, Argentina,, with discussions of the depositional settings and biostratigraphic constraints on the sections, using newly described ammonite, bivalve and nannofossil biostratigraphy.

Chapter 3 provides an overview of the carbon-isotope chemostratigraphy from bulk sediment and charcoalified wood from the four sections described in Chapter 2, and aims to correlate the data from the southern hemisphere with sections of a Pliensbachian–Toarcian age from other locations in the world, specifically Yorkshire, and Wales, UK; Kastelli, Greece; Valdorbia, Italy and Haida Gwaii, British Columbia, Canada. In addition the chapter examines how carbon-isotope chemostratigraphy from this study compares with recently published carbon-isotope data from Argentina, generated by Mazzini et al. (2011).

Chapter 4 gives a multi-proxy examination of two sections in the Neuquén Basin namely Arroyo Lapa North and Arroyo Lapa South. Proxies include biomarkers (homohopanes, steranes, pristine and phytane), organic carbon-isotopes and molybdenum-isotopes, hydrogen index, and pyrite framboids. This multi-proxy record is compared to data from sedimentary successions of similar age from the Tethyan region to document the degree of similarity and what can be inferred about the nature and extent of the Toarcian OAE.

Chater 5 is a summary of the principal findings and a discussion of future work that needs to be completed to improve understanding of the Toarcian OAE in the Southern Hemisphere.

References:

Al-Suwaidi, A.H., Angelozzi, G.N., Baudin. F., Damborenea, S.E., Hesselbo, S.P., Jenkyns, H.C., Manceñido, M.O., and Riccardi, A.C., 2010, First record of the Early Toarcian Oceanic Anoxic Event from the southern hemisphere, Neuquén Basin, Argentina: Journal of the Geological Society, London, v. 167, p. 633–636.

Anbar, A.D. and Rouxel, O., 2007, Metal stable isotopes in paleoceanography: Annual Review Earth and Planetary Science, v. 35, p. 717–746.

Ando, A., Kakegawa, T., Takashima, R. and Saito, T., 2002, New perspective on Aptian carbon isotope stratigraphy: data from $\delta^{13}C$ records of terrestrial organic matter: Geology, v. 30, p. 227–230, doi:10.1130/0091-7613(2002) 030<0227-NPOACI>2.0.CO;2,

Ando, A., Kakegawa, T., Takashima, R. and Saito, T., 2003, Stratigraphic carbon isotope fluctuations of detrital woody materials during the Aptian Stage in Hokkaido, Japan: comprehensive $\delta^{13}C$ data from four sections of the Ashibetsu area: Journal of Asian Earth Sciences, v. 21, p. 835–847, doi:10.1016/S1367-9120(02)0012-8.

Arens, N. C. and Jahren, A. H., 2000, Carbon isotope excursion in atmospheric CO_2 at the Cretaceous–Tertiary boundary: evidence from terrestrial sediments: Palaios, v. 15, p. 314–322.

Arrhenius, S., 1896, On the influence of carbonic acid in the air upon the temperature of the ground: Philosophical Magazine, v. 41, p. 237–279.

Arnold, G.L., Anbar, A.D., Barling, J., and Lyons, T.W., 2004, Molybdenum isotope evidence for widespread anoxia in mid-Proterozoic oceans: Science, v. 304, p. 87–90 , doi:10.1126/science.1091785.

Bailey, T.R., Rosenthal, Y., McArthur, J.M., van de Schootbrugge, B., and Thirlwall, M.F., 2003, Paleoceanographic changes of the Late Pliensbachian–Early Toarcian interval: a possible link to the genesis of an Oceanic Anoxic Event: Earth and Planetary Science Letters, v. 212, p. 307–320.

Barnard, P.D.W., 1973, Mesozoic floras: Special Papers in Palaeontology, v. 12, p. 175-187

Beerling, D.J. and Royer, D.L., 2002a, Reading a CO_2 signal from fossil stomata: New Phytologist, v. 153, p. 387–397.

Beerling, D.J. and Royer, D.L., 2002b, Fossil Plants as indicators of the phanerozoic global carbon cycle: Annual Review Earth and Planetary Science, v. 30, p. 527–556, doi:10.1146/annurev.earth.30.091201.141413.

Beerling, D.J., Lomas, M.R. and Gröcke, D.R., 2002, On the nature of methane gas-hydrate dissociation during the Toarcian and Aptian Oceanic Anoxic Events: American Journal of Science, v. 302, p. 28–49.

Berner, R.A. and Raiswell, R., 1983, Burial of organic carbon and pyrite sulfur in sediments over Phanerozoic time: a new theory: Geochemica et Cosmochimica Acta, v. 47, p. 855–862.

Berner, R.A. and Lasaga, A.C., 1989, Modeling the geochemical carbon cycle: Scientific American, v. 260, p. 74–81.

Berner, R.A., 1990, Atmospheric Carbon Dioxide Levels Over Phanerozoic Time: Science, v. 249, p.1382–1386.

Berner, R.A., 1991, A model for atmospheric CO_2 over Phanerozoic time: American Journal of Science, v. 291, p. 339–376.

Berner, R.A., 1999, A new look at the long-term carbon cycle: GSA Today, v. 9, p. 1–6.

Berner, R.A. and Kothavala, Z., 2001, GEOCARB III: A revised model of atmospheric CO_2 over Phanerozoic Time: American Journal of Science, v. 301, p. 182–204.

Bertine, K.K., and Turekian, K.K., 1973, Molybdenum in marine deposits: Geochimica et Cosmochimica Acta, v. 37, p. 1415–1434, doi: 10.1016/0016-7037(73)90080-X.

Blakey, R., 2007, Early Jurassic rectangular palaeogeographic map in mollewide: World Wide Web Address: http://jan.ucc.nau.edu/~rcb7/200marect.jpg

Bodin, S., Mattioli, E. Fröhlich, S., Marshall, J.D., Boutib, L., Lahsini, S., and Redfern, J., 2010, Toarcian carbon isotope shifts and nutrient changes from the Northern margin of Gondwana (High Atlas, Morocco, Jurassic): Palaeoenvironmental implications: Palaeogeography, Palaeoclimatology, Palaeoecology, v. 297, p. 377–390, doi:10.1016/j.palaeo.2010.08.018.

Bolin, B., 1970, The carbon cycle: Scientific American, v. 223, p. 124–132.

Bordenave, M.L., Espitalié, J., Leplat, P., Oudin, J.L. and Vandenbroucke, M., 1993, Screening techniques for source rock evaluation, *in*, Bordenave, M.L., ed., Applied Petroleum Geochemistry: Éditions Technip, Paris, France, p. 217–278

Caruthers, A.H., Gröcke, D.R., and Smith, P.L., 2011, The significance of an Early Jurassic (Toarcian) carbon-isotope excursion in Haida Gwaii (Queen Charlotte Islands), British Columbia, Canada: Earth and Planetary Science Letters, v. 307, p. 19–26 doi:10.1016/j.epsl.2011.04.013.

Calvert, S.E., and Pedersen, T.F., 1993. Geochemistry of recent oxic and anoxic marine sediments: Implications for the geological record: Marine Geology, v. 113, p. 67–88.

Cerling, T.E., 1991, Carbon dioxide in the atmosphere: evidence from Cenozoic and Mesozoic paleosols: American Journal of Science, V. 291, p. 377–400.

Coffin, M.F., Duncan, R.A., Eldhold, O., Fitton, J.G., Frey, F.A., Larsen, H.C., Mahoney, J.J., Saunders, A.D., Schlich, R. and Wallace, P.J., 2006, Large Igneous Provinces and scientific ocean drilling, status quo and a look ahead: Oceanography, v. 19, p. 150–160.

Cohen, A.S., 2004, The rhenium–osmium isotope system: applications to geochronological and palaeoenvironmental problems: Journal of the Geological Society, London, v. 161, p. 729–734.

Cohen, A.S. and Coe, A.L., 2007, The impact of the Central Atlantic Magmatic Province on climate and on the Sr- and Os-isotope evolution of seawater: Palaeogeography, Palaeoclimatology, Palaeoecology, v. 244, p. 374–390.

Cornford, C., Gardener, P. and Burgess, C., 1998, Geochemical truths in large data sets. I: Geochemical screening data: Organic Geochemistry, v. 29, p. 519–530.

Chamberlin, T.C., 1899, An attempt to frame a working hypothesis of the cause of glacial periods on an atmospheric basis: Journal of Geology, v. 7, p. 545–584.

Chandler, M.A., Rind, D. and Ruedy, R., 1992, Pangaean climate during the Early Jurassic: GCM simulations and the sedimentary record of paleoclimate: Geologic Society of America Bulletin, v. 104, p. 543–559, doi: 10.1130/0016-7606(1992)104<0543:PCDTEJ>2.3.CO;2.

Chaloner, W.G. and McElwain, J.C., 1997, The fossil plant record and global climatic change: Review of Palaeobotany and Palynology, v. 95, p. 73–82.

Crowley, T.J. and North, G.R., 1991, Paleoclimatology: Oxford University Press, UK, 349 p.

Dera, G., Brigaud, B., Monna, F., Laffont, R., Pucéat, E., Deconinck, J. -F., Pellenard, P., Joachimski, M. M. and Durlet, C., 2011, Climatic ups and downs in a disturbed Jurassic world: Geology, v. 39, p. 215–218, doi: 10.1130/G31579.1.

Dickens, G.R., Castillo, M. M. and Walker, J. C. G., 1997, A blast of gas in the latest Paleocene: Simulating first-order effects of massive dissociation of oceanic methane hydrates: Geology, v. 25, p. 259–262, doi:10.1130/0091-7613(1997)025<0259:ABOGIT>2.3.CO;2.

Dickens, G. R., 2003, Rethinking the global carbon cycle with a large dynamic and microbially mediated gas hydrate capacitor: Earth and Planetary Science Letters, v. 213, p. 169–183.

Dickens, G.R., 2011, Down the rabbit hole: toward appropriate discussion of methane release from gas hydrate systems during the Paleocene-Eocene thermal maximum and other past hyperthermal events: Climate of the Past, v. 7, p. 831–846, doi:10.5194/cp-7-831-2011.

Emerson, S.R. and Huested, S.S., 1991, Ocean anoxia and the concentrations of molybdenum and vanadium in seawater: Marine Chemistry, v. 34, p. 177–196.

Erba, E., 2004, Calcareous nannofossils and Mesozoic oceanic anoxic events: Marine Micropaleontology, v. 52, p. 85–106.

Espitalié, J., Deroo, G. and Marquis, F., 1985, Rock-Eval Pyrolysis and its Applications (Part One): Oil and Gas Science and Technology – Rev. IFP., v. 40, p. 563–579, doi:10.2516/ogst:1985035.

Eyles, N., 1993, Earth's glacial record and its tectonic setting: Earth-Science Reviews, v. 35, p. 1–248.

Falkowski, P.G., 1994, The role of phytoplankton photosynthesis in global biogeochemical cycles: Photosynthesis Research, v. 39, p. 235–258.

Falkowski, P., Scholes, R.J., Boyle, E., Canadell, J., Canfield, D., Elser, J., Gruber, N., Hibbard, K., Högberg, P., Linder, S., MacKenzie, F.T., Moore III, B., Pedersen, T., Rosenthal, Y., Seitzinger, S., Smatacek, V. and Steffen, W., 2000, The global carbon cycle: a test of our knowledge of earth as a system: Science, v. 290, p. 291–295, doi:10.1126/science.290.5490.291.

Fletcher, B.J., Beerling, D.J., Royer, D.L., Brentnall, S.J., 2005, Fossil bryophytes as recorders of ancient CO_2 levels: experimental evidence and a Cretaceous case study: Global Biogeochemical Cycles, v. 19, GB3012, doi:10.1029/

2005GB002495.

Fletcher, B.J., Brentnall, S.J., Anderson, C.W., Berner, R.A., and Beerling, D.J., 2008, Atmospheric carbon dioxide linked with Mesozoic and early Cenozoic climate change: Nature Geoscience, v. 1, p. 43–48, doi:10.1038/ngeo.2007.29

Forster, A., Schouten, S., Morriya, K, Wilson, P.A. and Sinninghe Damsté, J.S., 2007, Tropical warming and intermittent cooling during the Cenomanian/Turonian oceanic anoxic event 2: Sea surface temperature records from the equatorial Atlantic: Paleoceanography, v. 22, PA1219, 14 p., doi:10.1029/ 2006PA001349.

Frakes, L.A. and Francis, J.E., 1988, A guides to Phanerozoic cold polar climates from high latitude ice-rafting in the Cretaceous: Nature, v. 333, p. 547–549.

Frakes, L.A., Francis, J.E., Syktus, J.I., 1992, Climate modes of the Phanerozoic: Cambridge Univ. Press, Cambridge, UK, 274 p.

Gibbs, M. T., Bluth, G. J. S., Fawcett, P. J. and Kump, L. R., 1999, Global chemical erosion over the last 250 MY: variations due to changes in paleoceanography, paleoclimate, and paleogeology: American Journal of Science, v. 299, p. 611–651.

Golonka J. and Ford, D., 2000, Pangean (Late Carboniferous–Middle Jurassic) paleoenvironment and lithofacies: Palaeogeography, Palaeoclimatology, Palaeoecology, v. 161, p. 1–34.

Golonka, J., 2007, Late Triassic and Early Jurassic palaeogeography of the World: Palaeogeography, Palaeoclimatology Palaeoecology, v. 244, p. 297–307, doi:10.1016/j.palaeo.2006.06.041.

Gröcke, D.R., Hesselbo, S.P, and Jenkyns, H.C., 1999, Carbon isotope composition of Lower Cretaceous fossil wood: ocean-atmosphere chemistry and relation to sea-level change: Geology, v. 27, p. 155–158, doi:10.1130/0091-7613(1999)027<0155:CICOLC>2.3CO;2..

Gröcke, D.R., 2002, The carbon isotope composition of ancient CO_2 based on higher-plant organic matter: Phil. Trans. R. Soc. Lond., v. 360, p. 633–658, doi:10.1098/rsta.2001.0965

Gröcke, D.R., Hori, R.S., Trabucho-Alexandre, J., Kemp, D.B. and Schwark, L., 2011, An open marine record of the Toarcian oceanic anoxic event: Solid Earth Discussion, v. 3, p. 385-410, doi:10.5194/sed-3-385-2011.

Hallam, A., 1984, Continental humid and arid zones during the Jurassic and Cretaceous: Palaeogeography, Palaeoclimatology, Palaeoecology, v. 47, p. 195–223.

Hallam, A., 2001, A review of the broad pattern of Jurassic sea-level changes and their possible causes in the light of current knowledge: Palaeogeography, Palaeoclimatology, Palaeoecology, v. 167, p. 23–27.

Hallam, A., Crame, J. A., Manceñido, M.O., Francis, J.E. and Parrish, J.T., 1993, Jurassic climates as inferred from the sedimentary and fossil record [and discussion]: Philisophical Transactions: Biological Sciences, v. 341, p. 287–296.

Handley, L., Pearson, P.N., McMillan, I.K. and Pancost, R.D., 2008, Large terrestrial and marine carbon and hydrogen isotope excursions in a new Paleocene/Eocene boundary section from Tanzania: Earth and Planetary Science Letters, v. 275, p. 17–25, doi:10.1016/j.epsl.2008.07.030.

Hasegawa, T., 1997, Cenomanian–Turonian carbon isotope events recorded in terrestrial organic matter from northern Japan: Palaeogeography, Palaeoclimatology, Palaeoecology, v. 130, p. 1997,

Hasegawa, T., 2003, Cretaceous terrestrial paleoenvironments of northeastern Asia suggested from carbon isotope stratigraphy: Increased atmospheric pCO_2-induced climate: Journal of Asian Earth Sciences, v. 21, p. 849–859, doi:10.1016/S1367-9120(02)00109-8.

Helz, G.R., Miller, C.V., Charnock, J.M., Mosselmans, J.F.W., Pattrick, R.A.D., Garner,

C.D., and Vaughan, D.J., 1996. Mechanism of molybdenum removal from the sea and its concentration in black shales: EXAFS evidence: Geochimica et Cosmochimica Acta, , v. 60, p. 3631–3642.

Herman, A. B., and Spicer, R. A., 1996, Palaeobotanical evidence for a warm Cretaceous Arctic Ocean: Nature, v. 380, p. 330–333, doi:10.1038/ 380330a0.

Hesselbo, S.P., Gröcke, D.R., Jenkyns, H.C., Bjerrum, C.J., Farrimond, P., Morgans Bell, H.S., and Green, O.R., 2000, Massive dissociation of gas hydrate during a Jurassic Oceanic Anoxic Event: Nature, v. 406, p. 392–395.

Hesselbo, S.P., Jenkyns, H.C., Duarte, L.V., and Oliveira, L.C.V., 2007, Carbon-isotope record of the Early Jurassic (Toarcian) Oceanic Anoxic Event from fossil wood and marine carbonate (Lusitanian Basin, Portugal): Earth and Planetary Science Letters, v. 253, p. 455–470.

Hesselbo, S. P. and Piénkowski, G., 2010, Stepwise atmospheric carbon-isotope excursion during the Toarcian Oceanic Anoxic Event: Earth and Planetary Science Letters, v. 301, p. 365–372, doi: 10.1016/j.epsl.2010.11.021.

Jahren, A. H., Arens, N. C., Sarmiento, G. , Guerrero, J. and Amundson, R., 2001, Terrestrial record of methane hydrate dissociation in the Early Cretaceous: Geology, v. 29, p. 159–162, doi: 10.1130/0091-7613(2001)029<0159: TROMHD>2.0.CO;2.

Jenkyns, H.C., 1988, The Early Toarcian (Jurassic) anoxic event; stratigraphic, sedimentary and geochemical evidence: American Journal of Science, v. 288, p. 101–151.

Jenkyns, H.C., 2003, Evidence for rapid climate change in the Mesozoic–Palaeogene greenhouse world: Philosophical Transactions of the Royal Society, London, v. 231, p. 1885–1916, doi:10.1098/rsta.2003.1240.

Jenkyns, H.C., 2010, Geochemistry of oceanic anoxic events: Geochemistry, Geophysics, Geosystems, v. 11, Q03004, doi: 10.1029/2009GC002788.

Jenkyns, H.C. and Clayton, C. J., 1986, Black shales and carbon isotopes in pelagic sediments from the Tethyan Lower Jurassic: Sedimentology, v. 33, p. 87–106.

Jenkyns, H.C. and Clayton, C. J., 1997, Lower Jurassic epicontinental carbonates and mudstones from England and Wales: chemostratigraphic signals and the early Toarcian anoxic event: Sedimentology, v. 44, p. 687–706.

Jenkyns, H.C., Gröcke, D.R. and Hesselbo, S.P., 2001, Nitrogen isotope evidence for water mass denitrification during the early Toarcian (Jurassic) oceanic anoxic event: Paleoceanography, v. 16, p. 593–603.

Jenkyns, H.C., Jones, C.E., Gröcke, D.R., Hesselbo. S.P. and Parkinson, D.N., 2002, Chemostratigraphy of the Jurassic System: applications, limitations and implications for palaeoceanography: Journal of the Geological Society, London, v. 159, p. 351–378.

Jenkyns, H.C., Forster, A., Schouten, S., and Sinninghe Damsté, J.S., 2004, High temperatures in the Late Cretaceous Arctic Ocean: Nature, v. 432, p. 888892

Jones, C.E. and Jenkyns, H.C., 2001, Seawater Strontium Isotopes, Oceanic Anoxic Events, and seafloor hydrothermal activity in the Jurassic and Cretaceous: American Journal of Science, v. 301, p. 112–149.

Jourdan, F., Féraud, G., Bertrand, H., and Kampunzi, A. 2005, Karoo large igneous province: Brevity, origin, and relation to mass extinction questioned by new $^{40}Ar/^{39}Ar$ age data: Geology, v. 33, p. 745–748, doi: 10.1130/G21632.1.

Kafousia, N., Karakitsios, V., Jenkyns, H.C. and Mattioli, E., 2011, A global event with a regional character: the Early Toarcian Oceanic Anoxic Event in the Pindos Ocean (northern Peloponnese, Greece): Geological Magazine, v. 148, p. 619–631.

Kemp, D.B., Coe, A.L., Cohen, A.S., and Schwark, L., 2005, Astronomical pacing of methane release in the Early Jurassic period: Nature, v. 437, p. 396–399, doi:10.1038/nature04037.

Kump, L.R. and Arthur, M.A., 1999, Interpreting carbon-isotope excursions: carbonates and organic matter: Chemical Geology, v. 161, p. 181–198.

Kump, L.R., Bralower, T.J. and Ridgwell, A., 2009, Ocean Acidification in Deep Time: Oceanography, v. 22, p. 94–107.

Kurtz. A.C., Kump, L.R., Arthur, M.A., Zachos, J. C. and Paytan, A., 2003, Early Cenezoic decoupling of the global carbon and sulfur cycles: Paleoceanography, v. 18, 1090, 14 p., doi: 10.1029/2003PA000908.

Küspert, W. ,1982, Environmental changes during oil shale deposition as deduced from stable isotope ratios, in: Cyclic and Event Stratification, Einsele, G. and Seilacher eds., A. p. 482–501, Springer, Berlin.

Kuypers, M. M., Pancost, R.D., Sinninghe Damsté, J.S., 1999, A large and abrupt fall in atmospheric CO_2 concentration during Cretaceous times: Nature, v. 399, p. 324–345, doi:10.1038/20659.

Krassilov, V.A., 1972, Phytogeographical classification of Mesozoic floras and their bearing on continental drift: Nature, v. 237, p. 49-50.

Kvenvolden, K.A., 2002, Methane hydrate in the global carbon cycle: Terra Nova, v. 14, p. 302–306.

Langford, F.F. and Blanc-Valleron, M.-M., 1990, Interpreting Rock-Eval Pyrolysis data using graphs of pyrolizable hydrocarbons vs. Total Organic Carbon: The American Association of Petroleum Geologists Bulletin, v. 74, p. 799–804.

Lyons, T.W., Anbar, A.D., Severmann, S., Scott, C. and Gill, B.C., 2009, Tracking euxinia in the ancient ocean: A multiproxy perspective and Proterozoic case study: Annual Review Earth and Planetary Science, v. 37, p. 507–534. doi: 10.1146/annurev.earth.36.031207.124233.

Lüthi, D., Le Floch, M., Bereiter, B., Blunier,T., Barnola, J.-M., Siegenthaler, U., Raynaud, D., Jouzel, J., Fischer, H., Kawamura, K. and Stocker, T.F., 2008, High-resolution carbon dioxide concentration record 650,000–800,000 years before present: Nature, v. 453, p. 379–382.

Markwick, P.J., Rowley, D.B., 1998, The geological evidence for Triassic to Pleistocene glaciations: implications for eustacy, *in,* Pindell, J., and Drake, C.L., eds., Paleogeographic Evolution and Non-Glacial Eustacy: Northern South America. SEPM Special Publication, v. 58, p. 17–43.

Marzoli, A., Renne, P.R., Piccirillo, E. M., Ernesto, M., Bellieni, G. and De Min, A., 1999, Extensive 200-million-year-old continental flood basalts of the Central Atlantic Magmatic Province: Science, V. 284, p. 616–618.

Mazzini, A., Svenson, H., Leanza, H.A., Corfu, F. and Planke, S., 2010, Early Jurassic shale chemostratigraphy and U-Pb ages from the Neuquén Basin (Argentina): Implications for the Toarcian Oceanic Anoxic Event: Earth and Planetary Science Letters, v. 297, p. 633-645. doi:10.1016/j.epsl.2010.07.017.

McArthur, J.M., Algeo, T.J., van de Schootbrugge, B., Li, Q., and Howarth, R.J., 2008, Basinal restriction, black shales, Re-Os dating, and the Early Toarcian (Jurassic) oceanic anoxic event: Paleoceanography, v. 23, PA4217, doi:10.1029/2008PA001607.

McElwain, J.C., Wade-Murphy, J. and Hesselbo, S.P., 2005, Changes in carbon dioxide during an oceanic anoxic event linked to intrusion into Gondwana coals: Nature, v. 435, p. 479–482, doi:10.1038/nature03618.

Menegatti, A.P., Wesissert, H., Brown, R.S., Tyson, R. V., Farrimond, P., Strasser, A. and Caron, M., 1998, High resolution $\delta^{13}C$ stratigraphy through the early Aptian "Livello Selli" of the Alpine Tethys: Paleoceanography, v. 13, p. 530–545.

Morford, J.L. and Emmerson, S., 1999, The geochemistry of redox sensitive trace metals in sediments: Geochimica et Cosmochimica Acta, v. 63, p. 1735–1750, doi:10.1016/S0016-7037(99)00126-X.

Page, K.N., 2003, The Lower Jurassic of Europe: its subdivision and correlation, *in* Ineson, J.R. and Surlyk, F., eds., The Jurassic of Denmark and Greenland. Geological:

Geological Survey of Denmark and Greenland Bulletin, 1, GEUS, Copenhagen, Denmark p. 23-59.

Pálfy, J., and Smith, P.L., 2000, Synchrony between Early Jurassic extinction, oceanic anoxic event, and the Karoo-Ferrar flood basalt volcanism: Geology, v. 28, p. 747–750.

Palliani, R.B., Mattioli, E. and Riding, J.B., 2002, The response of marine phytoplankton and sedimentary organic matter to the early Toarcian (Lower Jurassic) oceanic anoxic event in northern England: Marine Micropaleontology, v. 46, p. 223–245.

Pancost, R.D., Sinninghe Damsté, J.S., De Lint, S., van der Maarel, M.J.E.C., Gottschal, J.C., and The Medinaut Shipboard Scientific Party, 2000, Biomarker evidence for widespread anaerobic methane oxidation in Mediterranean sediments by a consortium of methanogenic archae and bacteria: Applied and Environmental Microbiology, v. 66, p. 1126–1132.

Pancost, R.D., Crawford, N., Magness, S., Turner, A., Jenkyns, H.C. and Maxwell, J.R., 2004, Further evidence for the development of photic-zone euxinic conditions during Mesozoic oceanic anoxic events: Journal of the Geological Society, London, v. 161, p. 353–364.

Pankhurst, R.J., Riley, T.R., Fanning, C.M. and Kelley, S.P., 2000, Episodic Silicic Volcanism in Patagonia and the Antractic peninsula: chronology of magmatism Associated with the break-up of Gondwana: Journal of Petrology, v. 41, p. 605–625.

Parrish, J.T., Ziegler, A. M. and Scotese, C. R., 1982, Rainfall patterns and the distribution of coals and evaporites in the Mesozoic and Cenozoic: Palaeogeography, Palaeoclimatology, Palaeoecology, v. 40, p. 67–101.

Parrish, J.T., 1993, Climate of the Supercontinent Pangea: The Journal of Geology, v. 101, p. 212–233.

Pasley, M.A., Gregory, W.A. and Hart, G.F., 1991, Organic matter variations in transgressive and regressive shales: Organic Geochemistry, v. 17, p. 483–509.

Pearce, C.R., Cohen, A.S., Coe, A.L. and Burton, K.W., 2008, Molybdenum isotope evidence for global ocean anoxia coupled with perturbations to the carbon cycle during the Early Jurassic: Geology, v. 36, p. 231–234, doi:10.1130/ G24446A.1.

Peucker-Ehrinbrink, B. and Ravizza, G., 2000, The marine osmium record: Terra Nova, v. 12, p. 205–219, doi:10.1046/j.1365-3121.2000.00295.x.

Peters, K.E., 1986, Guidelines for Evaluating Petroleum Source Rock Using Programmed Pyrolysis: American Association of Petroleum Geologists Bulletin, v. 70, p. 318–329, doi: 10.1306/ 94885688-1704-11D7-8645000102C1865D

Peter, K.E., Walters, C.C. and Moldowan, J.M., 2005, The Biomarker Guide vol. 1: Biomarkers in the Environment and Human History: Cambridge University Press. Cambridge, UK, 490 p.

Petit, J.R., Jouzel, J., Raynaud, D., Barkov, N.I., Barnola, J.-M., Basile, I., Bender, M., Chappellaz, J., Davis, M., Delaygue, G., Delmotte, M., Kotlyakov, V.M., Legrand, M. Lipenkov, V.Y., Lorius, C., Pépin, L., Ritz, C., Saltzman, E., Stievenard, M., 1999, Climate and atmospheric history of the past 420, 000 years from the Vostock ice core, Antarctica: Nature, v. 399, p. 429–436.

Poulson, R. L., Siebert, C., McManus, J. and Berelson, W.M., 2006, Authigenic molybdenum isotope signatures in marine sediments: Geology, v. 34, p. 617–620, doi:10.1130/G22485.1

Price, G.D., 1999, The evidence and implications of polar ice during the Msozoic: Earth-Science Reviews, v. 48, p. 183–210.

Price, G.D., 2010, Carbon-isotope stratigraphy and temperature change during the Early–Middle Jurassic (Toarcian–Aalenian), Raasay, Scotland, UK: Palaeogeography, Palaeoclimatology, Palaeoecology, v. 285, p. 255–263, doi:10.1016/j.palaeo.2009.11.018.

Price, G.D., Valdes, P.J., and Sellwood, B.W., 1995, Sedimentological evaluation of general circulation model simulations for the “greenhouse” earth: Cretaceous and Jurassic case studies: Sedimentary Geology, v. 100, p. 159–180.

Price, G.D., Valdes, P.J., and Sellwood, B.W., 1997, Prediction of modern bauxite occurrence: implications for climate reconstruction: Palaeogeography, Palaeoclimatology, Palaeoecology, v. 131, p. 1–13.

Rahmstorf, S., Cazenave, A., Church, J.A., Hansen, J.E., Keeling, R.F., Parker, D.E. and Somerville, R.C.J., 2007, Recent Climate Observations Compared to Projections: Science, v. 316, p. 709, doi:10.1126/science.1136843.

Rees, P. MCA., Ziegler, A. M., and Valdes, P., 2000, Jurassic phytogeography and climates: new data and model comparisons, *in* Huber, B.T., MacLeod, K.G., and Wing, S.L., eds., Warm Climates in Earth History: Cambridge, UK, Cambridge University Press, p. 297–318.

Retallack, G. J., 2001, A 300-million-year record of atmospheric carbon dioxide from fossil plant cuticles: Nature, v. 411, p. 287–290.

Retallack, G.J., 2002, Carbon dioxide and climate over the past 300 Myr.: Philosophical Transactions of the Royal Society, London, v. 360, p. 659–673, doi:10.1098/rsta.2001.0960.

Revelle, R. and Suess. H. E., 1957, Carbon dioxide exchange between atmosphere and ocean and the question of an increase of atmospheric CO_2 during the past decades: Tellus, v. 9, p. 18–27.

Rogov, M.A. and Zakharov, Jurassic and lower Cretaceous glendonite occurrences and their implication for arctic paleoclimate reconstructions and stratigraphy: Earth Science Frontiers, v. 17, p. 345–347.

Royer, D. L., Berner, R. A., Montañez, I. P., Tabor, N. J. and Beerling, D. J., 2004, CO_2 as a primary driver of Phanerozoic climate: GSA Today, v. 14, p. 4–10, doi: 10.1130/1052-5173(2004)014<4:CAAPDO>2.0.CO;2

Royer, D.L., 2006, CO_2- forced climated thresholds during the Phanerozoic: Geochimica et Cosmochimica Acta, v. 70, p. 5665–5675.

Sabatino, N., Neri, R., Bellanca, A., Jenkyns, H.C., Baudin, F., Parisi, G. and Masetti, D., 2009, Carbon-isotope records of the Early Jurassic (Toarcian) oceanic anoxic event from the Valdorbia (Umbria–Marche Apennines) and Monte Mangart (Julian Alps) sections: palaeoceanographic and stratigraphic implications: Sedimentology, v. 56, p. 1307–1328, doi:10.1111/j.1365-3091.2008.01035.x.

Sarmiento, J.L. and Bender, M., 1994, Carbon biogeochemistry and climate change: photosynthesis research, v. 39, p. 209–234.

Schlanger, S.O. and Jenkyns, H.C., 1976, Cretaceous Oceanic Anoxic Events: causes and consequences: Geologie En Mijnbouw, v. 55, p. 179–184.

Scholle, P.A. and Arthur, M.A., 1980, Carbon isotope fluctuations in Cretaceous pelagic limestones: potential stratigraphic and petroleum exploration tool: American Association of Petroleum Geologists Bulletin, v. 64, p. 67–87, doi:10.1306/2F91892D-16CE-11D7-8645000102C1865D.

Schouten, S., van Kaam-Peters, H. M. E., Rijpstra, W. I. C., Schoell, M. and Sinninghe Damsté, J. S., 2000, Effects of an oceanic anoxic event on the stable carbon isotopic composition of Early Toarcian carbon: American Journal of Science, v. 300, p. 1–22.

Schouten, S., Forster, A., Elda Panoto, F. and Sinninghe Damsté, J. S., 2007, Towards calibration of the TEX_{86} palaeothermometer for tropical sea surface temperatures in ancient greenhouse worlds: Organic Geochemistry, v. 38, p. 1537–1546.

Sellwood, B.W., and Price, G.D., 1993, Sedimentary facies as indicators of Mesozoic palaeoclimate [and discussion]: Philosophical Transactions of the Royal Society, London, v. 341, p. 225–233.

Sellwood, B.W. and Valdes, P.J., 2006, Mesozoic climates: general circulation models and the rock record: Sedimentary Geology, v. 190, p. 269–287, doi:10.1016/j.sedgeo.2006.05.013.

Sellwood, B.W. and Valdes, P.J., 2008, Jurassic climates: Proceedings of the Geologists Association, v. 119, p. 5–17.

Seuss , E., Balzer, W., Hesse, K.-F., Müller, P.J., Ungerer, C.A. and Wefer, G., 1982, Calcium carbonate hexahydrate from organic-rich sediments of the Antarctic shelf: precursors of glendonite: Science, v. 206, p.1128–1130.

Siebert, C., Nägler, T.F., and Kramers, J.D., 2001, Determination of molybdenum isotope fractionation by double-spike multi-collector inductively coupled plasma mass spectrometry: Geochemistry, Geophysics, Geosystems, v. 2, 16 p. , doi:10.1029/2000GC000124.

Siebert, C., Nägler, T.F., von Blanckenburg, F. and Kramers, J.D., 2003, Molybdenum isotope records as a potential new proxy for paleoceanography: Earth and Planetary Science Letters, v. 211, p. 159–171, doi:10.1016/S0012-821X(03)00189-4.

Siebert, C., McManus, J., Bice, A., Poulson, R., and Berelson, W.M., 2006, Molybdenum isotope signatures in continental margin marine sediments: Earth and Planetary Science Letters, v. 241, p. 723–733, doi:10.1016/ j.epsl.2005.11.010.

Siegenthaler, U., Stocker, T.F., Monnin, E., Lüthi, D., Schwander, J., Stauffer, B., Raynaud, D., Barnola, J.-M., Fischer, H., Masson-Delmotte, V, Jouzel, J., 2005, Stable carbon cycle-climate relationship during the late Pleistocene: Science, v. 310, p. 1313–1317.

Sigman, D.M. and Haug, G.H., 2003, The Biological Pump in the Past, *in*, Treatise on Geochemistry, Holland, H. D. and Turekian, K.K., eds.: Pergamon, Oxford, UK, p. 491–528, doi:10.1016/B0-08-043751-6/06118-1

Spicer, R.A. Rees, P. M. and Chapman, J.L., 1993, Cretaceous Phytogeography and climate signals: Philosophical Transactions of the Royal Society, London: v. 341, p. 277–286.

Steiner, C., Hobson, A., Favre, P., Stampfli, G. M., and Hernandez, J., 1999. Mesozoic sequence of Fuerteventura (Canary Islands): witness of Early Jurassic sea-floor spreading in the central Atlantic: Geological Society of America Bulletin, v. 110, p. 1304–1317, doi: 10.1130/0016-7606(1998)110<1304:MSOFCI>2.3.C);2.

Suan, G., Nikitenko, B. L., Rogov, M. A., Baudin, F., Spangenberg, J. E., Kunazev, V. G., Glinskikh, L. A., Goryacheva, A. A., Adatte, T., Riding, J. B., Föllmi, K. B., Pittet, B., Mattioli, E. and Lécuyer, C., 2011, Polar record of Early Jurassic massive carbon injection: Earth and Planetary Science Letters, v. 312, p. 102–113, doi: 10.1016/j.epsl.2011.09.050.

Svensen, H., Planke, S., Chevallier, L., Malthe-Sørenssen, A., Corfu, F. and Jamtveit, B., 2007, Hydrothermal venting of greenhouse gases triggering Early Jurassic global warming: Earth and Planetary Science Letters, v. 256, p. 554–566, doi:10.1016/j.epsl.2007.02.013.

Tissot, B. P. and Welte, D. H., 1984, Petroleum Formation and Occurrence, 2nd edition: Springer-Verlag, New York, NY., USA, 699 p.

Vakhrameev, V.A., 1991, Jurassic and Cretaceous Floras and Climates of the Earth: Cambridge, Cambridge University Press, 318 p.

Valdes, P., 1993, Atmospheric general circulation models of the Jurassic: Philosophical Transactions of the Royal Society, London, v. 341, p. 317–326.

van Breugel, Y., Baas, M., Schouten, S., Mattioli, E. and Sinninghe Damsté, J.S., 2006, Isorenieratane record in black shales from the Paris Basin, France: Constraints on

recycling of respired CO_2 as a mechanism for negative carbon isotope shifts during the Toarcian oceanic anoxic event: Paleoceanography, v. 21, PA4220, 8 p., doi:10.1029/2006PA001305.

van de Schootbrugge, B., Bailey, T.R., Rosenthal, Y., Katz, M.E., Wright, J.D., Miller, K.G., Feist-Burkhardt, S. and Falkowski, P.G., 2005a, Early Jurassic climate change and the radiation of organic walled phytoplankton in the Tethys Ocean: Paleobiology, v. 31, p. 73–97.

van de Schootbrugge, McArthur, J.M., Bailey, T.R., Rosenthal, Y., Wright, J.D. and Miller, K.G., 2005b, Toarcian oceanic anoxic event: An assessment of global cuases using belemnite C isotope records: Paleoceanography, v. 20, PA3008, 12 p., doi:10.1029/2004PA001102.

Veevers, J.J., 2004, Gondwanaland from 650–500 Ma assembly through 320 Ma merger in Pangea to 185–100 Ma breakup: supercontinental tectonics via stratigraphy and radiometric dataing: Earth Science Reviews, v. 68, p. 1–132, doi:10.1016/j.earscirev.2004.05.002.

Veizer, J., Godderis, Y. and François, L. M., 2000, Evidence for decoupling of atmospheric CO_2 and global climate during the Phanerozoic eon: Nature, v. 408, p. 698–701.

Wasylenki, L.E., Rolfe, B.A., Weeks, C.L., Spiro, T.G., and Anbar, A.D., 2008, Experimental investigation of the effects of temperature and ionic strength on Mo isotope fractionation during adsorption to manganese oxides: Geochimica et Cosmochimica Acta, v. 72, p. 5997–6005, doi:10.1016/j.gca.2008.08.027.

Weissert, H., 2000, Deciphering methane's fingerprint: Nature, v. 406, p. 356–357, doi: 10.1038/35019230.

Weissert, H. and Erba, E., 2004, Volcanism, CO_2 and palaeoclimate: a Late Jurassic–Early Cretaceous carbon and oxygen isotope record: Journal of the Geological Society, London, v. 161, p. 695–702.

Wignall, P.B., Newton, R.J., and Little, C.T.S., 2005, The timing of paleoenvironmental change and cause-and-effect relationships during the early Jurassic mass extinction in Europe: American Journal of Science, v. 305, p. 1014-1032.

Wignall, P.B., McArthur, J. M., Little, C. T. S. and Hallam, A., 2006, Methane release in the Early Jurassic period: Nature, v. 441, E5, 1 p.

Ziegler, A. M., Parrish, J. M., Jiping, Y., Gyllenhaal, E. D., Rowley, D. B., Parrish, J. T., Shangyou, N., Bekker, A. and Hulver, M. L., 1993, Early Mesozoic phytogeography and climate: Philosophical Transactions of the Royal Society, London, v. 341, p. 297–305.

Chapter 2

The Late Pliensbachian to Early Jurassic of the Neuquén Basin, Argentina

Abstract

The Neuquén Basin is located in west central Argentina, on the eastern side of the Andes, between 32° and 41° S latitude; it is a roughly triangular back-arc basin, with a complicated multiphase tectonic history, dominated by rifting processes, related to the break up of Gondwana and extension of the South American Plate. The basin contains a sedimentary record spanning the Triassic–Cenozoic. During the Triassic, the basin underwent rifting followed by subsidence and marine transgression in the Late Triassic–Early Jurassic. Marine water from Panthalassa (proto-Pacific Ocean) fed into the basin through a volcanic island arc, the Chilean Coastal Cordillera, on its western side and through a wide deep channel in the north of the basin. Sedimentological and biostratigraphic examination of stratigraphic sections in three localities, following a North–South transect of the Neuquén Basin at Arroyo Serrucho, Arroyo Chacay Melehue and Arroyo Lapa reveals transgression and a relative sea level rise in the basin during the *tenuicostatum–hoelderi* Andean ammonite Zones and active volcanism during the Latest Pliensbachian to Early Toarcian.

2.1 Introduction:

The Neuquén Basin is located in west central Argentina, on the eastern side of the Andes, between 32° and 41° S latitude (Fig. 1). The basin is a roughly triangular, north – south oriented back-arc basin containing more than 6 km of Triassic to Cenozoic sediments, covering an area of about 120,000 km^2 (Howell et al., 2005). The basin has a complicated tectonic history related to the break-up of Gondwana, subduction of the proto-Pacific plate and the development of the Andean magmatic arc (Vergani et al., 1995).

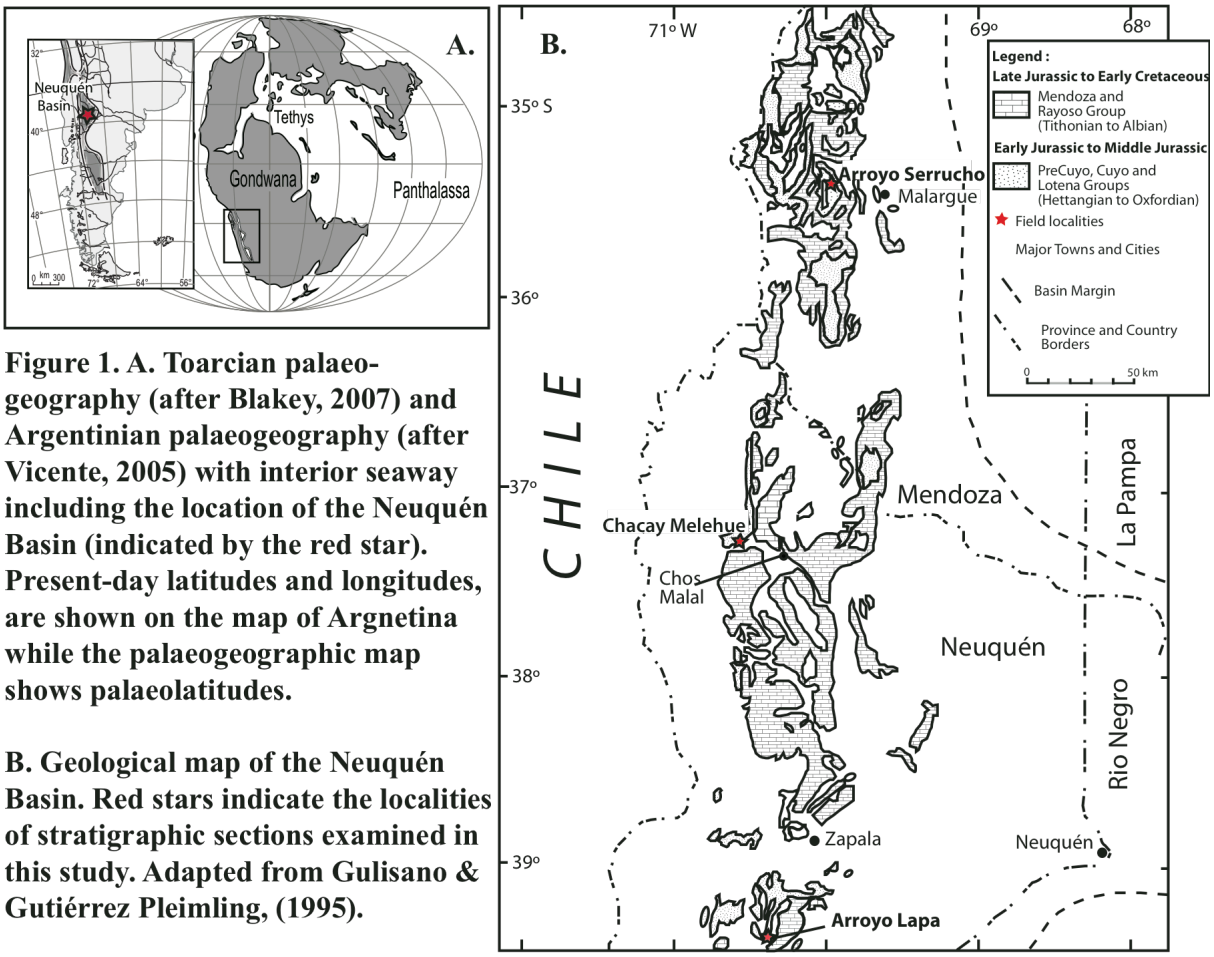


Figure 1. A. Toarcian palaeo-geography (after Blakey, 2007) and Argentinian palaeogeography (after Vicente, 2005) with interior seaway including the location of the Neuquén Basin (indicated by the red star). Present-day latitudes and longitudes, are shown on the map of Argnetina while the palaeogeographic map shows palaeolatitudes.

B. Geological map of the Neuquén Basin. Red stars indicate the localities of stratigraphic sections examined in this study. Adapted from Gulisano & Gutiérrez Pleimling, (1995).

The Neuquén Basin sediments occur in several depositional cycles representing deposition from pre-rifting to foreland basin development. This study is primarily concerned with sediments of the marine Cuyo or Cuyano Group (Early to Middle Jurassic) (Groeber,

1946). The sedimentation and deposition of the Cuyo Group is largely a result of marine transgression during subsidence in the post-rift phase of basin development. This chapter provides an overview of the palaeogeography of the Neuquén Basin from the Late Pliensbachian–Early Toarcian stages and the tectonic history associated with the deposition of the Cuyo group in the Neuquén Basin, specifically the Tres Esquinas and Los Molles Formations. Four sedimentary sections are described: Arroyo Lapa North and South, Chacay Melehue and Arroyo Serrucho, located in the Neuquén and Mendoza Provinces (Fig. 1).

2.2 Palaeogeography and Tectonic Setting of the Neuquén Basin

The Neuquén Basin is located on the eastern side of the Andes mountain range in Central Argentina (Northern Patagonia, Fig. 1). During the Jurassic, the basin was restricted on its western side by an active volcanic island arc (Digregorio et al., 1984), the Chilean Coastal Cordillera (Riccardi, 1983) (Fig. 2B); this volcanism is generally thought to have intermittently disrupted exchange of marine water from Panthalassa to the basin on its western margin, though exchange of marine water from Panthalassa continued through an opening in the northern part of the basin (Fig, 1, Vicente, 2005).

The development of the marine embayment in the Neuquén Basin is linked to the pre-rift and syn-rift phases of basin development (Fig. 2A & B). The pre-rift phase spans from the middle Triassic through the Early Jurassic (240–195 Ma) during this phase, extensional faulting along Palaeozoic terrane sutures resulted in rifting, continental deposition and bimodal magmatism, possibly related to an arc-trench system along the western margin of the South American Plate (Vergani et al., 1995; Franzese et al., 2003). The last stage of this tectonic event was the Latest Triassic–Early Jurassic extension of the South American Plate related to the collapse of the Gondwana orogen. As a result of this rifting, a series of fault-bounded long, narrow, depressions, oriented N–S, along the Panthalassic margin, opened.

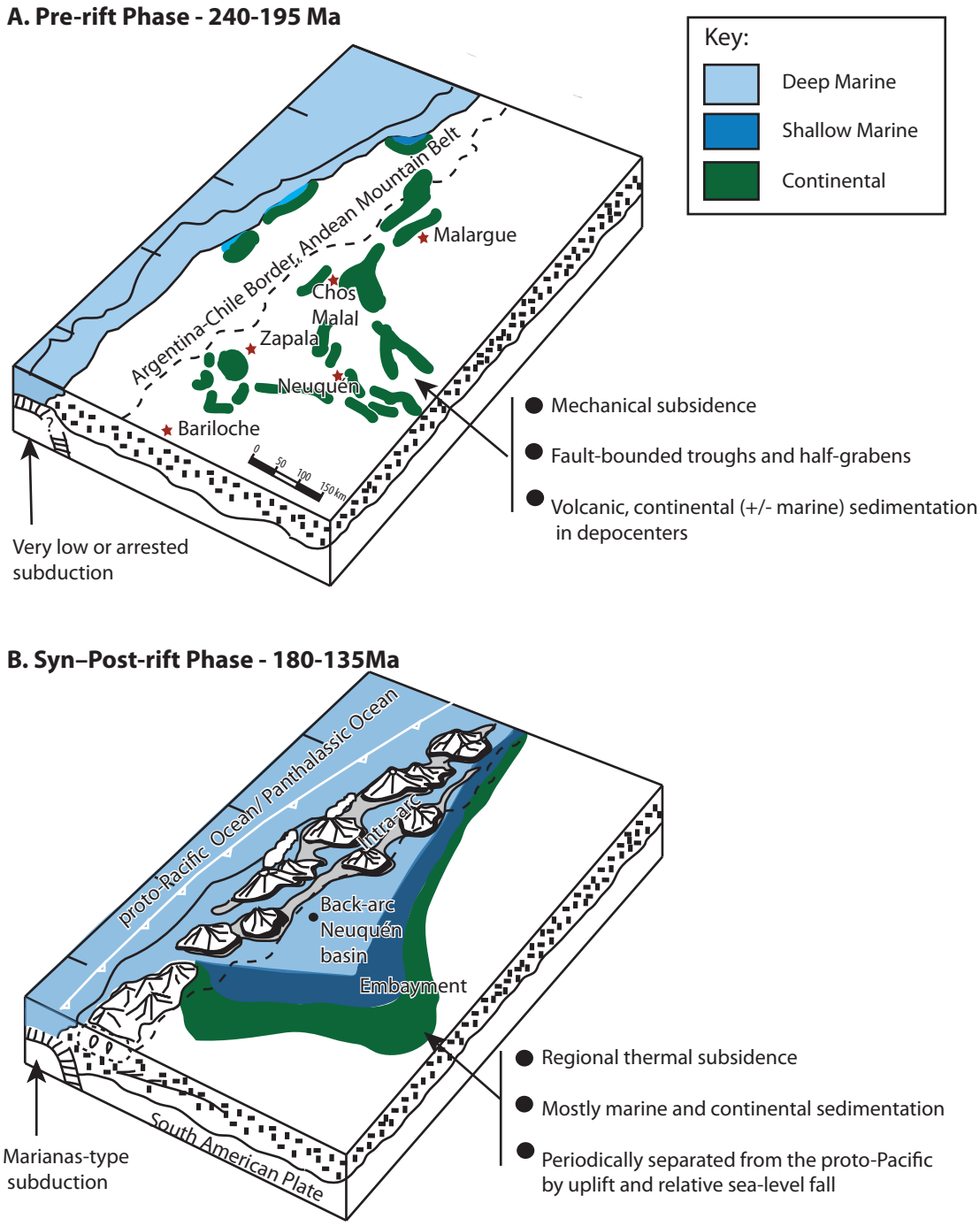


Figure 2. Schematic evolution of the Neuquén Basin from the Late Triassic to the Early Cretaceous. (A) Late Triassic to earliest Jurassic (240-195 Ma) characterized by pre-subduction rifting in a series of narrow grabens, with predominantly volcanic and continental sedimentation with some marine sedimentation along the western margin and (B) Early Jurassic to Cretaceous (180-150 Ma) onset of subduction along the western margin of Gondwana and the early development of the Andean chain. The basin was a large triangular embayment, dominated by marine basin fill and periodically separated from the proto-Pacific by the effects of intermittent volcanic activity, uplift and relative sea level fall. Adapted and modified from Howell et al. (2005), based on Vergani et al. (1995), Ramos (1999), Franzese & Spalleti (2001), Folguera & Ramos (2002) and Franzese et al. (2003).

Continental volcaniclastic rocks and local shallow marine deposits, dominated these rift basins (Fig. 2A).

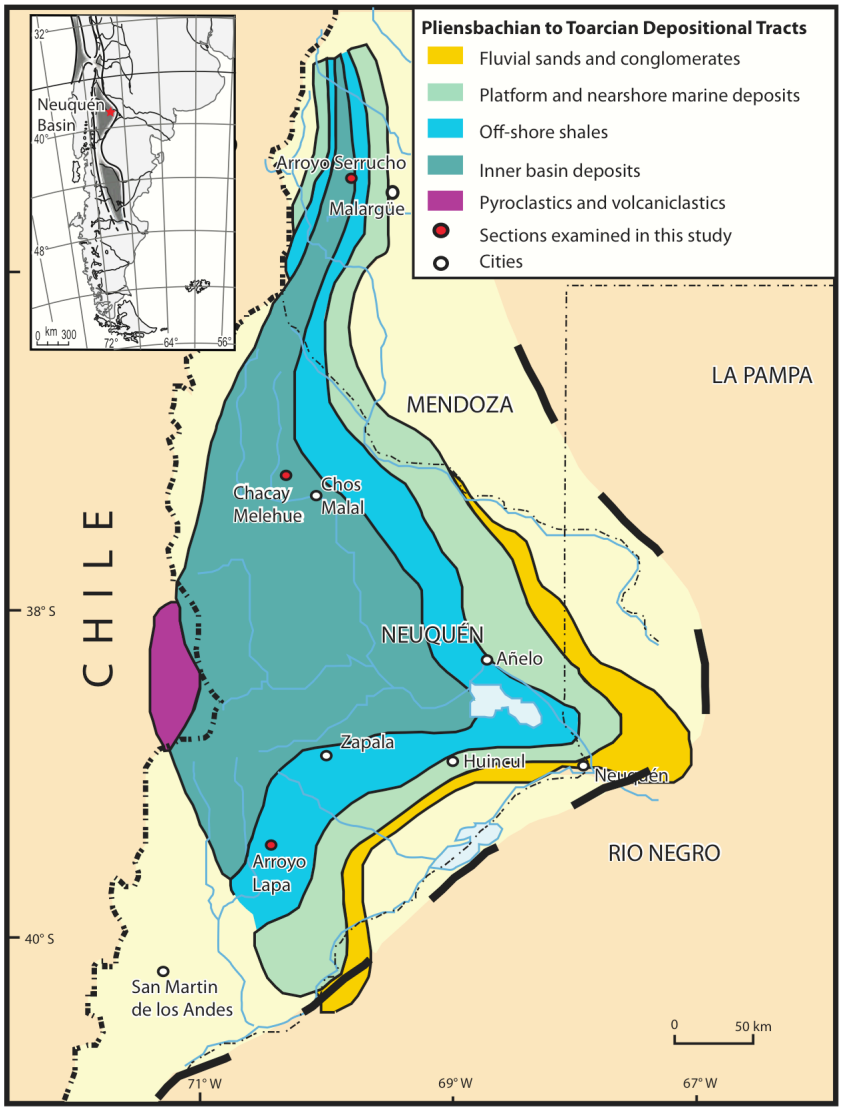


Figure 3. Map of the Neuquén Basin showing Pliensbachian to Toarcian depositional tracts within the basin. Red circles indicate field localities examined in this study. Map adapted from Riccardi et al. (2011), modified from Legareta & Uliana, (1996).

During the Early Jurassic, these depocenters were integrated into the Neuquén Basin where widespread lacustrine and shallow-marine facies developed. (Fig. 2B; Franzese & Spalletti, 2001; Franzese et al., 2003). The syn-rift phase (180–135Ma, Early Jurassic–Early Cretaceous) is characterized by thermal subsidence and regional back-arc extension, resulting in marine transgression and a general deepening of the Neuquén Basin. This transgression is

recorded in the deep-marine strata of the Los Molles Formation (Legarreta & Uliana, 1996; Franzese & Spalletti, 2001; Franzese et al., 2003; Howell et al., 2005). Figure 3 shows a palaeogeographic reconstruction of the different depositional tracts within the basin.

Sediment entered the Neuquén Basin from two main source areas during the pre- to post-rift stages of basin development. The Chilean Coastal Cordillera supplied immature volcaniclastic material (Caminos et al., 1982; Coira et al., 1982; Ramos et al., 1982; Dean, 1987; Eppinger & Rosenfeld, 1996), and material with a more mature provenance signature was supplied from cratonic areas to the south and northeast. In many locations within the Neuquén Basin provenance signatures of sediments are mixed, suggesting sediment supply from both island and cratonic sources (Burgess et al., 2000; Franzese et al., 2003).

2.3 Lithofacies and biostratigraphic framework of the Principal Localities

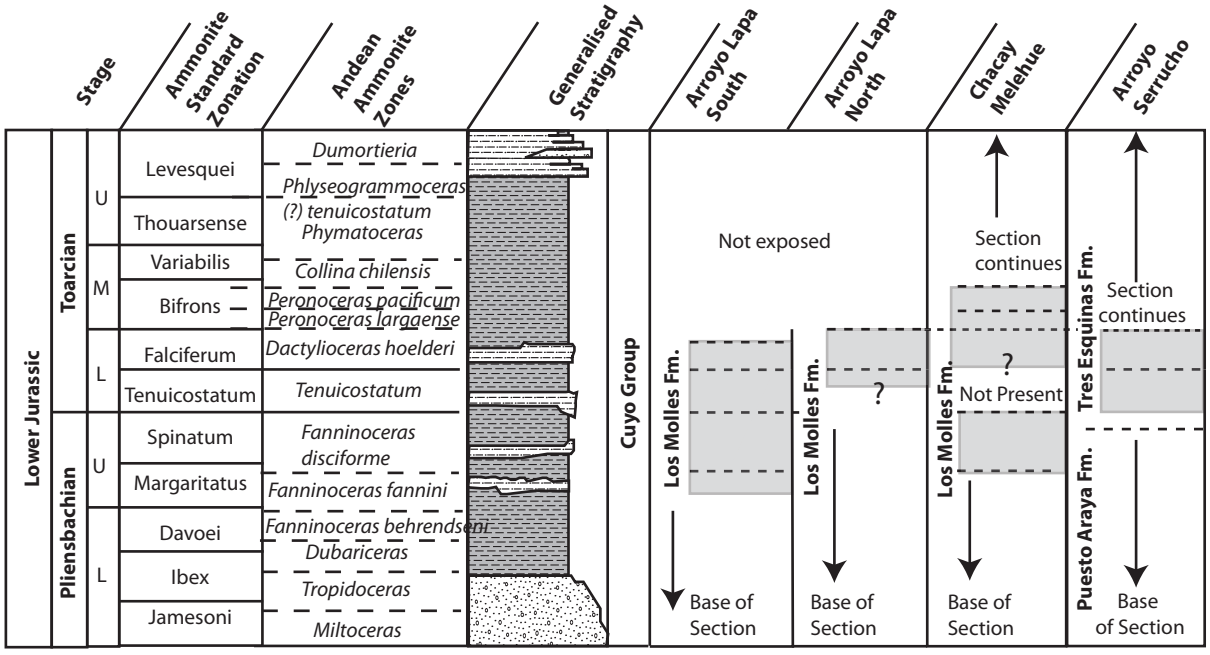


Figure 4. Generalized lithostratigraphic and biostratigraphic coloumn, for the Cuyo group, in the Neuquén Basin. Figure also shows the four field localities examined in this study, indicating stratigraphic and biostratigraphic intervals present within the studied sections. Ammonite biostratigraphy adapted from Riccardi (2008a, b). Generalized Cuyo Group lithostratigraphy adapted from Gulisano & Gutiérrez Pleimling, (1995).

Four stratigraphic sections, in three localities, within the Neuquén Basin, representing the Early Jurassic, Pliensbachian to Toarcian interval have been described for this study.

An overview of sedimentology, detailed new biostratigraphy (ammonites, bivalves and nannofossils) and a discussion of the depositional setting of these sections is provided below. These sections illustrate offshore shales and deep-marine deposits of the Cuyo Group, specifically the Los Molles and Tres Esquinas Formations, and are located at Arroyo Lapa (North and South), Arroyo Chacay Melehue and Arroyo Serrucho (Fig. 1, 3). An overview of the generalized stratigraphy and biostratigraphy, and the relationship between the measured sections, is given in Figure 4.

2.3.1 Arroyo Lapa North and South: Introduction

The Arroyo Lapa area includes two stratigraphically different sections on the North and South side of Arroyo Lapa creek about ~1 km apart from each other (Fig. 5). The creek is situated on the eastern slope of Sierra de Chacaico, about 50 km southwest of the town of Zapala in Neuquén Province (Fig. 1). The Arroyo Lapa section comprises about 900 m of Late Triassic–Early Jurassic sediments representing the pyroclastic deposits of the Lapa Formation, and Pliensbachian–Aalenian outer shelf to basinal shales and sandstones of the Los Molles Formation (Gulisano & Gutiérrez Pleimling, 1995). The stratigraphy of the Arroyo Lapa section has been previously studied on the basis of ammonites (von Hillebrandt, 1973, 1987, 2006; von Hillebrandt & Schmidt-Effing, 1981), teuthids (Riccardi, 2005), palynomorphs (Volkheimer, 1973), bivalves (Damborenea, 1987) and palaeomagnetic data (Iglesia Llanos & Riccardi, 2000). Ammonites were referred to a biostratigraphic zonation that is considered valid for the whole Andean region of Argentina and Chile (von Hillebrandt et al., 1992a; Riccardi, 2008a, b). A multiple zonal scheme,

based on ammonites, bivalves, brachiopods and calcareous microfossils has also been proposed for the Neuquén Basin (Riccardi et al., 2000, 2011).

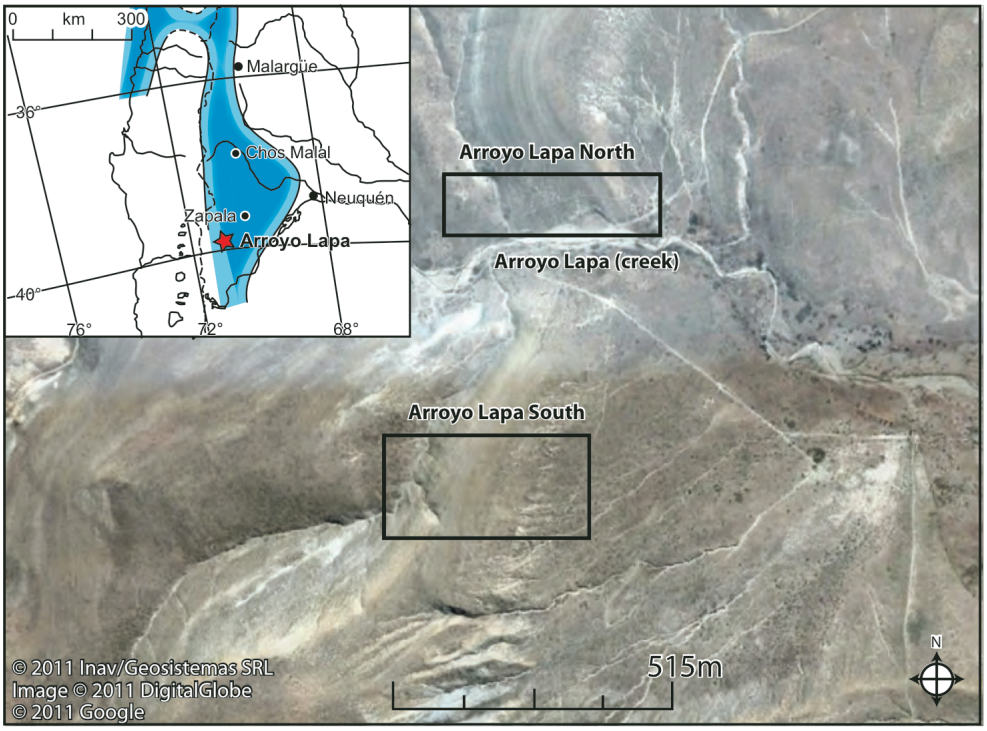


Figure 5. Satellite image of the Arroyo Lapa, field locality indicating the location of Arroyo Lapa South and Arroyo Lapa North, in the Sierra de Chacaico area, Neuquén Province Argentina, latitute and longitude, S 39º 24' 04", W 70º 25' 43", elevation 1311 m. Inset shows the approximate location of the field area, adapted from Vicente (2005), satellite image courtesy of Google Earth (2005).

There are three studied sections, in the Arroyo Lapa Creek area; (1) Arroyo Lapa South, 2008 (Pliensbachian to Early Toarcian, *fannini* to *hoelderi* ammonite Zones, Fig. 7); (2) Arroyo Lapa, South 2010; (Early Toarcian, *tenuicostatum to hoelderi* ammonite Zones, Fig. 8) and finally (3) Arroyo Lapa North, on the Northern side of the Arroyo Lapa creek (Early Toarcian, *tenuicostatum to hoelderi* ammonite zones, Fig. 10).

2.3.2 Lithostratigraphy: Arroyo Lapa South 2008 and 2010

The first Arroyo Lapa South section, examined in 2008 is ~72 m thick (Fig. 7), the second Arroyo Lapa South Section, examined in 2010, is a more detailed examination of the

upper part of the 2008 section, and extends a further ~7 m above this section (Fig. 8). The sections can be divided into 4 major depositional units A-D, with the overlap of the 2008 and 2010 section occurring in Unit B.

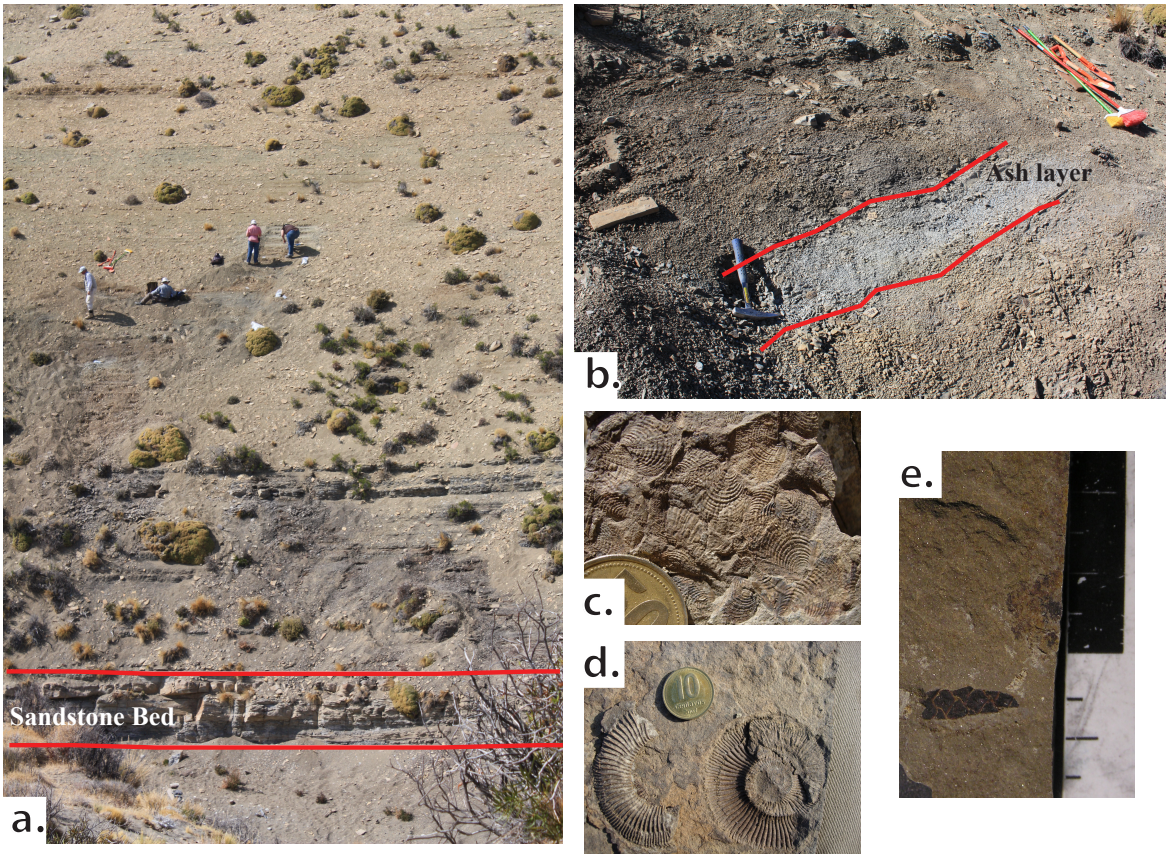


Figure 6. Outcrops in the Arroyo Lapa South area, representative of the of the Los Molles Formation. (a.) The upper part of the section as logged in 2010 (Fig. 8), the sandstone bed at the botom is Bed 21 (Fig. 8). (b) Thin volcaniclastic sandy units are present thrughout the section. This image represents the only thick (>10 cm) tuffaceous ash layer, interbedded in shale (Unit D, Fig. 8). Images c–e represent the typical fossils found throughout the section at Arroyo Lapa South, including (c.) *Posidonoitis cancellata* (Leanza), (d.) *Dactylioceras (Orthodactylites)* and (e.) fossil wood fragments are also common through out the section.

Unit A, the basal unit, comprises siltstones interbedded with sandstone. These sandstone Beds locally have scoured bases (e.g. Bed 5), though more commonly have sharp bases (e.g. Bed 8) with climbing ripple cross-lamination, indicative of rapid deposition. Sandstone Beds range in thickness from 2 to 20 cm, with very fine to medium grain particles; the Beds are typically laminated at the top. Sandstone Beds 5 and 6 show evidence of soft-sediment deformation, as do the surrounding siltstones in the Bed. Volcaniclastic material dominates a few of these sandstone Beds. At the top of Unit A is a ~50 cm-thick laminated

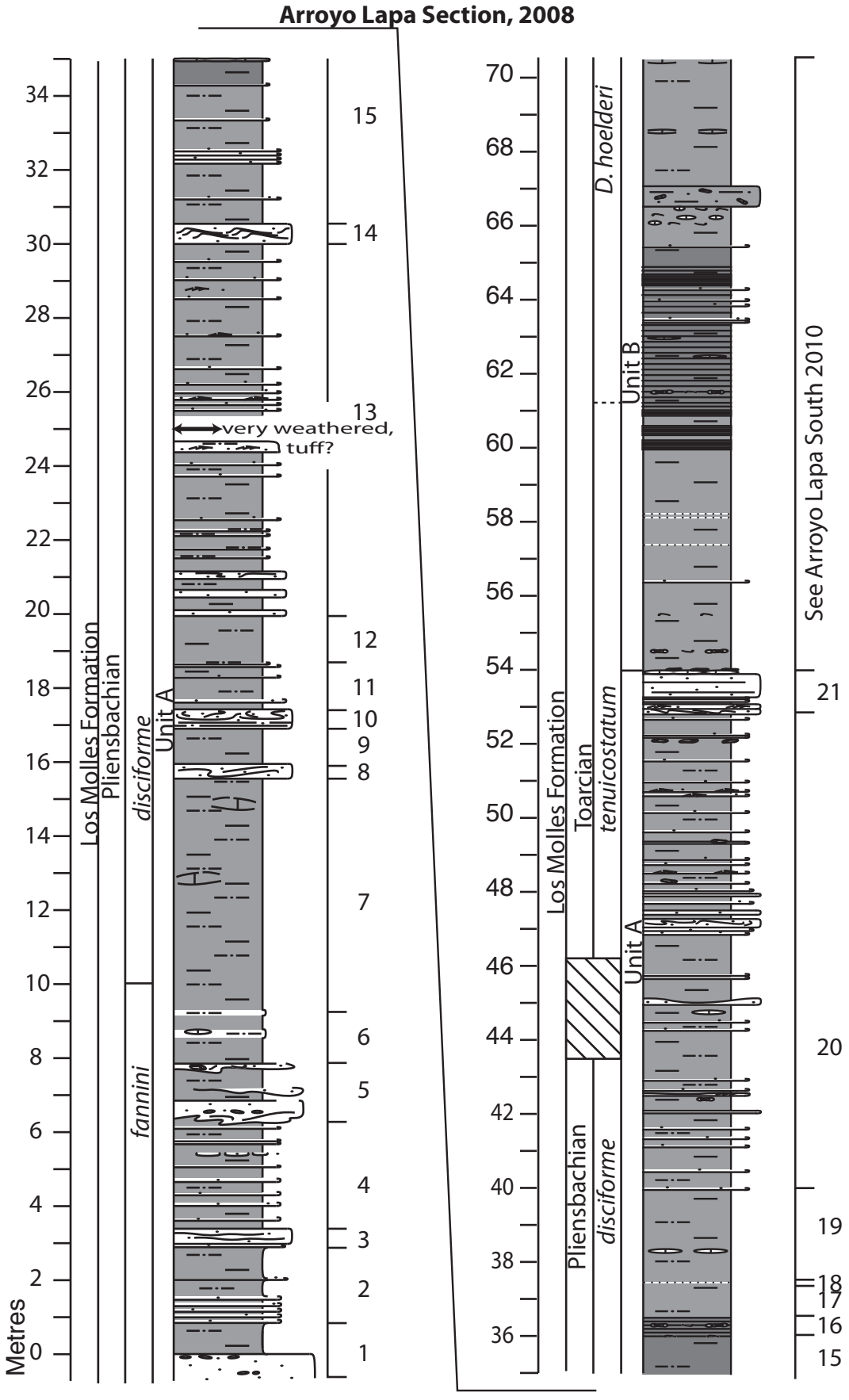


Figure 7. Detailed stratigraphic log of Arroyo Lapa South section logged in 2008. Legend and other symbols can be found in Fig. 12.

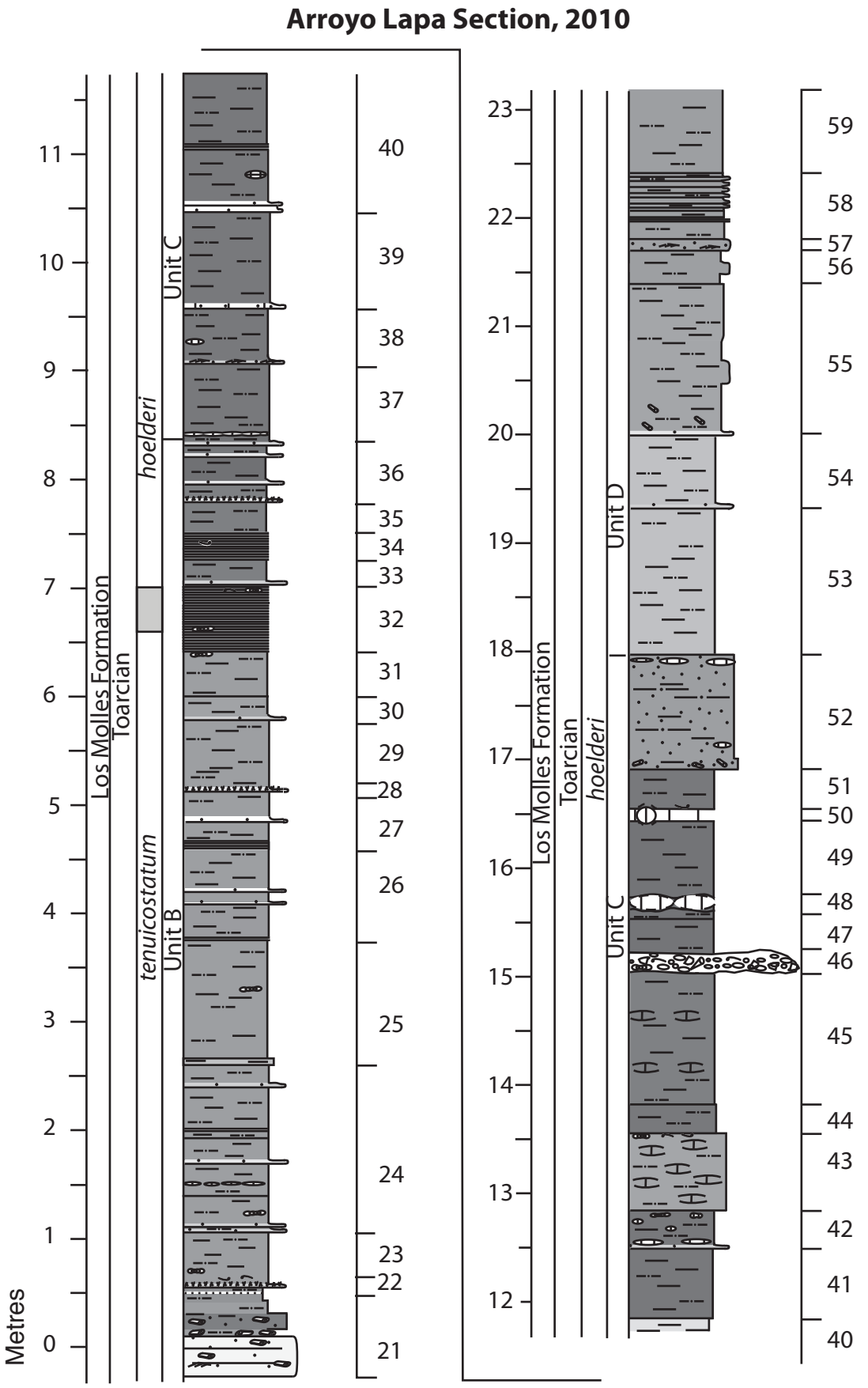


Figure 8. Detailed stratigraphic log of Arroyo Lapa South section logged in 2010. Legend and other symbols can be found in Fig. 12.

fine to very fine-grained sand, Bed 21, with poorly sorted, abundant wood fragments throughout the Bed. The base of Unit B is an 11cm thick, sharp based, very weathered tuff, Bed 22. Unit B is much finer grained than Unit A with laminated black shales (e.g. Beds 32 and 34), and siltstones interbedded with very thin, <5cm thick, very fine-grained sandstone and tuffaceous Beds.

Unit C comprises silty shales, and some very fine-grained sandstone Beds with cross-lamination. Thin cemented siltstone Beds and calcareous concretions are present throughout this unit. A major erosion surface truncates the section at Bed 46, scouring the underlying siltstone. It is marked by an abrupt change in lithology with poorly sorted conglomeratic lag (granule to cobble) with locally cemented fragments of bivalve, corals and ammonite fossils as well as wood fragments in a siltstone matrix. Clasts are rounded to sub-rounded, and the unit is in some places matrix supported and in other places clast supported, the unit is laterally lenticular. The final Unit at Arroyo Lapa South is Unit D, which comprises very fine-grained sand and siltstone with some laminated Beds. Wood fragments are common at the base of Bed 55, but in general there are significantly fewer bivalves and ammonites in this part of the section compared to lower Units.

2.3.4 Biostratigraphy: Arroyo Lapa South

Ammonites and other fossils were sampled wherever found in the section (full details of horizons and determinations given in Appendix A, Fig. 1 & 2). Biostratigraphic investigations of the Arroyo Lapa South 2008 section confirms the presence of sediments of Pliensbachian to earliest Toarcian age (Fig. 7) with ammonites that include *Canavaria* (*C*). cf. *naxensis* (Gemm.), *C.* (*C*). cf. *finitima* (Fuc.), *Canavaria* (*C*). cf. *pulcherrima* (Fuc.), *Protogrammoceras* sp., and *Lioceratoides* sp. (cf. von Hillebrandt, 2006, p. 34, 263), indicating the upper part of the Andean *disciforme* Zone of the Pliensbachian (~10 – 42.03

m), approximately equivalent to the Northwest European Province *spinatum* Zone (Page, 2003). In the lower part of this section, three nannofossil events were identified based, respectively, on the first occurrence (FO) of *Biscutum finchii* (Crux) (FO 8.52 m), *Lotharingius hauffii* Grün and Zwili (FO 10.05 m), and *Lotharingius barozii* Noël (FO 10.55 m), forms whose first occurrence is characteristic of the latest Pliensbachian ammonite zone in Europe (Mattioli and Erba, 1999) and in other localities of the Neuquen Basin.

The boundary between the Pliensbachian and Toarcian stages in the Arroyo Lapa 2008 section (~ 46.08 m, Fig. 7) is marked by the FO of *Terquemia andina* Damborenea (42.85 m), whilst *Dactylioceras (Orthodactylites*) cf. *directum* (Buck.) (cf. von Hillebrandt and Schmidt-Effing, 1981, pl. 1, Figs. 8-11) is represented between 54.55 and 62.05 m. This interval (43–62.05 m) belongs in the *tenuicostatum* Zone. From the same interval a fourth nannofossil event was identified with the first occurrences of *Calyculus* spp. and *Orthogonoides hamiltoniae* (FO 43.05 m) and *Lotharingius sigillatus* (Stradner) (FO 60.05 m) characteristic of the earliest Toarcian in Europe (Mattioli and Erba, 1999). The upper part of the Arroyo Lapa South 2008 section (62.55–70.55 m) includes ammonites from the Andean *hoelderi* Zone, the base of which is marked, at Arroyo Lapa, by the FO of *Harpoceras serpentinum* (Rein.) (cf. von Hillebrandt, 1987, pl. 5, Figs. 4-9; Howarth, 1992b, p. 109), *Hildaites* cf. *murleyi* (Moxon) (cf., von Hillebrandt, 1987, pl. 5, Fig. 3; Howarth, 1992b, p. 168), and *Cleviceras* sp.

In the Arroyo Lapa South 2010 section (Fig. 8, details in Appendix A, Fig. 2) the *tennuicostatim–hoelderi* boundary was refined to between ~6.5 and 7.2 m, and is marked by the FO of *Harpoceras serpentinum* (Schlotheim). The Andean *hoelderi* Zone is considered approximately equivalent to the *serpentinum* (= *falciferum*) ammonite Zone of northwestern Europe (von Hillebrandt and Schmidt-Effing, 1981; Page, 2004; Riccardi, 2008a, b). Other identified ammonites through the Arroyo Lapa South section that are indicative of the *hoelderi* Andean ammonite Zone include *Hildaites* cf. *murleyi* (Moxon) (cf. von Hillebrandt,

1987, pl. 5, Fig. 3; Howarth, 1992b, p. 168) and *Dactylioceras (Orthodactylites*) (cf. *hoelderi* Hillebarndt & Schmidt-Effing, 1981). There are three bivalve species in the Arroyo Lapa South section that have a range limited to the latest Pliensbachian to earliest Toarcian, which include *Entolium mapuche* (Damborenea) (FO 13.10 m) and *Weyla alata angustecostata* (Philippi) (FO 13.60 m); the bivalve *Posidonotis cancellata* (Leanza) is present through out both the 2008 and 2010 section and also has a range limited to the latest Pliensbachian to earliest Toarcian (Damborenea, 2002).

2.3.5 Lithostratigraphy: Arroyo Lapa North

Arroyo Lapa North is located on the northern side of the Lapa creek from Arroyo Lapa South (Fig. 5). This section is ~30m thick and is divided into a lower (~4.5 m) and upper (~22 m) section (Fig. 10) by an exposure gap of 3.8 m. The measured section can be divided up into 5 main lithostratigraphic units A through E. The base of the section, Bed 1, below Unit A, consists of ferruginous-cemented sandstone, and is overlain by Unit A, which comprises siltstone interbeded with very fine-grained sand. Some cemented concretions are present through this part of the section in Bed 3 and 5 and there is slight cementation in Beds 2 and 6. In Unit B there is a transition to laminated very fine-grained sand interbeded with mudstone. Above Bed 7 the section is lost due to scree and vegetation, resulting in an exposure gap of ~3.8 m.

The base of Unit C, Bed 8, is a green-grey mudstone with laminated very fine-grained sandstone beds with significant fossil plant material, and is representative of the entire unit. Concretions are present in Bed 12. The section continues with silty shales, and locally intermittent sandy beds. In Bed 17 there is evidence of sediment folds indicating slumping. In Bed 18 the sediment becomes a platy siltstone marking the beginning of Unit D.

Ammonites and fossil woody fragments are present within this siltstone. Irregular ferruginous concretions are present in Bed 19.

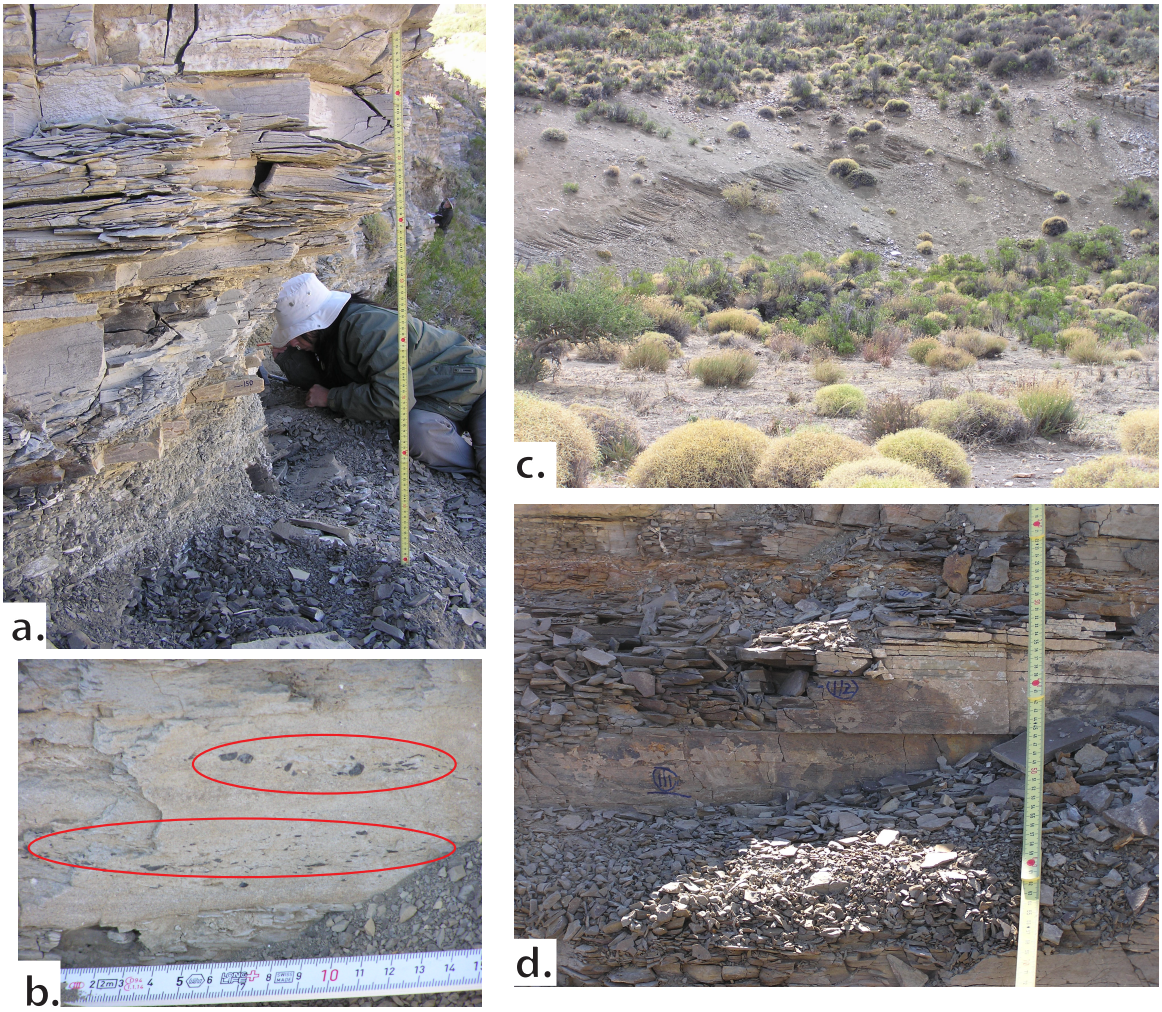


Figure 9. Outcrops in the Arroyo Lapa North Area area, representative of the of the Los Molles Formation. (a.) The section at Arroyo Lapa North is capped by a thick sandstone unit underlain by a dark grey shale interval (Fig. 10, Unit E, Bed 34–40). (b) The sandstone in the upper part of the section, (Unit E, Bed 39) contains common fossil wood lag as seen here. (c.) Overview of trenched section at Arroyo Lapa North beds alternate between sandy units and silty shales as seen in (d.) Shale intervals are very friable, while the sandy beds are muchmore lithified.

Unit E changes from siltstone to muddy siltstone with interbedded fine to very fine-grained sandstone. Ammonites are common in Bed 20, with a bivalve shell Bed ~0.5 m above this (Bed 22). There is an increase of very fine-grained sandy material in this unit compared with Unit D.

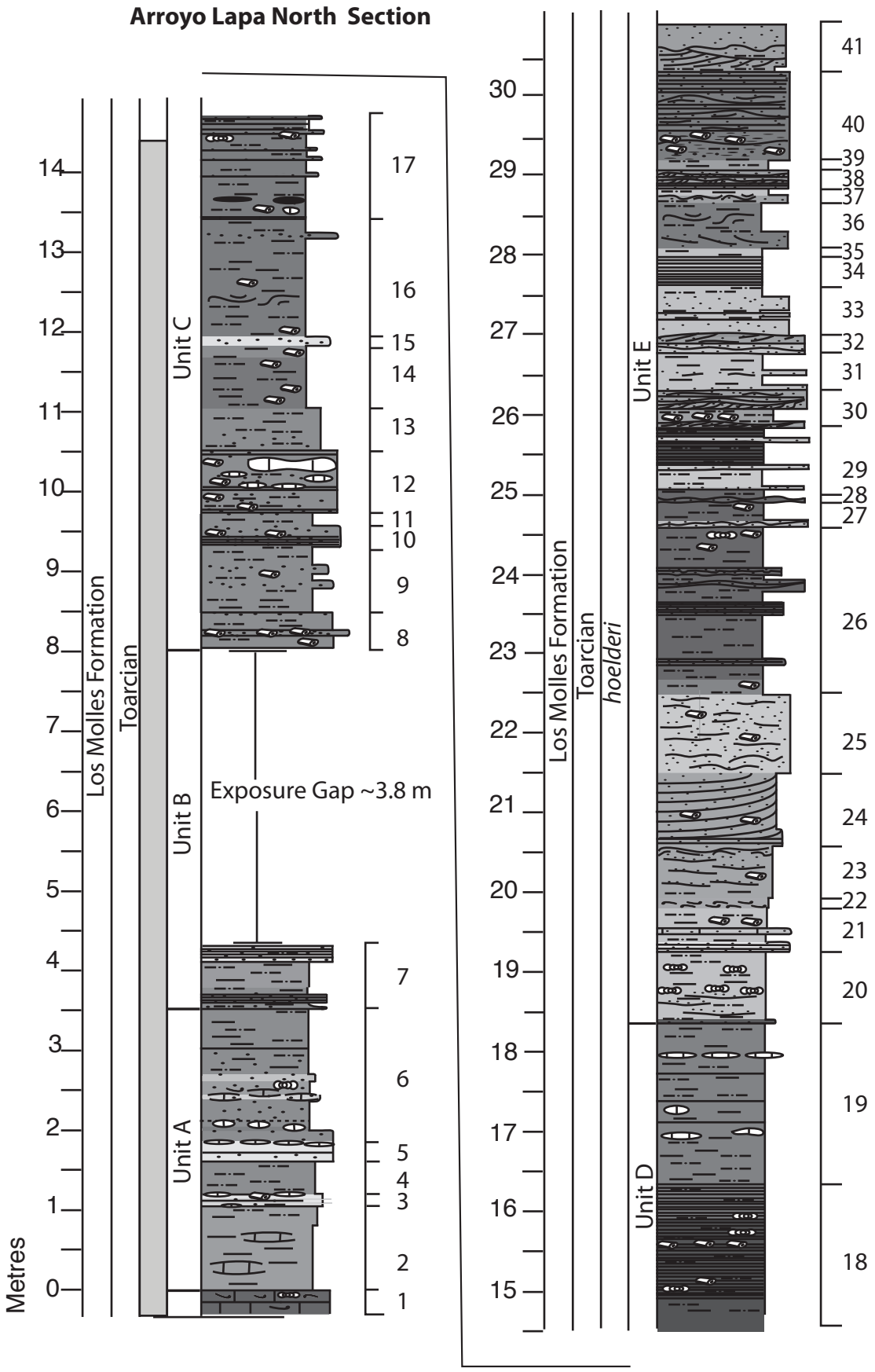


Figure 10. Detailed stratigraphic log of Arroyo Lapa North section logged in 2010. Legend and other symbols can be found in Fig. 12.

The sand content increases significantly in Unit E, with a prevalence of fine to very fine-grained sand, and some low angle wavy cross Bedding, in Bed 24. Bed 26 passes back to mudstone interbedded with laminated very fine-grained sandstone Beds. Groove marks scour the base of Bed 30 and there is an increase in the presence of fossil woody material through this unit. This charcoalifed woody material is graded, with coarser, 1-5cm pieces of woody lag at the base and smaller <1cm pieces of lag at the top. There is a transition from cross-bedded very fine-grained sand, in Bed 30, to laminated fine-grained sandstone at the top of the section, Bed 40. This upper sandy part of the section forms a topographic ridge.

2.3.6 Biostratigraphy: Arroyo Lapa North

Ammonites and other fossils were sampled wherever found in the section (full details of horizons and determinations given in Appendix A, Fig. 2). Biostratigraphic determination of the Arroyo Lapa North section confirms the presence of sediments of earliest Toarcian age. The base of the section Unit A–B lacks diagnostic ammonites, but units C–E includes ammonites from the Andean *hoelderi* Zone, the base of which is marked, at Arroyo Lapa North, by the FO of *Hildaites* cf. *murleyi* (Moxon) (14.70 m) (cf. von Hillebrandt, 1987, pl. 5, Fig. 3; Howarth, 1992b, p. 168). The Andean *hoelderi* Zone is considered approximately equivalent to the *serpentinum* (= *falciferum*) ammonite Zone of northwestern Europe (von Hillebrandt and Schmidt-Effing, 1981; Page, 2004; Riccardi, 2008a, b).

Two nannofossil events were identified in the Arroyo Lapa North section; the first event is based on the first occurrence (FO) of *Biscutum finchii* (Crux) and *Biscutum Novum* (Goy) (FO 10.80 m) as well as *Lotharingius hauffii* Grün and Zwili (FO 14.50 m). The first occurrence of these forms of nannofossils is characteristic of the latest Pliensbachian ammonite zone in Europe (Mattioli and Erba, 1999) and in other localities of the Neuquén Basin. From the same interval a second nannofossil event was identified from

Orthogonoides hamiltoniae (FO 14.90 m) and *Calyculus* sp. (FO 24.30 m), characteristic of the earliest Toarcian in Europe (Mattioli and Erba, 1999).

2.3.7 Arroyo Lapa, North and South Depositional setting

The deposits at Arroyo Lapa North and South are assumed to be a part of a similar depositional system, given the close proximity of these two sections. Turbidite deposits with coarse-grained sandstone bases, grading to fine mudstone units, dominate both Arroyo Lapa North and South. The presence of thin, relatively un-reworked tuffaceous material throughout the sections suggests close proximity to a volcanic source area. Sandstones are also dominated by volcaniclastic material. Burgess et al. (2000) examined the sandstones petrographically and confirmed the presence of fairly immature volcaniclastics, supporting close proximity to the adjacent volcanic system. Deposits of beds rich in charcolified wood indicate that the sections at Arroyo Lapa were relatively close to a continental source of sediment. Gulisano & Gutiérrez Pleimling (1995) interpreted the turbiditic part of the section as representing deposits from submarine fan channel-levee complexes, including finer overbank deposits. This channel-levee complex system may account for the difference in sedimentation from Arroyo Lapa South to Arroyo Lapa North. Arroyo Lapa North has more coarse-grained sandy material and woody debris, suggesting the dominanace of channel deposits while Arroyo Lapa South, which is dominated by fine-grained sands and shales, may represent a dominance of overbank deposits. The conglomeratic Bed at Arroyo Lapa South (Bed 46, Unit C, Fig. 8) has a lenticular lateral geometry, indicating that it is a channel deposit, with finer material over the top, suggesting channel migration in the fan complex (Richards et al., 1998; Bouma, 2000) .

Gulisano & Gutiérrez Pleimling (1995) hypothesized that the deposits at Arroyo Lapa represent transgressive-regressive marine cycles, with a decrease in sandy-turbiditic units

during transgression and marine highstand in the basin. The other possible reason for a decrease in sand could be a change in the grain size of the feeder system, as suggested by Burgess et al. (2000). Martinez et al. (2008) examined other similar sections on the eastern side of the Sierra de Chacaico near Arroyo Lapa, for palynological content and determined, based on the degree of preservation of woody material and the matrix in which the charcolified material was deposited, that sections on the eastern side of the of Sierra de Chacaico were deposited in a marginal marine environment close to a terrestrial source area.

The variation in deposition from sandy material to fine-grained shales back to sandier material at Arroyo Lapa North and South suggests the basin underwent marine transgression, recording deeper marine sedimentation during relative sea level rise, during the *tenuicostatum–hoelderi* ammonite Zones, and recording more marginal marine turbiditic deposits, with increased plant material during basin regression and a relative sea level fall, in the Pliensbachian units and later in the *hoelderi* ammonite Zone. Local variation between Arroyo Lapa North and South, in the amount of sand and fine sediments, during similar time intervals is most likely a result of migrating channel versus overbank deposits along the outer shelf of the Neuquén Basin.

2.3.8 Chacay Melehue: Introduction

The Chacay Melehue stratigraphic section is located 27 km northwest of the town of Chos Malal (Northern Neuquén Province) (Fig. 1). The section is located in the Chacay Melehue arroyo (creek), in the southern end of the Cordillera del Viento, which is a North–South oriented Mountain Chain. The Cordillera del Viento is an oval anticlinal fold (brachyanticline), with older rocks at its core and younger rocks around it. In this case the core outcrops comprise, marine sediments, plus plutonic and volcanic deposits of the upper Paleozoic (Andacollo Group, Huinganco Granite and Choiyoi Group), with Jurassic–

Cretaceous sediments of the Cuyo, Lotena and Mendoza Group around them (Gulisano & Gutiérrez Pleimling, 1995). The section at Arroyo Chacay Melehue is more than ~1200 m thick and spans the latest Pliensbachian to the Oxfordian (Riccardi, 1983; Damborenea, 1990). At the base of the section are epiclastic and pyroclastic deposits of the La Primavera Formation which are thought to derive from an andesitic strato-volcano complex on the western side of the Neuquén embayment during the latest Triassic–earliest Jurassic (Llambías & Leanza, 2005 and Schiuma & Llambias, 2008).

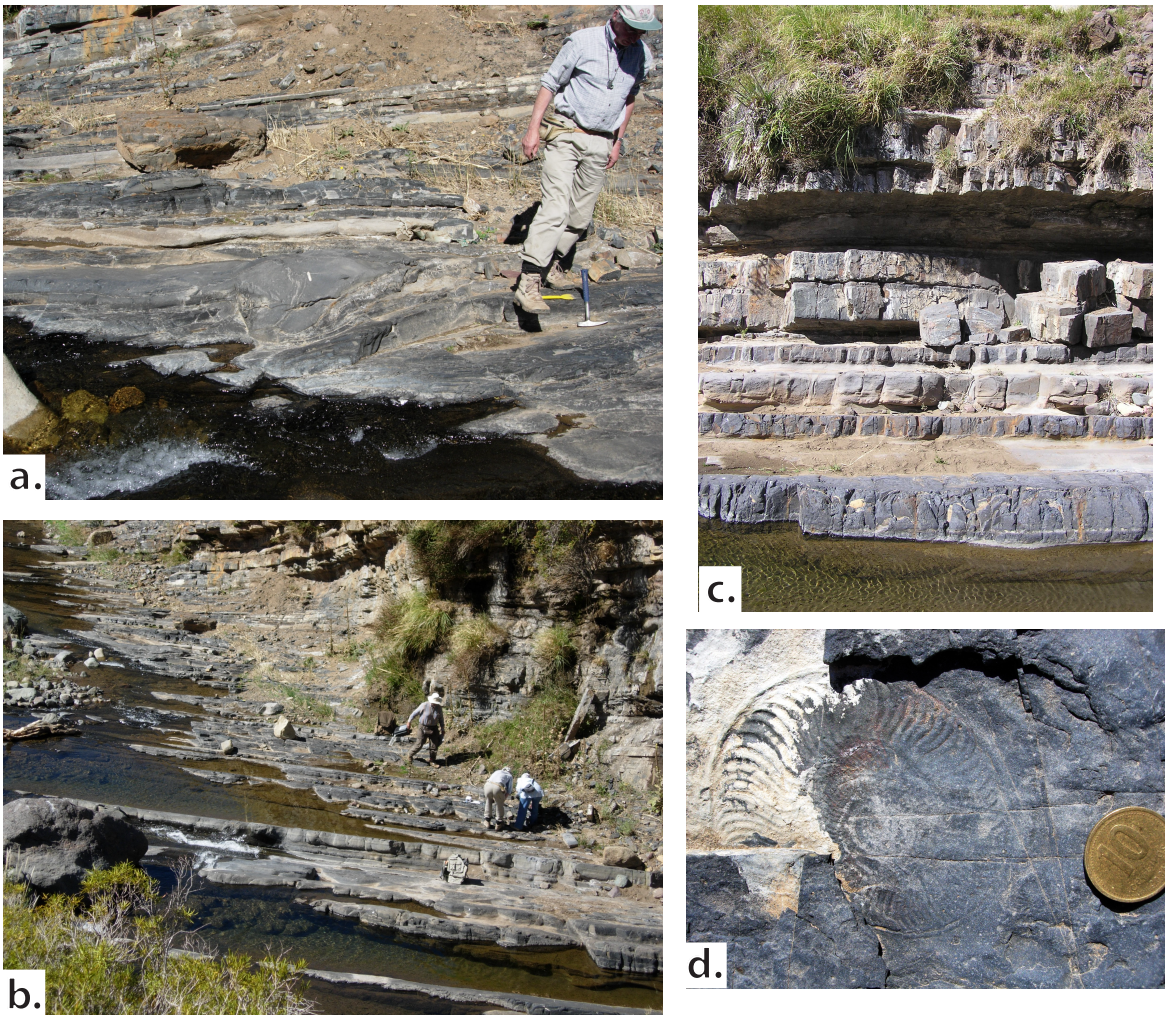


Figure 11. Outcrops in the Chacay Melehue area, representative of the Los Molles Formation. (a.) Large carbonate concretions disrupting shale beds, (see Unit 3., Fig. 12) (b.) Overview of the section at Chacay Melehue showing typical alternating dark limestone beds and thin laminated shales. (c.) Close up of the limestone beds, show typical hard blocky structure. Ammonite impressions are common on the tops of limestone beds and represent ammonites typical of the early Toarcian in the Neuquén Basin such as (d.) ***Harpoceras (sp.)*** **are common on the tops of these limestone units.**

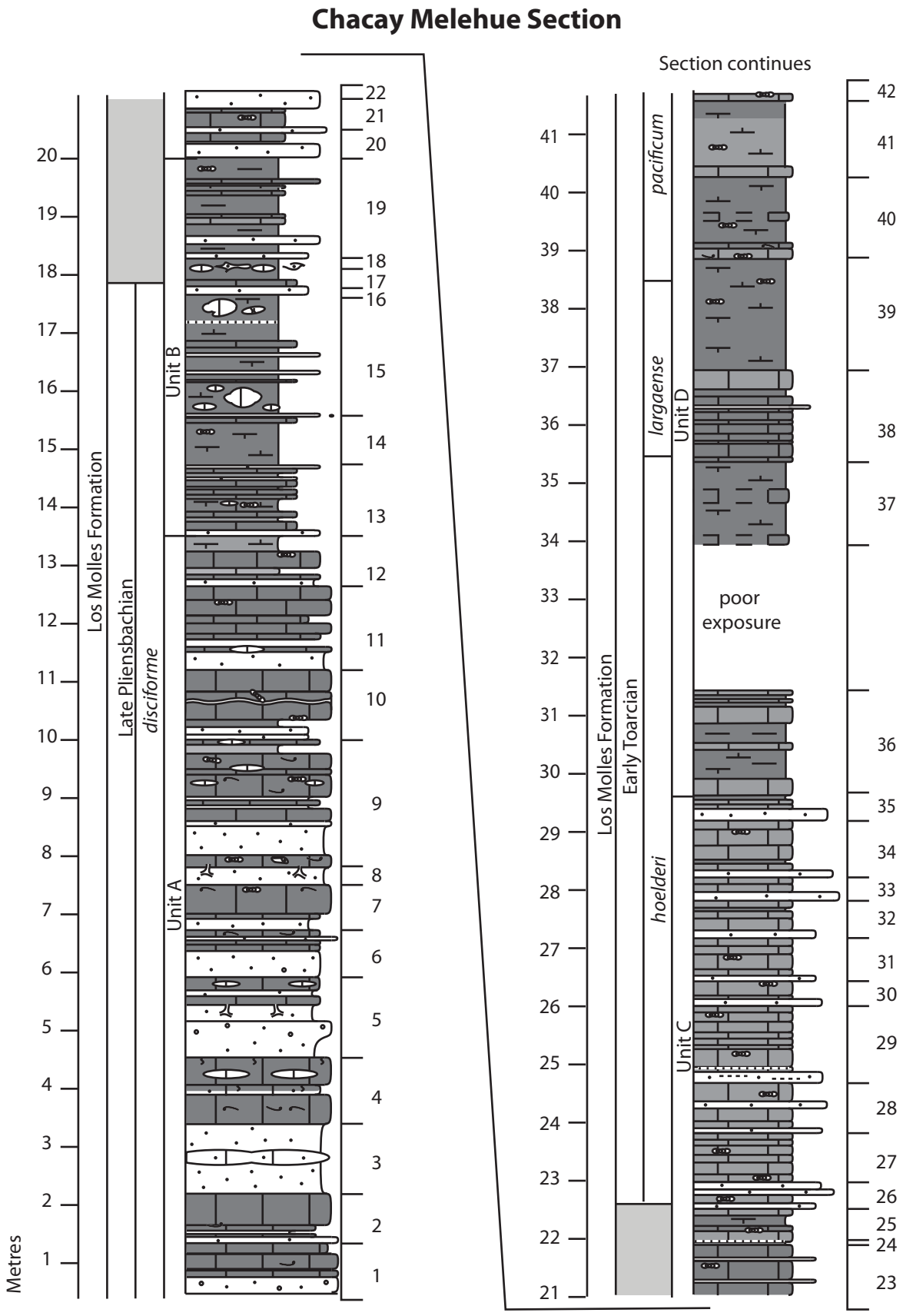


Figure 12. Detailed stratigraphic log of Chacay Melehue section logged in 2008. Legend and other symbols can be found in Fig. 12.

2.3.9 Lithostratigraphy: Chacay Melehue

The section studied at Chacay Melehue is ~42 m thick with a ~2.5 m exposure gap in the uppermost 10 m of the section (Fig. 12). The section can be divided up into four lithostratigraphic units A–D. Unit A comprises packages of sediment with buff-coloured tuffaceous sandstones at the base fining upwards into hard black limestones, with some small rounded aggregates, possibly volcaniclastic pebbles. These packages appear to be repeating or cyclical (i.e., Beds 1–12). Ammonites, bivalves and some wood are present through this unit. Large calcareous concretions are present in Beds 4, 5, 9 and 11. There is an abrupt transition at Bed 13, marking the beginning of Unit B with a significant decrease in coarse-grained material, tuffaceous sandy beds become thinner <5 cm, though there is a coarsening upwards in this unit of the section. The sediment is dark grey and well indurated with abundant ammonites; pyrite is also common in Beds 13–15, with large irregular calcretic concretions in Bed 15. The larger concretions disrupt overlying laminated mudstones. Slump folds are present in Bed 17. A medium–grained tuffaceous sandstone, Bed 20, marks the base of Unit C, overlying unit B.

In Unit C there is a transition back to packages of medium- to fine- grained tuffaceous sandstone overlain by a fining-upward sequence of silt to mudstone. These finer sediments are dark grey to black and are silicified, with common ammonite impressions. The final Unit in this succession, Unit D, is characterized by very fine grained mud and shale, and begins at Bed 36. There is a ~2.5 m exposure gap between Beds 36 and 37. Beds in Unit D are lithified and black. A few ammonites are present towards the top of the section, In Beds 39–42, with some bivalves at the base of Bed 40.

2.3.10 Biostratigraphy: Chacay Melehue

Ammonites and other fossils were sampled wherever found in the section (full details of horizons and determinations given in Appendix A, Fig. 4). Biostratigraphic determination of the Chacay Melehue section confirms the presence of sediments of Late Pliensbachian through earliest Toarcian age. Units A and B include ammonites from the Late Pliensbachian Andean *disciforme* Zone, approximately equivalent to the Northwest European Province *spinatum* Zone (Page, 2003). This is based on the First Occurrence (FO) of *Dactylioceras* (*Eodactylites*) cf. *simplex* (Fucini) (FO 11.21 m) (cf., von Hillebrandt, 2006, p. 34, 263). The bivalve *Kolymonectes weaveri* Damborenea is also present in Unit A, and has a range from the late Pliensbachian through the early Toarcian (Damborenea, 2002). Two main nannofossil events are present in unit B represented by the first appearance of *Lotharingius hauffii* Grün & Zwili, (FO 13.85 m), which is typical of the Late Pliensbachian, *Fanninoceras* Andean ammonite Zone equivalent to the *margaritatus* Northwest European Province ammonite Zone. The second nannofossil event is represented by the first occurrence of *Lotharingius barozii* Noël (FO 17.54 m) whose FO is characteristic of the latest Pliensbachian *disciforme* Andean ammonite zone equivalent to the latest *margaritatus–spinatum* Northwest European Province Ammonite Zone (Mattioli and Erba, 1999; Page, 2003; Riccardi 2008a, b).

The transition to Early Toarcian, is marked by the FO of *Dactylioceras* (*Orthodactylites*) sp. (FO 18.68 m) (cf. von Hillebrandt, 2006, p. 34, 263), importantly the *tenuicostatum* Zone appears to be absent in the section, which may be due to a hiatus in sedimentation or low sediment input in Unit B. The Andean *hoelderi* Zone, is the first Toarcian ammonite zone identified in the section and is marked by the FO of *Harpoceras serpentinum* (Schlotheim) (FO 21.76 m). The Andean *hoelderi* Zone is considered

approximately equivalent to the *serpentinum* (= *falciferum*) ammonite Zone of northwestern Europe (von Hillebrandt and Schmidt-Effing, 1981; Page, 2004; Riccardi, 2008a, b).

Unit D comprises two ammonite Zones, the first being the Andean *Peronoceras largaense* Assemblage Zone, which is equivalent to the northwestern European, uppermost *serpentinum* and *bifrons* Subzones, and is marked by the FO of *Harpoceras* cf. *serpentinum* (Sow.) at 34.41m. The final ammonite zone in the section and second in Unit D is the Andean *Peronoceras pacificum* assemblage Zone, which is equivalent to the northwestern European, uppermost *bifrons* and, *fibulatum–crassum* Subzones and is marked by the FO of *Harpoceras subplanatum* (Oppel) at 37.44 m. The bivalve *Bositra* sp. is also present in Unit D, at 37.24m, and is characteristic of the middle to late Toarcian (Damborenea, 2002).

2.3.11 Chacay Melehue Depositional Setting

Previous studies of sedimentary units at Chacay Melehue suggest that the section was deposited in a marginal marine to offshore environment, recording transgressive-regressive cycles of sedimentation within the Neuquén Basin (e.g. Damborenea, 1987, Gulisano & Gutiérrez Pleimling, 1995; Iglesia Llanos & Riccardi, 2000). Measurements of slump folds within the unit indicate the slope lay to the southeast of the section (Vicente, 2005). Units A–C are turbiditic in nature, with deposition of coarse-grained sandstone, that is volcaniclastic in nature at the base, and fining upward sequences above. The presence of volcaniclastic units at the base of the section, and the dominance of volcaniclastic material in the sandstones at Chacay Melehue, suggests close proximity of the section to the Chilean Coastal Cordillera, Vicente (2005) suggested that the basal turbiditic units at Chacay Melehue represent lahar-type deposits. The dark colour of the shale units and the presence of pyrite and pyrite framboids in shale samples suggest deposition in an oxygen-limited environment. The decrease in sandy material through the section suggests that sedimentary units at Chacay

Melehue either represent a change in grain size from the source area or represent relative sea-level rise across the basin, resulting in an increase of distance between Chacay Melehue and sources of coarse-grained material, allowing a predominance of fine-grained sedimentation. Based on the palaeogeographic reconstruction (Fig. 3), Chacay Melehue would have been located in the deepest part of the basin during peak marine transgression.

2.3.12 Arroyo Serrucho: Introduction

The Arroyo Serrucho section is located about 30 km west of the city of Malargüe, in Mendoza Province, north of the Neuquén Province (Fig. 1). The Jurassic succession crops out on the eastern side of the Cerro Puchenque anticline, which has a N–S strike (Gulisano and Gutiérrez-Pleimling, 1995). The Arroyo Serrucho sections examined in this study were measured within the Tres Esquinas Formation, which is underlain by the late Pliensbachian–earliest Toarcian, Puesto Araya Formation, which was not examined in this study. Details of the sedimentology and biostratigraphy of the Puesto Araya Formation may be found in Gulisano & Gutiérrez-Pleimling (1995); and Damborenea (1987) .

The Puesto Araya Formation is considered to represent fan deltaic sediments grading into transgressive storm-dominated and carbonate-rich platform sediments in the Late Pliensbachian–Early Toarcian part of the formation, deposited during basin subsidence (Lanés, 2005; Valencio et al., 2005). Overlying the Puesto Araya Formation is the Tres Esquinas Formation (Stipanicic, 1965), with which this study is concerned.

The Tres Esquinas Formation, extends from the Early Toarcian through to the lowermost Bajocian and is roughly 300-450 m thick (Gulisano & Gutiérrez-Pleimling, 1995) and is regionally equivalent to the Los Molles Formation (Weaver, 1931), comprises sediments deposited in a relatively deep marine environment suggesting marine transgression and basin deepening (Valencio et al., 2005).

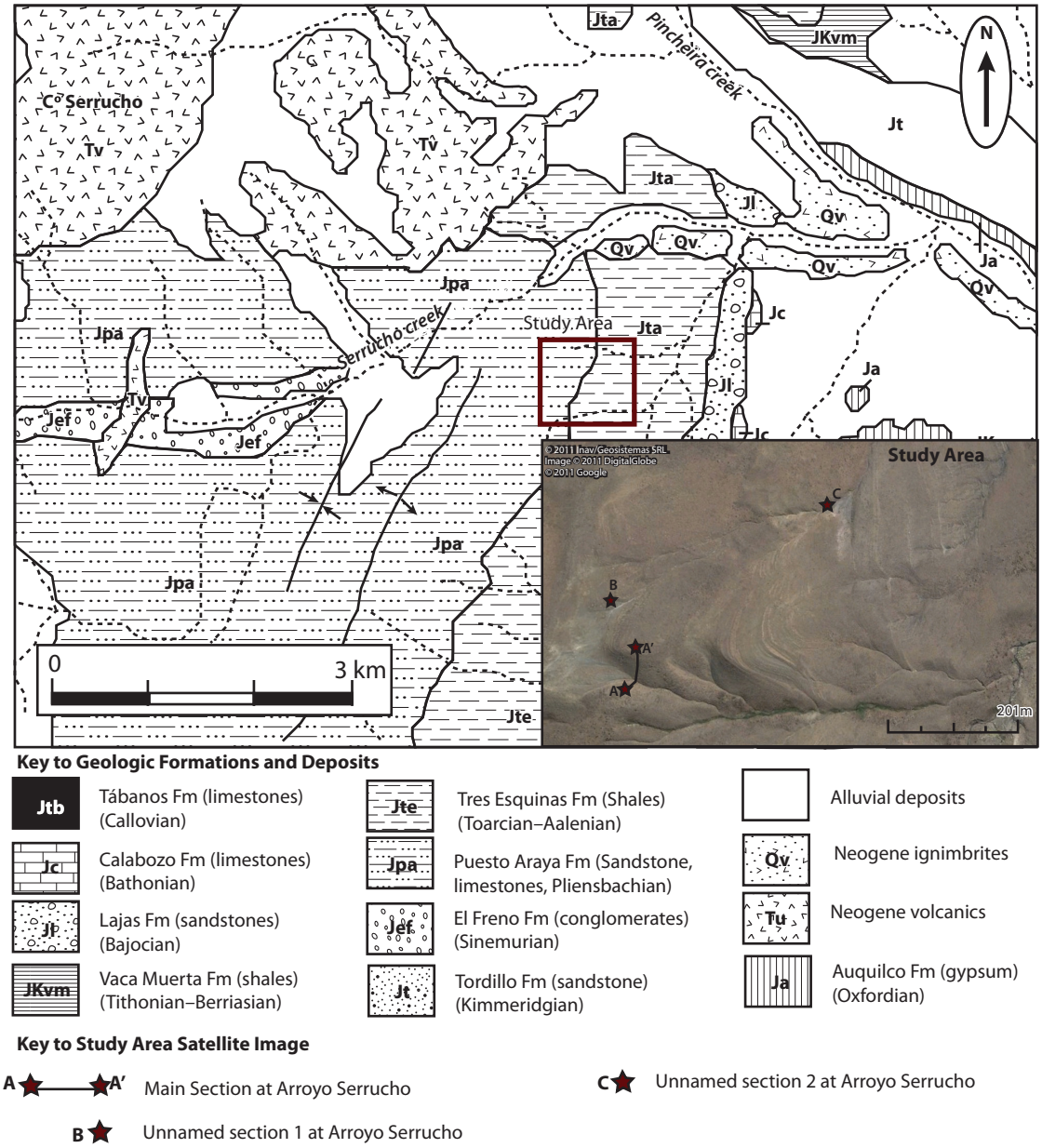


Figure 13. Geological map of the Arroyo Serrucho area, 30 km west of the city of Malargüe, in Mendoza Province, North of the Neuquén Province. Inset shows the satellite image of the study area and locations of the three measured sections at Arroyo Serrucho, the Main section, unnamed section 1 and unnamed section, latitute and longitude, S 35º 26' 24",W 69º 53' 59" W. Geological map adapted from Gulisano & Gutiérrez Pleimling (1995), satellite image courtesy of Google Earth (2006).









Figure 14. Outcrops in the Arroyo Serrucho area, representative of the of the Tres Esquinas Formation. (a.) Shale unit at base of section (Fig. 15, Bed 12). (b) Ammonites typical of the Early Toarcian are common in the limestone beds in this section, such as *Harpoceras* c.f. *Serpentinum* (c) Iron rich fossiliferous limestone units occur at 31 meters, (Fig 15, Bed 25), and are interbedded with shale. (d.) An overview of the typical silty sediments that can be found in the Arroyo Serrucho Section, with interbedded shale units.

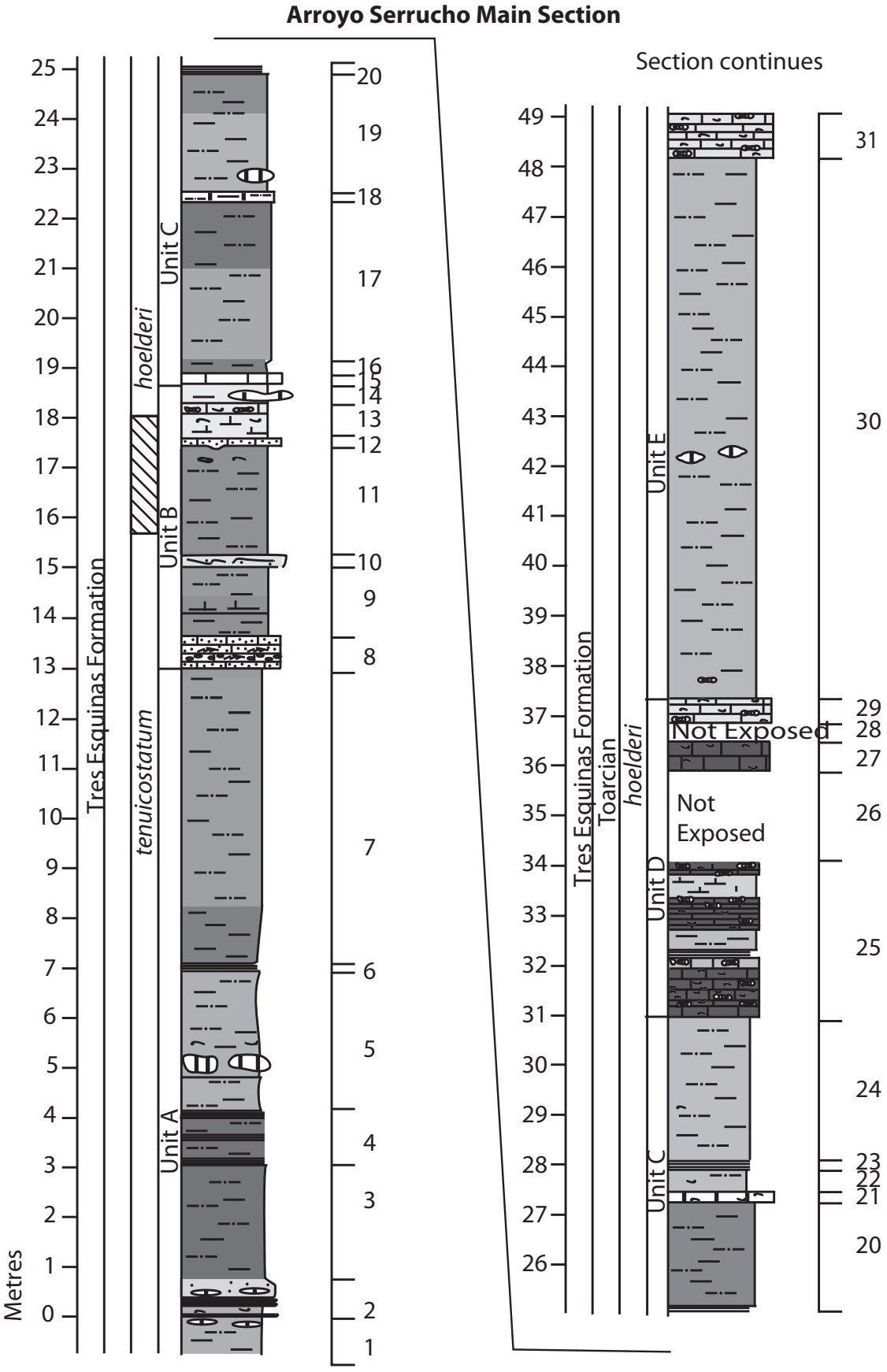


Figure 15. Detailed stratigraphic log of main section at Arroyo Serrucho logged in 2008. Legend and other symbols can be found in Fig. 12.

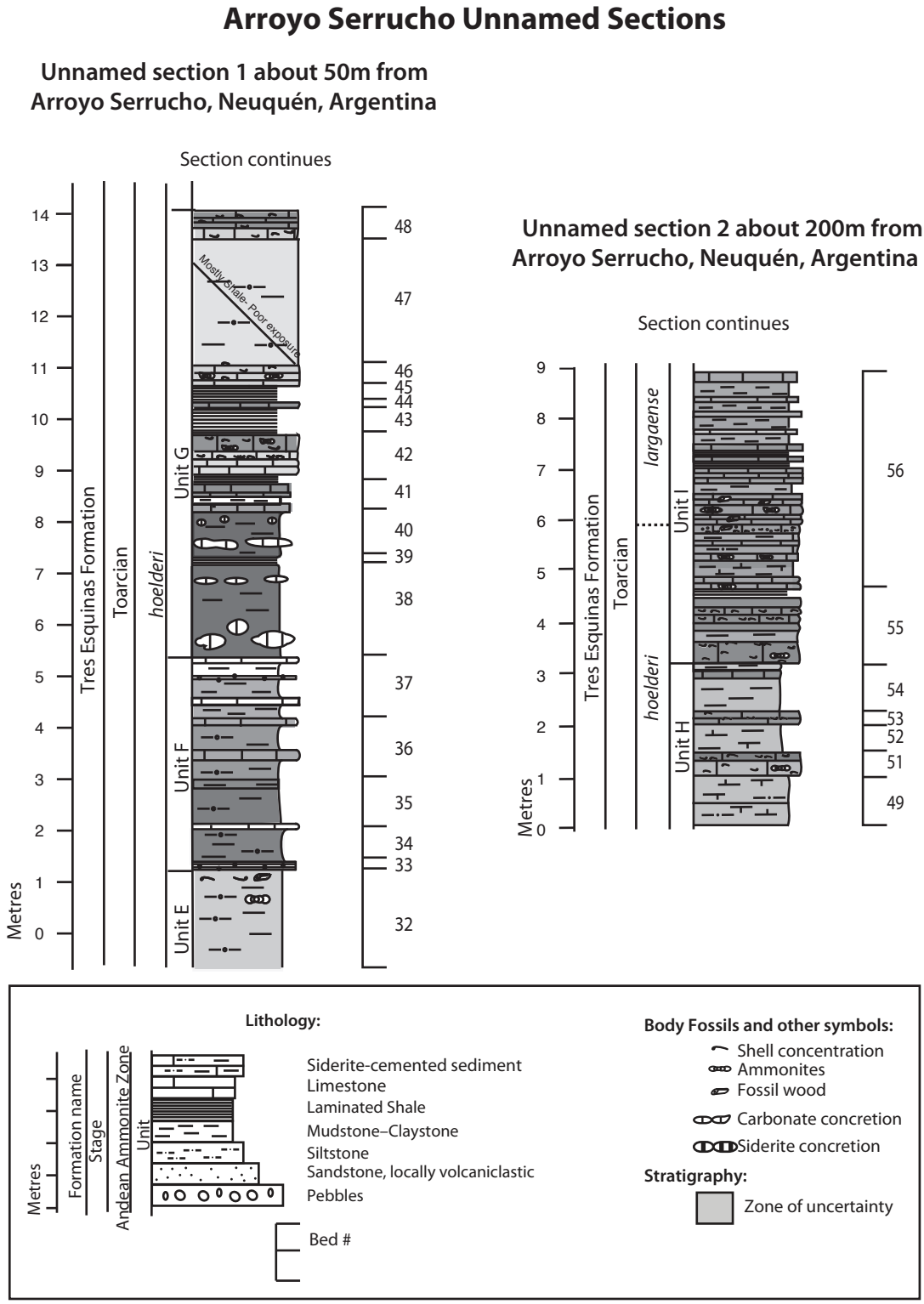


Figure 16. Detailed stratigraphic log of unnamed sections 1 and 2 at Arroyo Serrucho section logged in 2008 with legend to lithologies and other key elements illustrated in the stratigraphic logs.

2.3.13 Lithostratigraphy: Arroyo Serrucho

The Arroyo Serrucho section comprises three stratigraphic segments (Fig. 13). For the purposes of this description I will refer to them as Arroyo Serrucho Main section (Fig. 15), Unnamed section 1 and 2 (Fig. 16).

The main section at Arroyo Serrucho (Fig. 15) is ~49 m thick and comprises 5 distinct lithostratigraphic units, A–E. Unit A in the Arroyo Serrucho main section comprises medium grey to purple siltstone, with large 30–75cm wide elliptical/oval iron oxide-rich red concretions at the base of the unit, in Beds 1 and 2, and in Bed 5. The remainder of the unit is medium grey mudstone, with thin interbedded, buff-coloured very fine–grained sandstone beds and some laminated dark grey shales, Bed 4 and 6. An iron oxide-cemented very fine-grained sandstone with low-angle ripples and limestone intraclasts is located at the base of Unit B, Bed 8. There is an increase in the amount of sand in this unit. Two more siderite-cemented sandstones can be found within this unit, Bed 10 and 12. Bed 12 has gutter cast scouring into the underlying siltstone. The abundance of ammonites and bivalves increases upward through this part of the section. The uppermost Bed, Bed 13, is a fossiliferous light grey mudstone. This Bed is overlain by brown shale, Bed 16, marking the base of Unit C and passes to finer grained sediment. The brown shale in Bed 16 transitions into a medium grey mudstone. There are two iron oxide-cemented mudstones, Bed 18 and Bed 21, in this unit. Bed 18 is overlain by grey mudstone with a large 25 cm thick iron oxide nodule, while Bed 21 contains abundant bivalves.

The base of Unit D is marked by an increase in bivalves and ammonites, in beds of medium grey and red muddy limestone. These fossiliferous limestones are interbedded with pale grey mudstones and very weathered dark grey shale. Fossils vary in size and include abundant bivalves and ammonites, with some occurring in life position. Beds 26 and 28 are not exposed.

Unit E is marked by an abrupt transition from limestone to grey green mudstone, Bed 30, with some large red ferruginous concretions. A fossiliferous limestone occurs at the top of the main section at Arroyo Serrucho in Bed 31.

Unnamed section 1 is located about 50 m north of the main Arroyo Serrucho section and is ~14 m thick, with four sedimentologically distinct lithostratigraphic units, Units E–H (Fig. 16). The base of the section (Unit E, Bed 32) is a pale grey mudstone. Unit F comprises hard grey mudstone interbedded with thin iron oxide-cemented shales and laminated very fine-grained sandstone beds (Beds 33–37). Unit G comprises grey mudstone with large concretions (Beds 38 and 40); laminated black paper shale, Beds 39, 41, 43 and 45, and some cemented fossilferous mud and limestone in the upper parts of this unit, Beds 42, 46 and 48.

The final section, unnamed section 2, is located some 200 m northwest of the main section at Arroyo Serrucho and is ~9 m thick with two distinct sedimentological units, Units H and I (Fig. 16). The lower unit in the section, Unit H, comprises pale grey hard siltstone, interbedded with fossiliferous limestones (Bed 51 and 53). Above this unit follows the second and final unit, Unit I, which comprises alternating purple grey shale to limey mudstone and grey cemented fossiliferous limestone beds, with some dark grey paper shales towards the top of the section.

2.3.14 Biostratigraphy: Arroyo Serrucho

Ammonites and other fossils were sampled wherever found in the section (full details of horizons and determinations given in Appendix A, Fig. 5). Biostratigraphic determination of the Arroyo Serrucho sections confirms the presence of Early Toarcian sediments. 62 samples were collected for nannofossils, through out the section; only three samples yielded nannofossils, and those nannofossils do not record any major events.

The main section at Arroyo Serrucho (Fig. 15) includes ammonites from the *tenuicostatum* Zone, Early Toarcian, which is marked by the FO of *Dactylioceras* (*Orthodactylites*) cf. *anguinum* (Reinecke), from below the base of the section (cf., von Hillebrandt, 2006, p. 34, 263 & Schmidt-Effing, 1981, pl. 1, fig. 5-7), in Unit A. The onset of the Andean *hoelderi* Zone is marked by the FO of *Harpoceras serpentinum* (Schlotheim) (FO 18.00 m). The Andean *hoelderi* Zone is considered approximately equivalent to the *serpentinum* (= *falciferum*) ammonite Zone of northwestern Europe (von Hillebrandt and Schmidt-Effing, 1981; Page, 2004; Riccardi, 2008a, b). Unnamed section 1 (Fig. 16) also represents sediments from the *hoelderi* Zone, as indicated by the presence of *Hildaites* cf. *murleyi* (Moxon) (cf. von Hillebrandt, 1987, pl. 5, Fig. 3; Howarth, 1992b, p. 168) and *Harpoceras serpentinum* (Rein) (cf., von Hillebrandt, 1987, pl. 5, Figs. 4-9; Howarth, 1992b, p. 109) at 9.50 m and 11.09 m respectively.

Unnamed section 2 (Fig. 16) includes ammonites from the *hoelderi* Zone and the Andean *Peronoceras largaense* Assemblage Zone which is equivalent to the northwestern European, uppermost *serpentinum* and lowermost *bifrons*, Subzones. This assemblage zone is marked by the FO of *Harpoceras* cf. *falciferum* (Sow.) at 5.81 m.

A significant number of bivalves were also recovered from this section, two of which have a range limited to the Latest Pliensbachian to Earliest Toarcian, *Terquemia andina* (Damborenea) (FO 27.50 m) and *Entolium mapuche* (Damborenea) (FO 37.10 m) while *Parvamussium pumilum* (Lamarck) (FO 31.30 m), is limited to the Toarcian (Damborenea, 2002).

2.3.15 Arroyo Serrucho Depositional Setting:

Gulisano and Gutiérrez Pleimling (2005) interpreted the section at Arroyo Serrucho representing a transition from off-shore to near-shore depositional environments with

turbiditic deposits between the two depositional environments, suggesting a significant impact by transgression and regression, due to the close proximity of the section to the shelf of the basin. Examination of the palaeogeographic reconstruction of the Neuquén Basin (Fig. 3) supports this hypothesis, as the section would have been located in the narrow Northern strait of the basin, where water fed into the basin from Panthalassa. Sequences of fossiliferous limestone, Unit D and G, support the near-shore environment interpretation. Within these limestones, some bivalve fossils are present in life position, and the presence of bioturbation in some thin sections at the base of the section suggests deposition in a normal marine, oxygenated, near- shore environment. These limestone intervals are punctuated by darker, muddier, finer units, which may record basin deepening during relative sea level rise.

2.4 Summary & Conclusion

The four locations examined in this study provide a north–south transect of the Neuquén Basin, showing transition from near-shore to basinal off-shore deposits. Stratigraphic correlation based on the *tenuicostatum–hoelderi* ammonite Zone boundary is given in Fig. 17. In general, there is a transition from coarser grained sandy, turbiditic sedimentation to finer grained sedimentation in the middle of all the sections, during the *tenuicostatum–hoelderi* ammonite Zone interval, suggesting that this interval represents basin transgression, and a relative sea-level rise.

Upward through the *hoelderi* Zone towards the *largense* and *pacificum* Ammonite Zones, there is a transition back to increased coarse-grained sandy material, suggesting marine regression and a relative sea level fall. This phenomenon is apparent in both Arroyo Lapa and Chacay Melehue, which both represent more off shore, basinal deposits. While the more nearshore Arroyo Serrucho this transition is represented by a transition from limestone to shale, back to limestone in the *largense* ammonite Zone.The presence of volcaniclastic

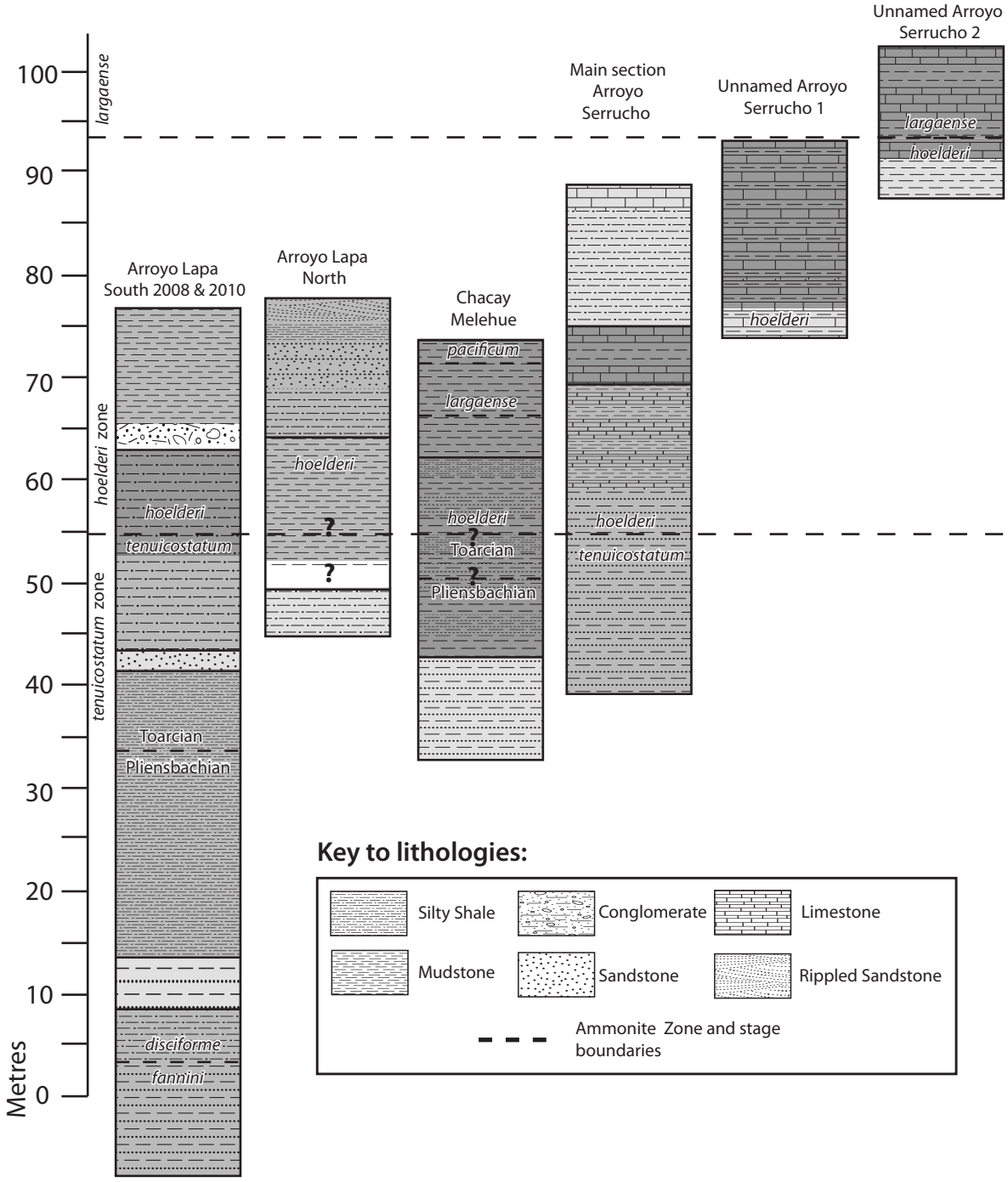


Figure 17. Correlation panel of the simplified measured stratigraphic sections. Figure shows simplified version of the measured stratigraphic sections correlated on the location of the *tenuicostatum–hoelderi* Andean ammonite zones. Arroyo Lapa South generalized log is based on a composite of the Arroyo Lapa South sections from 2008 and 2010 (Fig. 7 & 8). At Arroyo Lapa North and Chacay Melehue the *tenuicostatum* Zone is not identified so correlation is based on the presence of the *hoelderi* Zone only and the Earliest Toarcian is tentatively correlated with the *tenuicsotatum* Zone at Arroyo Serrucho and Arroyo Lapa South. The exact lithostratigraphic correlation between the unnamed sections at Arroyo Serrucho (Unnamed sections 1 and 2, Fig. 12) and the main section at Arroyo Serrucho (Fig. 11) is not known.

material in Arroyo Lapa, Chacay Melehue and in the upper part of Arroyo Serrucho indicates a close proximity of the three sections to the volcanic island arc, while the presence of charcoalifed fossil wood throughout the Arroyo Lapa and Arroyo Serrucho suggests that these sections had a close proximity to areas of terrestrial vegetation. While there is some woody material present in the Chacay Melehue section, it is not as common as in Arroyo Lapa and Arroyo Serrucho, further supporting the suggestion of a deeper, more basinal location for this section. More detailed petrographic work may also help to understand the change in provenance during basin transgression and regression.

References

Blakey, R., 2007, Early Jurassic rectangular palaeogeographic map in mollewide: http://jan.ucc.nau.edu/~rcb7/200marect.jpg (November, 2009).

Bouma, A. H., 2000, Coarse-grained and fine-grained trubidite systems as end member models: applicability and dangers: Marine and Petroleum Geology, v. 17, p. 137–143.

Burgess, P.M., Flint, S. and Johnson, S., 2000, Sequence stratigraphic interpretation of turbiditic strata: An example from Jurassic strata of the Neuquén Basin, Argentina: Geological Society of America Bulletin, v. 112, p. 1650–1666.

Caminos, R., Cingolani, C.A., Hervé, F. and Linares, E., 1982, Geochronology of the pre-Andean metamorphism and magmatism in the Andean Cordillera between latitudes 30º and 36º: Earth Science Reviews, v. 18, p. 333–352.

Coira, B., Davidson, J., Mpodozis, C., and Ramos. V., 1982, Tectonic and magmatic evolution of the Andes of northern Argentina and Chile: Earth Science Reviews, v. 18, p. 303–332.

Damborenea, S.E., 1987, Early Jurassic Bivalvia of Argentina. Part 1: Stratigraphical introduction and Superfamilies Nuculanacea, Arcacea, Mytilacea and Pinnacea: Palaeontographica, A, v. 199, p. 23–111.

Damborenea, S.E., 1990, Middle Jurassic inoceramids from Argentina: Journal of Paleontology, v. 64, p. 736–759.

Damborenea, S.E., 2002, Early Jurassic Bivalvia of Argentina. Part 3: Superfamilies Monotoidea, Pectinoidea, Plicatuloidea and Dimyoidea: Palaeontographica, A, v. 265, p. 1–119.

Dean, J.S., 1987, Depositional environments and palaeogeography of the lower to middle Cuyan Group, Neuquén Basin, Argentina. [PhD. Dissert.]: Golden, Colorado School of Mines, 586 p.

Digregorio, R.E., Gulisano, C.A., Gutiérrez Pleimling and Minitti, S.A., 1984, Esquema de la evolución geodinámica de la Cuenca Neuquina y sus implicancias paleogeográficas, *in* Proceedings 9th Congreso Geológico Argentino, Actas 2 Bariloche, Argentina: Asociación Geológica Argentina, Buenos Aires, Argentina, p. 147–162.

Eppinger, K.J. and Rosenfeld, U., 1996, Western margin and provenance of sediments in the Neuquén Basin (Argentina) in the Late Jurassic and Early Cretaceous. Tectonophysics, v. 259, p. 229–244.

Folguera, A. and Ramos, V.A., 2002, Los efectos producidos por la aproximación, colisión y subducción de dorsales pacíficas en los Andes Patagónicos: Acta Geológica Hispana, v. 37, p. 329–353.

Franzese, J. and Spalletti, L., 2001, Late Triassic–early Jurassic continental extension in southwestern Gondwana: tectonic segmentation and pre-break-up rifting: Journal of South American Earth Sciences, v. 14, p. 257–270.

Franzese, J., Spalletti, L., Gómez Pérez, I. and Macdonald, D., 2003, Tectonic and paleoenvironmental evolution of Mesozoic sedimentary basin along the Andean

foothills of Argentina (32º–54ºS): Journal of South American Earth Sciences, v. 16, p. 81–90.

Google Earth, 2005, Arroyo Lapa (Creek) , 31º24’04.87”S and 70º25’43.21”W August 7, 2011. Google Earth, Version 6.0.3.2197.

Google Earth, 2006, Arroyo Serrucho (Creek) , 35º26’24”S and 69º53’59”W October 1, 2011. Google Earth, Version 6.0.3.2197.

Groeber, P., 1946, Observaciones geológicas a lo largo del meridiano 70.1. Hoja Chos Malal: Revista de la Sociedad Geológica Argentina, v. 1, p. 177–208.

Gulisano, C.A. and Gutiérrez Pleimling, A.R., 1995, Field Guide. The Jurassic of the Neuquén Basin. (a) Neuquén Province. Asociación Geológica Argentina, Series E, No 2, Buenos Aires, Argentina, p. 1-111.

Hillebrandt, A. von., 1973, Die Ammonitengattungen Bouleiceras und Frechiella im Jura von Chile: Eclogae Geologicae Helvetiae, v. 66, p. 351–363.

Hillebrandt, A. von., 1987, Liassic ammonite zones of South America and correlations with other provinces. With description of new genera and species of ammonites, *in,* Volkheimer, W., ed.: Bioestratigrafía de los Sistemas regionales del Jurásico y Cretácico de América del Sur, Mendoza, Argentina, p. 111–157.

Hillebrandt, A. von., 2006, Ammoniten aus dem Pliensbachium (Carixium und Domerium) von Südamerika: Revue de Paléobiologie, v. 25, p 1–403.

Hillebrandt, A. von, and Schmidt-Effing, R., 1981, Ammoniten aus dem Toarcium (Jura) von Chile (Südamerika): Zitteliana, v. 6, p. 3–74.

Hillebrandt, A. von, Smith, P., Westermann, G.E.G. and Callomon, J.H., 1992a, Ammonite zones of the Circum-Pacific region, *in* Westermann, G.E.G., eds., The Jurassic of the Circum-Pacific: Cambridge University Press, Cambridge, p. 247–272.

Howarth, M.K., 1992b, The ammonite Family Hildoceratidae in the Lower Jurassic of Britain. Part 2: Monograph of the Palaeontographical Society London, v. 146, p. 107–200.

Howell, J.A., Schwarz, E., Spalletti, L.A., and Veiga, G.D., 2005, The Neuquén Basin: an overview, *in* Veiga, G.D., Spalletti, L.A., Howell, J.A., and Schwarz, E., eds., The Neuquén Basin, Argentina: a case study in sequence stratigraphy and basin dynamics: Geological Society, London, Special Publications, v. 252, p. 1–14.

Iglesia Llanos, M.P. and Riccardi, A.C., 2000, The Neuquén composite section: magnetostratigraphy and biostratigraphy of the marine Lower Jurassic from the Neuquén Basin (Argentina): Earth and Planetary Science Letters, v. 181, p. 443–457.

Lanés, S., 2005, Late Triassic to Early Jurassic sedimentation in northern Neuquén Basin, Argentina: tectosedimentary evolution of the first transgression, *in* Riccardi, A.C. ed. New Insights into the Jurassic Record of South America (Andes and Patagonia): Geologica Acta, v. 3, p. 81–106.

Legarreta, L. and Uliana, M.A., 1996, The Jurassic succession in west-central Argentina: stratal patterns, sequences and palaeogeographic evolution: Palaeogeography, Palaeoclimatology, Palaeoecology, v. 120, p. 303–330.

Llambías, E.J. and Leanza, H.A., 2005, Depósitos laháricos en la Formación Los Molles en Chacay Melehue, Neuquén: evidencia de volcanismo Jurásico en la Cuenca Neuqunia: Revista de la Asociacion Geológica Argentina, v. 60, p. 552–558.

Martinez, M.A., Prámparo, M.B., Quattrocchio, M.E. and Zavala, C.A., 2008, Depositional environments and hydrocarbon potential of the Middle Jurassic Los Molles Formation, Neuquén Basin, Argentina: palynofacies and organic geochemical data: Revista Geológica de Chile, v. 35, p. 279–305.

Mattioli, E. and Erba, E., 1999, Synthesis of calcareous nannofossil events in Tethyan Lower and Middle Jurassic successions: Rivista Italiana di Paleontologia e Stratigrafia, v. 105, p. 343–376.

Page, K.N., 2003, The Lower Jurassic of Europe: its subdivision and correlation, *in* Ineson, J.R. and Surlyk, F., eds., The Jurassic of Denmark and Greenland. Geological:

Geological Survey of Denmark and Greenland Bulletin, 1, GEUS, Copenhagen, Denmark, p. 23-59.

Page, K.N., 2004, A sequence of biohorizons for the subboreal province Lower Toarcian in Northern Britain and their correlation with a submediterranean standard: Rivista Italiana di Paleontologia e Stratigrafia, v. 110, p. 109-114.

Ramos, V.A., Niemeyer, H., Skarmeta, J. and Munoz, J., 1982, Magmatic evolution of the Austral Patagonian Andes: Earth Science Reviews, v. 18, p. 411–443.

Ramos, V.A., 1999, Evolución Tectónica de la Argentina, *in:* Caminos, R., ed., Geología Argentina: Instituto de Geología y Recursos Minerales, Anales, v. 29, p. 651–682.

Riccardi, A.C., 1983, The Jurassic of Argentina and Chile, *in*, Moullade, M. and Nairn, A.E.M., eds., Phanerozoic Geology of the World: The Mesozoic: Elsevier, Amsterdam, The Netherlands, v. B., p. 201–263.

Riccardi, A.C., 2005, First teuthid cephalopod from the Lower Jurassic of South America (Neuquén Basin, Argentina), *in,* Riccardi, A.C., ed., New Insights into the Jurassic Record of South America (Andes and Patagonia): Geologica Acta 3, v. 2, p. 179–184.

Riccardi, A.C., 2008a, The marine Jurassic of Argentina: a biostratigraphic framework: Episodes, v. 31, p. 326–335.

Riccardi, A.C., 2008b, El Jurásico de la Argentina y sus Amonites: Revista de la Asociación Geológica Argentina, v. 63, p. 625–643.

Riccardi, A.C., Leanza, H.A., Damborenea, S.E., Manceñido, M.O., Ballent, S.C. and Zeiss, A., 2000, Marine Mesozoic Biostratigraphy of the Neuquén Basin, *in*, Miller, H. and Hervé, F., eds., Zeitschrift für Angewandte Geologie, Sonderheft: 31st International Geological Congress, Rio de Janeiro, Brazil, p. 103–108.

Riccardi, A.C., Damborenea, S.E., Manceñido, M.O. and Leanza, H.A., 2011, Megainvertebrados Del Jurásico y su Importancia Geobiológica: Relatorio del 18th Congreso Geológico Argentino, Neuquén, Argentina, p. 441–464.

Richards, M., Bowman, M. and Reading, H., 1998, Submarine-fan systems I: characterization and stratigraphic pediction: Marine and Petroleum Geology, v. 15, p. 689–717.

Schiuma, M. and Llambías, E.J., 2008, New Ages and Chemical Analysis on Lower Jurassic Volcanism Close to the Dorsal De Huincul, Neuquén: Revista de la Asociacion Geológica Argentina, v. 63, p. 644–652.

Stipanicic, P.N., 1965, EL Jurásico de la Vega de la Veranada (Neuquén), el Oxfordense y el Diastrofismo Diveseano (Agassiz-Yaila) en Argentina: Revista de la Asociacion Geológica Argentina, v. 20, p. 403–478.

Valencio, S.A.; Cagnoni, M.C., Ramos, A.M., Riccardi, A.C. and Panarello, H.O., 2005, Chemostratigraphy of the Pliensbachian, Puesto Araya Formation (Neuquén Basin, Argentina), *in,* Riccardi, A.C., ed., New Insights into the Jurassic Record of South America (Andes and Patagonia): Geologica Acta 3, p. 147–154

Vergani, G.D., Tankard, A.J., Belotti, H.J. and Welsink, H.J., 1995, Tectonic evolution and paleogeography of the Neuquén Basin, Argentina, *in*, Tankard, A.J., Suárez Soruco, R. and Welsink, H.J., eds., Petroleum Basins of South America: American Association of Petroleum Geologists Memoir, v. 62, p. 383–402.

Vicente, J.C., 2005, Dynamic paleogeography of the Jurassic Andean Basin: pattern of transgression and localisation of main straits through the magmatic arc: Revista de la Asociación Geológica Argentina, v. 60, p. 221-250.

Volkheimer, W., 1973, Palinología estratigráfica del Jurásico de la Sierra de Chacai Có y adyacencias (Cuenca Neuquina, República Argentina). I. Estratigrafía de las Formaciones Sierra Chacai Có (Pliensbachiano), Los Molles (Toarciano, Aaleniano), Cura Niyeu (Bayociano) y Lajas (Caloviano inferior): Ameghiniana, v. 10, p. 105–131

Weaver, G.E.G., 1931, Paleontology of the Jurassic and Cretaceous of West Central Argentina: University of Washington, Memoir 1, Seattle, USA, 469 p..

Chapter 3

Early Jurassic (Pliensbachian-Early Toarcian) Carbon Isotope Chemostratigraphy, Neuquén Basin Argentina

Abstract

The Early Toarcian Oceanic Anoxic Event or T-OAE (Early Jurassic, *tenuicostatum-falciferum* ammonite Zones: ~183 Ma) is characterized by globally near-synchronous deposition of black shales relatively enriched in organic carbon. A broad positive and intervening stepped negative excursion in $\delta^{13}C$ (-2 to -7 ‰) is also recorded in marine and terrestrial organic matter and in pelagic and shallow-water carbonates deposited during the event. To date, all high-resolution studies of the T-OAE derive from European outcrops, leading some authors to question the global nature of the phenomenon. Organic-carbon isotope data ($\delta^{13}C_{org}$) of black shales from three locations in the Neuquén Basin, Argentina (30ºS to 40ºS) show a stepped negative (-6‰) excursion at the boundary of the *tenuicostatum* and *hoelderi* (approximately equivalent to *falciferum*) Andean ammonite Zones. This negative excursion is also recorded in the fossil wood record, lowest values of ~ -32.5 ‰, typical for Lower Toarcian black shales in Europe, and a stratigraphically associated relative enrichment in organic carbon. In addition to the early Toarcian, carbon isotope event new data from two locations in the Neuquén Basin, show a ~ -2‰ excursion in $\delta^{13}C_{org}$ at the Pliensbachian–Toarcian boundary, which can be correlated with an excursion of similar magnitude at this boundary recorded in Europe. This new data suggests that the Pliensbachian–Toarcian carbon isotope excursion and the T-OAE are global events likely caused by a globally synchronous increase in organic productivity with coincident injection of isotopically light carbon into the ocean–atmosphere system.

3.1 Introduction:

The Toarcian Oceanic Anoxic Event (T-OAE) was initially recognized on the basis of apparently coeval globally distributed black shales (Fig. 1) deposited in oxygen-depleted marine waters (Jenkyns, 1988). Burial of excess marine organic matter would imply the development of a positive $\delta^{13}C$ excursion due to preferential extraction and sequestration of the lighter isotope, ^{12}C, from the inorganic carbon pool in the marine environment. Although many European sections indicate such an overall positive excursion, a now defining character of the T-OAE is an interposed negative excursion, interpreted as due to a massive injection of isotopically light carbon into the ocean–atmosphere system, as a result of either gas hydrate dissociation (Hesselbo et al., 2000, 2007; Cohen et al, 2004, 2007; Kemp et al., 2005; Hesselbo and Pieńkowski, 2010) or thermogenic methane release from contact metamophism of Gondwana coals (McElwain et al., 2005; Svenson et al., 2007), during an interval of elevated organic-matter burial. This negative excursion has been recorded in marine carbonates and organic matter, as well as macroscopic fossil wood, indicating that the phenomenon must involve the global carbon cycle. Despite these geochemical and stratigraphical associations, a number of authors have depicted the T-OAE, and the associated negative carbon-isotope excursion, as a regional phenomenon related to particular oceanographic conditions in the Early Jurassic shelf seas of northern Europe (e.g. van de Schootbrugge et al., 2005;Wignall et al., 2005; McArthur et al., 2008), though new data from Argentina, Morroco, British Columbia, Japan, Greece, and Siberia and support the hypothesis that the Toarcian OAE extends outside Northern Europe (e.g. Al-Suwaidi et al., 2010, Bodin et al., 2011; Caruthers et al. 2011; Gröcke et al., 2011; Kafousia et al., 2011; Suan et al., 2011).

Given the presence of different ammonite bioprovinces, there have been arguments about the time-equivalence of the organic-rich strata in northern and southern Europe (Jenkyns et al., 2002; Mattioli et al., 2004; Wignall et al., 2005; Mailliot et al., 2006). This divergence in

opinion relates to problems of defining rigorously an OAE, because local environmental factors such as water depth, redox conditions and sedimentation rate control the preservation of organic carbon (e.g. Demaison and Moore, 1980) and deoxygenation in the marine environment likely took place before organic matter accumulated to any significant extent (Jenkyns, 2010). Consequently, exact time-equivalence of the most organic-rich strata would not necessarily be expected, even if an increase in organic productivity were globally synchronous, as has been suggested (Jenkyns et al., 2002).

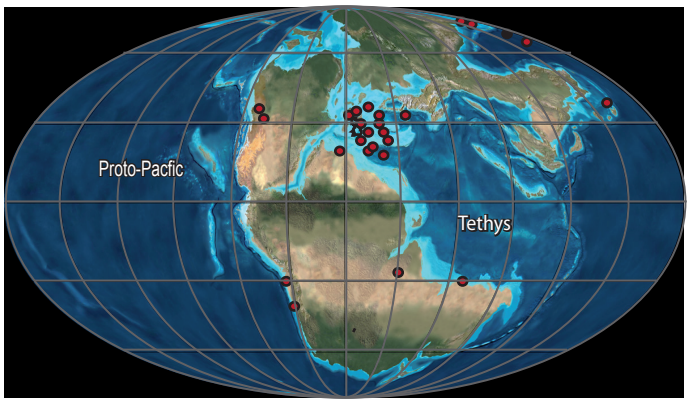


Figure 1. Paleogeographic map of the Toarcian ~183 Ma showing locationof organic rich black shales most of these localities are dated as *tenuicostatum-falcifurum* Ammonite Zones which corresponds with the Lower Toarcian stage (adapted from Jenkyns, 2001; Blakey, 2007).

To resolve the controversy surrounding the T-OAE it is necessary to move outside the European domain. This study examines new organic carbon data (isotope and total organic carbon from bulk sediment and fossil wood) from four stratigraphic sections from the Neuquén Basin, Argentina. The data is compared to coeval carbon-isotope data from other world localities, specifically Canada, Greece, Italy and the UK. The aims are to determine whether an increase in organic-matter deposition took place during the Andean equivalents of the *tenuicostatum* and *falciferum* Zones, the age of the T-OAE in NW Europe, and whether a stratigraphically associated negative carbon-isotope excursion can be detected. The palaeogeographic setting of the Neuquén Basin, detailed biostratigraphy and lithostratigraphy of the sections discussed in this chapter can be found in Chapter 2.

3.2 Methods.

Four stratigraphic sections along a North–South transect of the Neuquén Basin, Argentina were examined, Fig. 2, Arroyo Lapa North and South in the southern part of the basin, Chacay Melehue which is located centrally in the Neuquén Basin, and Arroyo Serrucho which is located in the Northern part of the basin.

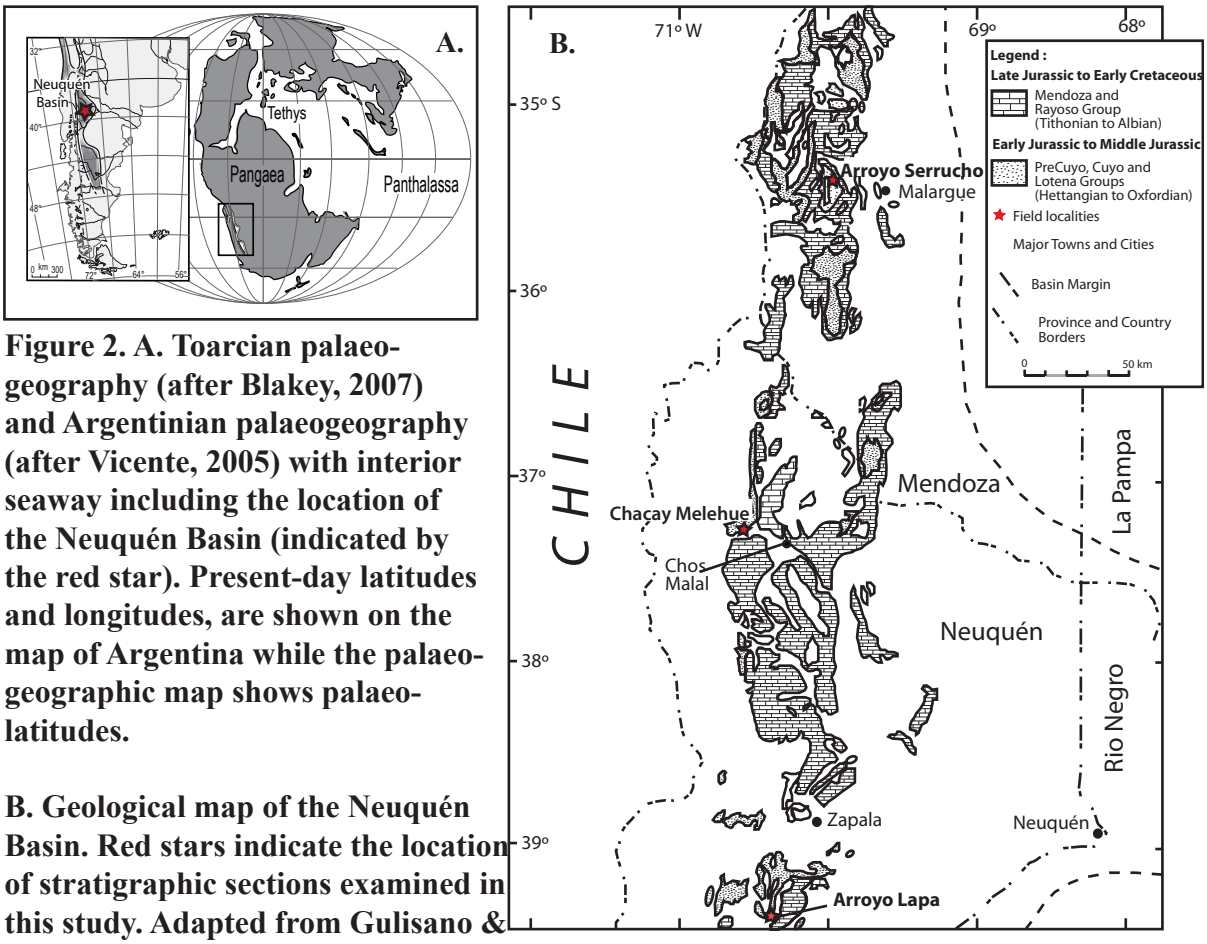


Figure 2. A. Toarcian palaeo-geography (after Blakey, 2007) and Argentinian palaeogeography (after Vicente, 2005) with interior seaway including the location of the Neuquén Basin (indicated by the red star). Present-day latitudes and longitudes, are shown on the map of Argentina while the palaeo-geographic map shows palaeo-latitudes.

B. Geological map of the Neuquén Basin. Red stars indicate the location of stratigraphic sections examined in this study. Adapted from Gulisano & Gutiérrez Pleimling, (1995).

Arroyo Lapa South was initially described in 2008 and a 50 cm resolution bulk organic matter $\delta^{13}C$ chemostratigraphic profile was generated, that spanned through the latest Pliensbachian and Early Toarcian (*disciforme–tenuicostauim* Andean ammonite Zone, roughly equivalent to the *spinatum–tenuicostatum* North West European ammonite Zone, (von Hillebrandt and Schmidt-Effing, 1981; Page, 2004; Riccardi, 2008)).

A second higher resolution examination of the upper 16 m of the Arroyo Lapa South 2008 section took place in 2010 and bulk sediment samples where collected at 10 cm intervals through the upper *tenuicosotatum–hoelderi* Andean ammonite Zone, approximately equivalent to the *tenuicostatum–serpentinum* (= *falciferum*) ammonite Zone of North West Europe (von Hillebrandt and Schmidt-Effing, 1981; Page, 2004; Riccardi, 2008), and an additional 7 m of section was measured and sampled to capture the entire Toarcian Carbon Isotope Excursion (T-CIE).

In the Arroyo Lapa South 2008 section a total of 15 fossil wood fragments were collected from outcrop, with an additional 13 samples recovered from bulk rock (full details of data are given in Appendix A, Fig. 1). A total of 52 wood fragments were recovered from bulk rock samples, in the Arroyo Lapa South 2010 section (full details are given in Appendix A, Fig. 2).

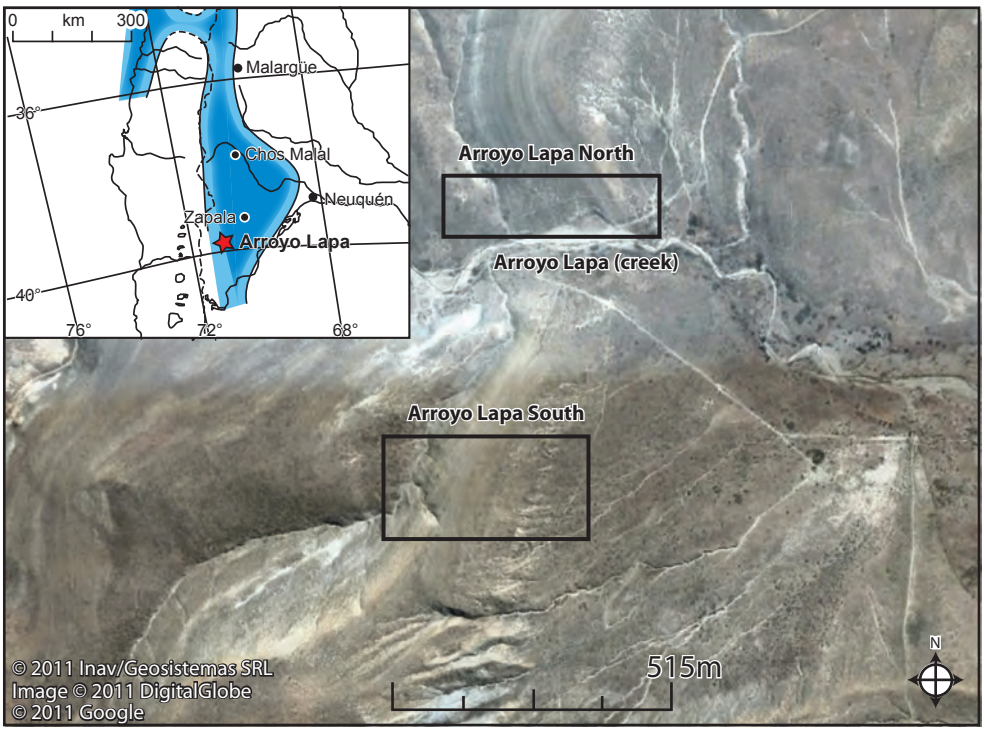


Figure 3. Satellite image of the Arroyo Lapa, field locality indicating the location of Arroyo Lapa South and Arroyo Lapa North, in the Sierra de Chacaico area, Neuquén Province Argentina, latitute and longitude, S 39º 24' 04", W 70º 25' 43" , elevation 1311 m. Inset shows the approximate location of the field area, adapted from Vicente (2005), satellite image courtesy of Google Earth (2005).

In the Arroyo Lapa North section, Fig .6, bulk sediment samples were collected at 10 cm intervals, a total of 34 fossil wood samples where recovered, 8 of these samples where recovered from bulk sediment samples, while the remaining were recovered from the section (full details are given in Appendix A, Fig. 3). In the Arroyo Serrucho section samples where collect at 50 cm intervals wherever possible. The samples come from two stratigraphic sections with a 16.7 m exposure gap, a total of 6 fossil wood samples where collected from outcrop at Arroyo Serrucho (full details of data are given in Appendix A, Fig. 5). At Chacay Melehue samples were collected at 10 cm intervals where possible (full details of data are given in Appendix A, Fig. 4).

An initial 50 cm resolution chemostratigraphy was generated for both Arroyo Lapa North and Chacay Melehue. Higher resolution examination of these two sections remains to be conducted. Samples have been catalogued and stored in the University of Oxford Department of Earth Science Rock Storage facility and are available for future work. Details of the method used for determination of total organic carbon (TOC) and organic $\delta^{13}C$ from bulk sediment and wood can be found in Chapter 1, sections 1.4.1–1.4.3.

3.3 Results:

3.3.1 Results: Arroyo Lapa South, 2008 and 2010

In the Arroyo Lapa South 2008 section (Fig. 4), $\delta^{13}C_{org}$ values at the Pliensbachian–Toarcian boundary (~14.3 m; Arroyo Lapa South 2008) fall to -26.7‰, from a background $\delta^{13}C_{org}$ of ~ -24‰, and is followed by a second negative step after the boundary, with values falling to -27.3‰ (22.55 m). This is also associated with a 2% increase in TOC weight percentages. A 4% increase in TOC weight percentages is recorded just before the *tenuicostatum–hoelderi* ammonite Zone boundary (~60 m), while bulk organic-carbon $\delta^{13}C$ values fall to ~ -31.3‰

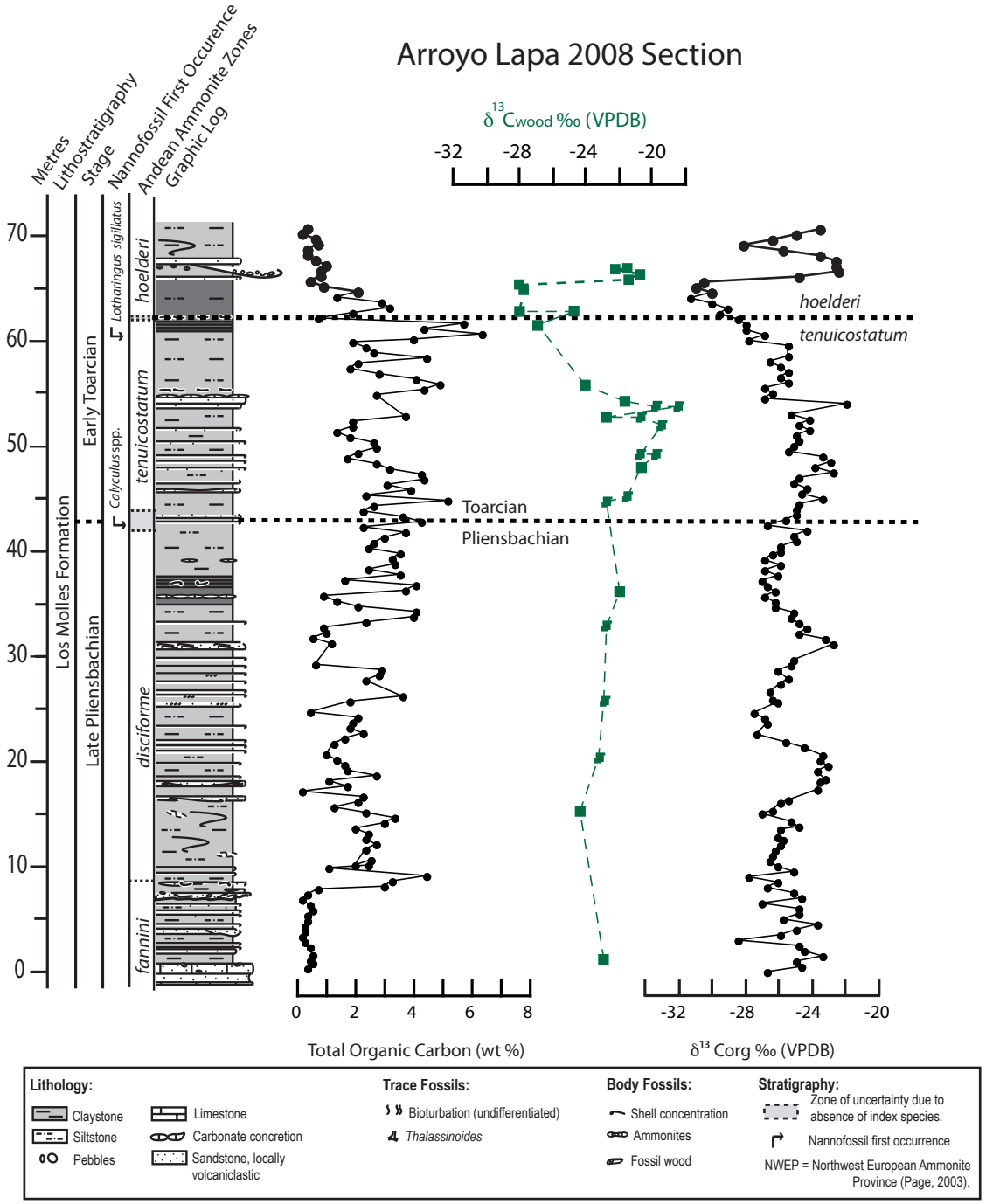


Figure 4. Section at Arroyo Lapa South examined in 2008, Neuquén Basin, Argentina, showing $\delta^{13}C_{org}$ values from bulk sediment and wood, and TOC profile. Dashed lines indicate the locations of the Toarcian–Pliensbachian boundary based on ammonite biostratigraphy from Arroyo Lapa, as well the zonal boundaries between the *tenuicostatum* and the overlying *hoelderi* (= ~*falciferum*) ammonite Zones. Note the increase in the TOC (from 3 to 6%) leading up to the top of the *tenuicostatum* Zone in Arroyo Lapa, as well as the negative -6‰ excursion in the $\delta^{13}C_{org}$ from both bulk sediment and wood. Also note a ~ -2‰ negative excursion in $\delta^{13}C_{org}$ at the Pliensbachian–Toarcian boundary in Arroyo Lapa that is correlative with new data from Yorkshire (Littler et al., 2010) details of this correlation can be found in Fig. 10 (adapted from Al-Suwaidi et al., 2010.)

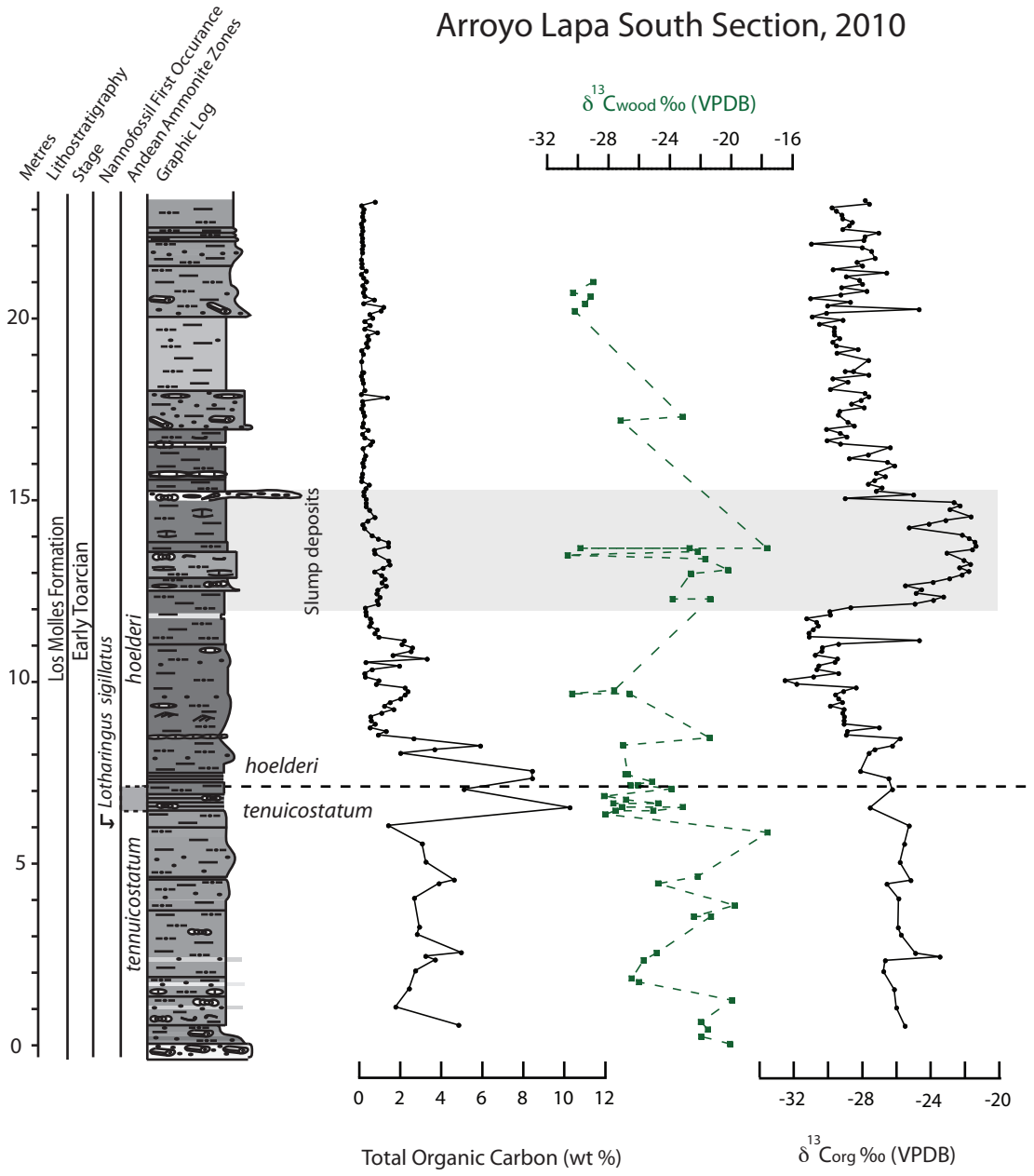


Figure 5. Section at Arroyo Lapa South examined in 2010, Neuquén Basin, Argentina, showing $\delta^{13}C_{org}$ values from bulk sediment and wood, and TOC profile. Dashed lines indicate the location of the refined zonal boundary between the *tenuicostatum* and *hoelderi* ammonite Zones. The grey shaded area indicates the location of a slump deposit in the Arroyo Lapa South section, where older sediment has been redposited resulting in a positive excursion, interupting the negative isotope excursion. Note the increase in the TOC (from ~2 to ~11%) leading up to the top of the *tenuicostatum* Zone in Arroyo Lapa, as well as the negative -6–7‰ excursion in the $\delta^{13}C_{org}$ from both bulk sediment and wood. Detailed key of lithologies and other key elements can be found in Fig. 4.

(~62 m, Fig. 4) and fossil wood $\delta^{13}C$ values falling to -28.5‰ at 64.05m after the *tenuicostatum–hoelderi* ammonite Zone boundary.

In the Arroyo Lapa South 2010 section (Fig. 5) , values fall to about -32.5‰ about 3 m above the revised *tenuicostatum–hoelderi* ammonite Zone boundary (10 m). Values of $\delta^{13}C_{org}$ in Arroyo Lapa South stay below -28‰ through the lower half of the *hoelderi* ammonite Zone, with a sharp positive excursion at 12.1 m to 14.90 m and values as high as -21.4 ‰. This interval contains reworked sediments from a slump deposit, disrupting the negative carbon isotope excursion. The isotopes during the slump interval are not indicative of the *hoelderi* ammonite Zone, and are much heavier. Suggesting that they represent some earlier time period prior to the excursion. The slump unit is caped by a conglomeratic unit that is fossilferous, but the units below show signs of soft sediment deformation, indicating reworking. In addition to this the $\delta^{13}C_{wood}$ shows a wide variety to of values from -30.66‰ to -17.6‰ which also suggests there is significant mixing in the sediment, resulting in a mixture of fossil wood from the CIE interval and from an interval with an unperturbed carbon cycle. The top of the slump deposit is marked by a negative shift back to $\delta^{13}C_{org}$ values between ~ -27 and -30‰ through the remaining 10 m of section. The $\delta^{13}C_{wood}$ record also shows the -6‰ negative excursion leading up to the *tenuicostatum–hoelderi* ammonite Zone boundary, with values falling to ~-30.66‰ at 9.6m. TOC weight percentages shows an increase of 6%, to 10.3% at 6.5m, followed by a stepped decrease after the *tenuicostatum-hoelderi* ammonite Zone boundary back to TOC values ≤ 3%.

3.3.2 Results: Arroyo Lapa North

In Arroyo Lapa North Section (Fig. 6: details in Appendix A, Fig. 3), index species indicative of the *tenuicostatum* ammonite Zone were not identified. The first diagnostic ammonites occur at 9.5 m and are indicative of the *hoelderi* ammonite Zone. Given that a

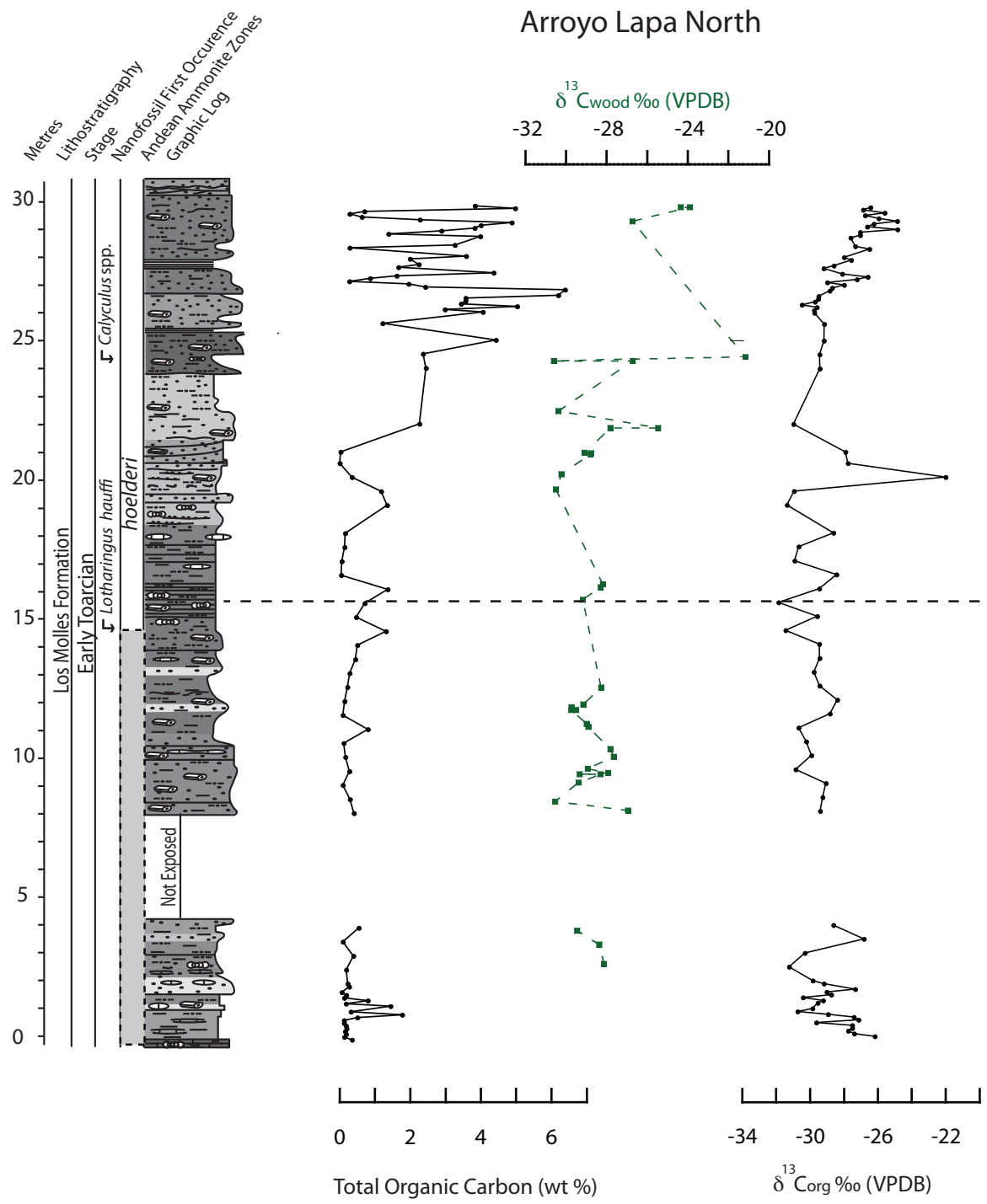


Figure 6. Section at Arroyo Lapa North examined in 2010, Neuquén Basin, Argentina, showing $\delta^{13}C_{org}$ values from bulk sediment and wood, and TOC profile. Dashed lines indicates the location of the most isotopically light sample with a value of -31.9‰, which corresponds with a 2% increase in TOC. $\delta^{13}C_{wood}$ values fall to 31.7‰, above the lightest bulk sediment values. There is a gradual positive recovery toward the top the section. Detailed key of lithologies and other key elements can be found in Fig. 4.

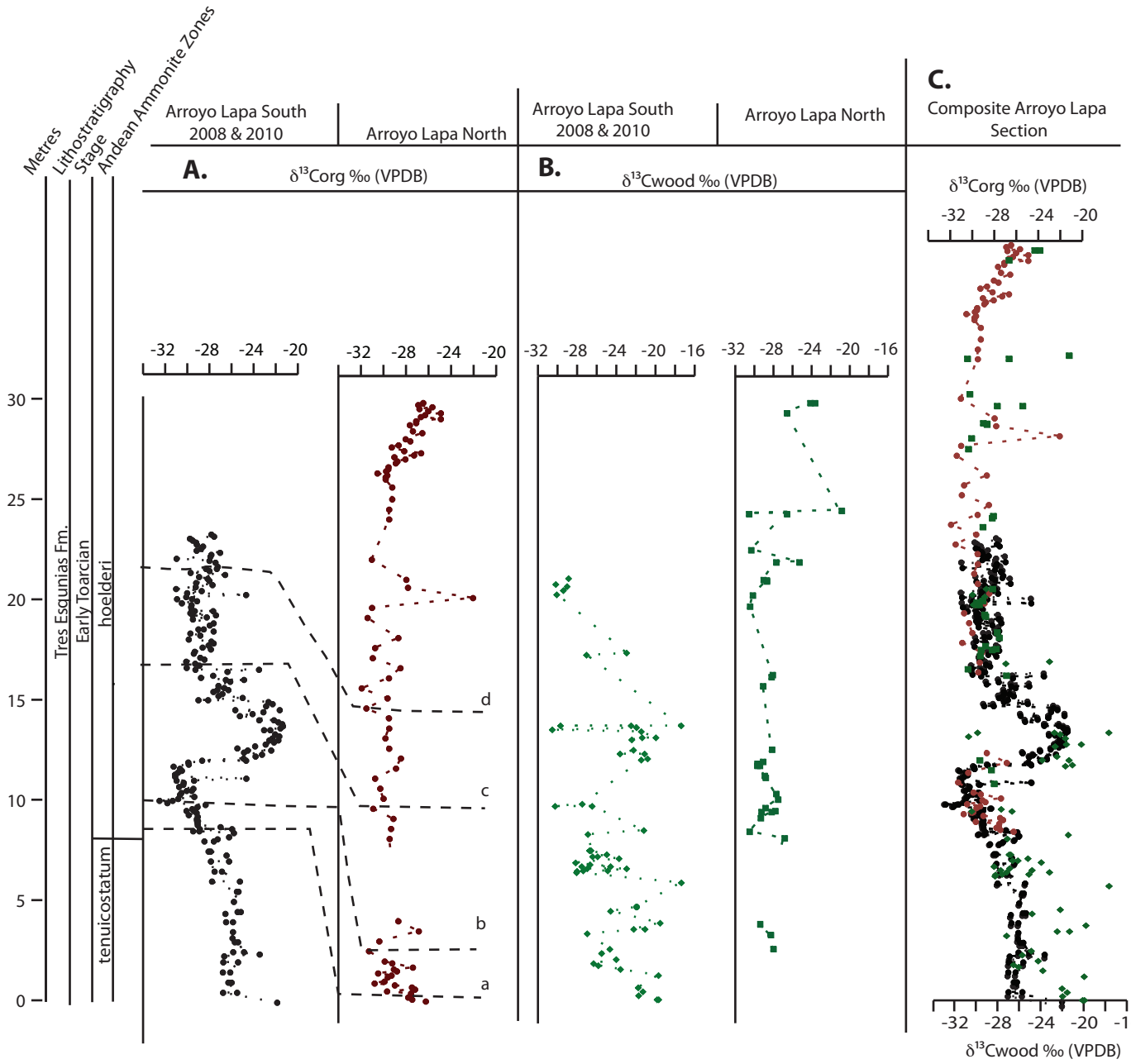


Figure 7. Comparison of data from Arroyo Lapa South (2008 and 2010) and Arroyo Lapa Northbased on $\delta^{13}C_{org}$ values from bulk sediment. A. Correlation of the two sections is indicated by dashed black lines a–d and is based on $\delta^{13}C_{org}$ values and the magnitude of negative steps in the chemostratigraphic profiles.(B) Comparison of the $\delta^{13}C_{wood}$ values from the two sections does not show any direct correlation. (C.) A composite of the bulk sediment and fossil wood data from Arroyo Lapa North and Arroyo Lapa South based on the correlation in A. It appears that regardless of local varaitions in deposition the chemostratigraphic signal can be correlated and shows a complete negative excursion and positive recovery in the *tenuicostatum-hoelderi* ammonite zone in the Arroyo Lapa area.

majority of $\delta^{13}C_{org}$ samples from Arroyo Lapa North have values < -27‰, and values as low as ~ -32‰ are present (7.5 m) it appears that the negative carbon isotope is recorded in this section, furthermore there is a positive recovery at the top of the section. Fossil wood values also remain light, < -26‰, with values as low as – 31.7 ‰, between 11.5m and 16.1m, though values become heavier (~ -24‰) at the top of the section.

The total organic carbon in this section is relatively low throughout, remaining below ~1% for about 15 m, and increases upward through the section. There is a slight increase at the *tenuicostatum–hoelderi* ammonite Zone boundary (14.5 m) with TOC increasing to ~ 2.5%. The amount of fossil wood increases up through the section with abundant fossil wood in the upper 5 m, which accounts for the elevated TOC in this part of the section. It is possible to correlate the $\delta^{13}C_{org}$ chemostratigraphy in Arroyo Lapa North with the composite 2008 and 2010, $\delta^{13}C_{org}$ chemostratigraphy from Arroyo Lapa South (Fig. 7). This correlation suggests that the section at Arroyo Lapa North sits slightly above the base of the Arroyo Lapa South 2010 section, and records the positive recovery, showing the complete record of the T-OAE in the southern hemisphere.

3.3.3 Results: Chacay Melehue

In the Chacay Melehue section, Fig.8, the *tenuicostatum–hoelderi* ammonite Zone boundary is missing, this may be due to a hiatus or very low sedimentation during this period, and is discussed in detail in Chapter 2. However, Chacay Melehue is still useful for chemostratigraphic comparison as the $\delta^{13}C_{org}$ chemostratigraphy can be correlated with equivalent aged sections from the Neuquén Basin (Arroyo Lapa South, this study) and Yorkshire, England (Littler et. al, 2010) indicating the presence of the Pliensbachian–Toarcian boundary, (*disciforme–tenuicostatum* Andean ammonite Zone, approximately

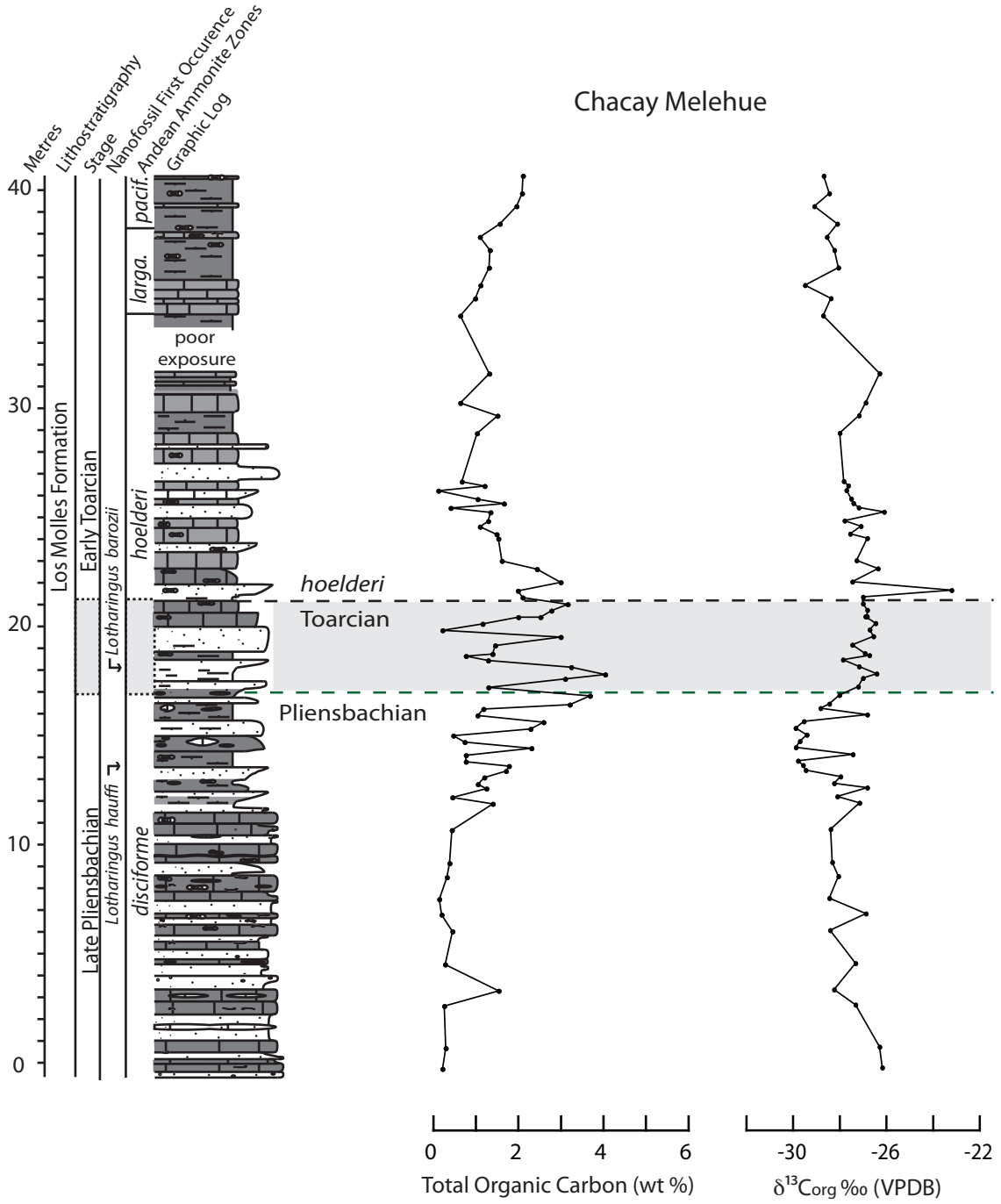


Figure 8. Section at Chacay Melehue, Neuquén Basin, Argentina, showing $\delta^{13}C_{org}$ values from bulk sediment and TOC profile. The green dashed line indicates the location of the last occurence of Pliensbachian ammonites and the black dashed line indicates the zonal boundary for the *hoelderi* ammonite Zone, in the Toarcian stage. The grey shaded area has no diagnostic ammonites and the *tenuicostatum* ammonite Zone assemblage was not identified in this section, indicating either a hiatus in or very low sedimentation in the earliest Toarcian *tenuicostatum* Zone. Note the increase in the TOC of 4% leading up to the top of the Pliensbachian part of the section, as well as the negative -4‰ excursion in the $\delta^{13}C_{org}$ in bulk sediment. Also note that as the *tenuicostatum–hoelderi* Zone boundary is missing, so is the negative excursion associated with this boundary. Biotratigraphic uncertainty due to absence of index species is indicated by grey shading. Detailed key of lithologies and other key elements can be found in Fig. 4.

equivalent to the Northwest European Province *spinatum–tenuicostatum* ammonite Zone (Page, 2003). Details of this correlation can be found in section 3.4.1.

In the Chacay Melehue section there is a stepped -2‰ negative $\delta^{13}C_{org}$ excursion with values falling to -29.9‰ (13.85 m) with a slight positive excursion at 16.8 m and values of -28‰ . There is also an enrichment in TOC at 16.8m, with TOC wt% increasing to 6%. TOC decreases upward through the section following this enrichment.

3.3.4 Results: Arroyo Serrucho

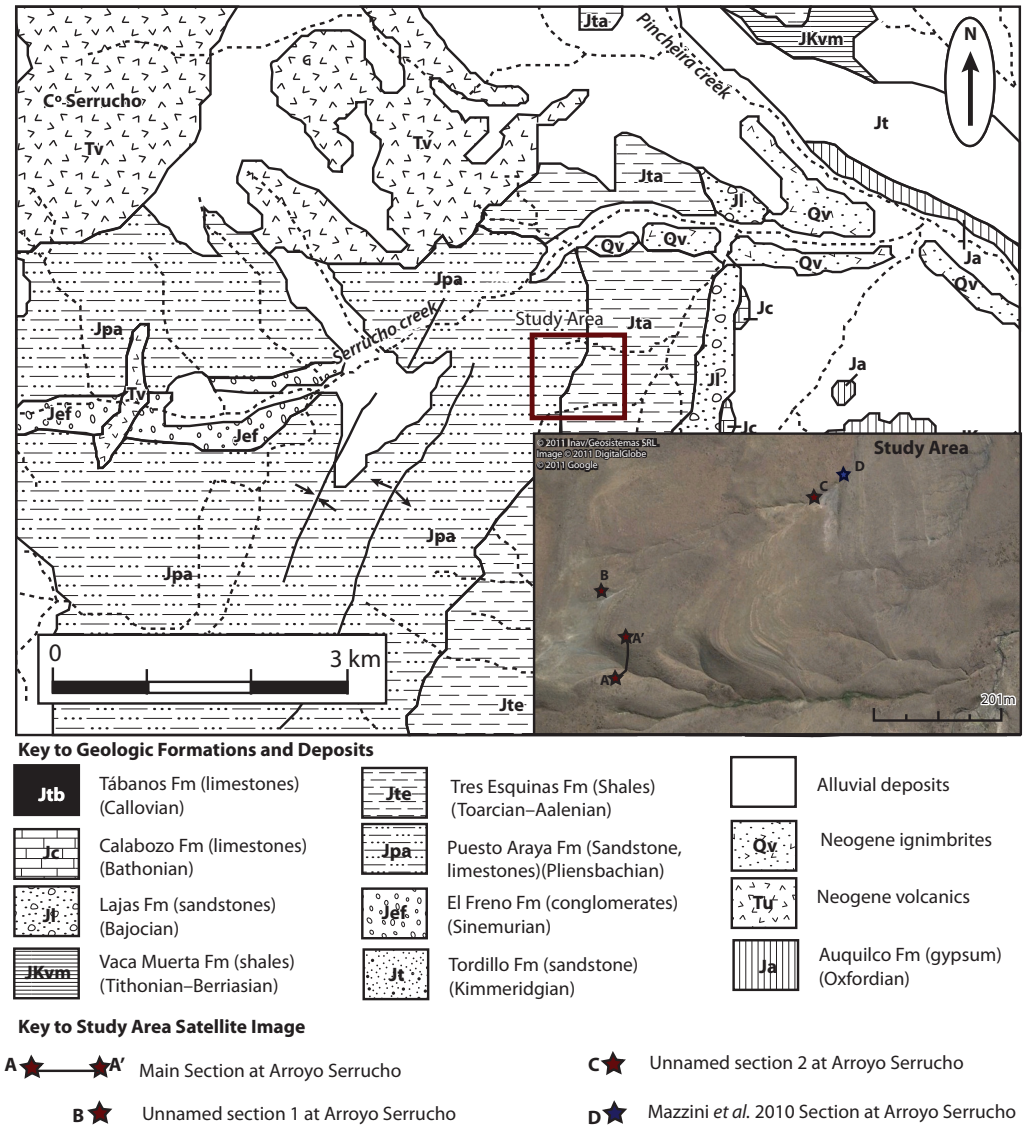


Figure 9. Geological map of the Arroyo Serrucho Area, 30 km west of the city of Malargüe, in Mendoza province, North of the Neuquén province, with inset showing the satellite image of the study area and locations of the three measured sections at Arroyo Serrucho, the Main section, unnamed section 1 and unnamed section, and the Mazzini et al. (2010) section. Latitute and longitude, S 35º 26' 24",W 69º 53' 59" W. Geologic map adapted from Gulisano & Gutiérrez Pleimling (1995), satellite image courtesy of Google Earth (2006).

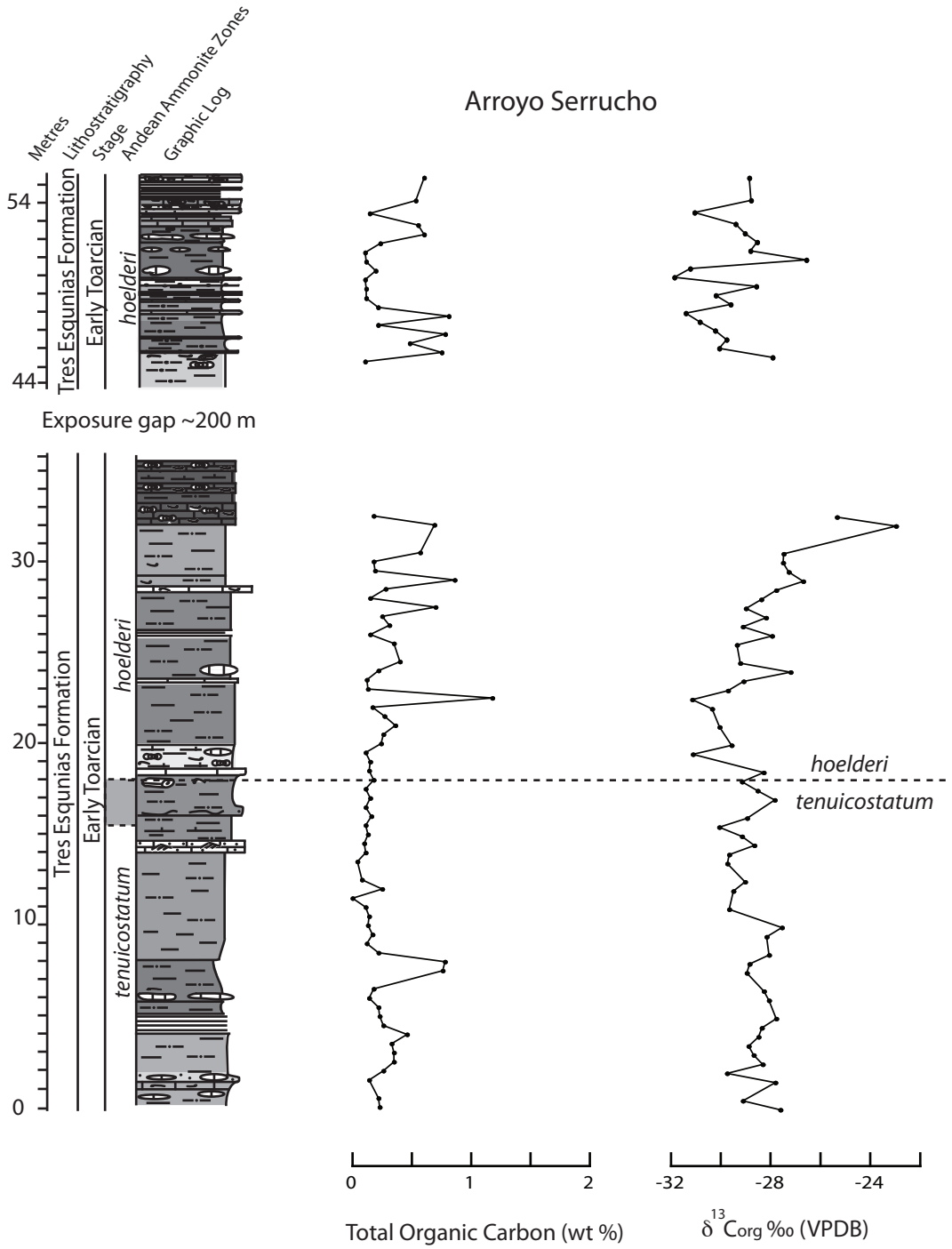


Figure 10. Two sections at Arroyo Serrucho, Neuquén Basin, Argentina, showing $\delta^{13}C_{org}$ values from bulk sediment and TOC profile. Dashed lines indicate the location of the zonal boundary for the *tenuicostatum– hoelderi* ammonite Zone. Note the TOC wt. % is very low in this section but increases upwards following the *tenuicostatum–hoelderi* ammonite Zone boundary. Also note the negative excursion in $\delta^{13}C_{org}$ in bulk sediment of -4‰ at the *tenuicostatum–hoelderi* ammonite Zone boundary, followed by a positive recovery towards the top of the lower section and a return to lighter values in the upper part of the section. Biotratigraphic uncertainty due to absence of index species is indicated by grey shading. Detailed key of lithologies and other key elements can be found in Fig. 4.

The Arroyo Serrucho section, is divided in to 2 sections separated by a 50 m exposure gap (Fig. 9–10). In the lower part of the section $\delta^{13}C_{org}$ values fall to -31.1‰, ~3 m above the *tenuicostatum–hoelderi* ammonite Zone boundary (18 m), this coincides with a relative enrichment in total organic carbon in the section. $\delta^{13}C_{org}$ values in this lower section become more positive upwards towards the top of the section, but remain below -28‰ through the lower part of the *hoelderi* Zone. Values then become heavier upward through the section, with an abrupt positive step at ~32m and $\delta^{13}C_{org}$ values increasing to -23‰ before decreasing again. In the upper section, which comprises sediments from the *hoelderi* Zone, shows $\delta^{13}C_{org}$ values remaining below -27‰ with a negative excursion of -3‰ and values falling to -31.8‰ at 49.7 m. The total organic carbon (TOC) in this section is relatively low through out, < 0.5% in most samples but values increase toward the *tenuicostatum–hoelderi* ammonite Zone boundary, and remain above 0.5% TOC through the lower part of the *hoelderi* Zone.

3.4 Discussion and Chemostratigraphic Correlation

3.4.1 Pliensbachian–Toarcian Boundary Excursion

The Pliensbachian–Toarcian boundary, which is located at the *spinatum–tenuicostatum* North West European ammonite Zone boundary, approximately equivalent to the *disciforme–tenuicostatum* Andean ammonite Zone boundary (von Hillebrandt and Schmidt-Effing, 1981; Page, 2004; Riccardi, 2008) and is recognized in Arroyo Lapa South, from the biostratigraphy and in Chacay Melehue by correlation of the $\delta^{13}C_{org}$ chemostratigraphy (ammonites indicative of the *tenuicostatum* ammonite Zone are absent in this section). Total Organic Carbon and $\delta^{13}C_{org}$ values from these two sections can be directly compared with equivalent aged sediments from Yorkshire, England (Fig. 11; Littler et al., 2010). The Yorkshire section shows a relative increase in TOC burial prior to the Pliensbachian–Toarcian boundary, a similar size increase in TOC burial is also present at Chacay Melehue, and at Arroyo Lapa South, where TOC increases

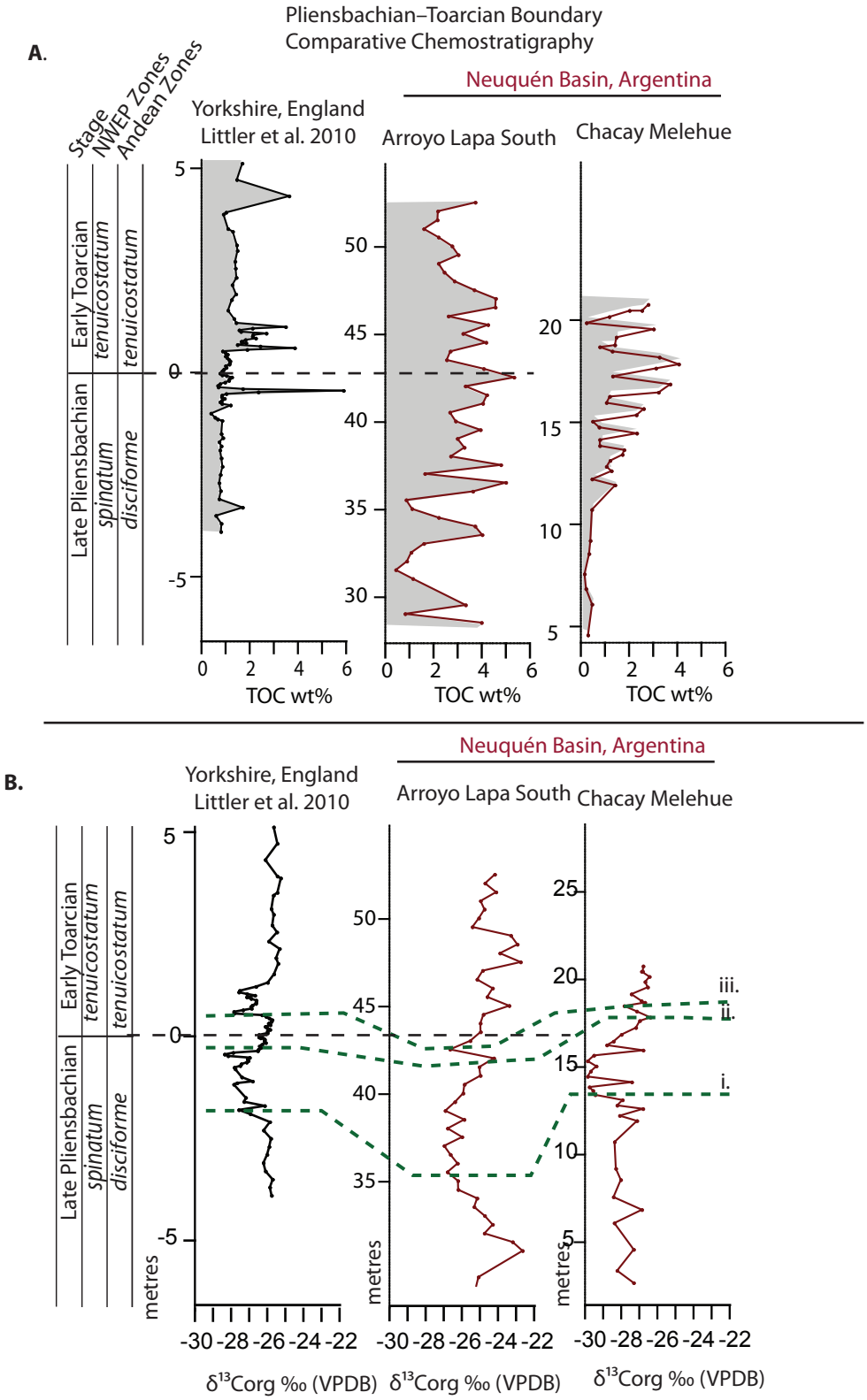


Figure 11. Comparative chemostratigraphy for the Pliensbachian–Toarcian Boundary, in Arroyo Lapa, 2008, Chacay Melehue and Yorkshire, England (Littler et al., 2010). Correlation is based on ammonite biostratigraphy (Yorkshire and Arroyo Lapa South) and $\delta^{13}C_{org}$ (all sections). (A) Comparison of TOC wt% in the three sections, note TOC wt % increases in all sections by ~4%, prior to and through the boundary. (B) Comparison of $\delta^{13}C_{org}$ in bulk sediment from the three sections. The dashed green line show the correlation between the sections and is based on values of $\delta^{13}C_{org}$: (i) indicates the -4‰ stepped excursion in all three sections before the Pliensbachian–Toarcian boundary, followed by (ii) a ~2‰ positive step in the excursion and (iii) a second -2‰ excursion following the Pliensbachian–Toarcian excursion. Followed by a recovery back to background values of in $\delta^{13}C_{org}$.

to about 6% at the boundary and then decreases again prior to the Toarcian negative carbon isotope excursion (Fig.11A).

In Yorkshire $\delta^{13}C_{org}$ values prior to the Pliensbachian–Toarcian boundary fall to -28.35‰, and are followed by a positive isotope excursion with values increasing to ~-25‰ before decreasing again to ~-27‰. In Arroyo Lapa South and in Chacay Melehue, values fall as low as -26.7‰ and -29.9‰, respectively prior to the Pleinsbachian-Toarcian boundary and follow a similar pattern of a positive recovery followed by another negative step after the boundary. It is important to note here that the background $\delta^{13}C_{org}$ values at Arroyo Lapa South are ~-24‰, so -26.7‰ is a -2‰ excursion. Both sections show an approximately ~2‰ negative carbon isotope excursion, which is comparable to that in Yorkshire (Fig. 11B). Hesselbo et al. (2007) also identified this excursion in both $\delta^{13}C$ from carbonate and in wood from Peniche, Portugal. While this CIE is not very well studied it may represent pulses of volcanic degassing of light carbon from the Karoo-Ferrar Large igneous province, which covered the southern part of Gondwana, or it may be related to shorter lived but similar events as those that resulted in the Toarcian CIE. Whatever the cause it now appears the Pliensbachian–Toarcian carbon isotope excursion is also a global event with a magnitude of ~ -2‰, and may be useful in identifying the boundary in sections of a similar age that lack good biostratigraphic control.

3.4.1 Toarcian Carbon Isotope Excursion

The $\delta^{13}C$ values from three of the sedimentary successions examined in Argentina, Arroyo Lapa South (2008 and 2010), Arroyo Lapa North and Arroyo Serrucho may be directly compared with coeval sediments from Yorkshire, England; Haida Gwaii, British Columbia (Carruthers et al., 2011); Mochras farm borehole, Wales (Jenkyns et al., 2001); Kastelli, Greece (Kafousia et al., 2011) and correlations in the steps of the negative excursion can be drawn (Fig. 12). Total Organic Carbon (TOC) weight percentages in all locations show an increasing trend

and similar absolute values in the *tenuicostatum* Zones. Organic $\delta^{13}C$ values from the high resolution Arroyo Lapa South 2010, section shows a stepwise negative shift with a magnitude of -6‰, as does the Arroyo Serrucho data; a feature characteristic of the T-OAE in Toarcian sections from Europe (Jenkyns et al., 2001; Hesselbo et al., 2000, 2007; Kemp et al., 2005; Sabatino et al., 2009, Kafousia et al, 2011). In the 2010 Arroyo Lapa South Section (Fig. 3), values fall to -32.53‰ at about 3 m above the *tenuicostatum–hoelderi* ammonite Zone boundary (~7m, Fig. 4–5), this can be correlated with the most negative values at Arroyo Lapa North, in the *hoelderi Zone*, where values fall to -31.94‰ (~15.5 m, Fig. 6–7), while in Arroyo Serrucho values fall to -31.14‰ about ~4 m above the *tenuicostatum–hoelderi ammonite Zone boundary* (Fig. 8).

Correlation can be made between the high-resolution record of Kemp et al., (2005) and Littler et al. (2010), with the composite record from the Arroyo Lapa Area (Fig. 13). At what is inferred to be the same biostratigraphic level in Yorkshire, very similar values are recorded by Hesselbo et al. (2000) and Jenkyns et al. (2002), but somewhat lower ones (~ -33‰) in the very high-resolution record of Kemp et al. (2005). Typical extreme $\delta^{13}C_{org}$ values at other locations in Europe for the T-OAE range from -30‰ to -33‰ (e.g., Jenkyns and Clayton, 1986; Schmid-Röhl et al., 2002; Sabatino et al., 2009; Jenkyns, 2010). Caruthers et al. (2011) recorded values as low as -31.8‰ from a section of similar age (*Kanese* North West American Ammonite Zone), at Haida Gwaii in British Columbia during the Toarcian CIE. In Yorkshire, values become heavier, approaching -26‰, through the lower part of the *falciferum* ammonite Subzone; values appear to do the same thing in Arroyo Lapa (Fig. 13) and Arroyo Serrucho indicating the positive recovery of the carbon isotope excursion.

Sediments examined by Caruthers et al. (2011) from Haida Gwaii, British Columbia, were expected to show a similar chemostratigraphic profile as those in Argentina, recording overall signal of the T-OAE in *Proto*-Pacific, but the section in British Columbia lacks the steps leading up to the Negative excursion. Though Carruthers et al. (2011) tentatively identified these, it is difficult to directly correlate these steps with the data from Argentina.

In Arroyo Serrucho, $\delta^{13}C_{org}$ values through the *hoelderi* ammonite Zone remain relatively light (<~-28‰), this may indicate a second isotope excursion later in the *hoelderi* (*falciferum)* ammonite Zone or may simply reflect local basin changes, or reworking of sediment from the *tenuicostatum–hoelderi* ammonite Zone. The section at Arroyo Serrucho was also examined by Mazzini et al. (2010), (Fig. 14) the location of the *tenuicostatum–hoelderi* ammonite Zone boundary was based on the presence of the bivalve bositra, which has a long range extending from the Pliensbachian through the Toarcian, and is not a particularly useful Zone boundary marker in the Southern Hemisphere. Furthermore Mazzini et al. (2010) recorded $\delta^{13}C_{org}$ values with a minimum of -29.8‰ through the *tenuicostatum–hoelderi* Zones, these $\delta^{13}C_{org}$ values are not typical of the minimum $\delta^{13}C_{org}$ values for the T-OAE in Argentina, or other sections from around the world (e.g. Sabatino et al., 2009; Caruthers et al., 2011; Gröcke et al., 2011, Kafousia et al., 2011). The chemostratigraphic profile generated by Mazzini et al., (2010) cannot be correlated with the chemostratigraphy in this study from Arroyo Serrucho or other sections in this study and while the ash dates appear to be correct for the Early Toarcian the poor chemostratigraphy and biostratigraphy raises questions about the depositional history of the ash beds sampled. It appears that Mazzini et al. (2010) misinterpreted the *tenuicostatum–hoelderi* ammonite Zone boundary at Arroyo Serrucho. Examination of the Mazzini et al. (2010) section indicates that it may sit above the measured section in this study but further field work is necessary at Arroyo Serrucho to determine the exact nature of the ash samples collected, and autochthony (primary ash) must be establish to determine the exact biostratigraphy of the area examined by Mazzini et al. (2010), and how it relates to the chemostratigraphy in this study. It would also be useful to reexamine the Arroyo Serrucho section in this study and establish the exact relationship between the upper section at Arroyo Serrucho and the lower section and determine if the sediments have been reworked in the upper section or if they do in fact represent a second excursion in the *hoelderi* ammonite Zone.

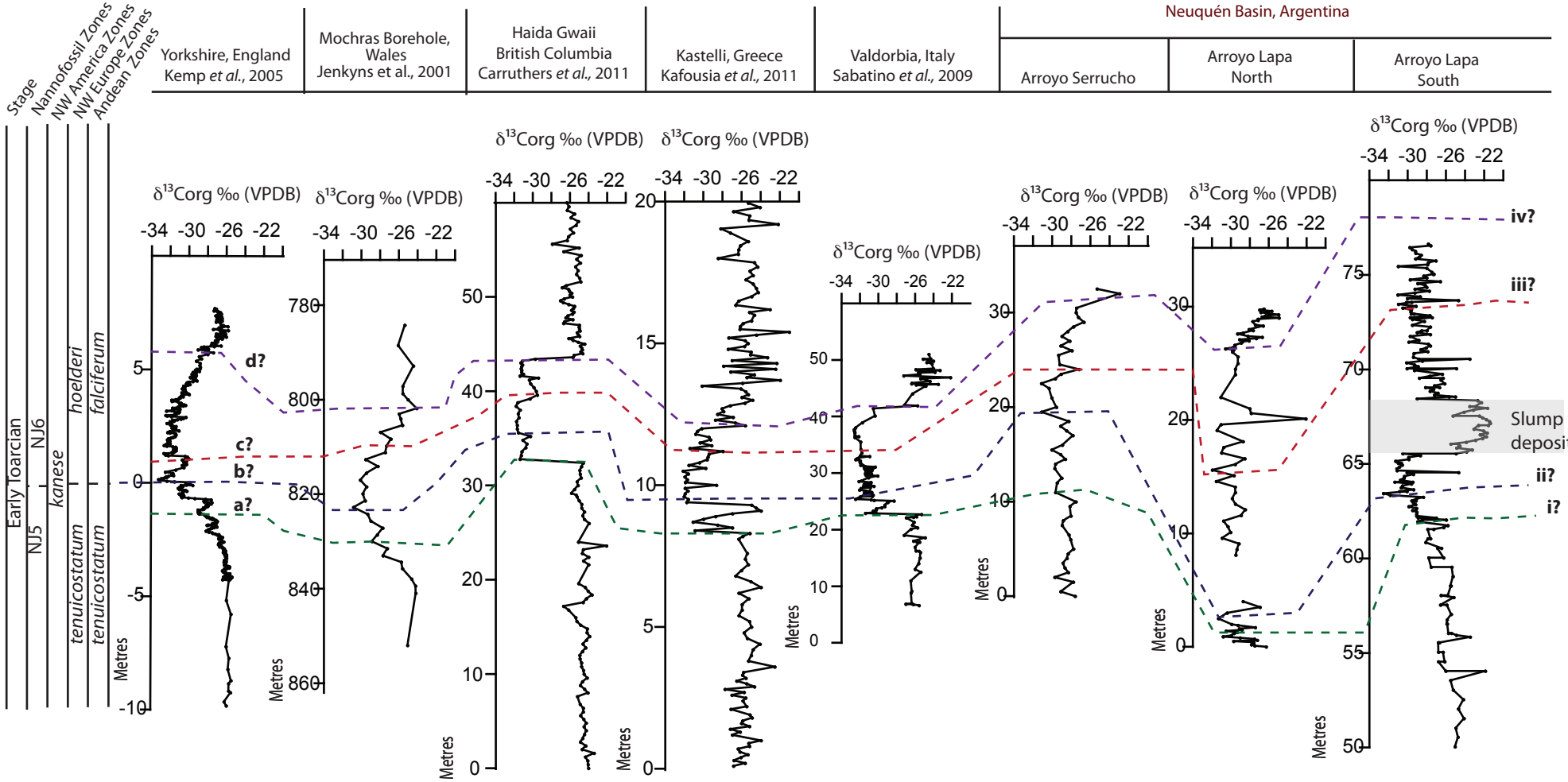


Figure 12. Comparative chemostratigraphy of the *tenuicostatum–hoelderi* ammonite Zone (~equivalent to the *tenuicostatum–falciferum* (=~*serpentinum*) North West European Ammonite Zone boundary or the North West American *Kanese* ammonite zone). Figures shows a comparison of data from Yorkshire, England (composite of data from Kemp et al, (2005); Mochras Borehole, Wales (Jenkyns et al. 2001); Haida Gwaii in British Columbia (Caruthers et al., 2011); Valdorbia, Italy, (Sabatino et al., 2009) and Kastelli, Greece (Kafousia et al., 2011) compared with data from Arroyo Serrucho, Arroyo Lapa North and composite data from Arroyo Lapa South (2008 and 2010). Correlation is based on the bulk sediment organic C-isotope steps. Green dashed line (i) is the initial ~-2–4‰ step, (ii) the blue dashed line shows the correlation in the chemostratigraphy at the most negative part of the excursion (δ^{13}Corg <-30‰) (iii) the red dashed line, indicates a final negative step prior to the final positive recovery (vi), indicated by the purple dashed line.

The $\delta^{13}C_{wood}$ record for Arroyo Lapa South and North both show a -6‰ negative shift leading up to the *tenuicostatum–hoelderi* ammonite Zone boundary, as is the case in Yorkshire and sections from Europe (Hesselbo et al., 2000, 2007). The fossil wood data provide an independent carbon-isotope record for the Southern Hemisphere that is not affected by any local oceanographic restriction of the Neuquén Basin. Combined biostratigraphic and chemostratigraphic data indicate that the T-OAE was recorded in the Southern Hemisphere and influenced the total ocean–atmosphere system. Although local factors, such as variable sedimentation rate and diagenesis, may have influenced values of TOC, the data are consistent with the hypothesis that the T-OAE represents an interval of globally increased organic productivity.

3.5 Conclusion.

Ammonite biostratigraphy, total organic carbon, and $\delta^{13}C_{org}$ values in wood and bulk sediment from the Neuquén Basin, Argentina, provide evidence for the Toarcian oceanic anoxic event in the Southern Hemisphere. The $\delta^{13}C$ values from bulk organic matter are comparable with carbon-isotope datasets from a coeval section of black shale in Yorkshire, England, Mochras, Wales and British Columbia, showing a stepped negative excursion of -6‰ leading up to the Andean *tenuicostatum–hoelderi* or its European equivalent the *tenuicostatum–serpentinum* (= *~falciferum*) ammonite Zonal boundary. These new data confirm the near-synchronous pattern of organic-matter burial in marine shale deposited over a considerable latitudinal range, here interpreted as due to a globally simultaneous increase in organic productivity. The new data from fossil wood provide an atmospheric record from the southern

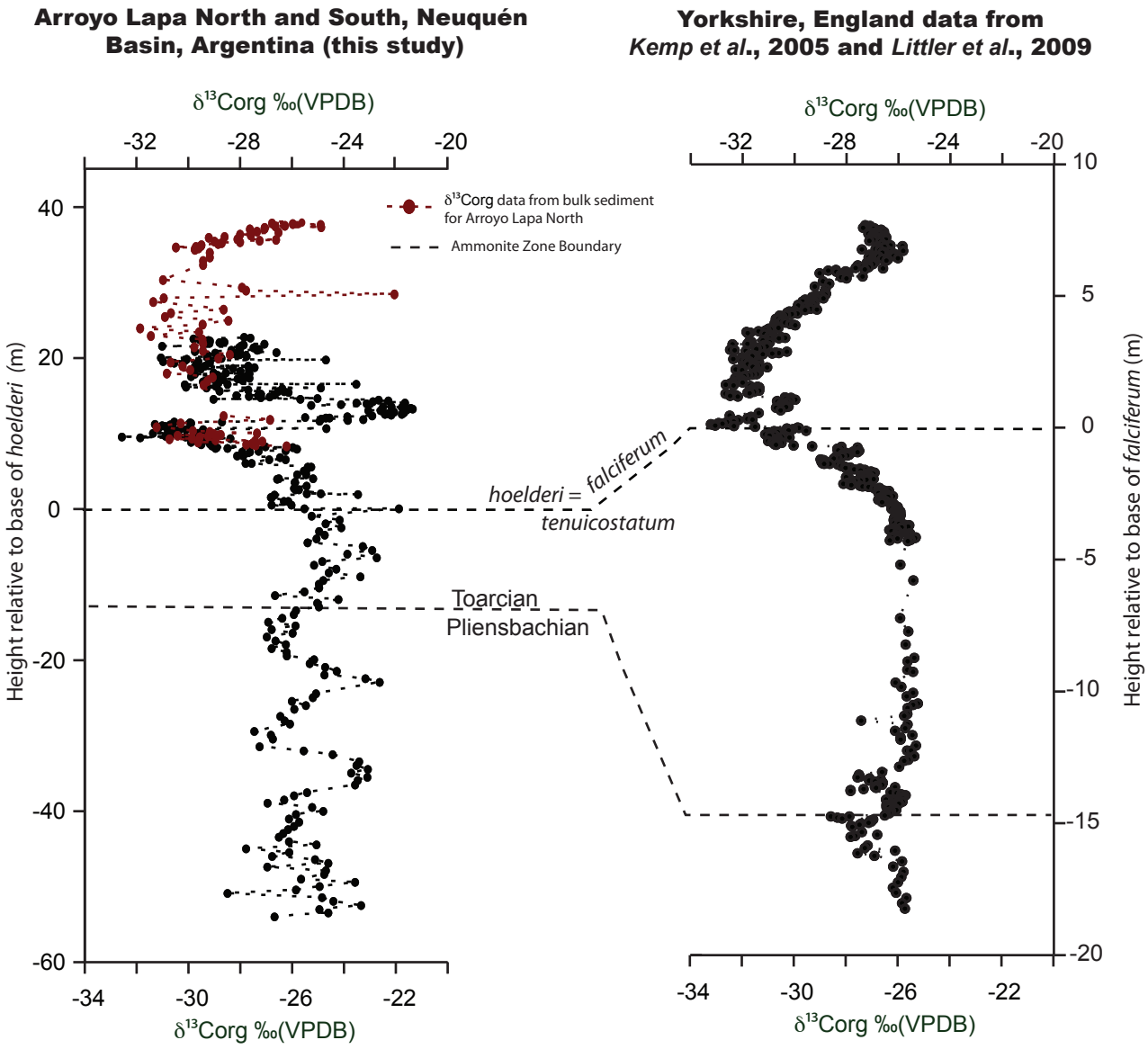


Figure 13. Comparative chemostratigraphy for the *tenuicostatum–hoelderi* (~equivalent to the *tenuicostatum–falciferum* (=~*serpentinum*) North West European Ammonite Zone boundary). Figures shows a comparison of δ^{13}Corg data from Yorkshire, England (composite of data from Kemp et al, (2005) and Littler et al. (2010) and the composite δ^{13}Corg data from Arroyo Lapa North and South. Both sections show a stepped negative δ^{13}Corg excursion with values falling to below -32‰ followed by a gradual positive recovery, with values staying below -28‰ through the lower part of the *hoelderi/falciferum* ammonite Zone.

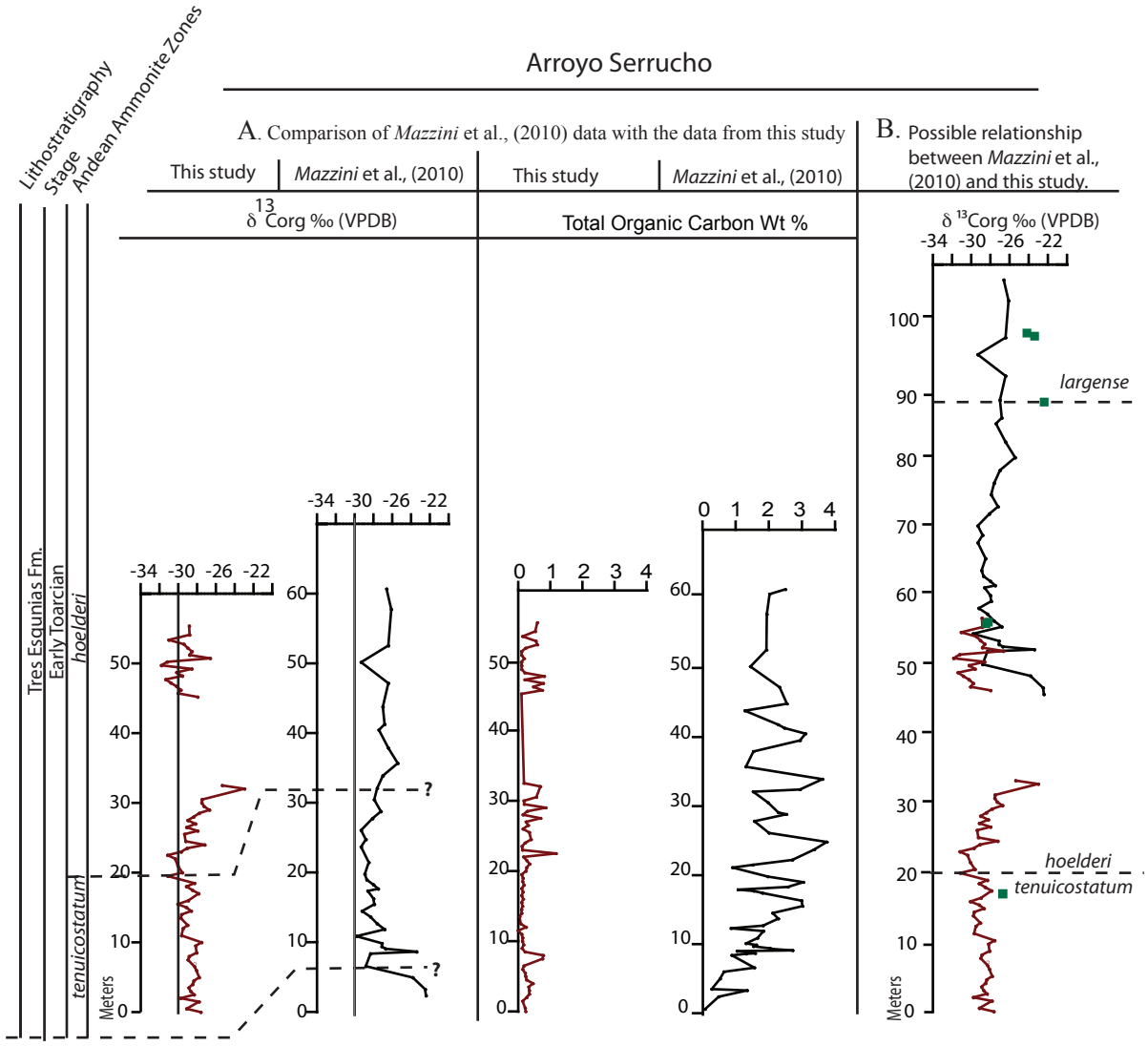


Figure 14 A. Figure showing a comparison of TOC wt% and $\delta^{13}C_{org}$ data from the Mazzini et al., (2010) study of Arroyo Serrucho compared to the Arroyo Serrucho data from this study. The Mazzini et al. (2010) biostratigraphy is poorly constrained and is based on the presence of the bivalve Bositra spp. which has a long range through the Pliensbachian–Toarcian, while the biostratigraphy in the Arroyo Serrucho sections in this study is based on detailed examination of ammonites through the sections. It is important to note that the Mazzini et al. (2010) $\delta^{13}C_{org}$ values are not indicative of typical T-OAE values from other sections in the Neuquén basin or around the world, values do not fall below -30‰. The Mazzini et al. (2010) data is not correlative with the data in this study from the *tenuicostatum–hoelderi* ammonite Zone boundary, in Arroyo Serrucho.

B. Based on field observations of the area and $\delta^{13}C_{org}$ correlation, the Mazzini et al. (2010) section sits above the Arroyo Serrucho section in this study as indicated in the composite $\delta^{13}C_{org}$ figure. Green squares indicate fossil wood $\delta^{13}C_{org}$ values.

hemisphere and confirm that introduction of isotopically light carbon into the atmosphere during the T-OAE was a phenomenon with global expression.

Furthermore, comparison of TOC and $\delta^{13}C_{org}$ from bulk sediment values from the Pliensbachian–Toarcian boundary show the presence of a negative carbon isotope excursion at this boundary, comparable to the excursion identified in sediments of a similar age in Yorkshire, England. The identification of this excursion may be a key stratigraphic tool in identifying this boundary in sections that lack good biostratigraphic or geochronological constraint. Further work needs to be conducted on other Southern Hemisphere sections of a similar age to develop a better understanding of the T-OAE outside the Tethyan and Boreal realm, but it appears that this event is globally synchronous.

References

Al-Suwaidi, A.H., Angelozzi, G.N., Baudin. F., Damborenea, S.E., Hesselbo, S.E., Jenkyns, H.C., Manceñido, M.O., and Riccardi, A.C., 2010, First Record of the Early Toarcian Oceanic Anoxic Event from the Southern Hemisphere, Neuquén Basin, Argentina: Journal of the Geological Society, v. 167, p. 633–636.

Blakey, R., 2007, Early Jurassic rectangular palaeogeographic map in mollewide: http://jan.ucc.nau.edu/~rcb7/200marect.jpg (November, 2009).

Bodin, S., Mattioli, E. Fröhlich, S., Marshall, J.D., Boutib, L., Lahsini, S., and Redfern, J., 2010, Toarcian carbon isotope shifts and nutrient changes from the Northern margin of Gondwana (High Atlas, Morocco, Jurassic): Palaeoenvironmental implications: Palaeogeography, Palaeoclimatology, Palaeoecology, v. 297, p. 377–390, doi:10.1016/j.palaeo.2010.08.018.

Caruthers, A.H., Gröcke, D.R., and Smith, P.L., 2011, The significance of an Early Jurassic (Toarcian) carbon-isotope excursion in Haida Gwaii (Queen Charlotte Islands), British Columbia, Canada: Earth and Planetary Science Letters, v. 307, p. 19–26 doi:10.1016/j.epsl.2011.04.013.

Cohen, A.S., 2004, The rhenium–osmium isotope system: applications to geochronological and palaeoenvironmental problems: Journal of the Geological Society, London, v. 161, p. 729–734.

Cohen, A.S. and Coe, A.L., 2007, The impact of the Central Atlantic Magmatic Province on climate and on the Sr- and Os-isotope evolution of seawater: Palaeoceanography, Palaeoclimatology, Palaoecology, v. 244, p. 374–390.

Demaison, G.J. and Moore, G.T., 1980, Anoxic environments and oil source bed genesis: AAPG Bulletin, v. 64, p. 1179–1209.

Gulisano, C.A. and Gutiérrez Pleimling, A.R., 1995, Field Guide. The Jurassic of the Neuquén Basin. (a) Neuquén Province. Asociación Geológica Argentina, Series E, No 2, Buenos Aires, Argentina, p. 1-111.

Gröcke, D.R., Hori, R.S., Trabucho-Alexandre, J., Kemp, D.B. and Schwark, L., 2011, An open marine record of the Toarcian oceanic anoxic event: Solid Earth Discussion, v. 3, p. 385-410. doi:10.5194/sed-3-385-2011.

Hesselbo, S.P., Gröcke, D.R., Jenkyns, H.C., Bjerrum, C.J., Farrimond, P., Morgans Bell, H.S. and Green, O.R., 2000, Massive dissociation of gas hydrate during a Jurassic oceanic anoxic event: Nature, v. 406, p. 392-395.

Hesselbo, S.P., Jenkyns, H.C., Duarte, L.V. and Oliveira, L.C.V., 2007, Carbon-isotope record of the Early Jurassic (Toarcian) oceanic anoxic event from fossil wood and marine carbonate (Lusitanian Basin, Portugal): Earth and Planetary Science Letters, v. 253, p. 455-470.

Hesselbo, S. P. and Piénkowski, G., 2010, Stepwise atmospheric carbon-isotope excursion during the Toarcian Oceanic Anoxic Event: Earth and Planetary Science Letters, v. 301, p. 365–372, doi: 10.1016/j.epsl.2010.11.021.

Hillebrandt, A., von, and Schmidt-Effing, R., 1981, Ammoniten aus dem Toarcium (Jura) von Chile (Südamerika): Zitteliana, v. 6, p. 3-74.

Jenkyns, H.C., 1988, The Early Toarcian (Jurassic) anoxic event; stratigraphic, sedimentary and geochemical evidence: American Journal of Science, v. 288, p. 101-151.

Jenkyns, H.C., 2010, Geochemistry of oceanic anoxic events: Geochemistry, Geophysics, Geosystems, v. 11, Q03004, doi. 10.1029/2009GC002788.

Jenkyns, H.C. and Clayton, C.J., 1986, Black shales and carbon isotopes in pelagic sediments from the Tethyan Lower Jurassic: Sedimentology, v. 33, p. 87-106.

Jenkyns, H.C., Gröcke, D.R. and Hesselbo, S.P., 2001, Nitrogen isotope evidence for water mass denitrification during the early Toarcian (Jurassic) oceanic anoxic event: Paleoceanography, v. 16, p. 593–603.

Jenkyns, H.C., Jones, C.E., Gröcke, D.R., Hesselbo, S.P. and Parkinson, D.N., 2002, Chemostratigraphy of the Jurassic system: applications, limitations and implications for palaeoceanography: Journal of the Geological Society, London, v. 159, p. 351-378.

Kafousia, N., Karakitsios, V., Jenkyns, H.C. and Mattioli, E., 2011, A global event with a regional character: the Early Toarcian Oceanic Anoxic Event in the Pindos Ocean (northern Peloponnese, Greece): Geoogical Magazine, v. 148, p. 619-631.

Kemp, D.B., Coe, A.L., Cohen, A.S. and Schwark, L., 2005, Astronomical pacing of methane release in the Early Jurassic period: Nature, v. 437, p. 396-399.

Littler, K., Hesselbo, S.P. and Jenkyns, H.C., 2010, A carbon-isotope perturbation at the Pliensbachian–Toarcian boundary: evidence from the Lias Group, NE England: Geological Magazine, v. 147, p. 181-192.

Mailliot, S., Mattioli, E., Guex, J. and Pittet, B., 2006, The Early Toarcian anoxia, a synchronous event in the Western Tethys? An approach by quantitative biochronology (Unitary Associations), applied on calcareous nannofossils: Palaeogeography, Palaeoclimatology, Palaeoecology, v. 240, p. 562-586.

Mattioli, E., Pittet, B., Bucefalo Palliani, R., Röhl, H.-J., Schmid-Röhl, A. and Morettini, E., 2004, Phytoplankton evidence for the timing and correlation of palaeoceanographical changes during the early Toarcian oceanic anoxic event (Early Jurassic): Journal of the Geological Society, London, v. 161, p. 685-693.

Mazzini, A., Svenson, H., Leanza, H.A., Corfu, F. and Planke, S., 2010, Early Jurassic shale chemostratigraphy and U-Pb ages from the Neuquén Basin (Argentina): Implications for the Toarcian Oceanic Anoxic Event: Earth and Planetary Science Letters, v. 297, p. 633-645. doi:10.1016/j.epsl.2010.07.017.

McArthur, J.M., Algeo, T.J., Schootbrugge, B. van de, Li, Q. and Howarth, R.J., 2008, Basinal restriction, black shales, Re-Os dating, and the Early Toarcian (Jurassic) oceanic anoxic event: Paleoceanography, v. 23, PA4217, doi:10.1029/2008PA001607.

McElwain, J.C., Wade-Murphy, J. and Hesselbo, S.P., 2005, Changes in carbon dioxide during an oceanic anoxic event linked to intrusion into Gondwana coals: Nature, v. 435, p. 479–482, doi:10.1038/nature03618.

Page, K.N., 2003, The Lower Jurassic of Europe: its subdivision and correlation, *in* Ineson, J.R. and Surlyk, F., eds., The Jurassic of Denmark and Greenland. Geological: Geological Survey of Denmark and Greenland Bulletin, 1, GEUS, Copenhagen, Denmark p. 23-59.

Page, K.N., 2004, A sequence of biohorizons for the subboreal province Lower Toarcian in Northern Britain and their correlation with a submediterranean standard: Rivista Italiana di Paleontologia e Stratigrafia, v. 110, p. 109-114.

Riccardi, A.C., 2008, El Jurásico de la Argentina y sus Amonites: Revista de la Asociación Geológica Argentina, v. 63, p. 625-643.

Sabatino, N., Neri, R., Bellanca, A., Jenkyns, H.C., Baudin, F., Parisi, G. and Masetti, D., 2009, Carbon-isotope records of the Early Jurassic (Toarcian) oceanic anoxic event from the Valdorbia (Umbria–Marche Apennines) and Monte Mangart (Julian Alps) sections: palaeoceanographic and stratigraphic implications: Sedimentology, v. 56, p. 1307-1328.

Schmid-Röhl, A., Röhl, H.-J., Oschmann, W., Frimmel, A. and Schwark, L., 2002, Palaeoenvironmental reconstruction of Lower Toarcian epicontinental black shales (Posidonia Shale, SW Germany): global versus regional control: Geobios, v. 35, p. 13-20.

Suan, G., Nikitenko, B.L., Rogov, M.A., Baudin, F., Spangenberg, J. E., Knyazev, V. G., Glinskikh, L.A., Goryacheva, A. A., Adatte, T., Riding, J.B., Föllmi, K.B., Pittet, B., Mattioli, E. and Lécuyer, C., 2011, Polar record of the Early Jurassic massive carbon injection: Earth and Planetary Science Letters, v. 312, p. 102–113, doi: 10.1016/ j.epsl.2011.09.050.

Svenson, H., Planke, S., Chevallier, L., Malthe-Sørenssen, A., Corfu, F. and Jamtveit, B., 2007, Hydrothermal venting of greenhouse gases triggering Early Jurassic global warming: Earth and Planetary Science Letters, v. 256, p. 554–566, doi:10.1016/j.epsl.2007.02.013.

van de Schootbrugge, McArthur, J.M., Bailey, T.R., Rosenthal, Y., Wright, J.D. and Miller, K.G., 2005b, Toarcian oceanic anoxic event: An assessment of global cuases using belemnite C isotope records: Paleoceanography, v. 20, PA3008, 12 p., doi:10.1029/2004PA001102.

Vicente, J.C., 2005, Dynamic paleogeography of the Jurassic Andean Bas*in,* pattern of transgression and localisation of main straits through the magmatic arc: Revista de la Asociación Geológica Argentina, v. 60, p. 221-250.

Wignall, P.B., Newton, R.J. and Little, C.T.S., 2005, The timing of paleoenvironmental change and cause-and-effect relationships during the Early Jurassic mass extinction in Europe: American Journal of Science, v. 305, p. 1014-1032.

.

Chapter 4

A Multiproxy Examination of the Toarcian Oceanic Anoxic Event, Arroyo Lapa, (North and South) Neuquén Basin, Argentina

Abstract:

The Toarcian, Early Jurassic, Oceanic Anoxic Event (T-OAE: ~183 Ma) was characterized by globally synchronous deposition of sediments rich in organic carbon (black shales), and is associated with an abrupt negative carbon isotope excursion, disrupting a positive carbon-isotope excursion during the *tenuicostatum–serpentinum* ammonite Zone boundary. These disturbances are recorded in bulk sedimentary organic matter, carbonate and fossil wood, the latter recording the isotopic composition of the atmosphere. The T-OAE has been extensively studied in Northern and Southern Europe and new studies from the southern hemisphere have provided chemostratigraphic evidence for the global imprint of the event. Here we present new geochemical data from the Neuquén Basin, Argentina: bulk-sediment $\delta^{13}C$ values fall to -32.5‰ and $\delta^{13}C$ values from fossil wood fall to -30.7 ‰, isotopic ratios that are comparable to those identified in Europe for the T-OAE. Hydrogen Index (HI) data for the T-OAE in Argentina give values ranging from 12 to 425 mg HC/ g TOC, indicating a mixture of terrestrial and marine organic components. Pristane/Phytane ratios and pyrite framboid distribution data indicative of anoxic conditions occur at some levels, and new $\delta^{98/95}Mo$ data, with values ranging from ~ -0.2 to 0.78 ‰, which contrast with previously published molybdenum-isotope values from T-OAE black shales of northern Europe.

4.1. Introduction

Ocean Anoxic Events, (OAE's) were initially recognized by a globally synchronous increase in the burial of organic carbon (Schalanger and Jenkyns, 1976), and by 1980 Scholle and Arthur had also recognized these events in the pelagic carbon-isotopic record. Today a wide array of tools are available to examine all aspects of OAEs; including carbon isotopes from wood, bulk sediment and carbonate; hydrogen index (e.g. Langford and Blanc-Valleron, 1990; Baudin et al., 1989; Sælen et al., 1996; Schouten et al., 2000; Palliani et al., 2002; Sabatino et al., 2009); pyrite framboid diameter distribution (e.g. Jenkyns et al., 2001, 2002; Sabatino et al., 2011); biomarker analysis including; Pristane, Phytane, Steranes, Hopanes, and isoreineratene (eg. Moldowan et al., 1985; Frimmel et al., 2004; Pancost et al., 2004; Peters et al., 2005 a, b; van de Schootbrugge et al., 2005a; van Breugal et al., 2006); and novel metal isotope analysis, including iron, thallium and molybdenum, which reflect redox potential in the water column (e.g. Emmerson and Huested, 1991; Morford and Emmerson, 1999; Siebert et al., 2003, 2006, 2011; Anbar and Rouxel, 2007; Archer and Vance, 2008; Pearce et al., 2008; Gill et al., 2011; Nielson et al., 2011) and isotopes of nitrogen; sulphur, strontium, uranium, and osmium (e.g. Peucker-Ehrinbrink and Ravizza, 2000; Jones and Jenkyns, 2001; Jenkyns et al., 2002, 2007; Cohen, 2004; Cohen and Coe, 2007; Jenkyns, 2010) with new isotope systems being developed such as calcium and chromium (Ellis et al., 2002; Johnson and Bullen, 2004, Amor et al., 2008; Lu et al., 2010; Blättler et al., 2011).

Many of these new proxies have been widely tested in modern euxinic settings such as the Black Sea and the Cariaco basin (e.g. Algeo and Lyons, 2006; Anbar and Rouxel, 2007 Lyons et al., 2009) but multi-proxy records of ancient OAEs are limited, and multiproxy records of the Toarcian, OAE (T-OAE, 183 Ma) are limited to European sections

from the Tethyan and Boreal region (e.g. Moldowan et al., 1985; Baudin et al., 1989; Jones and Jenkyns, 2001; Jenkyns et al. 2001, 2002, 2007; Cohen, 2004; van Breugal et al., 2006; McArthur et al., 2008; Pearce et al., 2008; Jenkyns, 2010; Suan et al., 2011).

In this chapter, new multiproxy data from two biostratigraphically constrained, Pliensbachian–Early Toarcian sections in the southern hemisphere, Arroyo Lapa North and South, Neuquén Basin Argentina are presented. Data includes an overview of biostratigraphy, sedimentology and carbon-isotope chemostratigraphy, $\delta^{13}C_{org}$ (details in Chapter 2 and 3); Hydrogen Index (HI) and total organic carbon (TOC) data; biomarker data (pristine, phytane, sterane and hopanes); molybdenum concentrations and isotopes ($^{98/97}Mo$) and data on pyrite framboid diameter. These data are compared with coeval records from the Northern Hemisphere, specifically the Posidonia Black Shale from SW Germany (Frimmel et al., 2004) and the Mulgrave Shale from Yorkshire, England (Kemp et al., 2005, Pearce et al., 2008), Pyrite Framboid diamters where also measured in samples from Port Mulgrave Yorkshire, to compare with coeval samples from the Neuquén Basin, to better understand the global impact of the Toarcian Ocean Anoxic Event.

4.2. Geological and paleogeographical setting: Arroyo Lapa North and South.

The Neuquén Basin is a roughly triangular back-arc basin, located on the eastern side of the Andes, with a complicated multiphase tectonic history. During the Early Jurassic, the Neuquén Basin was fed marine waters from Panthalassa through a volcanic island arc on its western margin and a northern channel. This study is concerned with sediments from the Arroyo Lapa area located in the southern part of the basin, on the eastern slope of Sierra de Chacacico, 50 km southwest of the town of Zapala in the Neuquén province. Three stratigraphic sections were examined in this area (1) Arroyo Lapa South, 2008 (Pliensbachian to Early Toarcian, *fannini* to *hoelderi* ammonite Zones); (2) Arroyo Lapa

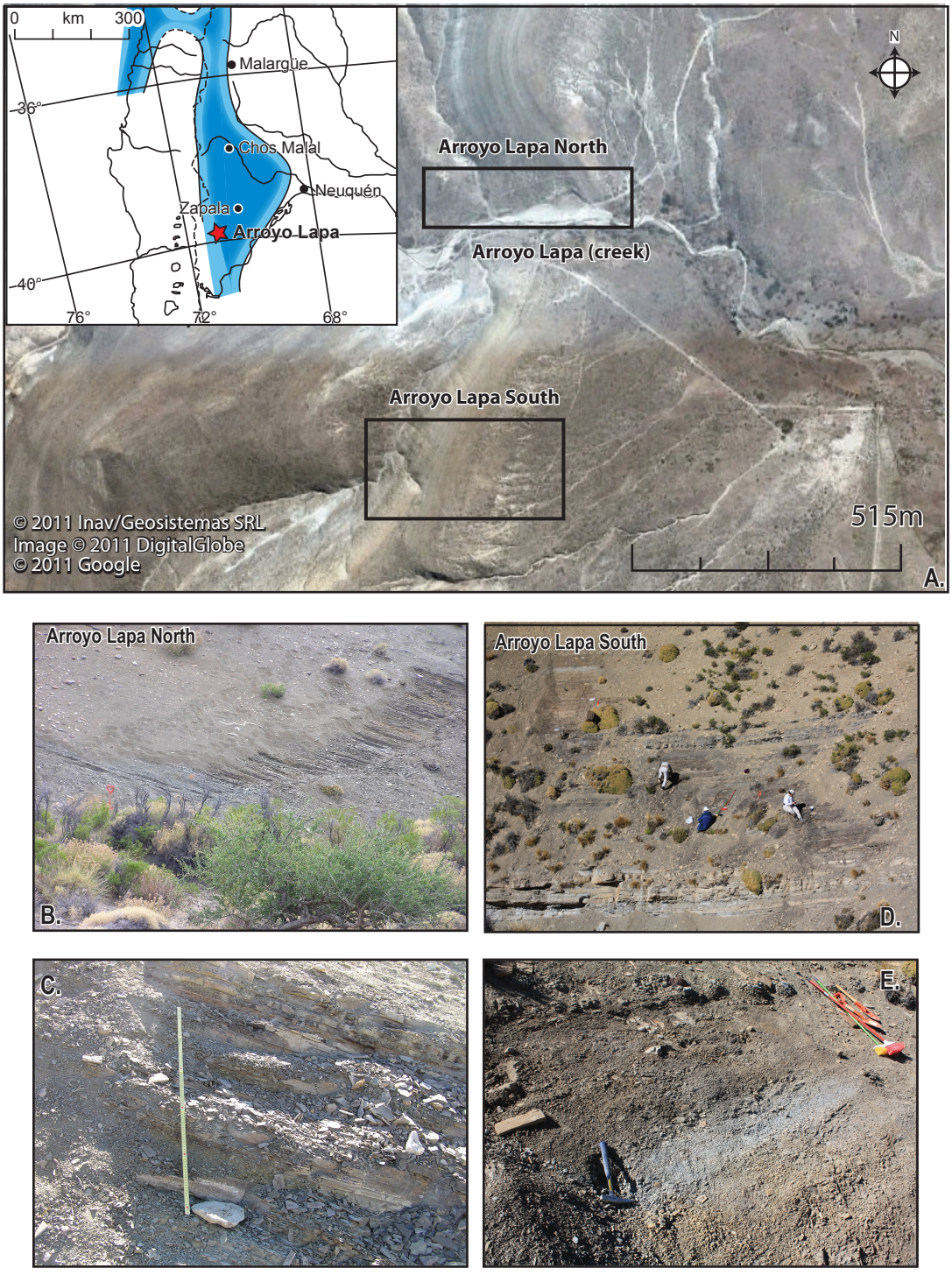


Figure 1 A. Satellite image of the Arroyo Lapa field locality indicating the location of Arroyo Lapa South and Arroyo Lapa North, in the Sierra de Chacaico area, Neuquén Province, Argentina, latitude and longitude, S 39º 24' 04", W 70º 25' 43" , elevation 1311 m. Inset shows the approximate location of the field area in the Neuquén Basin, adapted from Vicente (2005), satellite image courtesy of Google Earth (2005). Photographs B–C show the section at Arroyo Lapa North (B) and typical laminated shaly sediments (C). Photographs D–E show the section at Arroyo Lapa South (D) and typical sediments from the section (E).

South 2010 (Early Toarcian, *tenuicostatum to hoelderi* ammonite Zones) and finally (3) Arroyo Lapa North, on the Northern side of the Arroyo Lapa creek (Early Toarcian, *tenuicostatum to hoelderi* ammonite Zones).

The Arroyo Lapa Area comprises about 900 m of Late Triassic–Early Jurassic sediments representing the Late Triassic to Earliest Jurassic pyroclastic deposits of the Lapa Formation, and Pliensbachian–Aalenian outer shelf to basinal shales and sandstones of the Los Molles Formation (Gulisano & Gutiérrez Pleimling, 1995). The stratigraphy of the Arroyo Lapa section has been previously studied on the basis of ammonites (von Hillebrandt, 1973, 1987, 2006; von Hillebrandt & Schmidt-Effing, 1981), teuthids (Riccardi, 2005), palynomorphs (Volkheimer, 1973), bivalves (Damborenea, 1987) and palaeomagnetic data (Iglesia Llanos & Riccardi, 2000).

The deposits at Arroyo Lapa North and South are assumed to be a part of a similar depositional system, given the close proximity of these two sections. the Arroyo Lapa sections are both dominated by turbidite deposits with coarse grained sandstone bases, grading to fine mudstone units. The presence of thin, relatively un-reworked tuffaceous material throughout the sections suggests close proximity to a volcanic source area. Deposits of beds rich in charcoalified wood indicate that the sections at Arroyo Lapa were relatively close to a continental source of sediment. Gulisano & Gutiérrez Pleimling (1995) interpreted the turbiditic part of the section as representing deposits from submarine fan channel-levee complexes, including overbank finer deposits. This channel-levee complex system may account for the difference in sedimentation from Arroyo Lapa South to Arroyo Lapa North.

Details of the biostratigraphy, sedimentology and paleogeography of the sections examined in this study can be found in Chapter 2.

4.3. Materials and Methods:

Arroyo Lapa South was initially described in 2008 and a 50 cm resolution bulk organic matter $\delta^{13}C$ and TOC chemostratigraphic profile was generated that spanned from the latest Pliensbachian and Early Toarcian. A second higher resolution examination of the section took place in 2010 and bulk sediment samples were collected at 10 cm intervals through the upper *tenuicosotatum–hoelderi* Andean ammonite Zone, approximately equivalent to the *tenuicostatum–serpentinum* (= *falciferum*) ammonite Zone of northwestern Europe (von Hillebrandt and Schmidt-Effing, 1981; Page, 2004; Riccardi, 2008), and an additional 7 m of section was measured and sampled to capture the entire Toarcian Carbon Isotope Excursion (T-CIE). In the Arroyo Lapa South 2008 section, a total of 15 fossil wood fragments were collected from outcrop, with an additional 13 samples recovered from bulk rock (full details of data are given in Appendix A, Fig. 1). A total of 52 wood fragments were recovered from bulk rock samples, in the Arroyo Lapa South 2010 section (full details are given in Appendix A, Fig. 2).

In the Arroyo Lapa South, 2010 area a total of 22 samples were collected in glass for biomarkers, pyrite framboid diameter distribution and molybdenum analysis. An additional 7 samples were examined for biomarkers from the Arroyo Lapa South, 2008 section to determine background concentrations of the biomarkers examined. A total of 74 samples and 12 duplicates from Arroyo Lapa South 2008 and 2010 sections were examined using Rock-Eval pyrolysis for Hydrogen Index.

At Arroyo Lapa North, bulk sediment samples were collected at 10 cm intervals and a total of 34 fossil wood samples were recovered; 8 of these samples were recovered from bulk sediment samples, while the remaining were recovered from the section (full details are given in Appendix A, Fig. 3). High-resolution $\delta^{13}C$ and TOC analysis remains to be

completed for this section, and the current resolution of data is 50 cm, except in the upper 5 m where the resolution is 10 cm. In the Arroyo Lapa North section a total of 11 samples were collected in glass jars for biomarkers, pyrite framboid diameter distribution, molybdenum and Rock-Eval pyrolysis.

4.4. Results:

Table 1: Sample list including biostratigraphy, sediment type and pyrite framboid data

Equivalent Bulk Sed. Sample #	Height*(m)	Biomarker Sample #	Ammonite Zone	Sediment Type	Pyrite Frambs. Diameter $\bar{X} \pm \sigma$ (µm)
Arroyo Lapa South 2008					
AL-7	-50.93	ARG-AL-7	disciforme	Sandy Shale	
AL-11	-49.05	ARG-AL-11	disciforme	Shale	
AL-17	-46.03	ARG-AL-17	disciforme	Shale	
AL-44	-32.57	ARG-AL-44	disciforme	Shale	
AL-50	-29.50	ARG-AL-50	disciforme	Sandy Shale	
AL-66	-21.50	ARG-AL-66	disciforme	Shale	
AL-94	-7.50	ARG-AL-94	tenuicostatum	Shale	
Arroyo Lapa South 2010					
AL-215	1.00	AL-BM-1	tenuicostatum	Shale	4.37 ± 3.22
AL-225	2.00	AL-BM-8	tenuicostatum	Shale	26.67 ± 10.32
AL-235	3.00	AL-BM-2	tenuicostatum	Shale	9.00 ± 1.41
AL-245	4.00	AL-BM-9	tenuicostatum	Shale	no framboids
AL-255	5.00	AL-BM-3	tenuicostatum	shale	8.07 ± 6.05
AL-265	6.00	AL-BM-10	tenuicostatum	laminated Shale	no framboids
AL-275	7.00	AL-BM-4	hoelderi	Shale	no framboids
AL-285	8.00	AL-BM-11	hoelderi	Shale	no framboids
AL-295	9.00	AL-BM-5	hoelderi	Shale	6.20 ± 3.02
AL-305	10.00	AL-BM-12	hoelderi	Shale	no framboids
AL-315	11.00	AL-BM-6	hoelderi	Shale	7.27 ± 3.85
AL-325	12.00	AL-BM-13	hoelderi	Sandy Shale	5.83 ± 3.39
AL-335	13.00	AL-BM-7	hoelderi	Sandy Shale	no framboids
AL-345	14.00	AL-BM-14	hoelderi	Shale	8.13 ± 3.39
AL-355A	15.00	AL-BM-15	hoelderi	Shale	7.30 ± 3.15
AL-363	16.00	AL-BM-16	hoelderi	Shale	no framboids
AL-373	17.00	AL-BM-17	hoelderi	Sandy shale	no framboids
AL-383	18.00	AL-BM-18	hoelderi	Shale	no framboids
AL-393	19.00	AL-BM-19	hoelderi	Shale	no framboids
AL-403	20.00	AL-BM-20	hoelderi	Shale	6.58 ± 4.60
AL-413	21.00	AL-BM-21	hoelderi	Shale	no framboids
AL-423	22.00	AL-BM-22	hoelderi	Shale	7.83 ± 4.11
Arroyo Lapa North					
LN-304	0.4	LN-BM-12	tenuicostatum	Shale	no framboids
LN-314	1.4	LN-BM-13	tenuicostatum	Shale	no framboids

LN-324	2.4	LN-BM-9	tenuicostatum	Sandy Shale	7.27 ± 5.43
LN-334	3.4	LN-BM-10	tenuicostatum	Shale	11.59 ± 10.07
LN-343	4.3	LN-BM-11	tenuicostatum	Sandy Shale	no framboids
Exposure gap					
LN-1	8.1	LN-BM-1	tenuicostatum	Shale	16.80 ± 14.04
LN-21	10.1	LN-BM-2	tenuicostatum	Sandy Shale	no framboids
LN-41	12.1	LN-BM-3	tenuicostatum–hoelderi	Shale	Polyframboids common.
LN-61	14	LN-BM-4	tenuicostatum–hoelderi	shale	no framboids
LN-81	16	LN-BM-5	hoelderi	shale	no framboids
LN-101	18	LN-BM-6	hoelderi	shale	no framboids
LN-121	20	LN-BM-7	hoelderi	shale/fossilbed	no framboids
LN-141	24.1	LN-BM-8	hoelderi	Shale	5.50 ± 3.65

4.4.1. Fossil Wood and Bulk Sediment Organic Carbon Isotopes and Total Organic Carbon

In Arroyo Lapa South, (composite section 2008 and 2010) bulk organic-carbon $\delta^{13}C$ values fall to ~ -32.5‰ about 3 m above the *tenuicostatum–hoelderi* boundary (~10 m) and values remain below -28‰ through the lower part of the *hoelderi* Zone; at what is inferred to be the same biostratigraphic level in Yorkshire very similar values are recorded by Hesselbo et al. (2000) and Jenkyns et al. (2002), and slightly lower ones (~ -33‰) in the very high-resolution record of Kemp et al. (2005). Typical extreme $\delta^{13}C_{org}$ values have also been recorded in other locations in Europe, Morroco, Canada and Japan for the T-OAE range from -30‰ to -33‰ (e.g., Jenkyns and Clayton, 1986; Schmid-Röhl et al., 2002; Sabatino et al., 2009; Jenkyns, 2010; Bodin et al., 2011; Caruthers et al., 2011, Gröcke et al., 2011, Kafousia et al., 2011).

The $\delta^{13}C_{wood}$ record also shows the -6‰ negative shift leading up to the *tenuicostatum–hoelderi* boundary, as is the case in Yorkshire and sections elsewhere in Europe (Hesselbo et al., 2000, 2007). The fossil wood data provide an independent carbon-isotope record for the Southern hemisphere that is not affected by any local oceanographic restriction of the Neuquén Basin.

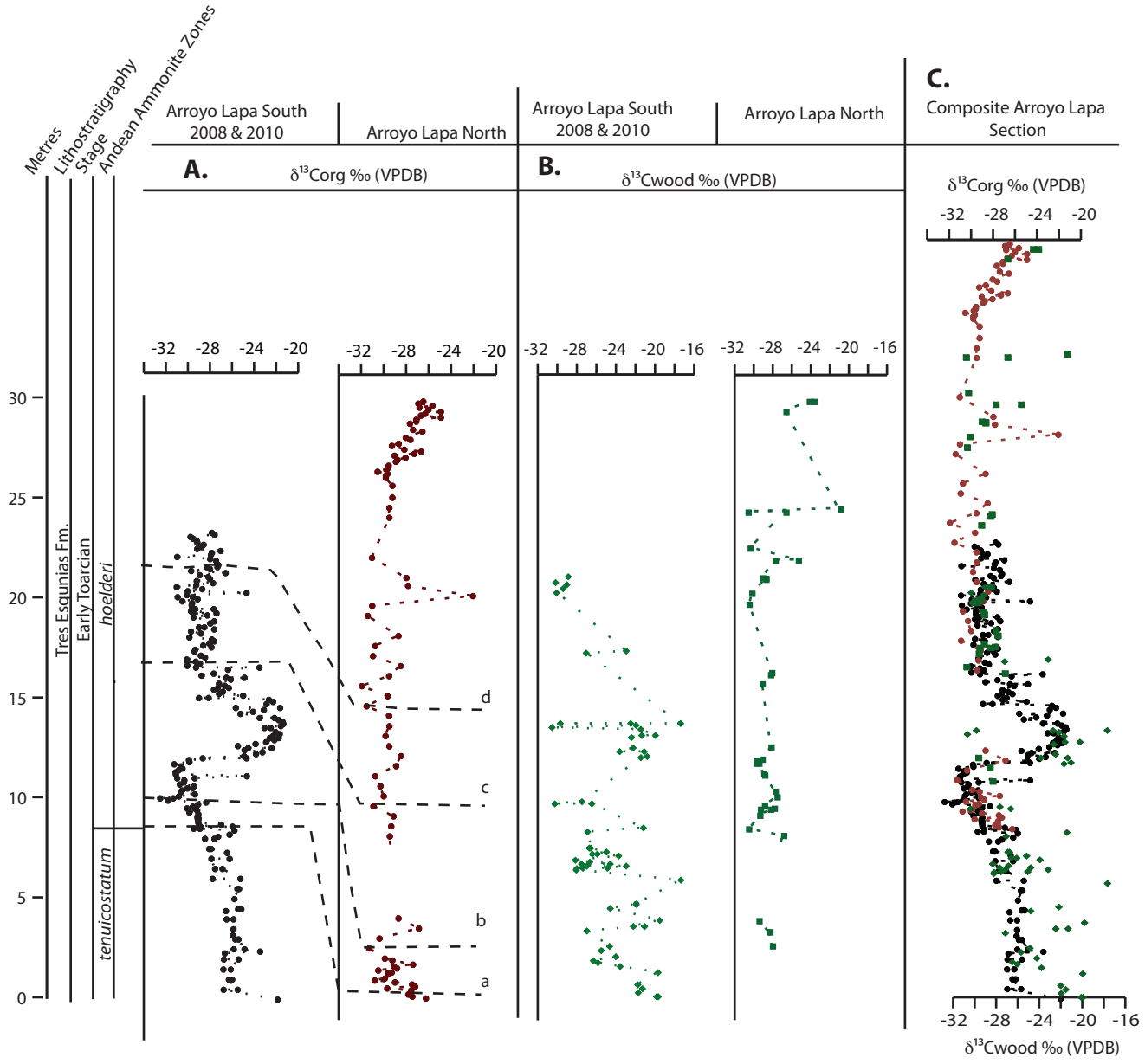


Figure 2. Comparison of data from Arroyo Lapa South (2008 and 2010) and Arroyo Lapa North based on $\delta^{13}C_{org}$ values from bulk sediment. (A) Correlation of the two sections is indicated bydashed black lines a–d and is based on $\delta^{13}C_{org}$ values and steps in the chemostratigraphic profiles. (B) Comparison of the $\delta^{13}C_{wood}$ values from the two sections does not show any direct correlation. (C) A composite of the bulk sediment and fossil wood data from Arroyo Lapa North and Arroyo Lapa South based on the correlation in A. It appears that regardless of local varaitions in deposition the chemostratigraphic signal can be correlated and shows a complete negative excursion and positive recovery in the *tenuicostatum–hoelderi* ammonite zone in the Arroyo Lapa area.

Total Organic Carbon (TOC) weight percentages range from 0.09 to a maximum of 10.26% at the summit of the *tenuicostatum* ammonite Zone. TOC increases towards the *tenuicostatum–hoelderi* ammonite Zone boundary and then decreases following it.

In the Arroyo Lapa North section index species indicative of the *tenuicostatum* ammonite Zone were not identified, and the $\delta^{13}C_{org}$ data can be used to correlate the section with the section at Arroyo Lapa South (Fig. 2), and indicates that the Arroyo Lapa North section records the summit of the negative excursion and its recovery. $\delta^{13}C_{org}$ values fall to -31.9‰ at ~7.5 m and remain below -28‰ through the *hoelderi* Zone. The $\delta^{13}C_{wood}$ record also shows a -9‰ negative shift with values falling as low as -30.7‰ at 2.5 m. Fossil wood values remain light (below -26‰), though the remainder of the section with somewhat heavier values (~ -24‰) at the top of the section.

The total organic carbon in this section is relatively low throughout, remaining below ~1% for about 15 m, and increases upward through the section. There is a slight increase at 14.5 m with TOC increasing to ~ 2.5%. The amount of fossil wood increases up through the section becoming abundant in the upper 5 m, which accounts for the elevated TOC in this part of the section. Details of the TOC, $\delta^{13}C$ chemostratigraphy and chemostratigraphic correlation between Arroyo Lapa North and South can be found in Chapter 3.

Table 2: Organic carbon-isotope data, total organic carbon and molybdenum data.

Biomarker Sample #	Height*(m)	TOC %	$\delta^{13}C$ ‰ (PDB)	$\delta^{98}Mo$ ‰	[Mo] ppm	1/[Mo]ppm
Arroyo Lapa South 2008						
ARG-AL-7	-50.93	0.07	-28.48			
ARG-AL-11	-49.05	0.32	-25.65			
ARG-AL-17	-46.03	2.97	-26.76			
ARG-AL-44	-32.57	1.24	-24.44			
ARG-AL-50	-29.50	0.34	-27.45			
ARG-AL-66	-21.50	0.82	-24.29			
ARG-AL-94	-7.50	4.28	-25.16			
Arroyo Lapa South 2010						
AL-BM-1	1.00	2.43	-26.14	0.78	4.8	0.2083
AL-BM-8	2.00	4.96	-24.9	0.40	1.5	0.6667

AL-BM-2	3.00			0.14	2.1	0.4762
AL-BM-9	4.00	4.62	-24.79	0.78	1.9	0.5263
AL-BM-3	5.00	3.06	-25.54	0.40	1.8	0.5556
AL-BM-10	6.00	10.26	-27.55	0.53	4.6	0.2174
AL-BM-4	7.00	8.43	-26.11	0.31	1.6	0.6250
AL-BM-11	8.00	0.91	-26.94	0.22	3.8	0.2632
AL-BM-5	9.00	2	-29.18	0.19	3.6	0.2778
AL-BM-12	10.00	0.31	-29.46	0.45		
AL-BM-6	11.00	0.49	-30.59	0.13	2.8	0.357
AL-BM-13	12.00	0.89	-24.56	-0.11	2.2	0.455
AL-BM-7	13.00	0.74	-23.07	-0.13	3.3	0.303
AL-BM-14	14.00	0.74	-21.66	0.39	2.1	0.476
AL-BM-15	15.00	0.11	-27.30	0.00	3.1	0.323
AL-BM-16	16.00	0.52	-29.29	-0.09	3	0.333
AL-BM-17	17.00	0.11	-27.90	0.08	2.4	0.417
AL-BM-18	18.00	0.2	-29.02	0.28	1.9	0.526
AL-BM-19	19.00	0.39	-29.67	0.14	3.4	0.294
AL-BM-20	20.00	0.72	-31.04	-0.01	3	0.333
AL-BM-21	21.00	0.12	-28.33	-0.07	2.8	0.357
AL-BM-22	22.00	0.13	-28.78	0.18	2.1	0.476
Arroyo Lapa North						
LN-BM-9	2.4	n/d	n/d	0.10	1.7	0.5882
LN-BM-10	3.4	n/d	n/d	n/d	n/d	n/d
LN-BM-11	4.3	n/d	n/d	n/d	n/d	n/d
Exposure gap						
LN-BM-1	8.1	0.424	-29.48	0.56	1.3	0.7692
LN-BM-2	10.1	0.187	-30.00	0.17	1.40	0.7143
LN-BM-3	12.1	0.161	-28.47	0.09	1.40	0.7143
LN-BM-4	14	0.526	-29.53	0.26	2.40	0.4167
LN-BM-5	16	1.38	-29.53	0.15	2.50	0.4000
LN-BM-6	18	0.182	-29.71	0.24		
LN-BM-7	20	0.378	-22.07	0.37	1.50	0.6667
LN-BM-8	24.1	2.468	-29.50	0.56	1.90	0.5263

4.4.2 Hydrogen Index and Total Organic Carbon

Bulk sediment samples from Arroyo Lapa were analysed using Rock Eval Pyrolysis (Espitalié et al., 1985a, b) as detailed Chapter 1.4.4. Table 4 shows the results of rock-eval pyrolysis for the Arroyo Lapa North and South sections as well as the total organic carbon as measured using a Coloumat 253 (Chapter 1.4.1). Hydrogen Index (HI) values in the sediments from Arroyo Lapa South range from 110 to 450 mg HC/g TOC, indicating a mixture of terrestrial and marine organic components in the section. More specifically, samples leading up to and just above the *tenuicostatum–hoelderi* ammonite Zone boundary

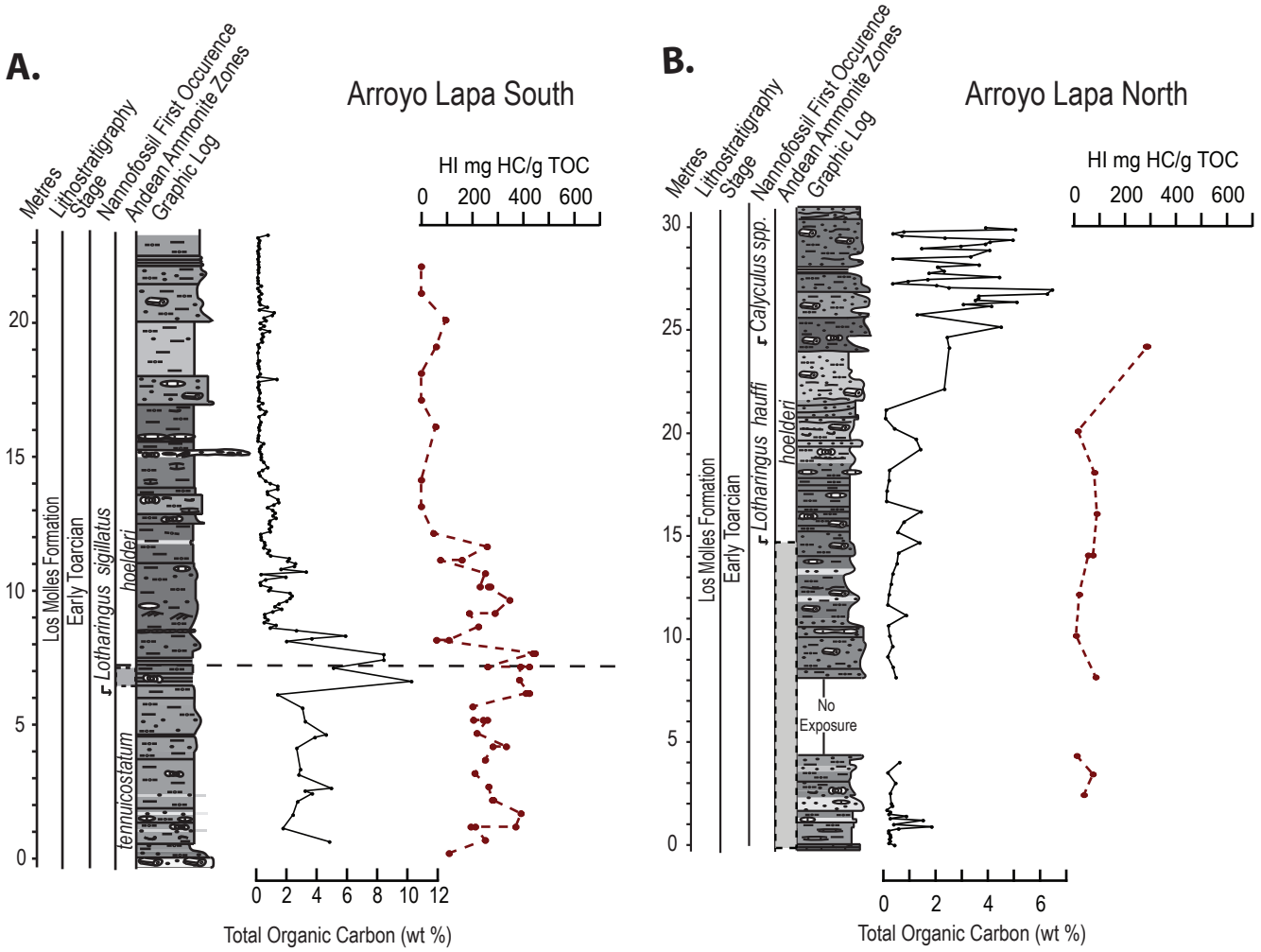


Figure 3. Hydrogen Index (HI) values and TOC in (A) Arroyo Lapa South and (B) Arroyo Lapa North. HI values indicate a mixture of terrestrial and marine organic components in the section. More specifically in Arroyo Lapa South samples, leading up to and just above the *tenuicostatum–hoelderi* boundary (~5m) give progressively increasing HI values, over the range 200 to 450 mg HC/g TOC, which show that the preservation of marine organic matter and/or its ratio to terrestrial organic matter increases in this interval (Baudin et al., 1990). The overall range of HI values in the section is very similar to that recorded in coeval Early Toarcian pelagic black shales in Italy and Greece (Baudin et al., 1990; Sabatino et al., 2009). HI values in Arroyo Lapa North are much lower, ranging from 12–293, suggesting the dominance of terrestrial organic matter in the section, with increased marine organic matter at the top of the section at 24.1m where values reach 293.

.

(~5–8m) give progressively increasing HI values, over the range 200 to 450 mg HC/g TOC, which is indicative of more marine and microalgal organic mater. In the upper part of the section (10–22 m), HI values decrease and range between 49 to 250 mg HC/g TOC, indicative of more terrestrial organic matter.

Table 4: Rock Eval Pyrolysis Results for Arroyo Lapa South 2008 and 2010

	Rock Eval. Pyrolysis Results					
Sample	Height*(m)	S1 mg/g	S2 mg/g	TOC %	Tmax °C	HI (mg HC/g TOC)
AL-79	-15.00	1.23	13.07	2.90	435	450
AL-80	-14.50	0.81	8.51	3.56	433	239
Duplicate Al-80	-14.50	0.87	8.17	3.44	430	237
AL-81	-14.00	0.60	7.20	3.24	432	222
AL-82	-13.50	1.06	3.91	3.28	436	119
AL-83	-13.00	0.52	5.88	2.97	432	197
AL-84	-12.50	0.76	7.63	3.60	432	211
AL-85	-12.00	0.33	2.63	2.00	436	131
AL-86	-11.50	0.73	12.77	4.47	431	285
AL-87	-11.00	0.77	9.22	3.03	431	304
AL-88	-10.50	0.37	2.90	2.03	436	142
AL-89	-10.00	0.57	3.83	2.60	436	147
Duplicate Al-89	-10.00	0.81	4.01	2.56	439	156
AL-90	-9.50	0.69	7.74	4.18	432	185
AL-91	-9.00	0.61	3.93	2.90	437	136
AL-92	-8.50	0.80	7.44	4.08	432	182
Duplicate Al-92	-8.50	0.56	5.41	3.84	437	141
AL-93	-8.00	0.60	4.72	2.88	434	163
AL-94	-7.50	0.75	8.92	4.27	438	208
AL-95	-7.00	0.65	8.97	4.02	436	223
AL-96	-6.50	0.61	4.78	3.87	433	124
AL-97	-6.00	0.38	2.07	1.46	435	141
AL-98	-5.50	0.56	2.04	1.47	436	138
Duplicate Al-98	-5.50	0.67	2.54	2.29	438	110
AL-99	-5.00	0.22	2.47	2.00	441	124
Duplicate Al-99	-5.00	0.26	2.47	1.98	438	125
AL-100	-4.50	1.10	6.22	2.91	431	213
AL-101	-4.00	0.63	4.85	2.44	432	198
AL-102	-3.50	0.50	2.50	1.77	436	141
AL-103	-3.01	0.59	2.03	1.37	435	148
AL-104	-2.51	0.71	3.02	1.67	436	180
AL-105	-2.00	0.72	3.62	1.67	432	216
AL-106	-1.50	0.48	8.93	3.51	434	254
AL-109	0.00	0.95	2.73	2.46	436	110
AL-110	0.50	0.97	6.82	2.70	432	252
AL-215	1.00	0.72	4.77	2.25	438	212
Duplicate Al-215	1.00	1.43	4.76	2.44	438	195
AL-111	1.00	0.90	13.77	3.71	431	371

AL-112	1.50	0.70	17.72	4.52	431	392
AL-225	2.00	0.88	11.84	4.17	431	283
AL-113	2.00	0.63	10.90	3.90	431	279
AL-235	2.50	0.29	5.00	1.88	435	265
AL-114	2.50	0.32	7.18	2.35	433	305
AL-115	3.00	0.41	3.20	1.52	434	210
AL-116	3.50	0.27	4.45	1.77	434	251
AL-245	4.00	0.57	11.43	4.05	431	282
AL-117	4.00	0.39	13.53	4.04	432	334
AL-118	4.50	0.31	5.86	2.69	434	218
		Rock Eval. Pyrolysis Results				
Sample	**Height*(m)**	**S1 mg/g**	**S2 mg/g**	**TOC %**	**Tmax °C**	**HI (mg HC/g TOC**
AL-255	5.00	1.32	8.02	3.08	437	260
AL-119	5.00	0.27	4.98	2.04	433	244
Duplicate AL-119	5.00	0.32	5.01	2.44	436	205
AL-120	5.50	0.29	3.03	1.50	435	202
AL-265	6.00	1.55	20.44	4.97	435	411
Duplicate Al-265	6.00	1.60	20.74	4.90	436	423
AL-121	6.00	0.45	16.13	3.80	430	424
AL-122	6.50	0.66	25.55	6.64	432	385
AL-275	7.00	3.40	27.91	7.14	430	390
Duplicate Al-275	7.00	1.74	29.36	6.90	432	425
AL-123	7.00	0.13	12.70	4.87	429	261
AL-124	7.50	1.43	24.46	5.57	429	439
Duplicate Al-124	7.50	1.38	25.00	5.59	431	447
AL-285	8.00	0.08	0.55	0.91	443	60
AL-125	8.00	0.19	0.53	0.49	441	108
AL-126	8.50	0.57	4.02	1.79	438	225
AL-295	9.00	0.25	2.99	1.59	437	188
AL-127	9.00	0.35	8.82	3.04	432	290
Duplicate Al-127	9.00	0.74	9.32	3.21	433	290
AL-128	9.50	0.60	9.40	2.70	431	348
AL-305	10.00	0.93	5.05	1.91	438	264
Duplicate Al-305	10.00	0.99	5.32	1.95	435	272
AL-129	10.00	0.32	2.50	1.08	440	231
AL-130	10.50	0.47	5.58	2.21	435	252
AL-315	11.00	0.16	0.23	0.30		76
AL-131	11.00	0.15	0.98	0.61	439	160
AL-132	11.50	0.63	0.83	0.32	432	259
AL-325	12.00	0.49	0.36	0.73	438	49
AL-335	13.00	0.34	0.00	0.43		
AL-345	14.00					
AL-355A	15.00	0.00	0.01	0.06		
AL-363	16.00	0.02	0.20	0.35	440	57
AL-373	17.00	0.01	0.02	0.04		
AL-383	18.00	0.00	0.04	0.06		
AL-393	19.00	0.01	0.10	0.17	439	59
AL-403	20.00	0.01	0.49	0.51	446	96
AL-413	21.00	0.00	0.03	0.05		
AL-423	22.00	0.00	0.01	0.03		

In the Arroyo Lapa North section, HI values tend to remain fairly low, with a range of 12–293 mg HC/g TOC through the entire section. Values increase up section but in general remain low. These values are more indicative of a prevalence of terrestrial material, with some marine organic matter. Samples from the upper part of the section were not examined for HI as the abundance of fossil wood in this part of the section, which is the main cause of the increase in TOC, would have been the dominant HI signal.

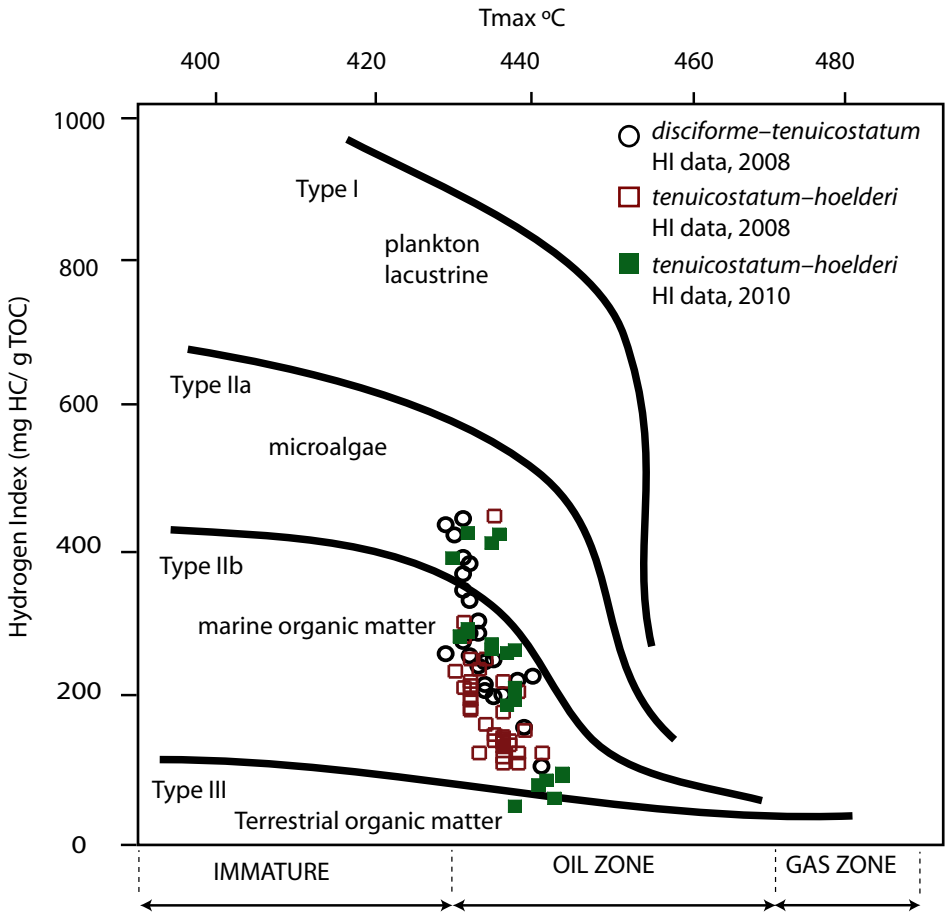


Figure 4. Tissot-Welte diagram showing a cross-plot of hydrogen Index (HC mg/g TOC) against T max ºC showing typical values for Type I–III kerogen, and the HI data from Arroyo Lapa North, and Arroyo Lapa South 2008 and 2010.

The preservation of marine organic matter and/or its ratio to terrestrial organic matter increases at towards the summit of the negative excursion in both sections (cf. Tissot and Welte, 1984; Baudin et al., 1989).

Table 5: Rock Eval Pyrolysis results for Arroyo Lapa North

		Rock Eval. Pyrolysis Results							
Biomarker Sample #	**Height (m)**	**Ctot %**	**CaCO3 %**	**Corg %**	**% TOC**	**Tmax °C**	**S1 mg/g**	**S2 mg/g**	**HI (mg HC/g TOC)**
Arroyo Lapa North									
LN-BM-9	2.4	0.63	3	0.27	0.27		0.81	0.12	44
LN-BM-10	3.4	0.78	0	0.78	0.46	441	0.47	0.36	78
LN-BM-11	4.3	0.17	0	0.17	0.12		0.45	0.02	16
Exposure gap									
LN-BM-1	8.1	0.46	0	0.46	0.30	444	0.24	0.27	90
LN-BM-2	10.1	0.02	0	0.02	0.08		0.37	0.01	12
LN-BM-3	12.1	0.45	0	0.45	0.16		0.54	0.04	25
LN-BM-4	14	0.24	0	0.24	0.30		1.13	0.18	60
Duplicate LN-BM-4					0.32	441	1.00	0.25	78
LN-BM-5	16				n/d	444	0.73	0.54	94
LN-BM-6	18	0.45	0	0.45	0.34	442	0.64	0.29	85
LN-BM-7	20	0.10	0	0.10	0.15		0.63	0.03	20
LN-BM-8	24.1	4.23	13.5	2.60	2.28	432	1.16	6.69	293

4.4.3. Pyrite Framboid Size Distribution Results

The examination of pyrite framboid numbers and morphology in rock samples, using a scanning electron microscope, can be used to determine the oxygenation state of the water column and the sediment during early diagensis (Wilkin et al. 1996; Wilkin and Barnes, 1997; Butler and Rickard, 2000; Taylor and Macquaker, 2000). The diameter distribution can be used to determine whether the pyrite formed is syngenetic: formed in the water column when free hydrogen sulphide is available, namely in euxinic settings or whether the pyrite framboids are diagnetic and formed within the anoxic pore waters of sediment underlying dysoxic or oxic water columns (Wilkin et al., 1996). Framboids that are syngenetic are on

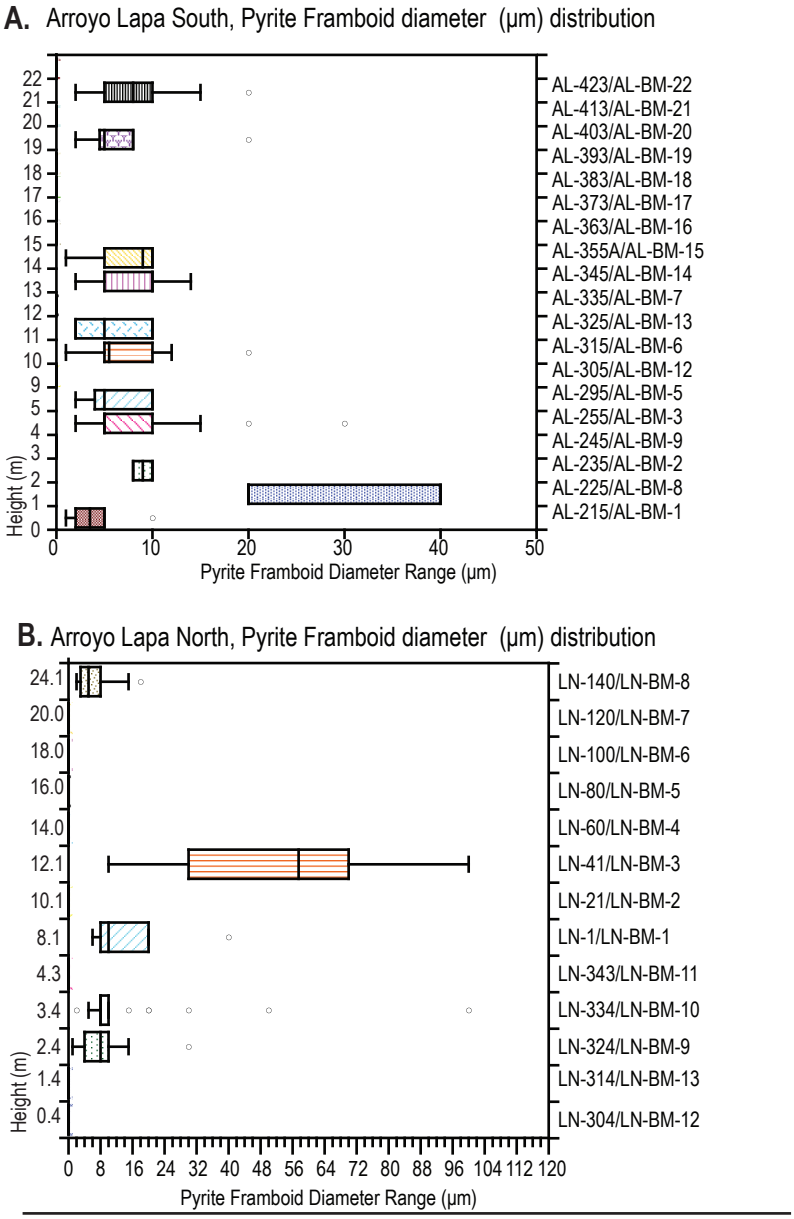


Figure 5. Box plots of pyrite framboid diameter distribution. (A) Shows pyrite framboid diameter distribution for Arroyo Lapa South; (B) Pyrite framboid diameter distribution for Arroyo Lapa North. Note that the pyrite framboid average diameter range for Aroryo Lapa South is much smaller than in Arroyo Lapa North. (C) Cross plot of Pyrite framboid mean diameter against standard devation of samples from Arroyo Lapa North and South and samples examined from Port Mulgrave, Yorkshire. Note that the Yorkshire samples have a much smaller average diameter than those from Arroyo Lapa, Argentina.

average smaller in diameter and less variable in size then framboids formed during diagenesis.

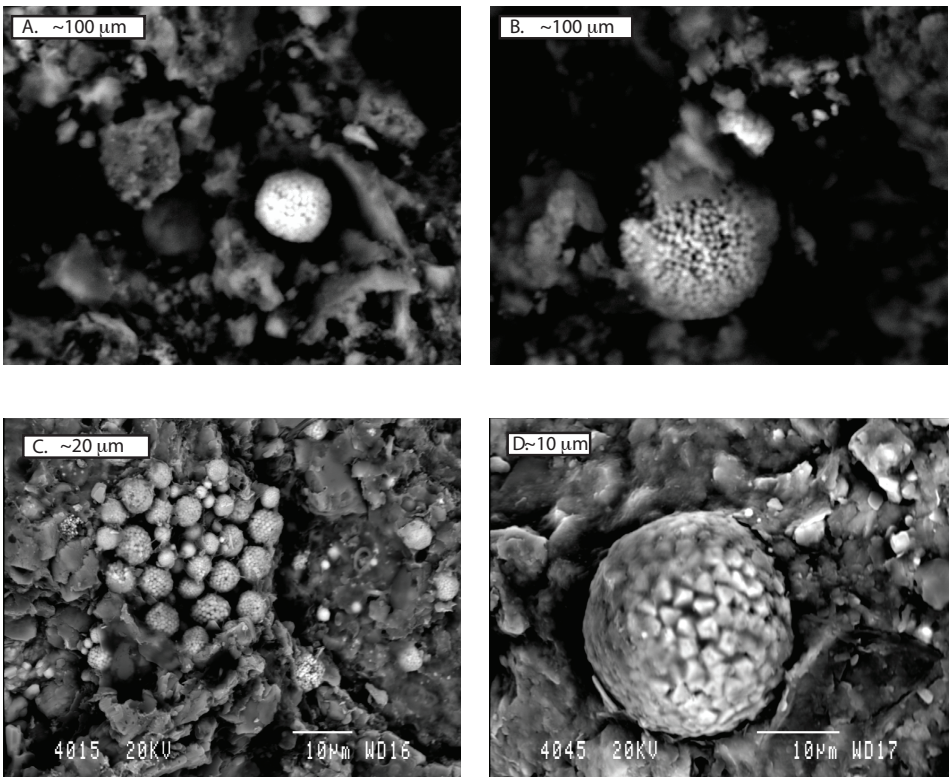


Figure 6. Scanning electron microscope images of pyrite framboids. Images A–B are images from Arroyo Lapa North and South, and show the typical size and structure of pyrite framboids from these sections. Images C–D are from samples from Port Mulgrave Yorkshire. Note that the pyrite framboids from Port Mulgrave, Yorkshire are much smaller and more spherical than those in the Arroyo Lapa sections.

In many of the examined samples no pyrite framboids were present and on average pyrite framboids tend to have a diameter of less than 10 μm in the Arroyo Lapa South section (Fig. 5A), while in the Arroyo Lapa North section, only 4 samples have pyrite framboids and the pyrite framboid diameter is significantly more variable with larger framboids (Fig. 5B). This can be compared with T-OAE pyrite framboid diameter data from Port Mulgrave Yorkshire (Fig. 5C). The Port Mulgrave pyrite framboids tend to have an average diameter of <5 μm, which is a lower mean pyrite framboid diameter compared to the data from Arroyo Lapa North and South. Data from Port Mulgrave, Yorkshire can be found in Appendix B, Table 1.

4.4.4. Biomarkers Results

Biomarker data from Arroyo Lapa South extend from the Pliensbachian–Toarcian (*disciforme (=spinatum)–tenuicostatum)* boundary through the *tenuicostatum–hoelderi* ammonite Zones, and includes 7 samples from the 2008 section and 22 samples from the 2010 section, samples.

C_{27} regular steranes *vs.* C_{35} regular hopanes (St/H) shows values ranging from 0.02 to 5.9 (Fig. 7A). Values of St/H ≥1 tend to reflect marine organic matter with contributions from planktonic and/or benthic algae (i.e. Moldowan et al., 1985, Peters et al., 2005b p. 524–525), and values of St/H <1 are typical of terrigenous and microbially reworked organic matter (e.g. Tissot and Welte, 1984). In the Arroyo Lapa South section the St/H ratio is high at the onset of the negative isotope excursion with values reaching the maximum of 5.97 at 1 m. Values are also high immediately after the *tenuicostatum–hoelderi* Zone boundary (3.63 at 7m). This increase in St/H corresponds with elevated HI values (390–425) and an increase in TOC to ~7%. St/H values from other samples in the section are typically <1.

In Arroyo Lapa North, St/H values range from 0.09 to 6.08 (Fig. 7B). St/H values increase to 1.48 at 12.1 m, at ~11m, though in general are < 1 through the section, except for the final sample at 24.1 m, where the St/H is 6.08. This value corresponds to a rise in TOC and HI values of 293, suggesting that there is an increase in deposition of terrestrial plant material. Field observations show an increase in the abundance of fossil wood in the section above this height.

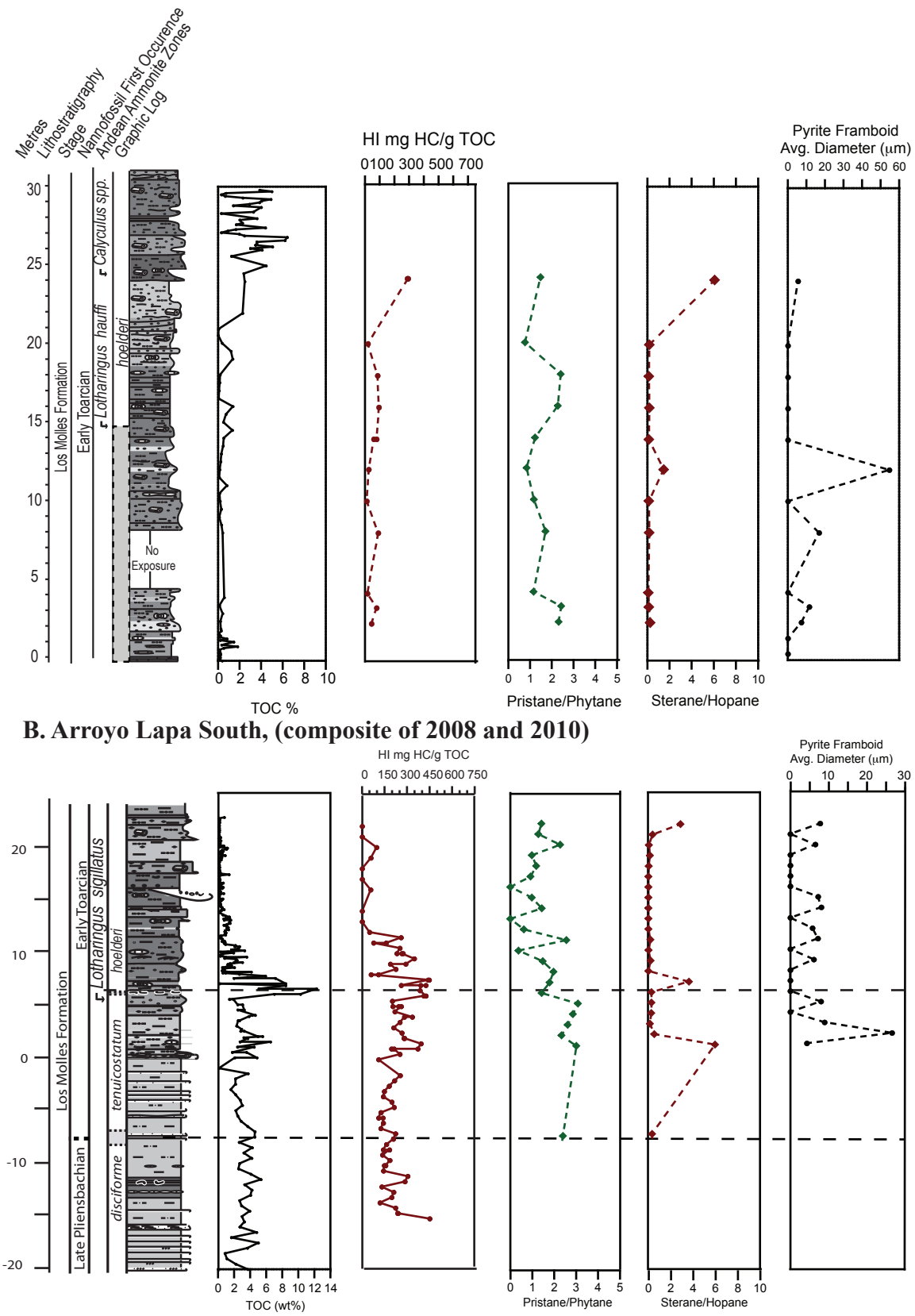


Figure 7. (A.) Arroyo Lapa North and (B.) Arroyo Lapa South plot showing TOC, HI, Pristane/Phytane ratios, Sterane/Hopane, and pyrite framboid average diameter distribution through the section. Arroyo Lapa South data include a composite of data from the 2008 and the 2010 sections.

Table 6: Hopane and Sterane Results

Biomarker Sample #	Height (m)	Hopanes Amt. Homohopanes (ppm)	Steranes Total [Sterane (ppm)]	Sterane/Hopane
Arroyo Lapa South 2008				
ARG-AL-7	-50.93	0.09	0.01	0.08
ARG-AL-11	-49.05	0.01	0.00	0.19
ARG-AL-17	-46.03	0.69	0.10	0.14
ARG-AL-44	-32.57	0.08	0.02	0.28
ARG-AL-50	-29.50	0.04	0.01	0.19
ARG-AL-66	-21.50	0.11	0.02	0.22
ARG-AL-94	-7.50	0.27	0.09	0.33
AL-BM-1	1.00	1.28	7.64	5.97
AL-BM-8	2.00	0.37	0.20	0.52
AL-BM-2	3.00	0.43	0.06	0.14
AL-BM-9	4.00	0.46	0.12	0.27
AL-BM-3	5.00	0.56	0.15	0.27
AL-BM-10	6.00	0.54	0.15	0.27
AL-BM-4	7.00	0.07	0.25	3.63
AL-BM-11	8.00	0.22		
AL-BM-5	9.00	0.32	0.06	0.20
AL-BM-12	10.00	0.07	0.00	0.02
AL-BM-6	11.00	0.29	0.05	0.19
AL-BM-13	12.00	0.04	0.00	
AL-BM-7	13.00	0.60	0.00	0.01
AL-BM-14	14.00		0.00	
AL-BM-15	15.00	1.03	0.00	0.00
AL-BM-16	16.00			
AL-BM-17	17.00	0.54	0.00	0.01
AL-BM-18	18.00	0.20	0.01	0.03
AL-BM-19	19.00	0.04	0.01	0.13
AL-BM-20	20.00	0.52	0.03	0.05
AL-BM-21	21.00	0.05	0.02	0.37
AL-BM-22	22.00	0.05	0.27	2.88
Arroyo Lapa North				
LN-BM-9	2.4	0.05	0.01	0.25
LN-BM-10	3.4	0.20	0.03	0.14
LN-BM-11	4.3	0.03	0.00	0.09
Exposure gap				
LN-BM-1	8.1	0.10	0.02	0.17
LN-BM-2	10.1	0.01	0.00	0.14
LN-BM-3	12.1	0.00	0.00	1.48
LN-BM-4	14	0.19	0.03	0.15
LN-BM-5	16	0.13	0.02	0.19
LN-BM-6	18	0.22	0.03	0.13
LN-BM-7	20	0.09	0.02	0.19
LN-BM-8	24.1	0.08	0.02	6.08

Pristane/Phytane (Pr/Ph) ratios are applied as an indicator of palaenenvironmental redox, salinity and terrestrial organic matter input but caution is suggested in interpreting Pr/Ph ratios as being indicative of specific palaeoenvironmental conditions without supporting data (Ten Haven et al., 1987; Peters et al, 2005b, p. 499–502). Pr/Ph ratios describe the relationship between proportions of phytol diagensis products generated under aerobic (pristine) and anaerobic (phytane) conditions (Didyk et al., 1978). There is a weak correlation with depositional redox conditions; high Pr/Ph values >3.0 indicates terrestrials organic- matter input under oxic to suboxic conditions while low <0.8 typify anoxic, associated with evaporite, and/or carbonate environments (Peters et al, 2005b).

In the Arroyo Lapa South section (Fig. 7A), Pristane/Phytane (Pr/Ph) values range from 0 to 3.22. Values of Pr/Ph decrease to 0.38 at 10 m, which corresponds with $\delta^{13}C_{org}$ values of -32.53‰ at the summit of the negative carbon-isotope excursion, indicating anoxic bottom waters in the *hoelderi* Zone. HI values are 252–264, suggesting a dominance of marine organic matter in this part of the section, with TOC values of 0.98%. Higher values > 3, of Pr/Ph in the Arroyo Lapa South section, correlate with intervals where fossil wood samples where found, i.e. 1 m, Pr/Ph= 3.02, 5m; Pr/Ph = 3.09. Pr/Ph values in the rest of the section are generally between 0.8–3 and are more indicative of normal oxygenated settings.

In the Arroyo Lapa North section Pr/Ph (Fig. 7B) values range from 0.77 to 2.44. Pr/Ph values at 12.1 m fall to 0.84 corresponding with $\delta^{13}C_{org}$ of -28.47, TOC of 0.16% and HI of 25 at 12m and 0.77 at 20 m at the onset of the recovery from the negative carbon-isotope excursion, corresponding with a $\delta^{13}C_{org}$ of -22.07, with a TOC of 0.38%,and HI of 20. In the rest of the section, values typically range between ~1–2.5, indicating normal oxygenated settings.

Table 7: Pristane and Phytane Data

Biomarker Sample #	Height*(m)	TLE (wt%)	Pristane & Phytane		
			Amt. Pr (ppm)	Amt Ph (ppm)	Pr/Ph
Arroyo Lapa South 2008					
ARG-AL-7	-50.93	0.20	0.10	0.15	0.65
ARG-AL-11	-49.05	0.13	0.00	0.00	3.11
ARG-AL-17	-46.03		2.68	1.14	2.35
ARG-AL-44	-32.57	0.11	0.49	0.37	1.31
ARG-AL-50	-29.50	0.25	0.01	0.00	3.22
ARG-AL-66	-21.50	0.02	0.43	0.32	1.36
ARG-AL-94	-7.50	0.69	2.64	1.10	2.41
Arroyo Lapa South 2010					
AL-BM-1	1.00	0.65	2.86	0.95	3.02
AL-BM-8	2.00	0.43	3.97	1.70	2.34
AL-BM-2	3.00	0.31	2.48	0.95	2.62
AL-BM-9	4.00	0.40	5.07	1.77	2.86
AL-BM-3	5.00	0.22	3.28	1.06	3.09
AL-BM-10	6.00	0.78	6.30	4.40	1.43
AL-BM-4	7.00	1.45	9.06	5.03	1.80
AL-BM-11	8.00	0.26	0.65	0.33	1.98
AL-BM-5	9.00	0.45	2.02	1.36	1.48
AL-BM-12	10.00	0.01	0.00	0.01	0.38
AL-BM-6	11.00	1.10	1.00	0.39	2.56
AL-BM-13	12.00	0.81	0.29	0.47	0.62
AL-BM-7	13.00	0.28	0.00	0.00	0.00
AL-BM-14	14.00	0.03	0.05	0.03	1.44
AL-BM-15	15.00	0.03	0.02	0.02	0.98
AL-BM-16	16.00	0.35			
AL-BM-17	17.00	0.12	0.48	0.52	0.92
AL-BM-18	18.00	0.88	0.00	0.00	1.18
AL-BM-19	19.00	0.44	0.06	0.07	0.98
AL-BM-20	20.00	0.08	0.58	0.25	2.28
AL-BM-21	21.00	2.24	0.28	0.22	1.29
AL-BM-22	22.00	0.37	4.29	3.02	1.42
Arroyo Lapa South 2010					
LN-BM-9	2.4	0.03	0.06	0.03	2.31
LN-BM-10	3.4	0.04	0.14	0.06	2.44
LN-BM-11	4.3	0.13	0.01	0.01	1.17
Exposure gap~					
LN-BM-1	8.1	0.22	0.06	0.03	1.72
LN-BM-2	10.1	0.04	0.00	0.00	1.17
LN-BM-3	12.1	0.03	0.01	0.01	0.84
LN-BM-4	14	0.29	0.09	0.07	1.23
LN-BM-5	16	0.29	0.09	0.04	2.28
LN-BM-6	18	0.14	0.09	0.04	2.41
LN-BM-7	20	1.15	0.01	0.01	0.77
LN-BM-8	24.1	0.35	0.14	0.09	1.48

Samples were also examined for the presence of isorenieratane, a biomarker for green sulphur bacteria, which is anoxygenic prototroph that fixes carbon dioxide, and is indicative of photic-zone anoxia or euxinia (Peters et al., 2005b, p. 593). Though none was found in the samples examined, it is possible that some of the samples have isorenieratane derivatives that were not identified in this study. The samples examined for biomarkers were collected systematically, without knowledge of TOC content and not based on sedimentology alone. Some samples were sandy and not ideal for biomarker work. Detailed examination of the section and identification of more organic rich samples may be key to further examination of biomarkers from the Arroyo Lapa sections.

4.4.5 Molybdenum Isotopes Results

Molybdenum (Mo) enrichment in sediments is generally considered to be diagnostic of reducing depositional settings due to Mo being readily removed from solution in anoxic to euxinic environments, resulting in Mo enrichment in these settings. In comparison, Mo tends to be un-reactive in oxygenated aqueous solution. Because these two sinks (anoxic and euxinic) of Mo have unique isotope signatures, the Mo isotopic values of sediments have been proposed to record ocean redox conditions through time (Siebert et al., 2003; Poulson et al. 2006). Fig 8 shows the molybdenum geochemical cycle and typical MO concentrations and $\delta^{98/95}$Mo values.

. $\delta^{98/95}$Mo in samples from Arroyo Lapa South range from -0.13 to 0.78‰. Concentrations of Mo range from 1.5 to 4.8 ppm through the section (Fig. 9A). At the onset of the negative carbon-isotope excursion, where TOC enrichment begins just prior to the *tennuicostatum-hoelderi* ammonite Zone boundary there is a significant increase in TOC of ~10%, which is accompanied by an increase in the concentration of Mo of about +3 ppm, and an increase in the $\delta^{98/95}$Mo of about + 0.3‰ prior to the negative carbon-isotope excursion.

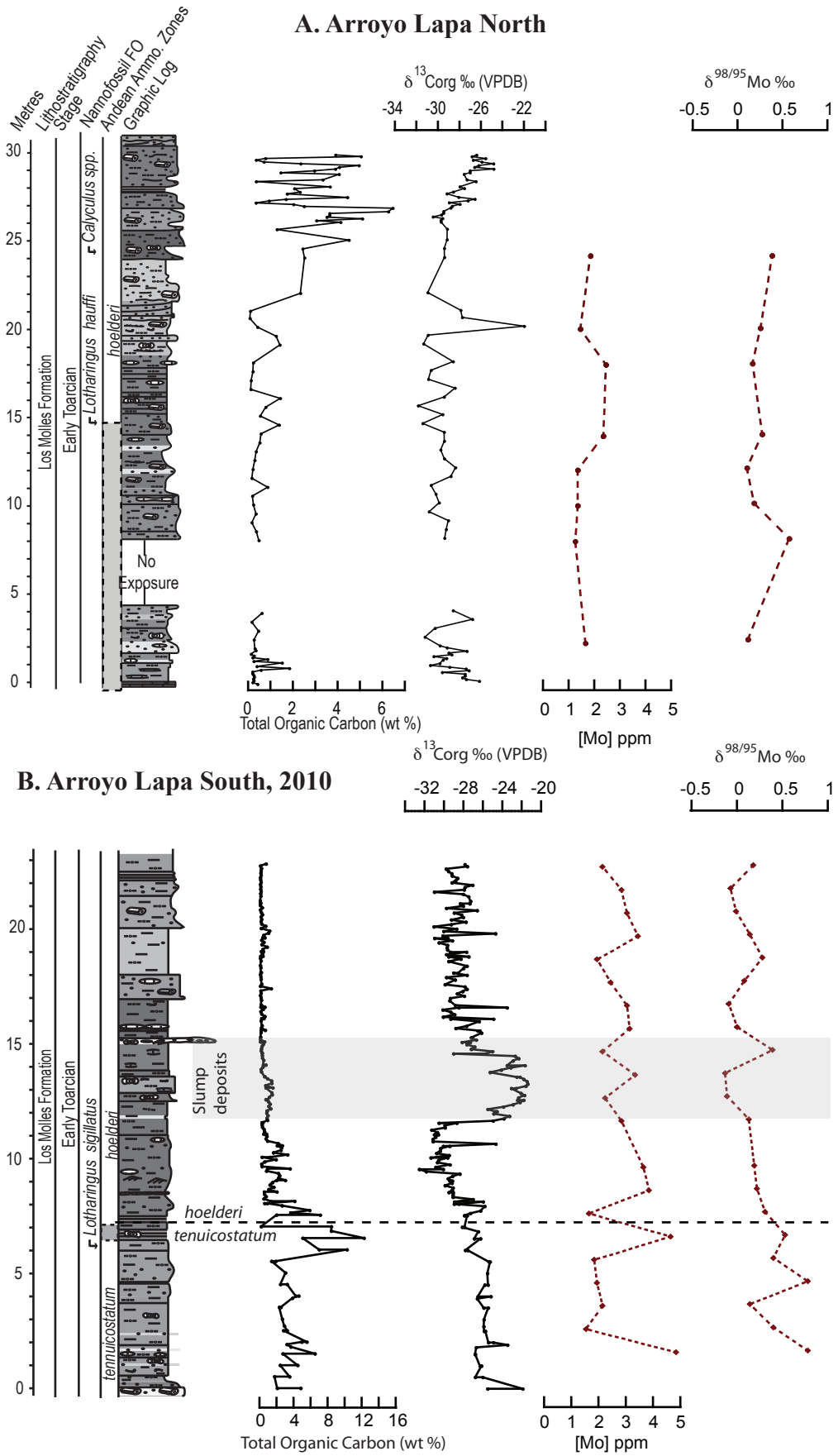


Figure 8. Comparison of δ^{13}Corg, TOC, $\delta^{98}/^{95}$Mo, and [Mo] ppm from bulk sediment for Arroyo Lapa North (B) and South (A), Argentina. Note the step at the *tenuicostatum–hoelderi* boundary at Arroyo Lapa South that corresponds with a marked increase in total organic carbon and the negative excursion.

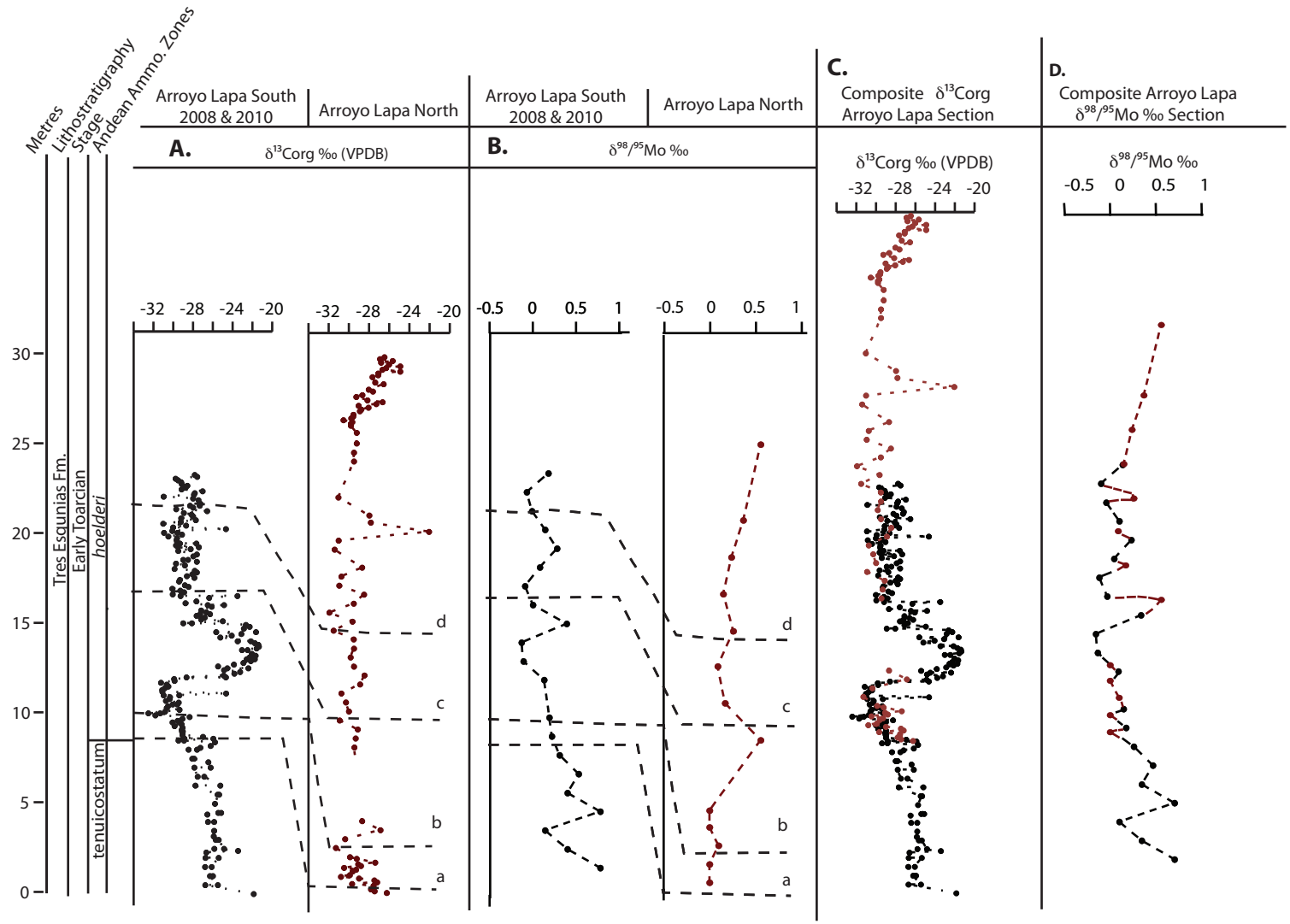


Figure 9. Comparison of $\delta^{13}C_{org}$ and $\delta^{98}/^{95}Mo$ data from Arroyo Lapa South (2008 and 2010) and Arroyo Lapa North. A. Correlation of the two sections is indicated by dashed black lines a–d and is based on $\delta^{13}C_{org}$ values and steps in the chemostratigraphic profiles.(B) Comparison of the $\delta^{98}/^{95}Mo$ values from the two sections correlation is based on the correlation of $\delta^{13}C_{org}$. (C.) A composite of the bulk sediment Arroyo Lapa North an South based on the correlation in A. (D.) Composite $\delta^{98}/^{95}Mo$ chemostratigraphy for Arroyo Lapa North and South based on the correlation in A.

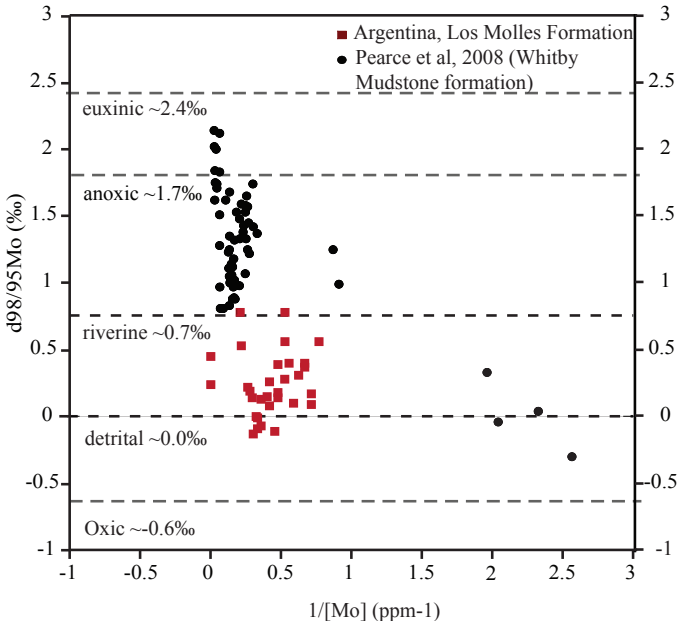


Figure 10. Cross plot of $\delta^{98}/^{95}$Mo vs 1/[ppm], for data from Arroyo Lapa North and South and data from Yorkshire, England (Pearce et al., 2008). Dashed lines indicate typical values of $\delta^{98}/^{95}$Mo for various depositional settings.

The values of $\delta^{98/95}$Mo from Arroyo Lapa North (Fig 9B) are comparable to those in Arroyo Lapa South with a range of 0.09 to 0.56 ‰ and concentrations varying from 1.3 to 2.5 ppm. The total-organic carbon content of the Arroyo Lapa North section is much lower, with values never exceeding 7% even at the height of the excursion. But given this, there is still an increase in the concentration of Mo corresponding with the lightest carbon isotope values (δ^{13}C > 28‰), 16 m, with values reaching their maximum concentration of 2.5 ppm at the ~15m, though the $\delta^{98/95}$Mo remains relatively low, 0.15‰.

Given the chemostratigraphic correlation of Arroyo Lapa North and South based on the $\delta^{13}C_{org}$ data, this correlation can be applied to the molybdenum-isotope data to create a composite molybdenum chemostratigraphic profile for the CIE (Fig. 10).

4.5. Discussion and Conclusion

The various proxy data sets can be compared with coeval chemo-stratigraphic data from Europena sections. Specifically, the biomarker and HI data can be compared with data

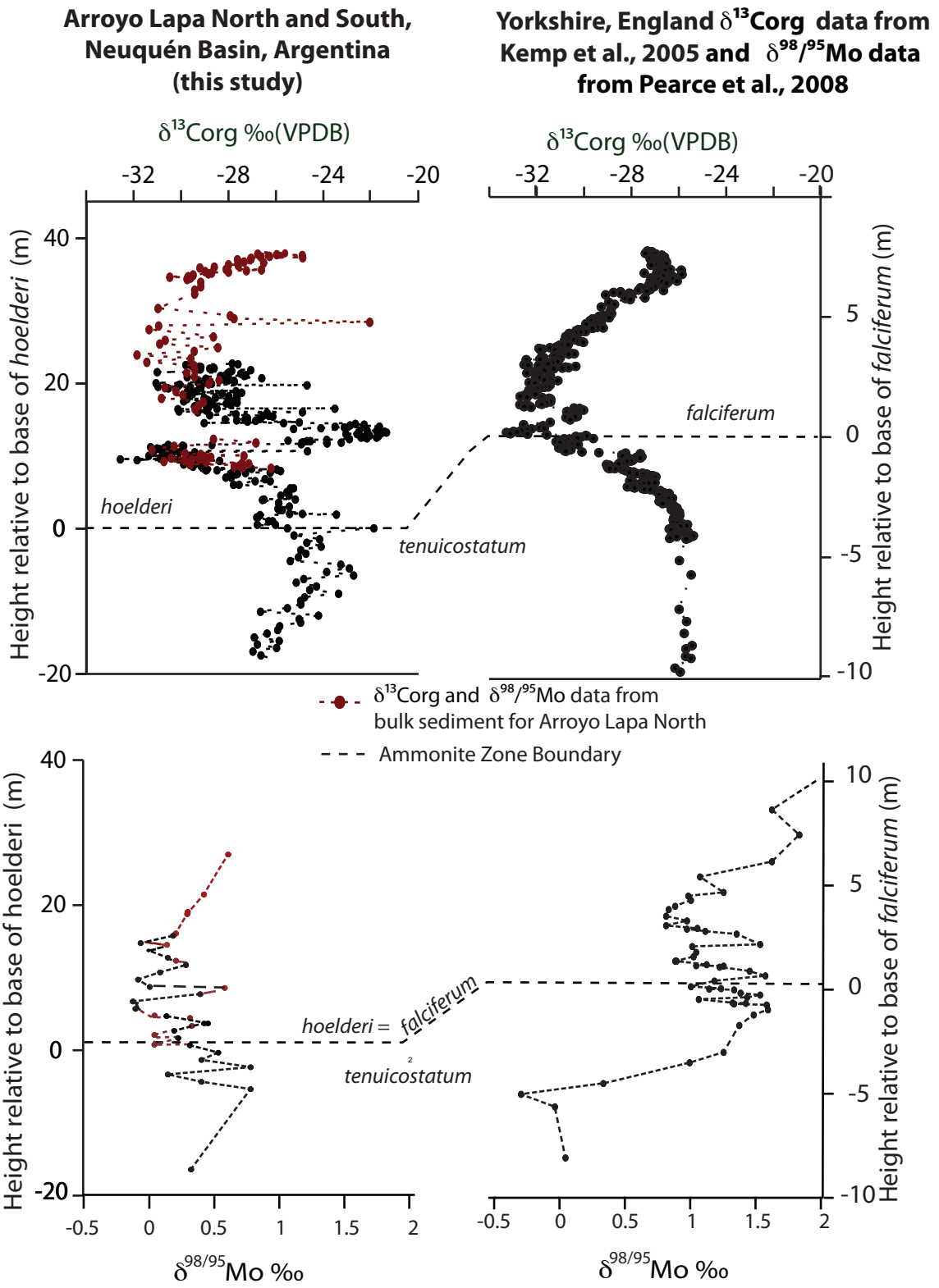


Figure 11. Comparison of δ^{13}Corg , and $\delta^{98}/^{95}$Mo from a Arroyo Lapa (North and South composite) and Yorkshire, England (Pearce et al., 2008). Note the negative excursion in $\delta^{98}/^{95}$Mo in Arroyo Lapa and Yorkshire, England, occurs just after the summit of the negative excursion. Also note that the magnitude of the excursion is about ~-0.5 ‰ in Yorkshire and Arroyo Lapa.

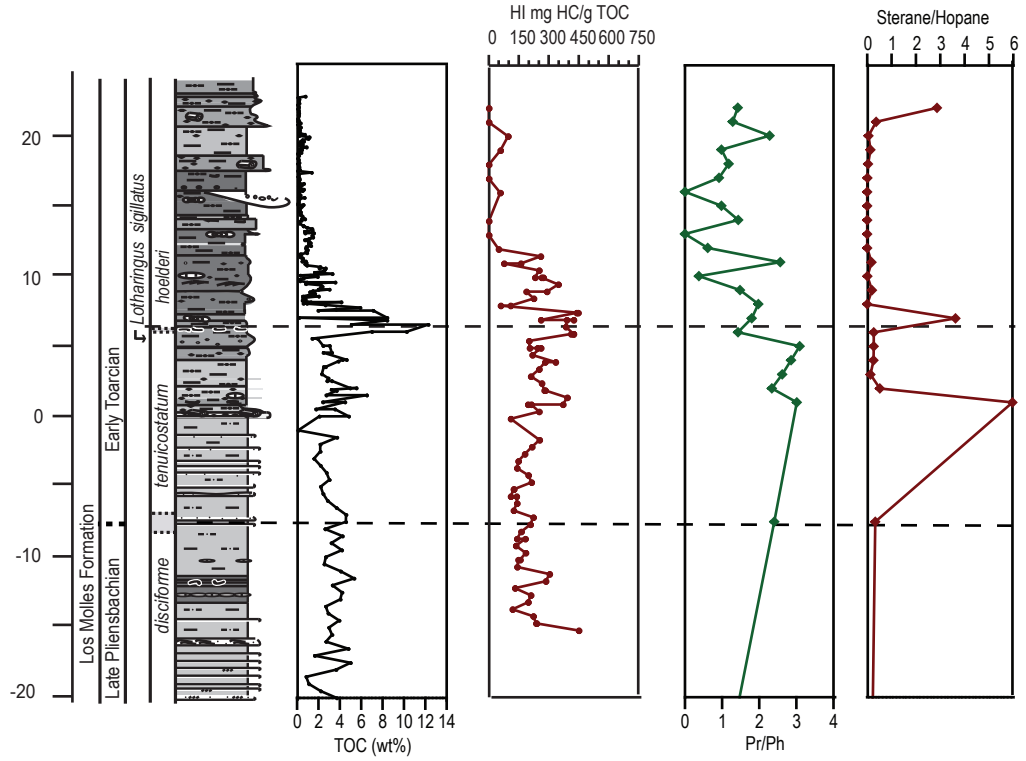
from the Posidonia Black Shale, SW Germany (Frimmel et al., 2004), while the $\delta^{98/95}$Mo, $\delta^{13}C_{org,}$TOC and pyrite framboid data from bulk sediment can with be compared with data sets from Yorkshire, England, specifically pyrite framboid data from Port Mulgrave, analysed in this study, and $\delta^{98/95}$Mo, $\delta^{13}C_{org,}$TOC from Hawskers Bottoms (Kemp et al., 2005; Pearce et al., 2008; Littler et al., 2010). Details of the $\delta^{13}C_{org}$ data and correlation of this data with other data sets can be found in Chapter 3.

The $\delta^{13}C_{org}$ data shows a -6‰ step wise negative carbon-isotope excursion at the *tenuicostatum–hoelderi* ammonite Zone boundary, interrupting an overall positive excursion, this is also recorded in fossil wood, and can be correlated with coeval sections from the UK, Canada, Greece and Italy as presented in Chapter 3.

Composite $\delta^{98/95}$Mo data from Arroyo Lapa North and South can be compared to data from the Cleveland Basin, Yorkshire, England (Figs. 11–12; Pearce et al., 2008). This comparison shows a stepped $\delta^{98/95}$Mo isotope profile through the *tenuicostatum–hoelderi* ammonite Zone of a similar magnitude to that recorded by Pearce et al. (2008), though the absolute molybdenum values recorded in the Cleveland Basin, are heavier than those recorded in the Neuquén Basin. This difference may be due a result of local restriction within the north European area, and the presence of a significant amount of volcaniclastics in the Arroyo Lapa sections; such that a detrital Mo signal is present which dilutes the $\delta^{98/95}$Mo signal in the Neuquén Basin. However hydrogenated Mo asserts its signal where TOC is high in Arroyo Lapa. Values heavier than ~0.78‰ occur prior to the *tennuicostatum–hoelderi* ammonite Zone boundary (Fig. 11) indicating anoxic settings for at least a short interval in the Neuquén Basin. An anoxic environment is also reflected in the Pr/Ph ratio, while the HI and Sterane/Hopane ratios indicate that, during the summit of the negative excursion marine organic matter dominated, specifically from marine phytoplankton.

The more continuous St/H and Pr/Ph data from Arroyo Lapa South can be compared to data from the Posidonia Shale, SW Germany (Fig., 13; Frimmel et al., 2004). Pr/Ph values

Arroyo Lapa South, Neuquén Basin, Argentina



Early Toarcian Posidonia Shale, SW Germany, Frimmel et al. (2004).

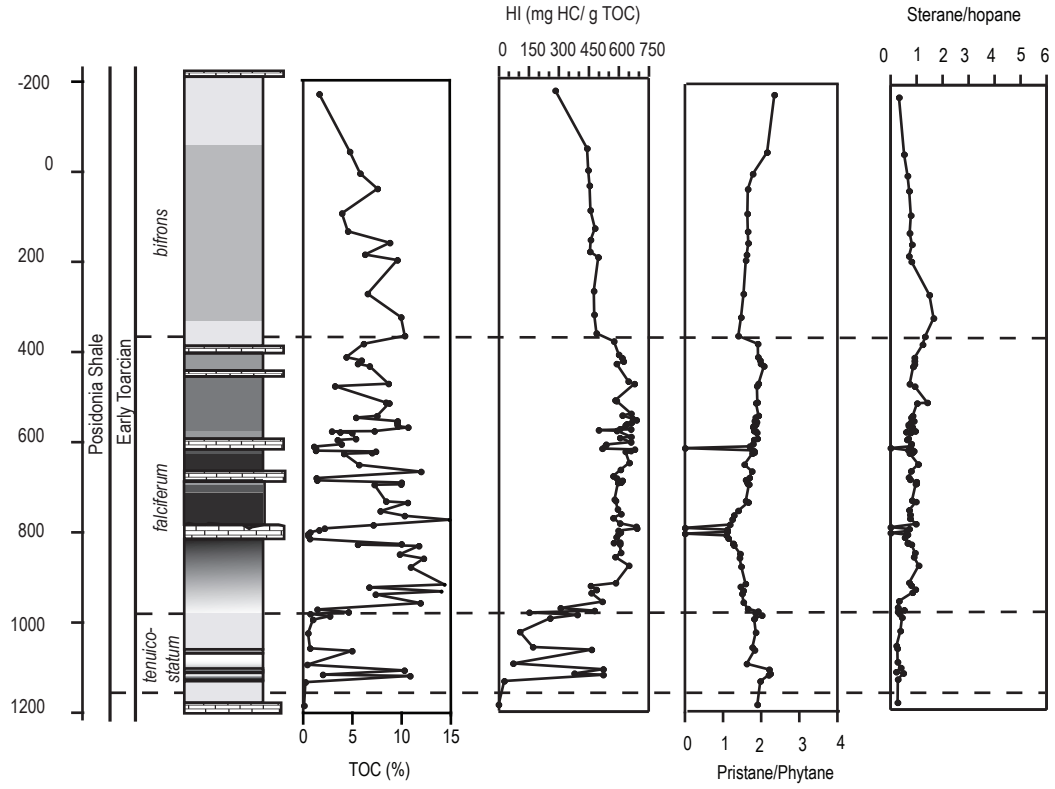


Figure 12. Comparison of TOC, Hydrogen Index, Pristane/Phytane and Sterane/Hopane data from Arroyo Lapa South and the Posidonia Shale SW Germany (Frimmel et al., 2004). Note the increase in HI and TOC at the *tenuicostatum–hoelderi* (= *serpentinum*) ammonite Zone Boundary in both sections. Pr/Ph values in the Arroyo Lapa section are lower (< 2) than in the Posidonia Shale section.

increase just prior to the *tenuciostatum–hoelderi* ammonite Zone boundary (~6 m), to a maximum of 3.09 at 5 m in the Arroyo Lapa South section and then gradually decrease to 0.38 after the boundary at 10 m. In the Posidonia shale s Pr/Ph values, increase to ~2 at the *tenuciostatum–falciferum* ammonite Zone boundary, and then remain between 1–2 throughout the section, which is too high for the sediment to be considered strictly anoxic, the authors attribute this to an increase in the input of non-phytol pristine and local basin variability (Frimmel et al., 2004). Sterane/Hopane ratio values are also much lower in the Posidonia Shale (< 2) with high HI values (> 200), indicating that the origin of organic matter in this section is predominantely marine, while the sections from Arroyo Lapa North and South show a much more mixed signal, with the dominance of terrestrial organic matter in some parts and the dominance of marine organic matter in other parts of the section. Hydrogen Index values in the Arroyo Lapa Sections (North and South) range from 12–450 while in the Posidonia Shale values range from 79–689.

Pyrite framboid data from the Arroyo Lapa sections, when compared with coeval data from Port Mulgrave, Yorkshire that were measured in this study (Fig. 5C). Data show that framboids from Arroyo Lapa, have much greater variability in size and there is a mixture of syngenetic and diagenetic framboids, suggesting brief intervals of anoxia and/or euxinia in the basin. In the Port Mulgrave data set, framboids are routinely syngenetic and indicate a persistent euxinic setting in the Cleveland Basin through the Early Toarcian.

While no isorenieratane or its deravatives was identified in this study, it is possible that isorenieratane may be found in other samples from the section, and higher resolution sampling targeted at shale intervals only may be important for the examination of biomarkers in theses large sections. The $\delta^{98/95}$Mo, Pristane/Phytane ratios and pyrite framboid data suggest that the Neuquén Basin, if it was anoxic was only anoxic for a short time. In order to determine if the Neuquén Basin is reflecting the Panthalssic Ocean it is important to create higher resolution data sets for sections such as Arroyo Lapa North and South, so that a more

detailed examination of the proxy record of the Neuquén Basin can be generated. It would also be useful to examine the potential of other more open Early Toarcian sections, such as the sections from Japan, (Gröcke et al., 2011; Kafousia et al., 2011) for the study of $\delta^{98/95}$Mo isotopes, biomarkers and other proxies. Such studies would help resolve the full oceanographic chemical record of the Toarcian Oceanic Anoxic Event.

References:

Algeo, T. J. and Lyons, T. W., 2006, Mo-total organic carbon covariation in modern anoxic marine environments: Implications for analysis of paleoredox and paleohydrographic conditions: Paleoceanography, v, 21, PA1016, doi: 10.1029/2004PA00112.

Al-Suwaidi, A.H., Angelozzi, G.N., Baudin. F., Damborenea, S.E., Hesselbo, S.E., Jenkyns, H.C., Manceñido, M.O., and Riccardi, A.C., 2010, First record of the Early Toarcian Oceanic Anoxic Event from the southern hemisphere, Neuquén Basin, Argentina: Journal of the Geological Society, v. 167, p. 633–636.

Amor, K., Al-Suwaidi, A. H., Hesselbo, S. P., Jenkyns, H.C., and Porcelli, D., 2008, Chromium isotope stratigraphy of the Toarcian OAE from Yorkshire, North East England: AGU Fall Meeting 2008, San Fransisco, PP31C-1495.

Anbar, A.D. and Rouxel, O., 2007, Metal stable isotopes in paleoceanography: Annual Review Earth and Planetary Science, v. 35, p. 717–746.

Archer, C. and Vance, D., 2008, The isotopic signature of the global riverine molybdenum flux and anoxia in the ancient oceans: Nature Geoscience, v. 1, p. 597–600, doi: 10.1038/ngeo282.

Baudin, F., Herbin, J.-P. and Vandenbroucke, M., 1989, Mapping and geochemical characterization of the Toarcian organic matter in the Mediterranean Tethys and Middle East: Advances in Organic Geochemistry, v. 16, p. 677–687.

Blakey, R., 2007, Early Jurassic rectangular palaeogeographic map in mollewide: http://jan.ucc.nau.edu/~rcb7/200marect.jpg (November, 2009).

Bodin, S., Mattioli, E. Fröhlich, S., Marshall, J.D., Boutib, L., Lahsini, S., and Redfern, J., 2010, Toarcian carbon isotope shifts and nutrient changes from the Northern margin of Gondwana (High Atlas, Morocco, Jurassic): palaeoenvironmental implications: Palaeogeography, Palaeoclimatology, Palaeoecology, v. 297, p. 377–390, doi:10.1016/j.palaeo.2010.08.018.

Blättler, C.L., Jenkyns, H.C., Reynard, L.M., and Henderson, G.M., 2011, Significant increases in global weathering during Oceanic Anoxic Events 1a and 2 indicated by calcium isotopes: Earth and Planetary Science Letters, v. 309, p. 77–88, doi:10.1016/j.epsl.2011.06.029.

Burgess, P.M., Flint, S. and Johnson, S., 2000, Sequence stratigraphic interpretation of turbiditic strata: An example from Jurassic strata of the Neuquén Basin, Argentina: Geological Society of America Bulletin, v. 112, p. 1650–1666.

Butler, I. B. and Rickard, D., 2000, Framboidal pyrite formation via the oxidation of iron (II) monosulfide by hydrogen sulfide: Geochimica et Cosmochimica Acta, v. 64, p 2665–2672, doi: 10.1016/ S00016-7037(00)00387-2.

Caruthers, A.H., Gröcke, D.R., and Smith, P.L., 2011, The significance of an Early Jurassic (Toarcian) carbon-isotope excursion in Haida Gwaii (Queen Charlotte Islands), British Columbia, Canada: Earth and Planetary Science Letters, v. 307, p. 19–26 doi:10.1016/j.epsl.2011.04.013.

Cohen, A.S., 2004, The rhenium–osmium isotope system: applications to geochronological and palaeoenvironmental problems: Journal of the Geological Society, London, v. 161, p. 729–734.

Cohen, A.S. and Coe, A.L., 2007, The impact of the Central Atlantic Magmatic Province on climate and on the Sr- and Os-isotope evolution of seawater: Palaeoceanography, Palaeoclimatology, Palaoecology, v. 244, p. 374–390.

Damborenea, S.E., 1987, Early Jurassic Bivalvia of Argentina. Part 1: Stratigraphical introduction and Superfamilies Nuculanacea, Arcacea, Mytilacea and Pinnacea: Palaeontographica, A, v. 199, p. 23–111.

Didyk, B., Simmoneit, B.R.T., Brassel, S.C., Eglington, G., 1978, Organic geochemical indicators of palaeoenvironmental conditions of sedimentation: Nature, v. 272, p. 216–222.

Ellis, A.S., Johnson, T. M., and Bullen, T.D., 2002, Chromium isotopes and the fate of hexavalent chromium in the envionrment: Science, v. 295, p. 2060–2062.

Emerson, S.R. and Huested, S.S., 1991, Ocean anoxia and the concentrations of molybdenum and vanadium in seawater: Marine Chemistry, v. 34, p. 177–196.

Espitalié, J., Deroo, G. and Marquis, F., 1985a, Rock-Eval Pyrolysis and its applications (Part One): Oil and Gas Science and Technology – Rev. IFP., v. 40, p. 563–579, doi:10.2516/ogst:1985035.

Espitalié, J., Deroo, G. and Marquis, F., 1985b, Rock-Eval Pyrolysis and its applications (Part Two): Oil and Gas Science and Technology – Rev. IFP., v. 40, p. 755–785.

Frimmel, A., Oschmann, W. and Schwark, L., 2004, Chemostratigraphy of the Posidonia Black Shale, SW Germany: I. influence of sea-level variation on organic facies evolution: Chemical Geology, v. 206, p. 199–230, doi: 10.1016/j.chemgeo.2003.12.007.

Google Earth, 2005, Arroyo Lapa (Creek) , 31º24’04.87”S and 70º25’43.21”W August 7, 2011. Google Earth, Version 6.0.3.2197.

Gill, B.J., Lyons, T.W., and Jenkyns, H.C., 2011, A global perturbation to the sulfur cycle during the Toarcian Oceanic Anoxic Event: Earth and Planetary Science Letters, v. 312, p. 484–496, doi: 10.1016/j.epsl.2011.10.030.

Gröcke, D.R., Hori, R.S., Trabucho-Alexandre, J., Kemp, D.B. and Schwark, L., 2011, An open marine record of the Toarcian oceanic anoxic event: Solid Earth Discussion, v. 3, p. 385-410, doi:10.5194/sed-3-385-2011.

Gulisano, C.A. and Gutiérrez Pleimling, A.R., 1995, Field Guide. The Jurassic of the Neuquén Basin. (a) Neuquén Province. Asociación Geológica Argentina, Series E, No 2, Buenos Aires, p. 1-111.

Hesselbo, S.P., Gröcke, D.R., Jenkyns, H.C., Bjerrum, C.J., Farrimond, P., Morgans Bell, H.S., and Green, O.R., 2000, Massive dissociation of gas hydrate during a Jurassic Oceanic Anoxic Event: Nature, v. 406, p. 392–395.

Hesselbo, S.P., Jenkyns, H.C., Duarte, L.V., and Oliveira, L.C.V., 2007, Carbon-isotope record of the Early Jurassic (Toarcian) Oceanic Anoxic Event from fossil wood and marine carbonate (Lusitanian Basin, Portugal): Earth and Planetary Science Letters, v. 253, p. 455–470.

Hillebrandt, A. von. 1973. Die Ammonitengattungen Bouleiceras und Frechiella im Jura von Chile. Eclogae Geologicae Helvetiae, 66, 351-363.

Hillebrandt, A. von., 1987, Liassic ammonite zones of South America and correlations with other provinces. With description of new genera and species of ammonites. In: Volkheimer, W. (ed) Bioestratigrafía de los Sistemas regionales del Jurásico y Cretácico de América del Sur, Mendoza, p. 111-157.

Hillebrandt, A. von., 2006, Ammoniten aus dem Pliensbachium (Carixium und Domerium) von Südamerika: Revue de Paléobiologie, v. 25, p 1–403.

Hillebrandt, A. von, and Schmidt-Effing, R., 1981, Ammoniten aus dem Toarcium (Jura) von Chile (Südamerika): Zitteliana, v. 6, p. 3–74.

Iglesia Llanos, M.P. and Riccardi, A.C., 2000, The Neuquén composite section: magnetostratigraphy and biostratigraphy of the marine Lower Jurassic from the Neuquén basin (Argentina): Earth and Planetary Science Letters, v. 181, p. 443–457.

Jenkyns, H.C., 2010, Geochemistry of oceanic anoxic events: Geochemistry, Geophysics, Geosystems, v. 11, Q03004, doi: 10.1029/2009GC002788.

Jenkyns, H.C. and Clayton, C. J., 1986, Black shales and carbon isotopes in pelagic sediments from the Tethyan Lower Jurassic: Sedimentology, v. 33, p. 87–106.

Jenkyns, H.C. and Clayton, C. J., 1997, Lower Jurassic epicontinental carbonates and mudstones from England and Wales: chemostratigraphic signals and the early Toarcian anoxic event: Sedimentology, v. 44, p. 687–706.

Jenkyns, H.C., Gröcke, D.R. and Hesselbo, S. P., 2001, Nitrogen Isotope evidence for water mass denitrification during the early Toarcian (Jurassuc) oceanic anoxic event: Paleoceanography, v. 16, p. 593–603.

Jenkyns, H.C., Jones, C.E., Gröcke, D.R., Hesselbo. S.P. and Parkinson, D.N., 2002, Chemostratigraphy of the Jurassic System: applications, limitations and implications for palaeoceanography: Journal of the Geological Society, London, v. 159, p. 351–378.

Jenkyns, H.C., Forster, A., Schouten, S., and Sinninghe Damsté, J.S., 2004, High temperatures in the Late Cretaceous Arctic Ocean: Nature, v. 432, p. 888–892

Jenkyns, H.C., Matthews, A., Tsikos, H. and Erel, Y., 2007, Nitrate reduction, sulfate rediction, and sedimentary iron isotope evolution during the Cenomanian–Turonian oceanic anoxic event: Paleoceanography, v. 22, PA3208, 17 p., doi: 10.1029/2006PA001355.

Johnson, T.M. and Bullen, T.D., 2004, Mass-dependant fractionation of selenium and chromium isotopes in low-temperature environments: Reviews of Mineralogy Geochemistry, v. 55, p. 290–317.

Jones, C.E. and Jenkyns, H.C., 2001, Seawater Strontium Isotopes, Oceanic Anoxic Events, and seafloor hydrothermal activity in the Jurassic and Cretaceous: American Journal of Science, v. 301, p. 112–149.

Kafousia, N., Karakitsios, V., Jenkyns, H.C. and Mattioli, E., 2011, A global event with a regional character: the Early Toarcian Oceanic Anoxic Event in the Pindos Ocean (northern Peloponnese, Greece): Geological Magazine, v. 148, p. 619–631.

Kemp, D.B., Coe, A.L., Cohen, A.S., and Schwark, L., 2005, Astronomical pacing of methane release in the Early Jurassic period: Nature, v. 437, p. 396–399, doi:10.1038/nature04037.

Langford, F.F. and Blanc-Valleron, M.-M., 1990, Interpreting Rock-Eval Pyrolysis data using graphs of pyrolizable hydrocarbons vs. Total Organic Carbon: The American Association of Petroleum Geologists Bulletin, v. 74, p. 799–804.

Littler, K., Hesselbo, S.P. and Jenkyns, H.C., 2010, A carbon-isotope perturbation at the Pliensbachian–Toarcian boundary: evidence from the Lias Group, NE England: Geological Magazine, v. 147, p. 181-192.

Lu, Z., Jenkyns, H.C. and Rickaby, E. M., 2010, Iodine to calcium ratios in marine carbonate as paleo-redox proxy during oceanic anoxic events: Geology, v. 38, p. 1107–1110, doi: 10.1130/ G31145.1.

Lyons, T. W., Anbar, A. D., Severmann, S., Scott, C. and Gill, B. C., 2009, Tracking Euxinia in the ancient ocean: a multiproxy perspective and Proterozoic case study: Annu. Rev. Earth Planet. Sci., v. 37, p. 507–534, doi: 10.1146/annurev.earth.36.031207.124233.

McArthur, J.M., Algeo, T.J., van de Schootbrugge, B., Li, Q., and Howarth, R.J., 2008, Basinal restriction, black shales, Re-Os dating, and the Early Toarcian (Jurassic) oceanic anoxic event: Paleoceanography, v. 23, PA4217, doi:10.1029/2008PA001607.

Morford, J.L. and Emmerson, S., 1999, The geochemistry of redox sensitive trace metals in sediments: Geochimica et Cosmochimica Acta, v. 63, p. 1735–1750, doi:10.1016/S0016-7037(99)00126-X.

Moldowan, J.M., Sundararaman, P., and Schoell, M., 1985, Sensitivity of biomarker properties to depositional environment and/or source input in the Lower Toarcian of SW-Germany: Advances in Organic Geochemistry, v. 10, p. 915–926.

Nielsen, S. G., Goff, M., Hesselbo, S. P., Jenkyns, H.C., LaRowe, D. E. and Lee, C. A., 2011, Thallium isotopes in early diagentic pyrite- a paleoredox proxy: Geochimica et Cosmochimica Acta, v. 75, p. 6690–6704, doi: 10.1016/j.gca.2011.07.047.

Page, K.N., 2004, A sequence of biohorizons for the subboreal province Lower Toarcian in Northern Britain and their correlation with a submediterranean standard: Rivista Italiana di Paleontologia e Stratigrafia, v. 110, p. 109-114.

Palliani, R.B., Mattioli, E. and Riding, J.B., 2002, The response of marine phytoplankton and sedimentary organic matter to the early Toarcian (Lower Jurassic) oceanic anoxic event in northern England: Marine Micropaleontology, v. 46, p. 223–245.

Pancost, R.D., Crawford, N., Magness, S., Turner, A., Jenkyns, H.C. and Maxwell, J.R., 2004, Further Evidence for the development of photic-zone euxinic conditions during Mesozoic oceanic anoxic events: Journal of the Geological Society, London, v. 161, p. 353–364.

Pearce, C.R., Cohen, A.S., Coe, A.L. and Burton, K.W., 2008, Molybdenum isotope evidence for global ocean anoxia coupled with perturbations to the carbon cycle during the Early Jurassic: Geology, v. 36, p. 231–234, doi:10.1130/ G24446A.1.

Peucker-Ehrinbrink, B. and Ravizza, G., 2000, The marine osmium record: Terra Nova, v. 12, p. 205–219, doi:10.1046/j.1365-3121.2000.00295.x.

Peter, K.E., Walters, C.C. and Moldowan, J.M., 2005a, The Biomarker Guide vol. 1: Biomarkers in the environment and human history: Cambridge University Press. Cambridge, UK, 492 p.

Peter, K.E., Walters, C.C. and Moldowan, J.M., 2005b, The Biomarker Guide vol. 2: Biomarkers in petroleum systems and Earth history: Cambridge University Press. Cambridge, UK, 704 p.

Poulson, R. L., Siebert, C., McManus, J. and Berelson, W.M., 2006, Authigenic molybdenum isotope signatures in marine sediments: Geology, v. 34, p. 617–620, doi:10.1130/G22485.1

Riccardi, A.C., 2005, First teuthid cephalopod from the Lower Jurassic of South America (Neuquén Basin, Argentina), *in,* Riccardi, A.C., ed., New Insights into the Jurassic Record of South America (Andes and Patagonia): Geologica Acta 3, v. 2, p. 179–184.

Riccardi, A.C., 2008, The marine Jurassic of Argentina: a biostratigraphic framework: Episodes, v. 31, p. 326–335.

Sabatino, N., Neri, R., Bellanca, A., Jenkyns, H.C., Baudin, F., Parisi, G. and Masetti, D., 2009, Carbon-isotope records of the Early Jurassic (Toarcian) oceanic anoxic event from the Valdorbia (Umbria–Marche Apennines) and Monte Mangart (Julian Alps) sections: palaeoceanographic and stratigraphic implications: Sedimentology, v. 56, p. 1307–1328, doi:10.1111/j.1365-3091.2008.01035.x.

Sabatino, N., Neri, R., Bellanca, A., Jenkyns, H.C., Masetti, D. and Scopeliti, G., 2011, Petrography and high-resolution geochemical records of Lower Jurassic manganese-rich deposits from Monte Mangart, Julian Alps: Palaeogeography, Palaeoclimatology, Palaeoecology, v. 299, p. 97–109, doi: 10.1016/j.palaeo.2010.10.039.

Sælen, G., Doyle, P. and Talbot, M. R., 1996, Stable-isotope analyses of belemnite rostra from the Whitby Mudstone Fm., England: surface water conditions during deposition of marine black shale: PALAIOS, v. 11, p. 97–117.

Schlanger, S.O. and Jenkyns, H.C., 1976, Cretaceous Oceanic Anoxic Events: causes and consequences: Geologie En Mijnbouw, v. 55, p. 179–184.

Scholle, P.A. and Arthur, M.A., 1980, Carbon isotope fluctuations in Cretaceous pelagic limestones: potential stratigraphic and petroleum exploration tool: American Association of Petroleum Geologists Bulletin, v. 64, p. 67–87, doi:10.1306/2F91892D-16CE-11D7-8645000102C1865D.

Schouten, S., van Kaam-Peters, H. M. E., Rijpstra, W. I. C., Schoell, M. and Sinninghe Damsté, J. S., 2000, Effects of an oceanic anoxic event on the stable carbon isotopic composition of Early Toarcian carbon: American Journal of Science, v. 300, p. 1–22.

Schmid-Röhl, J., Röhl, H.-J., Oschmann, W., Frimmel, A., and Schwark, L., 2002, Palaeoenvironmental reconstruction of Lower Toarcian epicontinental black shales (Posidonia Shale, SW Germany): global versus regional control: Geobios, v. 35, p. 13–20.

Siebert, C., Nägler, T.F., von Blanckenburg, F. and Kramers, J.D., 2003, Molybdenum isotope records as a potential new proxy for paleoceanography: Earth and Planetary Science Letters, v. 211, p. 159–171, doi:10.1016/S0012-821X(03)00189-4.

Siebert, C., McManus, J., Bice, A., Poulson, R., and Berelson, W.M., 2006, Molybdenum isotope signatures in continental margin marine sediments: Earth and Planetary Science Letters, v. 241, p. 723–733, doi:10.1016/ j.epsl.2005.11.010.

Siebert, C., Ross, A., and McManus, J., 2006, Germanium measurements of high-temperature geothermal fluids using double-spike hydride generation MC-ICP-MS: Geochimica et Cosmochimica Acta, v. 70, p. 3986–3995, doi:10.1016j/j.gca.2006.06.007.

Siebert, C., Ross, A., and McManus, J., 2011, Erratum to Siebert, C., Ross, A., and McManus (2006) “Germanium measurements of high-temperature geothermal fluids using double-spike hydride generation MC-ICP-MS”: Geochimica et Cosmochimica Acta, v. 75, p. 6267–6269, doi:10.1016j/j.gca.2011.07.032.

Suan, G., Nikitenko, B. L., Rogov, M. A., Baudin, F., Spangenberg, J. E., Kunazev, V. G., Glinskikh, L. A., Goryacheva, A. A., Adatte, T., Riding, J. B., Föllmi, K. B., Pittet, B.,

Mattioli, E. and Lécuyer, C., 2011, Polar record of Early Jurassic massive carbon injection: Earth and Planetary Science Letters, v. 312, p. 102–113, doi: 10.1016/j.epsl.2011.09.050.

Taylor, K. G., and Macquaker, J. H. S., 2000, Early diagenetic pyrite morphology in a mudstone-dominated succession: the Lower Jurassic Cleveland Ironstone Formation eastern England, Sedimentary Geology, v. 131, p. 77–86, doi: 10.1016/S0037-0738(00)00002-6.

Ten Haven, H.L., de Leeuw, J. W., Sinninghe Damsté, J.S., 1987, Restricted utility of the pristine/phytane ratio as palaeoenvironmental indicator: Nature, v. 330, p. 641–643.

Tissot, B. P. and Welte, D. H., 1984, Petroleum formation and occurrence, 2nd edition: Springer-Verlag, New York, NY., USA, 699 p.

van Breugel, Y., Baas, M., Schouten, S., Mattioli, E. and Sinninghe Damsté, J.S., 2006, Isorenieratane record in black shales from the Paris Basin, France: Constraints on recycling of respired CO_2 as a mechanism for negative carbon isotope shifts during the Toarcian oceanic anoxic event: Paleoceanography, v. 21, PA4220, 8 p., doi:10.1029/2006PA001305.

van de Schootbrugge, B. , Bailey, T.R., Rosenthal, Y., Katz, M.E., Wright, J.D., Miller, K.G., Feist-Burkhardt, S. and Falkowski, P.G., 2005a, Early Jurassic climate change and the radiation of organic walled phytoplankton in the Tethys Ocean: Paleobiology, v. 31, p. 73–97.

Volkheimer, W., 1973, Palinología estratigráfica del Jurásico de la Sierra de Chacai Có y adyacencias (Cuenca Neuquina, República Argentina). I. Estratigrafía de las Formaciones Sierra Chacai Có (Pliensbachiano), Los Molles (Toarciano, Aaleniano), Cura Niyeu (Bayociano) y Lajas (Caloviano inferior): Ameghiniana, v. 10, p. 105–131

Wilkin, R. T., Barnes, H. L. and Brantley, S. L., 1996, The size distribution of framboidal pyrite in modern sediments: an indicator of redox conditions: Geochimica et Cosmochimica Acta, v. 60, p. 3897–3912.

Wilkin, R. T. and Barnes, H. L., 1997, Formation processes of framboidal pyrite: Geochimica et Cosmochimica Acta, v. 61, p. 323–339.

Chapter 5

Conclusions

In order to understand the global extent of the Toarcian Oceanic Anoxic Event and its associated Carbon Isotope Excursion it was important to identify sections in the southern hemisphere, specifically in the Neuquén Basin, Argentina that contained sediments of Early Toarcian age, from the *tennuicostatum–hoelderi* (= *serpentinum*) Andean ammonite Zone boundary, which could be correlated with the record of the event it sections from the Northern Hemisphere.

Examination of sediments from the Neuquén Basin, Argentina, reveals a marine transgression in the basin at the *tennuicostatum–hoelderi* ammonite Zone boundary. An increase in burial of marine derived organic matter and a stepped -6‰ negative carbon-isotope excursion, recorded in wood and bulk sediment from the *tennuicostatum–hoelderi* ammonite zone boundary in the southern hemisphere. The $\delta^{13}C_{org}$ values from three of the successions in Argentina, Arroyo Lapa South (2008 and 2010), Arroyo Lapa North and Arroyo Serrucho may be directly compared with coeval sediments from Yorkshire, England; Haida Gwaii, British Columbia (Carruthers et al., 2011); Mochras farm borehole, Wales (Jenkyns et al., 2001); Kastelli, Greece (Kafousia et al., 2011) and direct correlations of the steps leading up to the negative excursion and the recovery can be drawn. Furthermore the identification of a ~2‰ negative carbon-isotope excursion at the Pliensbachian–Toarcian Boundary, that can be correlated with coeval data from Yorkshire, England (Littler et al., 2010), suggests that this excursion can be used to identify the boundary in sections were good biostratigraphic constraint is lacking.

The data from Arroyo Serrucho can be compared with data collected from the Arroyo Serrucho area by Mazzini et al., (2010), and reveals that due to a lack of good biostratigraphic constraint the data in the Mazzini et al. (2010) study does not record the T-OAE.

Multiproxy data from the Neuquén Basin, Argentina, specifically pyrite framboid diameter distribution, Pr/Ph and $\delta^{98/95}$Mo data reveal that the basin was anoxic for short intervals of time during the T-OAE and this anoxia occurs at the summit of the negative carbon isotope excursion in the Neuquén Basin. The Pyrite framboid diameter data can be compared to coeval data from Port Mulgrave, Yorkshire and reveals a mixture of syngenetic and diagenetic pyrite in Arroyo Lapa North and South, indicating periodic anoxia/euxinia, however the data from Yorkshire suggest predominantly sygnetic pyrite framboids indicating prolonged anoxia in the Cleveland basin during the T-OAE.

The Pristane/Phytane ratio, Sterane/Hopane ratio and Hydrogen Index data can be compared with data from the Posidonia Shale, SW Germany (Frimmel et al., 2004) and reveals that while there is significant variation in organic matter types deposited, marine organic matter dominates during the T-OAE.

The new $\delta^{98/95}$Mo data can be compared with coeval data from the Cleveland Basin, Yorkshire (Pearce et al., 2008) and reveals that while the overall trends and magnitude of the excursion in molybdenum are similar the absolute values of $\delta^{98/95}$Mo and the Mo concentration are affected by local basin depositional settings and sediment types.

These findings contribute to our understanding of the global extent of the Toarcian Oceanic Anoxic Event and the record of the negative carbon isotope excursion, confirming that the event is recorded globally and is captured in a wide array of proxies, with an emphasis on the importance of generating more, higher resolution proxy data from the southern hemisphere and other more open marine locations. It is also important to note that while the Neuquén Basin captures a record of the T-OAE and its associated CIE, it is apparent that local basin depositional settings have a direct affect on the proxy record in each basin. It is therefore important when utilizing proxies, to have a good understanding of basin morphology, depositional history, sediment and organic matter types.

During the collection of samples from Arroyo Lapa in 2010, several tuffaceous ash beds where identified and sampled, these samples have been sent to the Radiogenic Isotope Lab at MIT to be dated by Dr. Sam Bowring. At present zircon crystals have been identified and picked from the samples and sample analysis is pending, but was not completed in time for inclusion in this thesis. A significant number of samples also remain to be analysed for $\delta^{13}C_{org}$ from Arroyo Lapa North and Arroyo Chacay Melehue. Furthermore identification and examination of organic rich fine grained sediments from Arroyo Lapa, (North and South) for biomarkers may be important to determine if isorenieratane is present in the sedimentary succession at Arroyo Lapa, during the T-OAE.

References

Caruthers, A.H., Gröcke, D.R., and Smith, P.L., 2011, The significance of an Early Jurassic (Toarcian) carbon-isotope excursion in Haida Gwaii (Queen Charlotte Islands), British Columbia, Canada: Earth and Planetary Science Letters, v. 307, p. 19–26 doi:10.1016/j.epsl.2011.04.013.

Frimmel, A., Oschmann, W. and Schwark, L., 2004, Chemostratigraphy of the Posidonia Black Shale, SW Germany: I. influence of sea-level variation on organic facies evolution: Chemical Geology, v. 206, p. 199–230, doi:10.1016/j.chemgeo.2003.12.007.

Jenkyns, H.C., Gröcke, D.R. and Hesselbo, S.P., 2001, Nitrogen isotope evidence for water mass denitrification during the early Toarcian (Jurassic) oceanic anoxic event: Paleoceanography, v. 16, p. 593–603.

Kafousia, N., Karakitsios, V., Jenkyns, H.C. and Mattioli, E., 2011, A global event with a regional character: the Early Toarcian Oceanic Anoxic Event in the Pindos Ocean (northern Peloponnese, Greece): Geoogical Magazine, v. 148, p. 619-631.

Kemp, D.B., Coe, A.L., Cohen, A.S. and Schwark, L., 2005, Astronomical pacing of methane release in the Early Jurassic period: Nature, v. 437, p. 396-399.

Littler, K., Hesselbo, S.P. and Jenkyns, H.C., 2010, A carbon-isotope perturbation at the Pliensbachian–Toarcian boundary: evidence from the Lias Group, NE England: Geological Magazine, v. 147, p. 181-192.

Mazzini, A., Svenson, H., Leanza, H.A., Corfu, F. and Planke, S., 2010, Early Jurassic shale chemostratigraphy and U-Pb ages from the Neuquén Basin (Argentina): Implications for the Toarcian Oceanic Anoxic Event: Earth and Planetary Science Letters, v. 297, p. 633-645. doi:10.1016/j.epsl.2010.07.017.

Pearce, C.R., Cohen, A.S., Coe, A.L. and Burton, K.W., 2008, Molybdenum isotope evidence for global ocean anoxia coupled with perturbations to the carbon cycle during the Early Jurassic: Geology, v. 36, p. 231–234, doi:10.1130/ G24446A.1.

Sabatino, N., Neri, R., Bellanca, A., Jenkyns, H.C., Baudin, F., Parisi, G. and Masetti, D., 2009, Carbon-isotope records of the Early Jurassic (Toarcian) oceanic anoxic event from the Valdorbia (Umbria–Marche Apennines) and Monte Mangart (Julian Alps) sections: palaeoceanographic and stratigraphic implications: Sedimentology, v. 56, p. 1307-1328.

Appendix A: Detailed Stratigraphic Logs with Geochemical Data and Biostratigraphy

Figure 1: Arroyo Lapa South, 2008, Detailed Stratigraphic Log with Data.

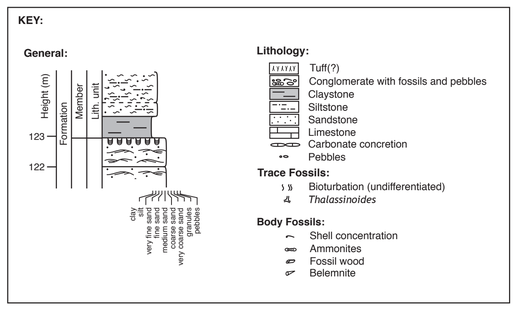
Figure 2: Arroyo Lapa South, 2010, Detailed Stratigraphic Log with Data.

Figure 3: Arroyo Lapa North, Detailed Stratigraphic Log with Data.

Figure 4: Chacay Melehue, Detailed Stratigraphic Log with Data.

Figure 5: Arroyo Serrucho, Detailed Stratigraphic Logs with Data.

Figure 1
Arroyo Lapa South 2008, Neuquén, Argentina
Hesselbo notebook 26.3.08 – 28.3.08
Samples: Al-Suwaidi, Damborenea, Hesselbo, Jenkyns, Manceñido



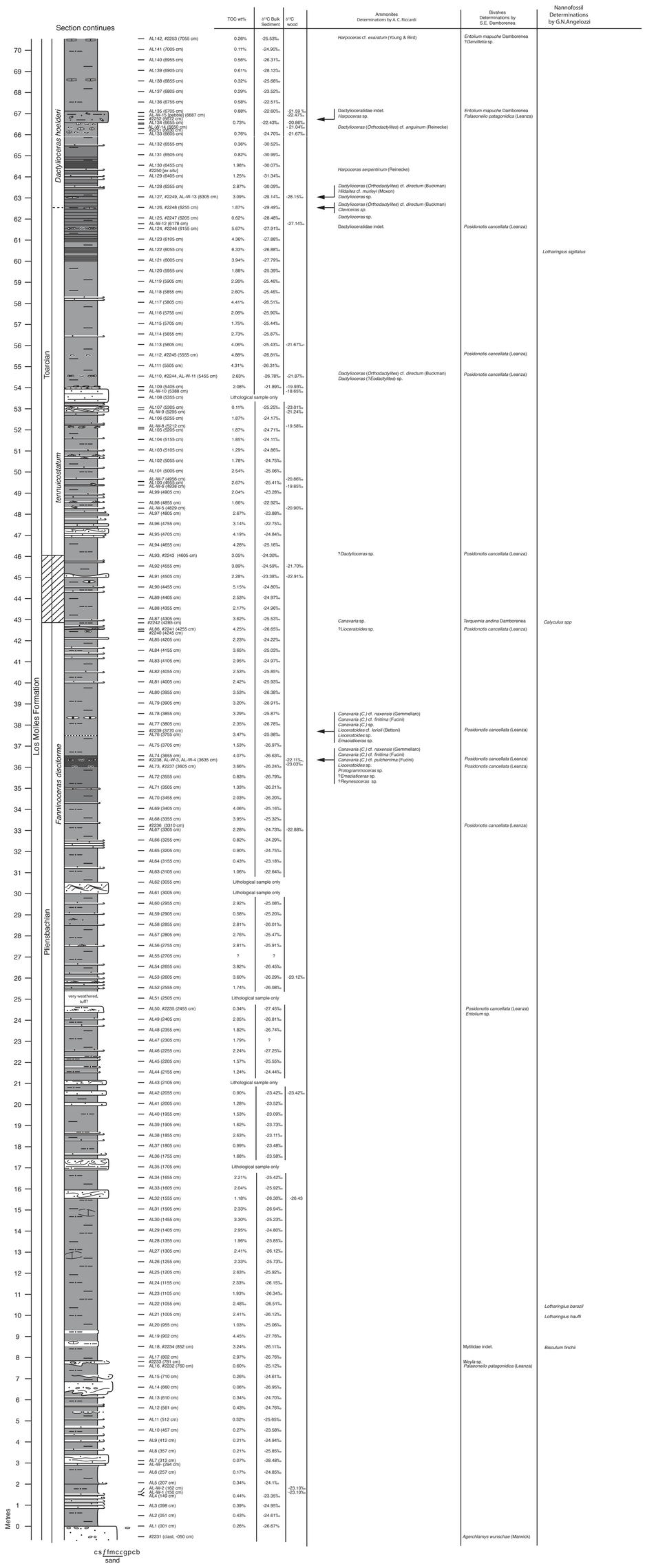
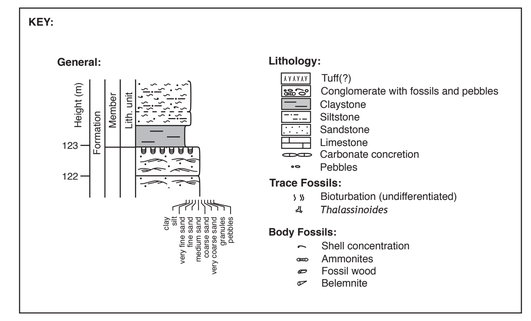
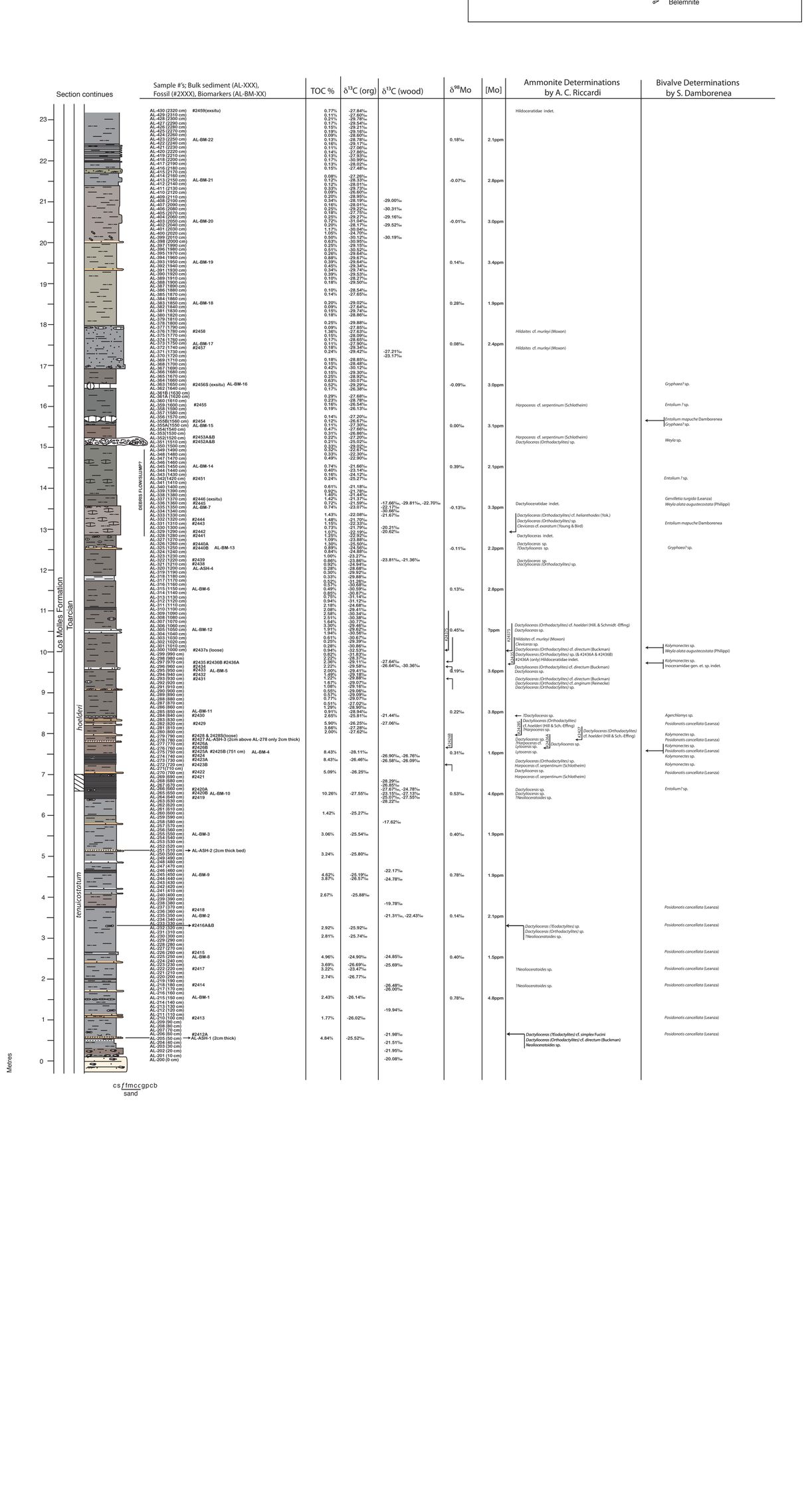


Figure 2
Arroyo Lapa South 2010, Neuquén, Argentina
Hesselbo notebook 4.4.10 – 6.4.10
Samples: Al-Suwaidi, Damborenea, Hesselbo, Jenkyns, Manceñido, Ros





Appendix A: Detailed Stratigraphic Log with Data

Figure 3
Arroyo Lapa North, Neuquén, Argentina
Hesselbo notebook 4.4.10 – 6.4.10
Samples: Al-Suwaidi, Damborenea, Hesselbo, Jenkyns, Manceñido, Ros

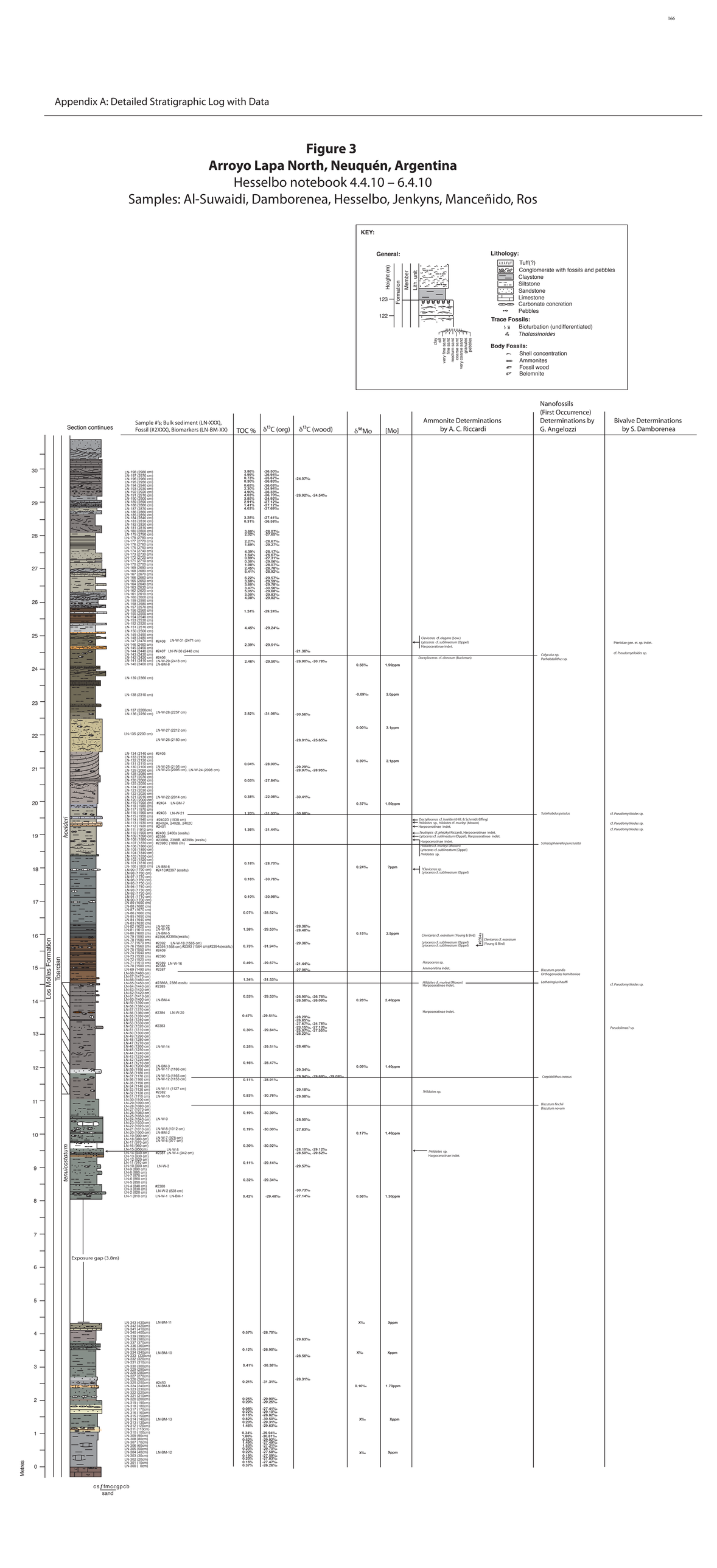
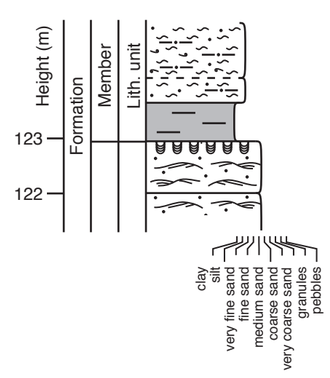


Figure 4
Chacay Melehue, Neuquén, Argentina
Hesselbo notebook 30.3.08 – 2.4.08
Samples: Al-Suwaidi, Damborenea, Hesselbo, Jenkyns, Mancinado

KEY:

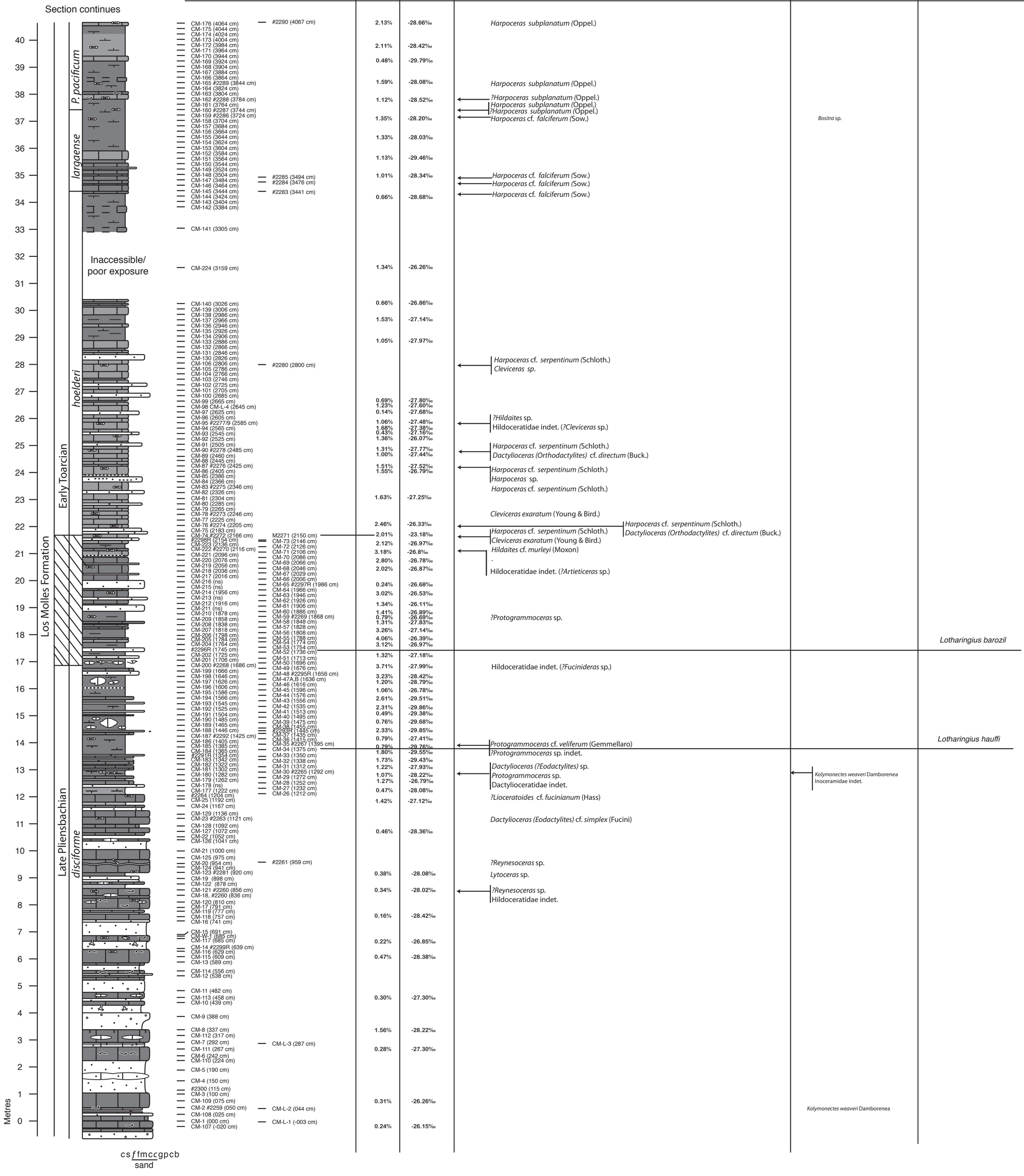
General:



Lithology:
- Tuff(?)
- Conglomerate with fossils and pebbles
- Claystone
- Siltstone
- Sandstone
- Limestone
- Carbonate concretion
- Pebbles

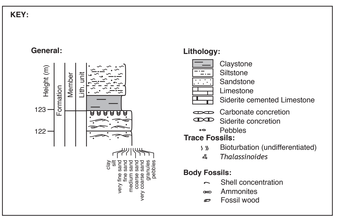
Trace Fossils:
- Bioturbation (undifferentiated)
- *Thalassinoides*

Body Fossils:
- Shell concentration
- Ammonites
- Fossil wood
- Belemnite

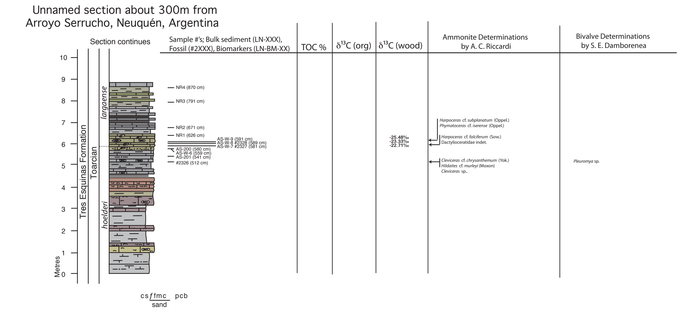


Appendix A: Detailed Stratigraphic Log with Data

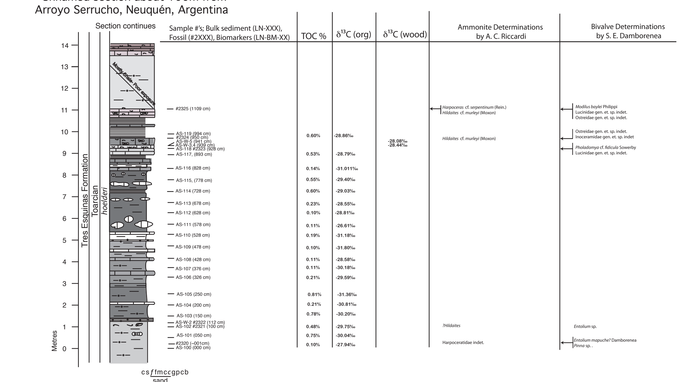
Figure 5
Arroyo Serrucho, Neuquén, Argentina
Hesselbo notebook 06.04.08 – 08.04.08,
Samples: Al-Suwaidi, Damborenea, Hesselbo, Jenkyns, Manceñedo



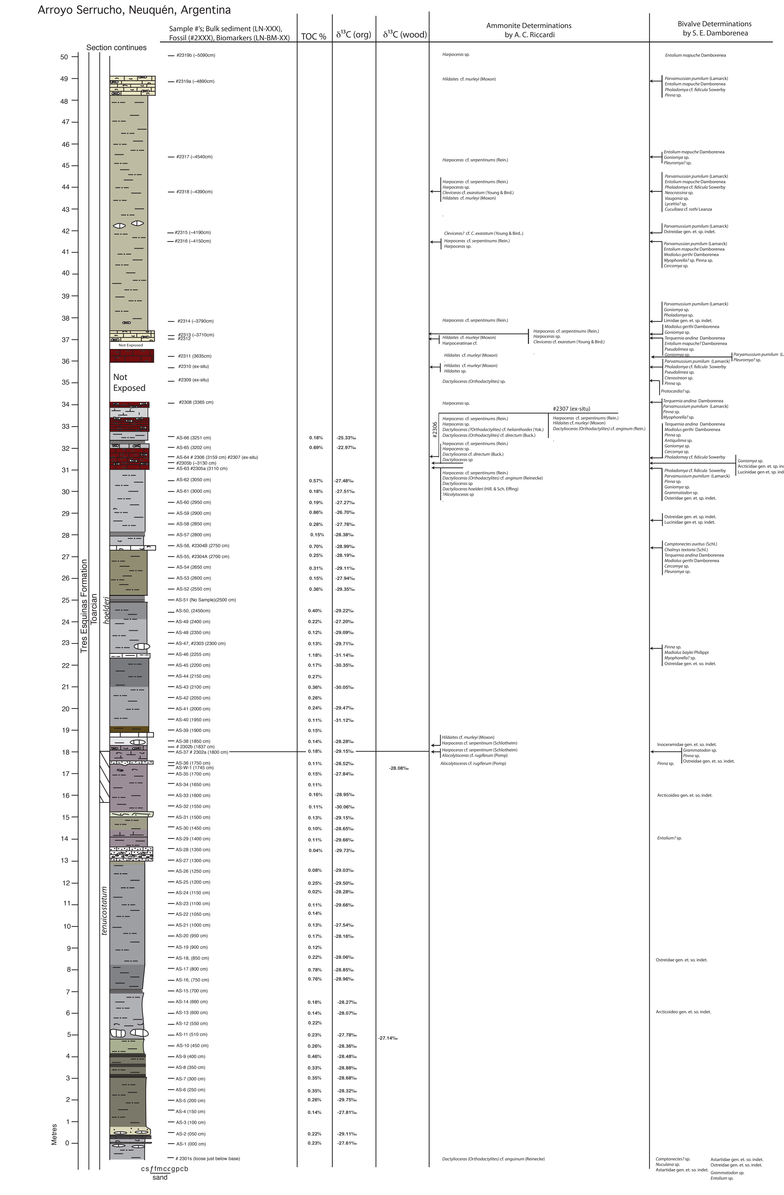
Unnamed section about 300m from Arroyo Serrucho, Neuquén, Argentina



Unnamed section about 100m from Arroyo Serrucho, Neuquén, Argentina



Arroyo Serrucho, Neuquén, Argentina



Appendix B: Raw Geochemical Data

B1. Arroyo Lapa South 2008- Bulk Sediment Organic Carbon Isotope and Total Organic Carbon Data

Sample	$\delta^{13}C_{org}$ (VPDB)	Height (m)	TOC (%) Coloumetric	TOC (wt %)
AL-1	-26.67	0	0.26	0.670433145
AL-2	-24.61	0.51	0.43	0.379104478
AL-3	-24.95	0.98	0.39	0.304405874
AL-4	-23.35	1.49	0.44	0.593220339
AL-5	-24.41	2.07	0.34	0.335025381
AL-6	-24.85	2.57	0.17	0.267387944
AL-7	-28.48	3.12	0.07	0.118518519
AL-8	-25.85	3.57	0.21	0.124528302
AL-9	-24.94	4	0.21	0.232758621
AL-10	-23.58	4.57	0.27	0.249566724
AL-11	-25.65	5	0.32	0.442265795
AL-12	-24.76	5.61	0.43	0.396850394
AL-13	-24.7	6.1	0.34	0.422572178
AL-14	-26.95	6.6	0.06	0.076190476
AL-15	-24.61	7.1	0.26	0.272511848
AL-16	-25.12	7.6	0.60	0.562962963
AL-17	-26.76	8.02	2.97	3.127118644
AL-18	-26.11	8.52	3.24	3.455357143
AL-19	-27.76	9.02	4.45	4.871428571
AL-20	-25.06	9.55	1.03	1.085858586
AL-21	-26.12	9.98	2.41	3.404580153
AL-22	-26.51	10.55	2.48	3.156716418
AL-23	-26.34	11.05	1.93	2.642105263
AL-24	-26.15	11.55	2.33	3.314285714
AL-25	-25.92	11.98	2.63	3.515873016
AL-26	-25.73	12.55	2.33	3.10738255
AL-27	-26.12	12.98	2.41	3.45323741
AL-28	-25.85	13.55	1.96	2.680272109
AL-29	-24.8	13.98	2.95	3.581967213
AL-30	-25.23	14.48	3.30	4.256637168
AL-31	-26.94	15.05	2.33	2.401197605
AL-32	-26.3	15.48	1.18	1.802752294
AL-33	-25.92	16.05	2.04	2.093959732
AL-34	-25.42	16.48	2.21	2.6
AL-36	-23.58	17.48	1.68	1.514450867
AL-37	-23.48	18.05	0.99	0.884
AL-38	-23.11	18.48	2.63	2.825174825
AL-39	-23.73	19.05	1.62	1.424581006
AL-40	-23.09	19.55	1.53	1.401129944
AL-41	-23.52	20.05	1.28	1.261627907
AL-42	-23.42	20.55	0.9	1.286324786
AL-44	-24.44	21.48	1.24	1.433179724
AL-45	-25.55	21.98	1.57	1.755555556
AL-46	-27.25	22.55	2.24	2.291666667
AL-48	-26.74	23.55	1.82	1.99408284
AL-49	-26.81	24.05	2.05	2.186335404
AL-50	-27.45	24.55	0.34	0.662900188
AL-52	-26.08	25.55	1.74	1.851485149
AL-53	-26.29	25.98	3.60	4.672413793

!

Sample	! $^{13}C_{org}$ ‰ (VPDB)	Height (m)	TOC (%) Coloumetric	TOC (wt %)
AL-54	-26.45	26.55		4.352112676
AL-56	-25.91	27.48	2.31	3.007092199
AL-57	-25.47	27.98	2.76	3.606666667
AL-58	-26.01	28.55	2.81	3.992592593
AL-59	-25.2	29.05	0.58	0.824761905
AL-60	-25.08	29.55		3.334862385
AL-63	-22.64	31.05	1.06	1.144366221
AL-64	-23.18	31.55	0.43	0.442391417
AL-65	-24.75	32.05	0.90	0.892433053
AL-66	-24.29	32.55	0.82	1.072607261
Al-67	-24.73	33.05	2.28	1.603860106
AL-68	-25.32	33.55	3.95	4.022395402
AL-69	-25.16	34.05	4.06	3.725490196
AL-70	-26.2	34.55	2.03	2.220183486
AL-71	-26.21	35.05	1.33	1.106481481
AL-72	-26.79	35.55	0.83	0.874125874
AL-73	-26.24	36.05	3.66	3.642160499
AL-74	-26.63	36.55	4.07	5
AL-75	-26.97	37.05	1.53	1.644444444
AL-76	-25.98	37.55	3.47	4.794117647
AL-77	-26.78	38.05	2.35	2.716981132
AL-78	-25.87	38.55	3.29	3.279661017
AL-79	-26.91	39.05	3.20	2.999239539
AL-80	-26.38	39.55	3.53	3.95412844
AL-81	-25.93	40.05	2.42	2.918367347
AL-82	-25.85	40.55	2.53	2.68503937
AL-83	-24.97	41.05	2.95	4.05
AL-84	-25.03	41.55	3.65	4.218956169
AL-85	-24.22	42.05	2.23	3.329192547
AL-86	-26.65	42.55	4.25	5.339805825
AL-87	-25.53	43.05	3.62	4.079646018
AL-88	-24.96	43.55	2.17	2.54954955
AL-89	-24.97	44.05	2.53	2.700066529
AL-90	-24.8	44.55	5.15	4.18705036
AL-91	-23.38	45.05	2.28	3.221767864
AL-92	-24.59	45.55	3.89	4.263157895
AL-93	-24.3	46.05	3.05	2.621359223
AL-94	-25.16	46.55	4.28	4.564356436
AL-95	-24.84	47.05	4.19	4.581632653
Al-96	-22.75	47.55	3.14	3.688777115
AL-97	-23.88	48.05	2.67	2.875968992
AL-98	-22.92	48.55	1.66	2.448275862
AL-99	-23.28	49.05	2.04	2.213492353
AL-100	-25.41	49.55	2.67	3.031458238
AL-101	-25.06	50.05	2.54	2.772058824
AL-102	-24.75	50.55	1.78	2.206451613
AL-103	-24.96	51.04	1.29	1.601941748
AL-104	-24.11	51.54	1.85	2.167567568
AL-105	-24.71	52.05	1.87	2.177777778
AL-106	-24.17	52.55	3.65	3.734265734
AL-107	-25.25	53.05		0.114942529
AL-109	-21.89	54.05		2.081739343
AL-110	-26.78	54.55	2.63	3.547368421

!

Sample	! $^{13}C_{org}$ ‰(VPDB)	Height (m)	TOC (%) Coloumetric	TOC (wt %)
AL-111	-26.31	55.05	4.31	4.490322581
AL-112	-26.81	55.55	4.88	6.527472527
AL-113	-25.43	56.05	4.06	5.552631579
AL-114	-25.87	56.55	2.73	3.25
AL-115	-25.44	57.05	1.75	2.329842932
AL-116	-25.9	57.55	2.06	2.507142857
AL-117	-26.51	58.05	4.41	4.259259259
AL-118	-25.46	58.55	2.60	2.456
AL-120	-25.39	59.55	1.88	1.919080962
AL-121	-27.79	60.05	3.94	7.011695906
AL-122	-26.88	60.55	6.33	12.27358491
AL-123	-27.88	61.05	4.36	0.194444444
AL-124	-27.91	61.55	5.67	7.134146341
AL-125	-28.48	62.05	0.62	0.605691057
AL-126	-29.49	62.55	1.87	2.031746032
AL-127	-29.14	63.05	3.09	3.017241379
AL-128	-30.09	63.55	2.87	3.575221239
AL-129	-31.34	64.05	1.25	1.247524752
AL-130	-30.07	64.55	1.98	2.670520231
AL-131	-30.99	65.05	0.82	0.825454545
AL-132	-30.52	65.55	0.36	0.388686131
AL-133	-24.70	66.05	0.76	0.8515253
AL-134	-22.43	66.55	0.73	0.952177759
AL-135	-22.6	67.05	0.88	1.564971751
AL-136	-22.51	67.55	0.58	0.588693957
AL-137	-23.52	68.05	0.29	0.449612403
AL-138	-25.68	68.55	0.32	0.299802761
AL-139	-28.13	69.05	0.61	0.586446426
AL-140	-26.31	69.55	0.56	0.682073054
AL-141	-24.9	70.05	0.11	0.253496503
AL-142	-23.53	70.55	0.26	0.62472713
Mean	**-25.60**		2.09	
Maximum	**-21.89**		6.33	
Minimum	**-31.34**		0.06	
Std Dev. ±	**1.74**			

B2. Arroyo Lapa South 2008- Fossil Wood Organic Carbon Isotope Data

Sample	$\delta^{13}C_{wood}$ (VPDB)	Height (m)
AL-W-1	-23.1	1.5
AL-W-2	-23.1	1.62
AL-32W	-26.43	15.55
AL-42W	-23.42	20.55
AL-53W	-23.12	26.05
AL-67W	-22.88	33.05
AL-W-3	-22.11	36.35
AL-W-4	-23.03	36.35
AL-91w	-22.91	45.05
AL-92w	-21.7	45.55
AL-W-5	-20.9	48.29
AL-W-6	-19.85	49.38
AL-W-7	-20.86	49.56
AL-W-8	-19.58	52.12
AL-W-9	-21.24	52.95
AL-107w	-23.01	53.05
AL-W-10	-20.65	53.88
AL-109w	-19.93	54.05
AL-W-11	-23.77	54.55
AL-113w	-24.22	56.05
AL-W-12	-27.14	61.78
AL-W-13	-28.15	63.05
AL-133w	-21.67	66.05
AL-W-14	-21.04	66.5
AL-134w	-20.86	66.55
AL-W-15	-22.47	66.87
AL-135w	-21.59	67.05
	Mean	**-22.55**
	Minimum	**-28.15**
	Maximum	**-19.58**
	Std. Dev. ±	**2.11**

!

B3. Arroyo Lapa South 2010- Bulk Sediment Organic Carbon Isotope and Total Organic Carbon Data

Name	! $^{13}C_{org}$ (VPDB)	Height (m)	TOC (%)
AL-205	-25.52	0.50	4.84
AL-210	-26.02	1.00	1.77
AL-215	-26.14	1.50	2.43
AL-220	-26.78	2.00	2.74
AL-223	-26.67	2.30	3.69
AL-224	-23.47	2.40	3.22
AL-225	-24.90	2.50	4.96
AL-230	-25.74	3.00	2.81
AL-232	-25.92	3.20	2.92
AL-240	-25.88	4.00	2.67
AL-244	-26.57	4.40	3.87
AL-245	-25.19	4.50	4.62
AL-250	-25.80	5.00	3.24
AL-255	-25.54	5.50	3.06
AL-260	-25.27	6.00	1.42
AL-265	-27.55	6.50	10.26
AL-270	-26.25	7.00	5.09
AL-273	-26.46	7.30	8.43
AL-275	-28.11	7.50	8.43
AL-280	-27.62	8.00	2.00
AL-281	-27.28	8.10	3.66
AL-282	-26.25	8.20	5.90
AL-284	-25.81	8.40	2.65
AL-285	-28.94	8.50	0.91
AL-286	-25.97	8.60	4.13
AL-286	-28.90	8.60	1.29
AL-287	-27.02	8.70	0.51
AL-288	-29.07	8.80	0.77
AL-289	-29.09	8.90	0.57
AL-290	-29.06	9.00	0.55
AL-291	-29.16	9.10	1.08
AL-292	-29.07	9.20	1.67
AL-293	-29.88	9.30	1.22
AL-294	-29.18	9.40	1.49
AL-295	-29.41	9.50	2.00
AL-296	-29.58	9.60	2.22
AL-297	-29.11	9.70	2.36
AL-298	-28.37	9.80	2.22
AL-299	-31.83	9.90	0.82
AL-300	-32.53	10.00	0.94
AL-301	-30.86	10.10	0.28
AL-302	-29.39	10.20	0.25
AL-303	-30.67	10.30	0.61
AL-304	-30.56	10.40	1.94
AL-305	-29.62	10.50	0.31
AL-306	-29.46	10.60	3.30
AL-307	-30.77	10.70	1.64
AL-308	-30.38	10.80	2.51
AL-309	-30.34	10.90	2.58
AL-310	-29.41	11.00	2.08
AL-311	-24.68	11.10	2.18
AL-312	-31.12	11.20	0.94

!

Name	! $^{13}C_{org}$ (VPDB)	Height (m)	TOC (%)
AL-313	-31.14	11.30	0.75
AL-314	-30.87	11.40	0.85
AL-315	-30.59	11.50	0.49
AL-316	-30.68	11.60	0.57
AL-317	-31.26	11.70	0.52
AL-318	-29.88	11.80	0.33
AL-319	-29.92	11.90	0.30
AL-320	-28.69	12.00	0.28
AL-321	-24.94	12.10	0.92
AL-322	-23.86	12.20	0.86
AL-323	-23.27	12.30	1.00
AL-324	-24.88	12.40	0.84
AL-325	-24.56	12.50	0.89
Al-326	-25.50	12.60	1.30
AL-327	-23.88	12.70	1.09
AL-328	-22.92	12.80	1.25
AL-329	-22.19	12.90	1.07
AL-330	-21.79	13.00	0.73
AL-331	-22.33	13.10	1.15
AL-332	-21.70	13.20	1.48
AL-333	-22.08	13.30	1.43
AL-335	-23.07	13.50	0.74
AL-336	-21.59	13.60	0.72
AL-337	-21.37	13.70	1.42
AL-338	-21.44	13.80	1.40
AL-339	-21.78	13.90	0.92
AL-340	-22.18	14.00	0.61
AL-342	-25.27	14.20	0.24
AL-343	-24.12	14.30	0.16
AL-344	-23.14	14.40	0.40
AL-345	-21.66	14.50	0.74
AL-347	-22.90	14.70	0.49
AL-348	-22.30	14.80	0.33
AL-349	-22.67	14.90	0.32
AL-350	-29.02	15.00	0.33
AL-351	-25.02	15.10	0.21
AL-352	-27.20	15.20	0.22
AL-353	-26.86	15.30	0.31
AL-354	-27.66	15.40	0.47
AL-355A	-27.30	15.50	0.11
AL-355B	-26.67	15.60	0.12
AL-356	-27.20	15.70	0.14
AL-358	-26.13	15.90	0.19
AL-359	-26.54	16.00	0.16
AL-360	-28.78	16.10	0.23
AL-361A	-27.68	16.20	0.29
AL-362	-26.38	16.40	0.17
AL-363	-29.29	16.50	0.52
AL-364	-30.07	16.60	0.63
AL-365	-28.92	16.70	0.25
AL-366	-29.30	16.80	0.15
AL-367	-30.12	16.90	0.42
AL-368	-28.48	17.00	0.15
AL-369	-28.85	17.10	0.18

!

Name	! $^{13}C_{org}$ (VPDB)	Height (m)	TOC (%)
AL-371	-29.42	17.30	0.24
AL-372	-29.34	17.40	0.18
AL-373	-27.90	17.50	0.11
AL-374	-28.65	17.60	0.17
AL-375	-28.09	17.70	0.15
AL-376	-27.63	17.80	1.36
AL-377	-27.85	17.90	0.09
AL-378	-29.88	18.00	0.25
AL-380	-28.86	18.20	0.18
AL-381	-29.74	18.30	0.15
AL-382	-27.64	18.40	0.09
AL-383	-29.02	18.50	0.20
AL-385	-28.54	18.50	0.14
AL-385	-27.99	18.70	0.15
AL-386	-27.65	18.80	0.10
AL-388	-29.50	19.00	0.18
AL-389	-28.27	19.10	0.10
AL-390	-29.53	19.20	0.39
AL-390	-27.44	19.20	0.12
AL-391	-29.74	19.30	0.34
AL-392	-27.68	19.40	0.20
AL-392	-29.34	19.40	0.45
AL-393	-29.64	19.50	0.39
AL-394	-29.67	19.60	0.88
AL-395	-29.64	19.70	0.26
AL-396	-30.52	19.80	0.51
AL-397	-29.15	19.90	0.25
AL-398	-30.95	20.00	0.63
AL-398	-29.60	20.00	0.36
AL-399	-30.12	20.10	0.50
AL-400	-24.70	20.20	1.05
AL-401	-30.04	20.30	1.17
AL-402	-28.71	20.40	0.20
AL-403	-31.04	20.50	0.72
AL-404	-29.27	20.60	0.25
AL-405	-27.75	20.70	0.18
AL-406	-29.23	20.80	0.25
AL-407	-28.01	20.90	0.16
AL-408	-28.19	21.00	0.34
AL-409	-28.95	21.10	0.20
AL-410	-26.60	21.20	0.09
AL-411	-29.73	21.30	0.33
AL-412	-28.01	21.40	0.12
AL-413	-28.33	21.50	0.12
AL-413	-27.34	21.50	0.13
AL-414	-27.26	21.60	0.08
AL-416	-27.48	21.80	0.15
AL-417	-28.02	21.90	0.13
AL-418	-30.99	22.00	0.17
AL-419	-27.93	22.10	0.13
AL-420	-27.86	22.20	0.14
AL-421	-27.06	22.30	0.11
AL-422	-29.17	22.40	0.16
AL-423	-28.78	22.50	0.13

!

Name	! $^{13}C_{org}$ (VPDB)	Height (m)	TOC (%)
AL-424	-28.60	22.60	0.09
AL-425	-29.16	22.70	0.19
AL-426	-29.21	22.80	0.15
AL-427	-29.54	22.90	0.17
AL-428	-29.78	23.00	0.21
AL-429	-27.60	23.10	0.11
Al-430	-27.84	23.20	0.77
Mean	**-27.71**		**0.58**
Maximum	**-21.37**		**3.30**
Minimum	**-32.53**		**0.078**
Std Dev. ±	**2.57**		

B4. Arroyo Lapa South- Fossil Wood Organic Carbon Isotope Data

Sample #	$\delta^{13}C_{wood}$ ‰ (VPDB)	Height
AL-200W	-20.09	0
AL-202W	-21.95	0.2
AL-204W	-21.52	0.4
AL-206W	-21.99	0.6
AL-212W	-19.94	1.2
AL-217W	-26.01	1.7
AL-218W	-26.48	1.8
AL-223W	-25.69	2.3
AL-225W	-24.85	2.5
AL-235W	-21.31	3.5
AL-235W	-22.43	3.5
AL-238W	-19.78	3.8
AL-244W	-24.78	4.4
AL-246W	-22.17	4.6
AL-258W	-17.63	5.8
AL-263W	-28.22	6.3
AL-264W	-27.55	6.4
AL-264W	-25.07	6.4
AL-265W	-23.15	6.5
AL-265W	-27.13	6.5
AL-266W	-27.67	6.6
AL-266W	-24.78	6.6
AL-267W	-26.85	6.7
AL-268W	-28.30	6.8
AL-270W	-23.91	7
AL-271W	-26.09	7.1
AL-271W	-26.58	7.1
AL-272W	-25.15	7.2
AL-274W	-26.90	7.4
AL-274W-F	-26.76	7.4
AL-282W	-27.06	8.2
AL-284W	-21.41	8.4
AL-296W	-26.64	9.6
AL-296W	-30.37	9.6
AL-297W	-27.64	9.7
AL-322W	-21.36	12.2
AL-322W	-23.81	12.2
AL-329W	-22.62	12.9
AL-330W	-20.21	13
AL-333W	-21.67	13.3
AL-334W	-30.66	13.4
AL-335W	-22.17	13.5
AL-336W	-22.70	13.6
AL-336W	-29.82	13.6
AL-336W	-17.66	13.6
AL-371W	-27.21	17.1
AL-370-371	-23.17	17.2
AL-399W	-30.19	20.1
AL-402W	-29.52	20.3
AL-404W	-29.17	20.5
AL-406W	-30.31	20.6
AL-408W	-29.00	20.9

!

Sample #	! $^{13}C_{wood}$ ‰ (VPDB)
Mean	**-24.90**
Maximum	**-17.63**
Minimum	**-30.66**
Std Dev.±	**3.43**

B5. Arroyo Lapa North- Bulk sediment Organic Carbon Isotope and TOC Data

Name	! $^{13}C_{org}$ ‰ (VPDB)	Height (m)	Adjusted Height w/ expo. Gap	TOC%
LN-300	-26.26	0	0	0.37
LN-301	-27.47	0.1	0.1	0.16
LN-302	-27.83	0.2	0.2	0.20
LN-303	-27.59	0.3	0.3	0.19
LN-304	-27.58	0.4	0.4	0.22
LN-305	-29.70	0.5	0.5	0.20
LN-306	-27.21	0.6	0.6	0.15
LN-307	-27.49	0.7	0.7	0.15
LN-308	-29.02	0.8	0.8	0.52
LN-309	-30.81	0.9	0.9	1.80
LN-310	-29.94	1	1	0.33
LN-312	-28.41	1.2	1.2	0.11
LN-312	-29.63	1.2	1.2	1.46
LN-313	-29.31	1.3	1.3	0.20
LN-314	-30.50	1.4	1.4	0.82
LN-315	-28.82	1.5	1.5	0.16
LN-316	-29.10	1.6	1.6	0.22
LN-317	-27.41	1.7	1.7	0.08
LN-319	-29.25	1.9	1.9	0.29
LN-320	-29.91	2	2	0.25
LN-325	-31.31	2.5	2.5	0.21
LN-330	-30.38	3	3	0.41
LN-335	-26.90	3.5	3.5	0.12
LN-340	-28.70	4	4	0.57

LN-1	-29.48	0.00	8.1	0.42
LN-6	-29.34	0.50	8.6	0.31
LN-11	-29.14	1.00	9.1	0.11
LN-16	-30.92	1.50	9.6	0.30
LN-21	-30.00	2.00	10.1	0.19
LN-26	-30.30	2.50	10.6	0.14
LN-31	-30.76	3.00	11.1	0.83
LN-36	-28.91	3.50	11.6	0.11
LN-41	-28.47	4.00	12.1	0.16
LN-46	-29.51	4.50	12.6	0.25
LN-51	-29.85	5.00	13.1	0.30
LN-56	-29.51	5.50	13.6	0.47
LN-61	-29.53	6.00	14.1	0.53
LN-66	-31.53	6.50	14.6	1.34
LN-71	-29.67	7.00	15.1	0.49
LN-76	-31.94	7.50	15.6	0.73
LN-81	-29.53	8.00	16.1	1.38
LN-86	-28.52	8.50	16.6	0.07
LN-91	-30.98	9.00	17.1	0.09
LN-96	-30.76	9.50	17.6	0.16
LN-101	-28.71	10.00	18.1	0.18
LN-111	-31.44	11.00	19.1	1.36
LN-116	-31.03	11.50	19.6	1.20

!

Name	! $^{13}C_{org}$ (VPDB)	Height (m)	Adjusted Height w/ expo. Gap	TOC%
LN-121	-22.08	12.00	20.1	0.38
LN-126	-27.84	12.50	20.6	0.03
LN-131	-28.00	13.00	21.1	0.05
LN-136	-31.06	14.40	22.5	2.28
LN-141	-29.50	16.10	24.2	2.47
LN-146	-29.51	16.60	24.7	2.39
LN-151	-29.25	17.10	25.2	4.45
LN-156	-29.24	17.60	25.7	1.24
LN-160	-29.82	18.00	26.1	4.08
LN-161	-29.83	18.10	26.2	3.00
LN-161	-30.24	18.10	26.2	3.08
LN-162	-29.68	18.20	26.3	5.05
LN-163	-30.56	18.30	26.4	3.47
LN-164	-29.78	18.40	26.5	3.60
LN-165	-29.59	18.50	26.6	3.60
LN-166	-29.57	18.60	26.7	6.22
LN-166	-29.02	18.60	26.7	1.55
LN-168	-28.52	18.80	26.9	0.35
LN-168	-28.92	18.80	26.9	6.41
LN-169	-28.78	18.90	27.0	2.45
LN-170	-28.07	19.00	27.1	1.98
LN-171	-29.06	19.10	27.2	0.30
LN-172	-27.31	19.20	27.3	0.89
LN-173	-26.67	19.30	27.4	1.64
LN-174	-28.17	19.40	27.5	4.39
LN-176	-29.28	19.60	27.7	1.69
LN-177	-28.67	19.70	27.8	2.27
LN-179	-27.65	19.90	28.0	2.02
LN-180	-28.07	20.00	28.1	3.61
LN-183	-26.58	20.30	28.4	0.31
LN-184	-27.41	20.40	28.5	3.28
LN-187	-27.69	20.8	28.9	4.01
LN-188	-27.12	20.70	28.8	1.41
LN-189	-27.12	20.80	28.9	2.91
LN-190	-24.92	20.90	29.0	3.85
LN-191	-26.70	21.10	29.2	4.03
LN-192	-26.33	21.20	29.3	4.90
LN-193	-24.94	21.30	29.4	2.30
LN-194	-26.03	21.40	29.5	0.65
LN-195	-26.83	21.50	29.6	0.30
LN-196	-25.67	21.60	29.7	0.73
LN-197	-26.94	21.70	29.8	4.99
LN-198	-26.50	21.80	29.9	3.86
Mean	**-28.72**			**1.48**
Maximum	**-22.08**			**6.41**
Minimum	**-31.94**			**0.03**
Std Dev. ±	**1.69**			**1.63**

B6. Arroyo Lapa North- Fossil Wood Organic Carbon Isotope Data

Sample #	$\delta^{13}C_{wood}$ ‰(VPDB)	Height (m)	Height adjusted with exposure gap (m)
LN-326W	-28.31	2.60	2.60
LN-333W	-28.56	3.30	3.30
LN-338W	-29.63	3.80	3.80
LN-W-1	-27.14	0.00	8.10
LN-W-2	-30.73	0.32	8.42
LN-10W	-29.57	1.00	9.10
LN-W-4	-28.50	1.30	9.40
LN-W-4	-29.52	1.30	9.40
LN-W-5	-28.10	1.35	9.45
LN-15W	-29.12	1.50	9.60
LN-W-8	-27.84	1.92	10.02
LN-W-9	-28.00	2.20	10.30
LN-W-10	-29.08	3.00	11.10
LN-W-11	-29.18	3.10	11.20
LN-W-13	-29.94	3.60	11.70
LN-W-13R	-29.69	3.60	11.70
LN-37-W	-29.91	3.70	11.80
LN-W-17	-29.34	3.80	11.90
LN-W-14	-28.46	4.40	12.50
LN-W-18	-29.36	7.55	15.65
LN-W-19	-28.48	8.00	16.10
LN-W-32	-28.37	8.10	16.20
LN-W-21	-30.68	11.50	19.60
LN-W-22	-30.41	12.05	20.15
LN-W-23	-28.97	12.75	20.85
LN-W-24	-28.95	12.80	20.90
LN-W-25	-29.29	12.82	20.92
LN-W-26	-28.01	13.70	21.80
LN-W-26	-25.65	13.70	21.80
LN-W-28	-30.57	14.30	22.40
LN-W-29F	-26.91	16.10	24.20
LN-W-29	-30.78	16.10	24.20
LN-W-30	-21.36	16.25	24.35
LN-191W	-26.92	21.10	29.20
LN-196W	-24.08	21.60	29.70
LN-191W	-24.54	21.60	29.70
Mean	**-28.44**		
Maximum	**-21.36**		
Minimum	**-30.78**		
Std Dev. ±	**1.98**		

B7. Arroyo Chacay Melehue- Bulk sediment Organic Carbon Isotope and TOC Data

Name	! $^{13}C_{org}$ ‰ (VPDB)	Height (m)	TOC%
CM-107	-26.15	-0.2	0.24
CM-109	-26.26	0.75	0.31
CM-111	-27.30	2.67	0.28
CM-8	-28.22	3.37	1.56
CM-113	-27.30	4.58	0.30
CM-115	-28.38	6.09	0.47
CM-117	-26.85	6.85	0.22
CM-118	-28.42	7.57	0.16
CM-121	-28.02	8.56	0.34
CM-123	-28.29	9.2	0.40
CM-127	-28.36	10.72	0.46
CM-25	-27.12	11.92	1.42
CM-177	-28.08	12.22	0.47
CM-179	-26.79	12.62	1.27
CM-180	-28.22	12.82	1.07
CM-31	-27.93	13.12	1.22
CM-183	-29.43	13.42	1.73
CM-184	-29.55	13.65	1.80
CM-185	-29.76	13.85	0.79
CM-36	-27.41	14.14	0.79
CM-188	-29.85	14.46	2.33
CM-39	-29.68	14.75	0.76
CM-191	-29.38	15.04	0.49
CM-42	-29.86	15.35	2.31
CM-194	-29.51	15.66	2.61
CM-45	-26.78	15.96	1.06
CM-197	-28.79	16.26	1.20
CM-198	-28.42	16.46	3.23
CM-200	-27.99	16.86	3.71
CM-202	-27.18	17.25	1.32
CM-204	-26.97	17.64	3.12
CM-205	-26.39	17.84	4.06
CM-207	-27.14	18.18	3.26
CM-58	-27.83	18.48	1.31
CM-59	-26.69	18.68	0.79
CM-210	-26.89	18.78	1.41
CM-212	-27.43	19.16	1.48
CM-214	-26.53	19.56	3.02
CM-65	-26.68	19.86	0.24
CM-217	-26.44	20.16	1.18
CM-68	-26.87	20.46	2.02
CM-220	-26.78	20.76	2.80
CM-71	-26.98	21.06	3.18
CM-223	-26.97	21.36	2.12
CM-74	-23.18	21.66	2.01
CM-76	-27.43	22.05	3.02
CM-79	-26.33	22.65	2.46
CM-81	-27.25	23.04	1.63
CM-86	-26.79	24.05	1.55
CM-87	-27.52	24.25	1.51
CM-89	-27.06	24.60	1.12

!

Name	! $^{13}C_{org}$ ‰ (VPDB)	Height (m)	TOC%
CM-90	-27.77	24.85	1.31
CM-92	-26.07	25.25	1.36
CM-93	-27.16	25.45	0.43
CM-94	-27.38	25.65	1.68
CM-95	-27.48	25.85	1.06
CM-97	-27.68	26.25	0.14
CM-98	-27.60	26.45	1.23
CM-99	-27.80	26.65	0.69
CM-133	-27.97	28.86	1.05
CM-137	-27.14	29.66	1.53
CM-140	-26.86	30.26	0.66
CM-224	-26.26	31.59	1.34
CM-144	-28.68	34.24	0.66
CM-148	-28.34	35.04	1.01
CM-151	-29.46	35.64	1.13
CM-155	-28.03	36.44	1.33
CM-159	-28.20	37.24	1.35
CM-162	-28.52	37.84	1.12
CM-165	-28.08	38.44	1.59
CM-169	-29.06	39.24	1.98
CM-172	-28.42	39.84	2.11
CM-176	-28.66	40.64	2.13
Mean	**-27.67**		**1.43**
Maximum	**-23.18**		**4.06**
Minimum	**-29.86**		**0.14**
Std Dev. ±	**1.13**		**0.92**

B8. Arroyo Serrucho- Bulk sediment Organic Carbon Isotope and TOC Data

Name	! $^{13}C_{org}$‰ (VPDB)	Height %	TOC%
AS-1	-27.61	0.00	0.23
AS-2	-29.11	0.50	0.22
AS-3		1.00	
AS-4	-27.81	1.50	0.14
AS-5	-29.75	2.00	0.26
AS-6	-28.32	2.50	0.35
AS-7	-28.68	3.00	0.35
AS-8	-28.88	3.50	0.33
AS-9	-28.48	4.00	0.46
AS-10	-28.36	4.50	0.26
AS-11	-27.78	5.00	0.23
AS-12		5.50	0.22
AS-13	-28.07	6.00	0.14
AS-14	-28.27	6.50	0.18
AS-15		7.00	
AS-16	-28.96	7.50	0.76
AS-17	-28.85	8.00	0.78
AS-18	-28.06	8.50	0.22
AS-19		9.00	0.12
AS-20	-28.16	9.50	0.17
AS-21	-27.54	10.00	0.13
AS-22		10.50	0.14
AS-23	-29.66	11.00	0.11
AS-24		11.50	0.00
AS-25	-29.50	12.00	0.25
AS-26	-29.03	12.50	0.08
AS-27		13.00	
AS-28	-29.73	13.50	0.04
AS-29	-29.66	14.00	0.11
AS-30	-28.65	14.50	0.10
AS-31	-29.15	15.00	0.13
AS-32	-30.06	15.50	0.11
AS-33	-28.95	16.00	0.16
AS-34		16.50	0.11
AS-35	-27.84	17.00	0.15
AS-36	-28.52	17.50	0.11
AS-37	-29.15	18.00	0.18
AS-38	-28.28	18.50	0.14
AS-39		19.00	0.15
AS-40	-31.12	19.50	0.11
AS-41-2	-29.57	20.00	0.24
AS-42		20.50	0.26
AS-43	-30.05	21.00	0.36
AS-44		21.50	0.27
AS-45	-30.35	22.00	0.17

!

Name	! $^{13}C_{org}$ ‰ (VPDB)	Height %	TOC%
AS-46	-31.14	22.50	1.18
AS-47	-29.71	23.00	0.13
AS-48	-29.09	23.50	0.12
AS-49	-27.20	24.00	0.22
AS-50	-29.22	24.50	0.40
AS-51		25.00	
AS-52	-29.35	25.50	0.35
AS-53	-27.94	26.00	0.15
AS-54	-29.11	26.50	0.31
AS-55	-28.19	27.00	0.25
AS-56	-28.99	27.50	0.70
AS-57	-28.38	28.00	0.15
AS-58	-27.78	28.50	0.28
AS-59	-26.70	29.00	0.86
As-60	-27.27	29.50	0.19
AS-61	-27.51	30.00	0.18
AS-62	-27.48	30.50	0.57
AS-63		31.10	
AS-64		31.59	
AS-65	-22.97	32.02	0.69
AS-66	-25.33	32.51	0.18
Exposure gap 16.7m			
AS-100	-27.94	45.21	0.10
AS-101	-30.04	45.71	0.75
AS-102	-29.75	46.21	0.48
AS-103	-30.20	46.71	0.78
AS-104	-30.81	47.22	0.21
AS-105	-31.36	47.71	0.81
AS-106	-29.59	48.21	0.21
AS-107	-30.18	48.71	0.11
AS-108	-28.58	49.23	0.11
AS-109	-31.80	49.73	0.10
AS-110	-31.18	50.23	0.19
AS-111	-26.61	50.73	0.11
AS-112	-28.81	51.23	0.10
AS-113	-28.55	51.73	0.23
AS-114	-29.03	52.23	0.60
AS-115	-29.40	52.75	0.55
AS-116	-31.01	53.4	0.14
AS-117	-28.79	54.1	0.53
AS-118		54.72	
AS-119	-28.86	55.37	0.60
Mean	**-28.84**		**0.29**
Maximum	**-22.97**		**1.18**
Minimum	**-31.80**		**0.00**
Std Dev. ±	**1.39**		**0.23**

!

Name	! $^{13}C_{org}$‰ (VPDB)	Height %	TOC%
Main Section			
AS-W-1	-28.08	17.45	
Unnamed section 1			
AS-W-4	-28.44	54.72	
AS-W-5	-28.08	54.72	
Unnamed section 2			
AS-W-7	-22.71	86.41	
AS-W-8	-23.33	90.41	
AS-W-9	-25.48	95.41	

B9. Rock Eval Pyrolysis Data Arroyo Lapa 2008.

Elemental Analyser Data		Oil Show Analyser Data						
Sample	%TOC	S1	S2	TOC	Tmax°C	HI		HI oxf
AL-79	3.2	1.23	13.07	2.90	435	450		408
AL-80	3.53	0.81	8.51	3.56	433	239		241
AL-80R		0.87	8.17	3.44	430	237		
AL-81	2.42	0.60	7.20	3.24	432	222		298
AL-82	2.53	1.06	3.91	3.28	436	119		155
AL-83	2.95	0.52	5.88	2.97	432	197		199
AL-84	3.65	0.76	7.63	3.60	432	211		209
AL-85	2.23	0.33	2.63	2.00	436	131		118
AL-86	4.25	0.73	12.77	4.47	431	285		300
AL-87	3.62	0.77	9.22	3.03	431	304		255
AL-88	2.17	0.37	2.90	2.03	436	142		134
AL-89	2.53	0.57	3.83	2.60	436	147		151
AL-89R		0.81	4.01	2.56	439	156		
AL-90	5.15	0.69	7.74	4.18	432	185		150
AL-91	2.28	0.61	3.93	2.90	437	136		172
AL-92	3.89	0.80	7.44	4.08	432	182		191
AL-92R		0.56	5.41	3.84	437	141		
AL-93	3.05	0.60	4.72	2.88	434	163		155
AL-94	4.28	0.75	8.92	4.27	438	208		208
AL-95	4.19	0.65	8.97	4.02	436	223		214
AL-96	3.14	0.61	4.78	3.87	433	124		152
AL-97	2.67	0.38	2.07	1.46	435	141		78
AL-98	1.66	0.56	2.04	1.47	436	138		123
AL-99R		0.67	2.54	2.29	438	110		
AL-99	2.04	0.22	2.47	2.00	441	124		121
AL-99R		0.26	2.47	1.98	438	125		
AL-100	2.67	1.10	6.22	2.91	431	213		233
AL-101	2.54	0.63	4.85	2.44	432	198		191
AL-102	1.78	0.50	2.50	1.77	436	141		140
AL-103	1.29	0.59	2.03	1.37	435	148		157
AL-104	1.85	0.71	3.02	1.67	436	180		163
AL-105	1.87	0.72	3.62	1.67	432	216		194
AL-106	3.65	0.48	8.93	3.51	434	254		245
AL-109	2.08	0.95	2.73	2.46	436	110		131
AL-110	2.63	0.97	6.82	2.70	432	252		259
AL-111	4.31	0.90	13.77	3.71	431	371		319
AL-112	4.88	0.70	17.72	4.52	431	392		363
AL-113	4.06	0.63	10.90	3.90	431	279		268
AL-114	2.73	0.32	7.18	2.35	433	305		263
AL-115	1.75	0.41	3.20	1.52	434	210		183
AL-116	2.06	0.27	4.45	1.77	434	251		216
AL-117	4.41	0.39	13.53	4.04	432	334		307
AL-118	2.6	0.31	5.86	2.69	434	218		225
AL-119	2.26	0.27	4.98	2.04	433	244		220
AL-119R		0.32	5.01	2.44	436	205		
AL-120	1.88	0.29	3.03	1.50	435	202		161
AL-121	3.94	0.45	16.13	3.80	430	424		409
AL-122	6.33	0.66	25.55	6.64	432	385		404

!

Elemental Analyser Data		Oil Show Analyser Data						
Sample	**%TOC**	**S1**	**S2**	**TOC**	**Tmax°C**	**HI**		**HI oxf**
AL-123	4.36	0.13	12.70	4.87	429	261		291
AL-124	5.67	1.43	24.46	5.57	429	439		431
AL-124R		1.38	25.00	5.59	431	447		
AL-125	0.62	0.19	0.53	0.49	441	108		85
AL-126	1.87	0.57	4.02	1.79	438	225		215
AL-127	3.09	0.35	8.82	3.04	432	290		285
AL-127R		0.74	9.32	3.21	433	290		290
AL-128	2.87	0.60	9.40	2.70	431	348		328
AL-129	1.25	0.32	2.50	1.08	440	231		200
AL-130	1.98	0.47	5.58	2.21	435	252		282
AL-131	0.82	0.15	0.98	0.61	439	160		120
AL-132	0.36	0.63	0.83	0.32	432	259		231

B10. Rock Eval Pyrolysis Data Arroyo Lapa South and North 2010.

Sample	Ctot %	$CaCO_3$ %	C_{org} %	TOC %	Tmax °C	S1 mg/g	S2 mg/g	HI mg HC/g TOC
AL-BM-1	2.91	0	2.91	2.25	438	0.72	4.77	212
AL-BM-1R				2.44	438	1.43	4.76	195
AL-BM-2	3.42	7	2.58	1.88	435	0.29	5.00	265
AL-BM-3	3.63	0	3.63	3.08	437	1.32	8.02	260
AL-BM-4	8.29	6	7.56	7.14	430	3.40	27.91	390
AL-BM-4R				6.90	432	1.74	29.36	425
AL-BM-5	1.60	0	1.60	1.59	437	0.25	2.99	188
AL-BM-6	0.33	0	0.33	0.30		0.16	0.23	76
AL-BM-7	2.43	14.5	0.69	0.43		0.34	0.00	0
AL-BM-8	4.76	0	4.76	4.17	431	0.88	11.84	283
AL-BM-9	4.25	0	4.25	4.05	431	0.57	11.43	282
AL-BM-10	9.29	32.5	5.39	4.97	435	1.55	20.44	411
AL-BM-10				4.90	436	1.60	20.74	423
AL-BM-11	0.74	0	0.74	0.91	443	0.08	0.55	60
AL-BM-12	2.37	0	2.37	1.91	438	0.93	5.05	264
AL-BM-12				1.95	435	0.99	5.32	272
AL-BM-13	0.11	0	0.11	0.73	438	0.49	0.36	49
AL-BM-15	nd	1.5		0.06		0.00	0.01	
AL-BM-16	nd	0.5		0.35	440	0.02	0.20	57
AL-BM-17	nd	3.0		0.04		0.01	0.02	
AL-BM-17 grey	nd	1.0		0.58		0.00	0.06	
AL-BM-18	nd	2.5		0.06		0.00	0.04	
AL-BM-19	nd	0.0		0.17	439	0.01	0.10	59
AL-BM-20	nd	6.5		0.51	446	0.01	0.49	96
AL-BM-21	nd	1.5		0.05		0.00	0.03	
AL-BM-22	nd	5.5		0.03		0.00	0.01	
LN-BM-1	0.46	0	0.46	0.30	444	0.24	0.27	90
LN-BM-2	0.02	0	0.02	0.08		0.37	0.01	12
LN-BM-3	0.45	0	0.45	0.16		0.54	0.04	25
LN-BM-4	0.24	0	0.24	0.30		1.13	0.18	60
LN-BM-4R				0.32	441	1.00	0.25	78
LN-BM-5	not determined			0.57	444	0.73	0.54	94
LN-BM-6	0.45	0	0.45	0.34	442	0.64	0.29	85
LN-BM-7	0.10	0	0.10	0.15		0.63	0.03	20
LN-BM-8	4.23	13.5	2.60	2.28	432	1.16	6.69	293
LN-BM-9				2.32	432	1.48	6.69	288
LN-BM-9	0.63	3	0.27	0.27		0.81	0.12	44
LN-BM-10	0.78	0	0.78	0.46	441	0.47	0.36	78
LN-BM-11	0.17	0	0.17	0.12		0.45	0.02	16
Mean	**2.34**		**1.92**	**1.55**	**437**	**0.68**	**4.61**	**#DIV/0!**

!

B11. Molybdenum Data for Arroyo Lapa North and Arroyo Lapa South 2010

Sample #	Biomarker Sample #	Height (m)	! ^{98}Mo	[Mo] ppm	1/[Mo] ppm
LN-304	LN-BM-12	0.4	x	x	x
LN-314	LN-BM-13	1.4	x	x	x
LN-324	LN-BM-9	2.4	0.10	1.7	0.5882
LN-334	LN-BM-10	3.4	x	x	x
LN-343	LN-BM-11	4.3	x	x	x
LN-1	LN-BM-1	8.1	0.56	1.3	0.7692
LN-21	LN-BM-2	10.1	0.17	1.40	0.7143
LN-41	LN-BM-3	12.1	0.09	1.40	0.7143
LN-60	LN-BM-4	14.0	0.26	2.40	0.4167
LN-80	LN-BM-5	16.0	0.15	2.50	0.4000
LN-100	LN-BM-6	18.0	0.24	x	x
LN-120	LN-BM-7	20.0	0.37	1.50	0.6667
LN-140	LN-BM-8	24.1	0.56	1.90	0.5263
Arroyo Lapa South 2010					
AL-215	AL-BM-1	1.50	0.78	4.8	0.2083
AL-225	AL-BM-8	2.50	0.40	1.5	0.6667
AL-235	AL-BM-2	3.50	0.14	2.1	0.4762
AL-245	AL-BM-9	4.50	0.78	1.9	0.5263
AL-255	AL-BM-3	5.50	0.40	1.8	0.5556
AL-265	AL-BM-10	6.50	0.53	4.6	0.2174
AL-275	AL-BM-4	7.50	0.31	1.6	0.6250
AL-285	AL-BM-11	8.50	0.22	3.8	0.2632
AL-295	AL-BM-5	9.50	0.19	3.6	0.2778
AL-305	AL-BM-12	10.50	0.45	x	x
AL-315	AL-BM-6	11.50	0.13	2.8	0.357
AL-325	AL-BM-13	12.50	-0.11	2.2	0.455
AL-335	AL-BM-7	13.50	-0.13	3.3	0.303
AL-345	AL-BM-14	14.50	0.39	2.1	0.476
AL-355A	AL-BM-15	15.50	0.00	3.1	0.323
AL-363	AL-BM-16	16.50	-0.09	3	0.333
AL-373	AL-BM-17	17.50	0.08	2.4	0.417
AL-383	AL-BM-18	18.50	0.28	1.9	0.526
AL-393	AL-BM-19	19.50	0.14	3.4	0.294
AL-403	AL-BM-20	20.50	-0.01	3	0.333
AL-413	AL-BM-21	21.50	-0.07	2.8	0.357
AL-423	AL-BM-22	22.50	0.18	2.1	0.476
Arroyo Lapa South 2008					
AL-116	A26		0.42	1.4	0.714
AL-89	T64		0.32	2.2	0.455

B12. Hopane Data from Arroyo Lapa North. Concentrations are in parts per million (ppm.)

Sample #	Height (m)	Biomarkers Sample #	[C27-TS]	[C27-TR]	[C29]
LN-304	0.4	LN-BM-12	n/a	n/a	n/a
LN-314	1.4	LN-BM-13	0.003	0.012	0.259
LN-324	2.4	LN-BM-9	0.002	0.003	0.009
LN-334	3.4	LN-BM-10	0.005	0.010	0.039
LN-343	4.3	LN-BM-11	0.001	0.002	0.006
LN-1	8.1	LN-BM-1	0.003	0.007	0.015
LN-21	10.1	LN-BM-2	0.000	0.001	0.002
LN-41	12.1	LN-BM-3	0.000	0.000	0.000
LN-60	14	LN-BM-4	0.005	0.009	0.024
LN-80	16	LN-BM-5	0.005	0.006	0.021
LN-100	18	LN-BM-6	0.005	0.010	0.043
LN-120	20	LN-BM-7	0.003	0.006	0.016
LN-140	24.1	LN-BM-8	0.002	0.005	0.011

Biomarker Sample #	[C30]	[C31R]	[C31S]	[C32R]	[C32S]
LN-BM-12	n/a	n/a	n/a	n/a	n/a
LN-BM-13	0.035	0.019	0.013	0.012	0.009
LN-BM-9	0.013	0.006	0.004	0.003	0.002
LN-BM-10	0.049	0.021	0.016	0.011	0.008
LN-BM-11	0.009	0.004	0.003	0.002	0.002
LN-BM-1	0.025	0.012	0.010	0.006	0.005
LN-BM-2	0.003	0.001	0.001	0.001	0.001
LN-BM-3	0.000	0.000	0.000	0.000	0.000
LN-BM-4	0.049	0.019	0.015	0.015	0.009
LN-BM-5	0.035	0.014	0.011	0.008	0.006
LN-BM-6	0.053	0.023	0.020	0.013	0.010
LN-BM-7	0.023	0.010	0.007	0.005	0.004
LN-BM-8	0.017	0.009	0.007	0.005	0.004

Biomarker Sample #	[C33R]	[C33S]	[C34R]	[C34S]	[C35R]
LN-BM-12	n/a	n/a	n/a	n/a	n/a
LN-BM-13	0.009	0.007	0.006	0.004	0.003
LN-BM-9	0.002	0.001	0.001	0.001	0.001
LN-BM-10	0.010	0.007	0.005	0.003	0.014
LN-BM-11	0.002	0.001	0.002	0.001	0.000
LN-BM-1	0.005	0.004	0.003	0.002	0.002
LN-BM-2	0.001	0.000	0.000	0.000	0.000
LN-BM-3	0.000	0.000	0.000	0.000	0.000
LN-BM-4	0.013	0.009	0.007	0.004	0.009
LN-BM-5	0.007	0.005	0.004	0.002	0.002
LN-BM-6	0.012	0.009	0.007	0.005	0.003
LN-BM-7	0.004	0.003	0.002	0.002	0.003
LN-BM-8	0.005	0.004	0.003	0.002	0.002

Biomarkers Sample #	[C35S]	Amt. Homohopanes (ppm)	C31R/C30	C29/C30
LN-BM-12	n/a	n/a	n/a	n/a
LN-BM-13	0.002	0.391	0.543	7.459
LN-BM-9	0.000	0.048	0.421	0.675
LN-BM-10	0.002	0.200	0.431	0.784
LN-BM-11	0.000	0.035	0.474	0.677
LN-BM-1	0.001	0.101	0.463	0.582
LN-BM-2	0.000	0.013	0.465	0.841
LN-BM-3	0.000	0.002	0.437	0.676
LN-BM-4	0.003	0.191	0.388	0.491
LN-BM-5	0.002	0.128	0.402	0.583
LN-BM-6	0.003	0.216	0.437	0.804
LN-BM-7	0.001	0.090	0.446	0.699
LN-BM-8	0.001	0.076	0.556	0.657

B13. Hopane Data from Arroyo Lapa South. Concentrations are in parts per million (ppm.)

Sample #	Height (m)	Biomarker Sample #	C27-TS	C27-TR	C29
Arroyo Lapa South 2008					
AL-7	3.12	ARG-AL-7	0.004	0.002	0.011
AL-11	5.12	ARG-AL-11	0.001	0.001	0.002
AL-17	8.02	ARG-AL-17	0.017	0.034	0.127
AL-44	21.55	ARG-AL-44	0.001	0.007	0.012
AL-50	24.55	ARG-AL-50	0.001	0.004	0.006
AL-66	32.55	ARG-AL-66	0.003	0.007	0.020
AL-94	46.55	ARG-AL-94	0.007	0.015	0.047
Arroyo Lapa South 2010					
AL-215	54.55	AL-BM-1	1.280	1.280	4.296
AL-225	55.95	AL-BM-8	0.374	0.871	2.438
AL-235	56.25	AL-BM-2	0.433	0.971	2.734
AL-245	57.95	AL-BM-9	0.462	1.163	2.805
AL-255	58.55	AL-BM-3	0.559	1.244	4.343
AL-265	59.55	AL-BM-10	0.545	1.137	2.815
AL-275	60.85	AL-BM-4	0.070	0.131	0.416
AL-285	61.95	AL-BM-11	0.219	0.544	1.261
AL-295	62.95	AL-BM-5	0.320	0.477	1.473
AL-305	63.95	AL-BM-12	0.071	0.271	0.385
AL-315	64.95	AL-BM-6	0.289	0.321	1.090
AL-325	65.95	AL-BM-13	0.040	0.014	0.047
AL-335	66.85	AL-BM-7	0.597	0.200	0.521
AL-345	67.95	AL-BM-14	n/a	n/a	n/a
AL-355A	68.95	AL-BM-15	1.033	0.598	1.636
AL-363	69.95	AL-BM-16	n/a	n/a	n/a
AL-373	70.95	AL-BM-17	0.535	0.949	2.815
AL-383	71.95	AL-BM-18	0.199	0.309	1.017
AL-393	72.95	AL-BM-19	0.038	0.045	0.150
AL-403	73.95	AL-BM-20	0.520	0.862	2.350
AL-413	74.95	AL-BM-21	0.049	0.063	0.221
AL-423	22.50	AL-BM-22	0.661	1.056	4.052

Sample #	C30	C31R	C31S	C32R	C32S
Arroyo Lapa South 2008					
ARG-AL-7	0.015	0.011	0.010	0.008	0.006
ARG-AL-11	0.003	0.002	0.001	0.001	0.001
ARG-AL-17	0.167	0.086	0.062	0.043	0.033
ARG-AL-44	0.015	0.011	0.008	0.005	0.003
ARG-AL-50	0.007	0.005	0.003	0.002	0.002
ARG-AL-66	0.024	0.014	0.010	0.007	0.005
ARG-AL-94	0.064	0.037	0.025	0.017	0.012
Arroyo Lapa South 2010					
AL-BM-1	4.692	2.468	1.773	12.600	0.971
AL-BM-8	3.904	2.011	1.444	1.099	0.830
AL-BM-2	4.134	2.220	1.619	1.268	0.959
AL-BM-9	4.235	2.135	1.519	1.131	0.843
AL-BM-3	4.645	2.412	1.742	1.269	0.974
AL-BM-10	5.480	2.479	1.743	1.436	1.029
AL-BM-4	0.735	0.358	0.250	0.220	0.008
AL-BM-11	2.207	1.049	0.737	0.576	0.430
AL-BM-5	3.033	12.765	0.951	1.100	0.077
AL-BM-12	0.649	0.379	0.264	0.159	0.115
AL-BM-6	1.831	0.749	0.581	0.419	0.297
AL-BM-13	0.048	0.027	0.020	0.022	0.004
AL-BM-7	0.712	0.334	0.257	0.168	0.128
AL-BM-14	n/a	n/a	n/a	n/a	n/a
AL-BM-15	2.085	1.064	0.764	0.652	0.530
AL-BM-16	n/a	n/a	n/a	n/a	n/a
AL-BM-17	3.544	1.662	1.221	0.852	0.631
AL-BM-18	1.274	0.599	0.450	0.275	0.221
AL-BM-19	0.229	0.093	0.075	0.056	0.036
AL-BM-20	3.626	1.588	1.144	0.685	0.527
AL-BM-21	0.347	0.147	0.125	0.108	0.080
AL-BM-22	6.348	2.550	2.576	1.957	1.287

Sample #	C33R	C33S	C34R	C34S	C35R
Arroyo Lapa South 2008					
ARG-AL-7	0.007	0.005	0.004	0.003	0.005
ARG-AL-11	0.001	0.000	0.000	0.000	0.000
ARG-AL-17	0.038	0.027	0.021	0.014	0.012
ARG-AL-44	0.003	0.002	0.002	0.001	0.007
ARG-AL-50	0.001	0.001	0.001	0.001	0.005
ARG-AL-66	0.006	0.004	0.004	0.002	0.001
ARG-AL-94	0.014	0.010	0.009	0.006	0.005
Arroyo Lapa South 2010					
AL-BM-1	1.303	0.813	0.690	0.439	0.346
AL-BM-8	1.088	0.741	0.637	0.396	0.432
AL-BM-2	1.327	0.857	0.642	0.408	0.447
AL-BM-9	1.139	0.822	0.633	0.396	0.353
AL-BM-3	1.225	0.838	0.645	0.418	0.330
AL-BM-10	1.451	1.006	0.873	0.531	0.315
AL-BM-4	0.245	0.166	0.125	0.088	0.094
AL-BM-11	0.658	0.441	0.339	0.209	0.209
AL-BM-5	1.036	0.803	0.689	0.462	0.360
AL-BM-12	0.101	0.021	0.055	0.039	0.036
AL-BM-6	0.368	0.245	0.206	0.141	0.095
AL-BM-13	n/a	n/a	n/a	n/a	0.106
AL-BM-7	0.118	0.083	0.067	0.043	0.036
AL-BM-14	n/a	n/a	n/a	n/a	n/a
AL-BM-15	0.471	0.290	0.212	0.140	0.298
AL-BM-16	n/a	n/a	n/a	n/a	n/a
AL-BM-17	0.706	0.489	0.366	0.231	0.168
AL-BM-18	0.228	0.157	0.128	0.087	0.046
AL-BM-19	0.051	0.036	0.041	0.028	0.279
AL-BM-20	0.598	0.381	0.300	0.193	0.124
AL-BM-21	0.090	0.077	0.076	0.046	0.048
AL-BM-22	1.961	1.438	1.117	0.689	0.735

Sample #	C35S	Total [Hopanes] (ppm)	C31R/C30	C29/C30	C35S/C34S
Arroyo Lapa South 2008					
ARG-AL-7	0.002	0.09	0.71	0.72	0.80
ARG-AL-11	0.000	0.01	0.64	0.91	0.29
ARG-AL-17	0.012	0.69	0.52	0.76	0.83
ARG-AL-44	0.001	0.08	0.74	0.80	0.67
ARG-AL-50	0.000	0.04	0.72	0.82	0.62
ARG-AL-66	0.002	0.11	0.61	0.84	0.65
ARG-AL-94	0.003	0.27	0.58	0.73	0.54
Arroyo Lapa South 2010					
AL-BM-1	0.350	33.30	0.53	0.92	0.80
AL-BM-8	0.323	16.59	0.52	0.62	0.81
AL-BM-2	0.332	18.35	0.54	0.66	0.82
AL-BM-9	0.307	17.94	0.50	0.66	0.78
AL-BM-3	0.258	20.90	0.52	0.93	0.62
AL-BM-10	0.503	21.34	0.45	0.51	0.95
AL-BM-4	0.088	3.00	0.49	0.57	1.00
AL-BM-11	0.144	9.02	0.48	0.57	0.69
AL-BM-5	0.314	23.86	4.21	0.49	0.68
AL-BM-12	0.027	2.57	0.58	0.59	0.70
AL-BM-6	0.085	6.72	0.41	0.60	0.60
AL-BM-13	n/a	n/a	0.55	0.99	
AL-BM-7	0.035	3.30	0.47	0.73	0.80
AL-BM-14	n/a	n/a	n/a	n/a	
AL-BM-15	0.114	9.89	0.51	0.78	0.81
AL-BM-16	n/a	n/a	n/a	n/a	
AL-BM-17	0.169	14.34	0.47	0.79	0.73
AL-BM-18	0.049	5.04	0.47	0.80	0.56
AL-BM-19	0.000	1.16	0.40	0.66	
AL-BM-20	1.204	14.10	0.44	0.65	6.22
AL-BM-21	0.038	1.52	0.42	0.64	0.82
AL-BM-22	0.524	26.95	0.40	0.64	0.76

B14. Sterane Data from Arroyo Lapa South. Concentrations are in parts per million (ppm.)

Sample #	Height (m)	Biomarker Sample #	[C27]	[C28]	[C29]
Arroyo Lapa South 2008					
AL-7	3.12	ARG-AL-7	0.003	0.001	0.002
AL-11	5.12	ARG-AL-11	0.001	0.001	0.001
AL-17	8.02	ARG-AL-17	0.025	0.018	0.047
AL-44	21.55	ARG-AL-44	0.005	0.006	0.009
AL-50	24.55	ARG-AL-50	0.002	0.002	0.003
AL-66	32.55	ARG-AL-66	0.008	0.004	0.011
AL-94	46.55	ARG-AL-94	0.025	0.016	0.041
Arroyo Lapa South 2010					
AL-215	54.55	AL-BM-1	1.638	1.787	3.344
AL-225	55.95	AL-BM-8	0.039	0.046	0.087
AL-235	56.25	AL-BM-2	0.013	0.015	0.022
AL-245	57.95	AL-BM-9	0.026	0.031	0.054
AL-255	58.55	AL-BM-3	0.041	0.028	0.070
AL-265	59.55	AL-BM-10	0.028	0.042	0.052
AL-275	60.85	AL-BM-4	0.053	0.071	0.093
AL-285	61.95	AL-BM-11	0.008	0.009	0.014
AL-295	62.95	AL-BM-5	0.018	0.013	0.023
AL-305	63.95	AL-BM-12	0.000	0.000	0.000
AL-315	64.95	AL-BM-6	0.014	0.013	0.023
AL-325	65.95	AL-BM-13	0.001	0.000	0.000
AL-335	66.85	AL-BM-7	0.002	0.001	0.001
AL-345	67.95	AL-BM-14	0.001	0.000	0.001
AL-355A	68.95	AL-BM-15	0.001	0.001	0.001
AL-363	69.95	AL-BM-16	n/a	n/a	n/a
AL-373	70.95	AL-BM-17	0.001	0.001	0.002
AL-383	71.95	AL-BM-18	0.002	0.001	0.003
AL-393	72.95	AL-BM-19	0.002	0.001	0.002
AL-403	73.95	AL-BM-20	0.009	0.007	0.011
AL-413	74.95	AL-BM-21	0.005	0.004	0.007
AL-423	75.95	AL-BM-22	0.068	0.057	0.117

Sample ID	[C30]	Total [Sterane (ppm)]	Sterane Index (C30)/(C27-C30)	C28/C29	St/H
ARG-AL-7	0.001	0.007	1.069	0.542	0.076
ARG-AL-11	0.000	0.002	0.025	0.512	0.190
ARG-AL-17	0.008	0.098	0.492	0.380	0.141
ARG-AL-44	0.002	0.022	1.106	0.632	0.281
ARG-AL-50	0.001	0.007	0.949	0.659	0.188
ARG-AL-66	0.002	0.024	0.309	0.364	0.217
ARG-AL-94	0.008	0.091	0.485	0.393	0.335
AL-BM-1	0.868	7.637	1.128	0.534	5.965
AL-BM-8	0.024	0.196	1.510	0.529	0.523
AL-BM-2	0.012	0.061	19.268	0.655	0.141
AL-BM-9	0.012	0.123	0.877	0.574	0.266
AL-BM-3	0.013	0.151	0.454	0.403	0.271
AL-BM-10	0.026	0.149	8.829	0.811	0.273
AL-BM-4	0.036	0.253	2.103	0.764	3.628
AL-BM-11	0.003	n/a	0.527	0.628	n/a
AL-BM-5	0.008	0.063	0.885	0.593	0.196
AL-BM-12	0.000	0.001	0.188	0.765	0.017
AL-BM-6	0.004	0.054	0.369	0.570	0.186
AL-BM-13	0.000	0.002	0.071	0.571	n/a
AL-BM-7	0.000	0.004	0.072	0.866	0.006
AL-BM-14	0.000	0.002	0.161	0.290	n/a
AL-BM-15	0.000	0.003	0.279	0.722	0.003
AL-BM-16	n/a	n/a	n/a	n/a	n/a
AL-BM-17	0.000	0.004	0.393	0.373	0.007
AL-BM-18	0.001	0.006	0.337	0.280	0.032
AL-BM-19	0.000	0.005	0.254	0.415	0.134
AL-BM-20	0.002	0.028	0.228	0.607	0.054
AL-BM-21	0.002	0.018	0.411	0.622	0.370
AL-BM-22	0.030	0.272	0.761	0.486	2.876

B15. Sterane Data from Arroyo Lapa North. Concentrations are in parts per million (ppm.)

Sample #	Height (m)	Biomarker Sample #	[C27]	[C28]	[C29]	[C30]
LN-304	0.4	LN-BM-12	n/a	n/a	n/a	n/a
LN-314	1.4	LN-BM-13	0.0086	0.0066	0.0153	0.0032
LN-324	2.4	LN-BM-9	0.0023	0.0029	0.0046	0.0012
LN-334	3.4	LN-BM-10	0.0068	0.0049	0.0111	0.0019
LN-343	4.3	LN-BM-11	0.0013	0.0005	0.0012	0.0002
Exposure gap ~4.3m						
LN-1	8.1	LN-BM-1	0.0042	0.0028	0.0072	0.0021
LN-21	10.1	LN-BM-2	0.0004	0.0005	0.0007	0.0001
LN-41	12.1	LN-BM-3	0.0010	0.0009	0.0010	0.0001
LN-60	14	LN-BM-4	0.0067	0.0095	0.0097	0.0032
LN-80	16	LN-BM-5	0.0064	0.0035	0.0101	0.0021
LN-100	18	LN-BM-6	0.0084	0.0044	0.0114	0.0027
LN-120	20	LN-BM-7	0.0048	0.0027	0.0072	0.0006
LN-140	24.1	LN-BM-8	0.0082	0.0032	0.0073	0.0015

	Total [Sterane] (ppm)	Sterane Index (C30)/(C27-C30)	C28/C29	St/H
LN-BM-12	n/a	n/a	n/a	n/a
LN-BM-13	0.037	0.606	0.429	0.095
LN-BM-9	0.012	1.185	0.627	0.250
LN-BM-10	0.027	0.398	0.440	0.136
LN-BM-11	0.003	0.205	0.449	0.086
LN-BM-1	0.017	1.045	0.387	0.170
LN-BM-2	0.002	0.684	0.731	0.145
LN-BM-3	0.003	0.082	0.834	1.483
LN-BM-4	0.029	0.943	0.980	0.151
LN-BM-5	0.024	0.495	0.349	0.186
LN-BM-6	0.027	0.483	0.388	0.126
LN-BM-7	0.017	0.133	0.373	0.189
LN-BM-8	0.018	0.228	0.433	6.079

B16. Pristane and Phytane Data from Arroyo Lapa South. Concentrations are in parts per million (ppm.)

Sample #	Height (m)	Biomarker Sample #	[Pristane] (ppm)	[Phytane] (ppm)	Pr/Ph
Arroyo Lapa South 2008					
AL-7	3.12	ARG-AL-7	0.095	0.147	0.650
AL-11	5.12	ARG-AL-11	0.003	0.001	3.108
AL-17	8.02	ARG-AL-17	2.683	1.141	2.351
AL-44	21.55	ARG-AL-44	0.486	0.370	1.311
AL-50	24.55	ARG-AL-50	0.014	0.004	3.218
AL-66	32.55	ARG-AL-66	0.429	0.316	1.357
AL-94	46.55	ARG-AL-94	2.639	1.097	2.405
Arroyo Lapa South 2010					
AL-215	54.55	AL-BM-1	2.858	0.947	3.017
AL-225	55.95	AL-BM-8	3.975	1.698	2.341
AL-235	56.25	AL-BM-2	2.480	0.947	2.619
AL-245	57.95	AL-BM-9	5.071	1.773	2.860
AL-255	58.55	AL-BM-3	3.275	1.060	3.090
AL-265	59.55	AL-BM-10	6.295	4.399	1.431
AL-275	60.85	AL-BM-4	9.063	5.033	1.801
AL-285	61.95	AL-BM-11	0.650	0.328	1.980
AL-295	62.95	AL-BM-5	2.017	1.361	1.482
AL-305	63.95	AL-BM-12	0.003	0.007	0.378
AL-315	64.95	AL-BM-6	1.001	0.390	2.564
AL-325	65.95	AL-BM-13	0.288	0.466	0.618
AL-335	66.85	AL-BM-7	0.000	0.000	0.000
AL-345	67.95	AL-BM-14	0.050	0.035	1.441
AL-355A	68.95	AL-BM-15	0.021	0.021	0.985
AL-363	69.95	AL-BM-16	0.000	0.000	0.000
AL-373	70.95	AL-BM-17	0.476	0.517	0.921
AL-383	71.95	AL-BM-18	0.000	0.000	1.180
AL-393	72.95	AL-BM-19	0.064	0.065	0.984
AL-403	73.95	AL-BM-20	0.576	0.253	2.281
AL-413	74.95	AL-BM-21	0.277	0.215	1.287
AL-423	75.95	AL-BM-22	4.292	3.016	1.423

B17. Pristane and Phytane Data from Arroyo Lapa South. Concentrations are in parts per million (ppm.)

Sample #	Height (m)	Biomarker Sample #	[Pristane] (ppm)	[Phytane] (ppm)	Pr/Ph
LN-304	0.4	LN-BM-12	n/a		
LN-314	1.4	LN-BM-13	0.1410	0.0733	1.9228
LN-324	2.4	LN-BM-9	0.0583	0.0252	2.3134
LN-334	3.4	LN-BM-10	0.1435	0.0588	2.4392
LN-343	4.3	LN-BM-11	0.0119	0.0102	1.1669
Exposure gap ~4.3m					
LN-1	8.1	LN-BM-1	0.0596	0.0347	1.7152
LN-21	10.1	LN-BM-2	0.0027	0.0023	1.1747
LN-41	12.1	LN-BM-3	0.0052	0.0062	0.8405
LN-60	14	LN-BM-4	0.0854	0.0693	1.2327
LN-80	16	LN-BM-5	0.0912	0.0400	2.2804
LN-100	18	LN-BM-6	0.0927	0.0384	2.4111
LN-120	20	LN-BM-7	0.0055	0.0071	0.7659
LN-140	24.1	LN-BM-8	0.1379	0.0930	1.4827

B18. Pyrite Framboid Data from Arroyo Lapa North and South.

Arroyo Lapa South

Biomarker Sample #	Height (m)	Mean Pyrite Framboid diameter size (m)	Std Dev.±
AL-BM-1	1.50	4.37	3.22
AL-BM-8	2.50	38.57	32.88
AL-BM-2	3.50	9.00	1.41
AL-BM-9	4.50	no frambs	n/a
AL-BM-3	5.50	8.07	6.05
AL-BM-10	6.50	no frambs	n/a
AL-BM-4	7.50	no frambs	n/a
AL-BM-11	8.50	no frambs	n/a
AL-BM-5	9.50	6.20	3.02
AL-BM-12	10.50	no frambs	n/a
AL-BM-6	11.50	7.27	3.85
AL-BM-13	12.50	5.83	3.62
AL-BM-7	13.50	no frambs	n/a
AL-BM-14	14.50	8.13	3.39
AL-BM-15	15.50	7.30	3.15
AL-BM-16	16.50	no frambs	n/a
AL-BM-17	17.50	no frambs	n/a
AL-BM-18	18.50	no frambs	n/a
AL-BM-19	19.50	no frambs	n/a
AL-BM-20	20.50	6.58	4.60
AL-BM-21	21.50	no frambs	n/a
AL-BM-22	22.50	7.83	4.11

Arroyo Lapa North

Biomarker Sample #	Height (m)		
LN-BM-12	0.4	no frambs	n/a
LN-BM-13	1.4	no frambs	n/a
LN-BM-9	2.4	7.27	5.43
LN-BM-10	3.4	14.53	18.93
LN-BM-11	4.3	no frambs	n/a
Exposure gap ~4.3m			n/a
LN-BM-1	0.00	16.80	14.04
LN-BM-2	2.00	no frambs	n/a
LN-BM-3	4.00	54.67	25.63
LN-BM-4	5.90	no frambs	n/a
LN-BM-5	7.90	no frambs	n/a
LN-BM-6	9.90	no frambs	n/a
LN-BM-7	11.90	no frambs	n/a
LN-BM-8	16.00	5.50	3.65

B18. Pyrite Framboid Data from Port Mulgrave, Yorkshire, England.

Sample #	Total Depth (cm)	Mean Pyrite Framboid diameter size (m)	Std Dev.±
PM-2	20	5.28	1.95
PM-3	40	5.7	2.59
PM-4	60	4.73	1.68
PM-5	80	3.98	2.7
PM-6	100	6.59	2.05
PM-7	120	4.97	2.19
PM-8	140	5.62	1.74
PM-9	160	4.13	1.93
PM-10	180	4.95	1.99
PM-11	190	4.78	1.56
PM-12	200	3.47	1.24
PM-13	220	4.73	1.68
PM-14	240	4.93	1.64
PM-15	260	5.37	7.3
PM-16	280	4.23	1.66
PM-17	290	4.3	1.66
PM-18	300	4.73	1.68
PM-19	310	5.47	1.26
PM-20	320	4.52	2.09
PM-21	325	4	1.53
PM-22	345	4.73	1.68
PM-23	377	3.97	1.56
PM-24	397	5.65	2.51
PM-25	417	3.86	1.42
PM-26	437	6.18	1.7
PM-27	457	4.43	1.24
PM-28	467	2.92	0.97
PM-29	477	3.65	1.37
PM-30	497	3.72	1.64
PM-31	517	3.23	1.15
PM-32	537	3.65	1.45
PM-33	557	6.65	2.68
PM-34	577	4.23	1.52
PM-35	597	3.4	1.16
PM-36	607	3.23	1.35
PM-37	617	3.8	1.24
PM-38	637	4.27	2.32
PM-39	657	3.55	1.28
PM-40	677	3.93	1.13
PM-41	697	4.73	1.68
PM-42	717	4.34	1.21
PM-43	737	4.57	1.87
PM-44	757	4	1.41
PM-45	777	4.32	1.86

B19. $\delta^{18}O/\ \delta^{13}C$ Carbonate Data from Chacay Melehue

Sample	Raw $\delta^{13}C$	Raw $\delta^{18}O$	Raw $\delta^{13}C$	Raw $\delta^{18}O$	Corrected $\delta^{13}C$	Corrected $\delta^{18}O$	Height (m)
CM-107	-8.421	-16.380	-6.632	-13.088	-6.638	-13.087	-0.2
CM-1	-4.495	-12.571	-3.183	-9.784	-3.067	-9.788	0
CM-108	-8.109	-16.913	-6.312	-13.613	-6.279	-13.613	0.25
CM-2	-7.995	-16.403	-6.102	-13.001	-6.076	-13.001	0.5
CM-109	-7.885	-15.940	-6.365	-12.933	-6.358	-12.932	0.75
CM-3	-9.072	-16.775	-7.310	-13.511	-7.347	-13.509	1
CM-110	-8.501	-15.293	-6.555	-11.834	-6.599	-11.832	2.24
CM-6	-7.256	-16.134	-5.911	-13.313	-5.861	-13.314	2.42
CM-111	-10.357	-16.882	-8.920	-13.963	-9.051	-13.958	2.67
CM-7	-7.814	-16.160	-6.432	-13.299	-6.417	-13.299	2.92
CM-112	-8.546	-16.610	-6.752	-13.312	-6.759	-13.311	3.17
CM-8	-4.876	-15.547	-3.338	-12.521	-3.140	-12.527	3.37
CM-10	-6.807	-15.632	-5.303	-12.642	-5.234	-12.643	4.39
CM-113	-7.787	-16.131	-6.364	-13.227	-6.347	-13.226	4.58
CM-12	-6.923	-15.632	-5.391	-12.612	-5.329	-12.613	5.38
CM-114	-6.520	-15.936	-4.879	-12.102	-4.800	-12.104	5.56
CM-13	-5.884	-14.547	-4.330	-11.504	-4.234	-11.506	5.89
CM-115	-6.262	-16.051	-4.860	-13.169	-4.743	-13.172	6.09
CM-116	-7.553	-16.353	-5.952	-13.260	-5.906	-13.261	6.29
CM-14	-8.483	-16.244	-7.050	-13.330	-7.077	-13.328	6.39
CM-117	-7.030	-16.071	-5.493	-13.046	-5.424	-13.048	6.85
CM-16	-4.929	-15.134	-3.544	-12.270	-3.368	-12.275	7.41
CM-118	-8.124	-12.370	-6.461	-8.512	-6.611	-8.507	7.57
CM-119	-9.349	-15.769	-7.415	-12.323	-7.500	-12.320	7.77
CM-17	-7.289	-16.805	-5.939	-13.978	-5.868	-13.980	7.91
CM-18	-7.840	-16.446	-6.066	-13.170	-6.031	-13.170	8.36
CM-21	-6.571	-14.845	-4.691	-11.456	-4.620	-11.457	10
CM-22	-3.603	-9.621	-2.004	-6.531	-1.919	-6.533	10.52
CM-23	-7.910	-15.927	-6.257	-12.778	-6.248	-12.778	11.21
CM-24	-8.159	-15.958	-6.389	-12.686	-6.393	-12.685	11.67
CM-26	-6.502	-16.869	-5.138	-14.028	-5.012	-14.031	12.12
CM-27	-6.233	-15.845	-4.780	-12.909	-4.666	-12.912	12.32
CM-28	-5.500	-16.228	-4.015	-13.259	-3.839	-13.264	12.52
CM-29	-7.175	-15.682	-5.640	-12.659	-5.593	-12.660	12.72
CM-30	-5.580	-16.500	-4.050	-12.785	-3.891	-12.789	12.92
CM-32	-11.526	-16.232	-10.009	-12.531	-10.262	-12.522	13.38
CM-34	-5.964	-16.398	-4.519	-12.775	-4.392	-12.778	13.75
CM-36	-8.196	-15.230	-6.499	-11.336	-6.556	-11.333	14.15
CM-40	-5.963	-16.828	-4.454	-13.135	-4.311	-13.139	14.95
CM-42	-8.258	-16.103	-6.672	-12.328	-6.706	-12.326	15.35
CM-44	-6.361	-16.613	-4.842	-12.910	-4.733	-12.913	15.76
CM-46	-5.692	-16.439	-4.206	-12.772	-4.059	-12.776	16.16
CM-48	-5.559	-16.297	-4.041	-12.595	-3.888	-12.599	16.56
CM-84	-6.831	-12.850	-5.290	-9.124	-5.340	-9.122	23.66
CM-86	-5.683	-15.963	-4.247	-12.349	-4.116	-12.353	24.05
CM-88	-4.898	-15.989	-3.454	-12.367	-3.270	-12.373	24.45
CM-90	-5.064	-16.771	-3.543	-13.066	-3.341	-13.072	24.85
CM-92	-6.133	-16.586	-4.435	-12.690	-4.306	-12.694	25.25
CM-94	-8.933	-15.748	-7.415	-12.046	-7.509	-12.043	25.65
CM-96	-4.900	-15.912	-3.347	-12.172	-3.161	-12.177	26.05
CM-98	-6.400	-16.597	-4.980	-13.001	-4.877	-13.004	26.45
CM-101	-9.228	-16.379	-7.793	-13.462	-7.865	-13.459	27.05
CM-103	-8.054	-15.719	-6.634	-12.818	-6.650	-12.817	27.46
CM-104	-8.011	-16.433	-6.577	-13.517	-6.564	-13.516	27.66

Sample	Raw $\delta^{13}C$	Raw $\delta^{18}O$	Raw $\delta^{13}C$	Raw $\delta^{18}O$	Corrected $\delta^{13}C$	Corrected $\delta^{18}O$	Height (m)
CM-105	-8.536	-16.333	-7.107	-13.423	-7.134	-13.421	27.86
CM-106	-8.211	-14.960	-6.725	-11.989	-6.774	-11.986	28.06
CM-38	#na	#na	#na	#na	#na	#na	

B20. $\delta^{18}O$/ $\delta^{13}C$ Carbonate Data from Arroyo Lapa South, 2008

Sample	Raw $\delta^{13}C$	Raw $\delta^{18}O$	Raw $\delta^{13}C$	Raw $\delta^{18}O$	Corrected $\delta^{13}C$	Corrected $\delta^{18}O$	Height (m)
AL-1	0.01	-2.628	-11.168	-1.094	-8.016	-0.897	-8.022
AL-13	6.10	-2.270	-11.221	-0.906	-8.464	-0.681	-8.471
AL-14	6.60	-3.521	-15.211	-2.194	-12.464	-1.921	-12.473
AL-18	8.52	-3.477	-11.138	-1.829	-7.901	-1.686	-7.906
AL-18	8.52	-2.774	-9.136	-1.392	-6.303	-1.273	-6.307
AL-19	9.02	-2.370	-9.789	-1.008	-6.965	-0.841	-6.970
AL-21	10.05	-2.858	-12.163	-1.262	-8.965	-1.044	-8.972
AL-21	10.05	-2.665	-11.199	-1.319	-8.382	-1.125	-8.389
AL-22	10.55	-2.302	-11.076	-1.008	-8.338	-0.794	-8.345
AL-22	10.55	-3.095	-11.938	-1.488	-8.732	-1.294	-8.738
AL-23	11.05	-5.108	-11.653	-3.829	-8.920	-3.786	-8.920
AL-23	11.05	-5.244	-12.733	-3.699	-9.574	-3.626	-9.575
AL-24	11.55	-2.130	-10.765	-0.803	-8.018	-0.586	-8.025
AL-26	12.55	-2.185	-10.500	-0.877	-7.701	-0.676	-7.707
AL-27	13.05	-2.568	-12.026	-1.024	-8.867	-0.793	-8.874
AL-27	13.05	-2.380	-11.507	-1.110	-8.725	-0.890	-8.732
AL-28	13.55	-2.730	-12.030	-1.119	-8.821	-0.896	-8.827
AL-28	13.55	-2.395	-11.173	-1.061	-8.362	-0.850	-8.368
AL-29	14.05	-2.528	-11.484	-0.830	-8.210	-0.609	-8.217
AL-29	14.05	-2.595	-10.740	-1.250	-7.924	-1.066	-7.929
AL-30	14.55	-2.936	-12.167	-1.295	-8.935	-1.080	-8.942
AL-30	14.55	-2.605	-11.014	-1.315	-8.223	-1.126	-8.229
AL-32	15.55	-4.698	-12.877	-3.335	-10.053	-3.220	-10.056
AL-33	16.05	-3.444	-10.892	-2.024	-8.042	-1.889	-8.046
AL-34	16.55	-4.267	-10.455	-2.881	-7.620	-2.818	-7.622
AL-35	17.05	-2.988	-14.200	-1.637	-11.381	-1.363	-11.390
AL-41	20.05	-2.267	-12.997	-0.914	-10.177	-0.631	-10.186
AL-44	21.55	-3.827	-11.072	-2.347	-8.194	-2.229	-8.198
AL-45	22.05	-6.629	-12.363	-5.272	-9.542	-5.306	-9.540
AL-46	22.55	-3.718	-11.924	-2.262	-9.057	-2.109	-9.062
AL-48	23.55	-2.572	-10.683	-1.231	-8.275	-1.035	-8.281
AL-49	24.05	-2.377	-10.048	-1.149	-7.825	-0.962	-7.830
AL-50	24.55	-5.677	-9.771	-3.904	-6.654	-3.943	-6.652
AL-52	25.55	-3.788	-12.404	-2.465	-9.598	-2.307	-9.603
AL-53	26.05	-1.474	-8.187	0.004	-5.553	0.192	-5.559
AL-54	26.55	-1.384	-8.086	-0.071	-5.724	0.118	-5.730
AL-55	27.05	-1.871	-9.389	-0.515	-6.955	-0.314	-6.961
AL-56	27.55	-1.550	-10.015	-0.034	-7.320	0.211	-7.328
AL-57	28.05	-1.093	-9.952	0.252	-7.136	0.510	-7.144
AL-58	28.55	-1.634	-9.665	-0.209	-7.118	0.018	-7.125
AL-59	29.05	-1.026	-7.714	0.334	-5.273	0.536	-5.280
AL-60	29.55	-1.195	-8.231	0.120	-5.865	0.327	-5.871
AL-61	30.05	-2.953	-12.953	-1.510	-10.377	-1.261	-10.385
AL-62	30.55	-4.304	-12.589	-2.864	-10.019	-2.719	-10.023
AL-63	31.05	-1.953	-9.290	-0.603	-6.537	-0.422	-6.542
AL-65	32.05	-1.740	-8.812	-0.312	-6.037	-0.128	-6.042
AL-66	32.55	-3.181	-10.454	-1.906	-7.722	-1.774	-7.726
AL-67	33.05	-1.966	-9.989	-0.412	-7.179	-0.197	-7.185
AL-68	33.55	-2.266	-9.459	-0.794	-6.672	-0.622	-6.677
AL-69	34.05	-2.179	-8.978	-0.709	-6.191	-0.548	-6.196
AL-70	34.55	-3.200	-13.100	-1.817	-10.337	-1.590	-10.344
AL-73	36.05	-1.180	-11.649	0.418	-8.826	0.745	-8.837
AL-74	36.55	-8.124	-10.389	-6.723	-7.622	-6.921	-7.615
AL-76	37.55	-2.273	-11.339	-0.966	-8.598	-0.741	-8.605
AL-77	38.05	-1.992	-11.064	-0.695	-8.325	-0.460	-8.333

Sample	Raw $\delta^{13}C$	Raw $\delta^{18}O$	Raw $\delta^{13}C$	Raw $\delta^{18}O$	Corrected $\delta^{13}C$	Corrected $\delta^{18}O$	Height (m)
AL-78	38.55	-1.994	-10.566	-0.692	-7.826	-0.474	-7.833
AL-79	39.05	-1.945	-10.802	-0.633	-8.059	-0.403	-8.066
AL-80	39.55	-2.112	-10.575	-0.818	-7.837	-0.609	-7.844
AL-81	40.05	-1.348	-10.009	0.094	-7.230	0.345	-7.238
AL-82	40.55	-2.284	-10.262	-0.754	-7.458	-0.552	-7.465
AL-85	42.05	-2.077	-12.540	-0.722	-9.785	-0.440	-9.794
AL-86	42.55	-1.336	-10.081	-0.051	-7.346	0.194	-7.354
AL-87	43.05	-1.310	-9.530	0.083	-6.765	0.318	-6.772
AL-89	44.05	-2.023	-9.573	-0.667	-6.818	-0.481	-6.824
AL-90	44.55	-1.906	-10.699	-0.551	-7.944	-0.320	-7.952
AL-91	45.05	-2.074	-12.564	-0.722	-9.810	-0.439	-9.819
AL-92	45.55	-1.196	-8.991	0.202	-6.224	0.426	-6.231
AL-93	46.05	-2.190	-9.427	-0.797	-6.589	-0.628	-6.594
AL-94	46.55	-4.518	-11.096	-2.951	-8.317	-2.869	-8.319
AL-95	47.05	-1.888	-10.706	-0.385	-7.578	-0.155	-7.585
AL-95	47.05	-0.941	-7.912	0.474	-5.382	0.688	-5.389
AL-96	47.55	-1.978	-9.670	-0.625	-7.242	-0.423	-7.248
AL-97	48.05	-1.973	-8.737	-0.463	-6.052	-0.290	-6.057
AL-98	48.55	-1.473	-13.696	0.072	-10.536	0.433	-10.548
AL-99	49.05	-2.108	-13.499	-0.581	-10.353	-0.270	-10.362
AL-99	49.05	-3.218	-12.116	-1.223	-8.636	-1.014	-8.642
AL-100	49.55	-2.377	-12.044	-0.859	-8.905	-0.616	-8.912
AL-101	50.05	-2.937	-11.011	-1.143	-7.860	-0.954	-7.866
AL-102	50.55	-2.261	-9.300	-0.833	-6.748	-0.661	-6.753
AL-103	51.05	-2.818	-11.161	-1.513	-8.811	-1.317	-8.817
AL-104	51.55	-2.571	-10.091	-1.060	-7.404	-0.882	-7.410
AL-105	52.05	-1.188	-12.179	0.327	-9.042	0.655	-9.052
AL-105	52.05	-4.793	-10.738	-2.943	-7.495	-2.889	-7.496
AL-106	52.55	-3.385	-10.624	-1.855	-7.906	-1.713	-7.910
AL-107	53.05	-3.032	-13.592	-1.534	-10.926	-1.268	-10.935
AL-108	53.55	-5.948	-13.077	-4.506	-10.502	-4.455	-10.504
AL-109	54.05	-4.379	-14.447	-2.689	-11.466	-2.483	-11.472
AL-110	54.55	-6.969	-9.789	-5.317	-6.870	-5.444	-6.866
AL-111	55.05	-3.256	-11.531	-1.944	-9.170	-1.766	-9.176
AL-112	55.55	-2.825	-10.869	-1.452	-8.408	-1.266	-8.413
AL-114	56.55	-4.420	-10.769	-2.831	-7.764	-2.760	-7.766
AL-115	57.05	-3.544	-11.341	-2.129	-8.509	-1.985	-8.514
AL-116	57.55	-2.634	-9.694	-1.228	-7.179	-1.068	-7.184
AL-117	58.05	-2.209	-9.393	-0.821	-6.588	-0.654	-6.594
AL-118	58.55	-3.778	-13.166	-2.349	-10.320	-2.159	-10.326
AL-120	59.55	-2.734	-9.775	-1.330	-6.955	-1.185	-6.959
AL-121	60.05	-2.307	-9.058	-0.652	-5.986	-0.494	-5.991
AL-122	60.55	-4.901	-7.990	-3.282	-5.125	-3.330	-5.123
AL-123	61.05	-2.629	-10.906	-1.204	-8.064	-1.012	-8.070
AL-124A	61.55	-4.368	-8.460	-3.001	-5.676	-3.012	-5.676
AL-124S	61.55	-5.041	-9.146	-3.510	-6.198	-3.538	-6.197
AL-127	63.05	-4.304	-7.360	-2.825	-4.724	-2.856	-4.723
AL-130	64.55	-3.236	-10.601	-1.770	-7.718	-1.628	-7.722
AL-132	65.55	-3.345	-10.480	-1.979	-8.031	-1.842	-8.035
AL-133	66.05	-2.350	-9.261	-0.618	-6.211	-0.449	-6.216
AL-134	66.55	-1.956	-9.311	-0.232	-6.274	-0.035	-6.280
AL-135	67.05	-2.931	-11.881	-1.652	-9.574	-1.440	-9.581
AL-137	68.05	-2.302	-9.099	-0.340	-5.672	-0.171	-5.678
AL-138	68.55	-3.536	-9.337	-2.017	-6.402	-1.937	-6.404
AL-139	69.05	-2.707	-9.094	-0.734	-5.649	-0.592	-5.653
AL-140	69.55	-1.644	-9.526	-0.251	-7.031	-0.030	-7.038
AL-141	70.05	-3.212	-11.346	-1.830	-8.871	-1.654	-8.876

Sample	Raw $\delta^{13}C$	Raw $\delta^{18}O$	Raw $\delta^{13}C$	Raw $\delta^{18}O$	Corrected $\delta^{13}C$	Corrected $\delta^{18}O$	Height (m)
AL-142	70.55	-5.799	-12.030	-4.289	-9.103	-4.271	-9.103

B21 Raw Nitrogen Isotope Data: Arroyo Lapa North

Sample	N/mg	$\delta^{15}N$
LN-300	17.34	-2.37
LN-301	0.01	-3.41
LN-303	0.03	-0.68
LN-304	0.02	0.48
LN-305	9.19	2.89
LN-306	0.01	-4.74
LN-307	0.01	-1.44
LN-308	0.05	-1.27
LN-309	0.04	-5.55
LN-31	15.17	-0.74
LN-310	24.25	0.10
LN-312	0.06	-6.52
LN-312	24.77	-1.51
LN-313	0.03	-1.67
LN-314	0.04	-4.26
LN-315	0.04	-2.12
LN-316	0.03	-1.41
LN-317	0.02	0.43
LN-319	0.03	-2.44
LN-320	18.47	-2.63
LN-325	16.05	2.72
LN-330	22.37	1.38
LN-335	13.13	1.78
LN-340	17.04	-5.03
LN302	0.03	4.12
LN312RR	0.03	-2.11
Exposure Gap		
LN-1	27.610	1.123
LN-6	19.743	-4.280
LN-11	18.724	-4.340
LN-11Rr	0.024	-1.110
LN-16	14.717	0.692
LN-21	25.048	0.215
LN-26	19.340	1.772
LN-36	22.630	-0.585
LN-36Rr	0.045	-1.260
LN-376	0.019	-1.500
LN-41	28.269	-1.798
LN-418	20.222	-3.217
LN-41Rr	0.049	-0.650
LN-46	24.215	-0.133
LN-51	37.267	-0.380
LN-56	19.877	-0.471
LN-61	26.858	3.297

Sample	N/mg	$\delta^{15}N$
LN-66	13.017	15.243
LN-71	24.159	10.746
LN-76	18.898	0.875
LN-81	20.942	-2.493
LN-86	19.093	-0.378
LN-91	17.073	-3.867
LN-96	28.923	-10.920
LN-101	23.610	-1.419
LN-111	16.481	4.843
LN-116	17.536	-2.853
LN-121	27.395	-5.574
LN-126	16.306	-1.724
LN-126Rr	0.028	-0.790
LN-131	17.335	-2.076
LN-131RR	0.031	-1.440
LN-141	12.239	2.023
LN-146	15.363	1.737
LN-151	14.940	3.416
LN-156	9.341	10.529
LN-160	0.018	-0.510
LN-161	0.013	-1.220
LN-161	18.825	22.223
LN-162	0.022	1.090
LN-163	0.016	0.240
LN-164	0.021	0.440
LN-165	0.022	-0.220
LN-166	0.013	-2.060
LN-166	44.965	3.966
LN-166RR	0.034	-1.780
LN-168	0.019	-0.550
LN-168	0.007	-5.160
LN-169	0.016	-0.020
LN-170	0.036	0.180
LN-171	6.681	13.715
LN-172	0.015	-2.100
LN-173	0.031	1.090
LN-174	0.020	-1.670
LN-176	11.345	-4.047
LN-177	0.016	-0.670
LN-179	0.012	-2.680
LN-180	8.366	9.516
LN-183	0.005	-6.040
LN-184	0.011	-1.510
LN-187	17.323	-9.736
LN-188	0.021	0.380
LN-189	0.017	-1.240

Sample	N/mg	$\delta^{15}N$
LN-191	33.320	-9.599
LN-192	0.021	0.480
LN-193	0.007	-1.160
LN-194	0.007	-6.000
LN-195	0.007	-6.260
LN-196	5.391	5.369
LN-197	0.020	-1.480
LN-198	0.022	0.020

Arroyo Lapa South Fossil Wood Nitrogen Data

Sample	N/mg	$\delta^{15}N$
Wood Samples		
LN-326W	4.308	10.353
LN-333W	7.746	2.817
LN-338W	11.839	3.402
Exposure Gap		
LN-W-1	6.702	6.009
LN-W-4	5.341	21.171
LN-10W	2.404	-46.588
LN-W-5	13.090	1.533
LN-15W	4.988	-22.762
LN-W-8	5.382	5.266
LN-W-9	5.938	-1.668
LN-W-10	5.607	7.931
LN-W-11	8.690	29.185
LN-W-14	2.323	41.685
LN-W-18	2.997	5.190
LN-W-21	17.315	0.807
LN-W-22	4.305	-9.081
LN-W-23	11.299	-6.479
LN-W-24	10.734	3.164
LN-W-26	34.301	0.216
LN-W-28	15.791	2.432
LN-W-29	2.772	-20.225
LN-W-30	1.032	-58.374
LN-W-32	7.158	14.546
LN-191W	14.852	-0.447
LN-191W	9.516	-2.373

B22. Raw Nitrogen Data: Arroyo Lapa South

Sample	N/mg	$\delta^{15}N$
AL-2	0.051	-0.38
AL-3	0.036	1.04
AL-6	0.024	-0.76
AL-7	0.02	-3.73
AL-10	0.032	0.8
AL-14	0.016	-0.44
AL-18	0.012	-2
AL-19	0.02	-1.06
AL-23	0.018	-0.61
AL-24	0.014	7.1
AL-26	0.014	0.85
AL-28	0.014	0.5
AL-40	0.011	-5.46
AL-41	0.009	-0.25
AL-42	0.011	-6.09
AL-48	0.015	-5.51
AL-52	0.014	-11.76
AL-53	0.019	2.56
AL-54	0.018	1.65
AL-58	0.017	2.13
AL-60	0.023	-1.12
AL-60	16.336	-3.289
AL-90R	0.012	0.92
AL-91	0.008	-3.76
AL-92	0.007	-10.7
AL-92	0.005	-35.31
AL-102	0.015	2.85
AL-105	0.007	-5.52
AL-105	0.015	-1.98
AL-106	0.011	-12.11
AL-107	0.003	-8.24
AL-107	0.007	-3.92
AL-107	0.007	-14.46
AL-109	0.003	11.76
AL-109	0.011	-1.57
AL-110	0.024	-2
AL-111	0.02	-1.89
AL-112	0.016	-2.98
AL-113	0.018	-4.77
AL-113	0.014	-10.11
AL-114	0.023	3.97
AL-115	0.018	-1.9
AL-116	0.015	-3.53
AL-118	0.017	1.4
AL-119	0.013	0.76
AL-121	0.036	-0.91
AL-122	0.032	-1.36
AL-123	0.005	-15.94
AL-123	0.025	-0.47
AL-124	0.016	-5.17

Sample	N/mg	$\delta^{15}N$
AL-126	0.021	-1.2
AL-128	0.017	-3.8
AL-129	0.018	-2.61
AL-130	0.022	1.93
AL-131	0.019	-4.4
AL-133	0.017	-4.86
AL-134	0.01	-3.21
AL-134	0.004	6.44
AL-135	0.011	-5.08
AL-135	0.007	-21.52
AL-138	0.026	-2.31
AL-200	7.745	-0.634
AL-205	11.607	0.525
AL-210	8.059	-0.174
AL-215	7.961	1.952
AL-220	11.333	5.317
AL-223	13.680	7.292
AL-224	23.855	-2.407
AL-225	11.187	19.792
AL-230	16.280	4.948
AL-232	9.095	-7.089
AL-240	9.078	-4.209
AL-244	10.638	-1.327
AL-245	10.333	3.884
AL-250	10.913	11.676
AL-255	10.113	-0.055
AL-260	11.246	-5.412
AL-265	11.012	1.170
AL-270	12.522	0.953
AL-272	15.720	-1.636
AL-273	15.584	-2.715
AL-275	11.857	-1.846
AL-280	16.780	1.279
AL-281	0.014	-1.440
AL-282	0.034	-2.540
AL-284	0.021	-0.820
AL-285	20.244	0.445
AL-286	0.014	-2.560
AL-286	0.019	0.920
AL-287	0.038	-0.680
AL-288	0.019	-0.680
AL-289	0.021	-0.890
AL-290	26.531	-6.272
AL-291	0.035	-0.080
AL-292	0.031	0.400
AL-293	0.022	-1.200
AL-294	0.030	-0.590
AL-295	16.860	-1.465
AL-296	0.013	-0.200
AL-296	23.310	-4.367
AL-296RR	0.013	-1.970
AL-297	0.015	-0.29

Sample	N/mg	$\delta^{15}N$
AL-299	0.013	-2.220
AL-300	14.489	-2.064
AL-301	0.007	-1.820
AL-302	0.014	-1.890
AL-303	0.011	-2.430
AL-304	0.015	-0.810
AL-305	4.445	-5.008
AL-306	0.014	0.010
AL-307	0.018	-0.360
AL-308	0.019	-0.870
AL-309	0.024	0.270
AL-310	12.085	-1.093
AL-311	0.021	0.340
AL-312	0.036	-0.240
AL-313	0.017	0.470
AL-314	0.018	-2.120
AL-315	17.434	-1.574
AL-316	0.024	-0.400
AL-317	0.026	-1.760
AL-317	0.018	-1.320
AL-318	0.030	-0.210
AL-319	0.028	-1.760
AL-320	27.967	-0.342
AL-321	0.031	-0.040
AL-322	0.029	-1.100
AL-323	0.027	-1.610
AL-324	0.029	-2.010
AL-325	19.182	0.638
Al-326	0.021	-1.540
AL-327	0.029	-0.700
AL-328	0.029	-0.380
AL-329	0.029	0.130
AL-330	13.092	-0.088
AL-331	0.023	-2.960
AL-332	10.253	2.429
AL-333	0.023	-5.550
AL-335	9.237	3.643
AL-336	0.025	-2.120
AL-337	0.025	-0.390
AL-338	0.027	-0.410
AL-339	0.029	-3.670
AL-340	17.116	-2.489
AL-342	0.012	-0.270
AL-343	0.018	0.080
AL-344	0.014	-2.590
AL-345	19.517	-2.667
AL-347	0.027	-0.640
AL-348	0.030	-0.710
AL-349	0.033	-0.590
AL-350	30.374	-2.569
AL-351	0.036	-1.080
AL-352	0.026	-0.650

Sample	N/mg	$\delta^{15}N$
AL-354	0.045	0.4
AL-355A	0.014	-0.210
AL-355B	0.014	-0.980
AL-356	0.018	-0.360
AL-358	0.033	-1.470
AL-359	0.031	-1.680
AL-360	30.443	-3.312
AL-361A	0.030	-0.640
AL-362	0.036	-0.800
AL-363	0.025	-5.370
AL-364	0.047	0.120
AL-365	0.043	-1.390
AL-366	0.025	-2.040
AL-367	0.021	-1.030
AL-368	17.415	-1.597
AL-368Rr	0.027	-0.870
AL-369	0.039	-1.290
AL-370	0.015	-4.360
AL-371	2.583	1.417
AL-372	0.030	-2.720
AL-373	0.036	-0.510
AL-374	0.041	-0.830
AL-375	0.025	-1.040
AL-376	0.033	-1.140
AL-377	0.029	-0.900
AL-378	17.999	3.621
AL-378Rr	0.029	-1.490
AL-379	0.029	-1.380
AL-380	0.020	-2.050
AL-381	0.022	-2.610
AL-382	0.030	-1.260
AL-383	23.241	-2.660
AL-385	0.042	4.390
AL-385	0.022	-2.480
AL-386	0.023	-1.930
AL-387	0.024	-1.090
AL-388	29.615	-1.092
AL-389	0.016	-1.950
AL-390	0.026	-2.650
AL-390	0.018	-0.840
AL-391	0.029	-0.710
AL-392	0.037	-0.170
AL-392	20.344	0.804
AL-393	0.030	-2.100
AL-394	0.047	-4.230
AL-395	0.030	-1.950
AL-396	0.029	-3.850
AL-397	0.032	-2.390
AL-398	0.026	-1.910
AL-398	20.358	-0.572
AL-399	0.021	-2.090
AL-400	0.040	-0.660

Sample	N/mg	$\delta^{15}N$
AL-402	0.028	-1.280
AL-403	16.153	-0.845
AL-404	0.024	-1.880
AL-405	0.021	-2.910
AL-406	13.811	-6.979
AL-407	0.035	-0.070
AL-408	19.429	0.318
AL-408	15.937	1.156
AL-408RR	0.027	-1.410
AL-409	0.012	-1.510
AL-410	0.026	-0.420
AL-411	12.992	-1.969
AL-411Rr	0.017	-0.950
AL-412	0.033	-2.080
AL-413	0.032	-0.870
AL-413	25.388	-4.239
AL-414	0.033	0.530
AL-416	0.037	0.040
AL-417	0.036	0.630
AL-419	0.038	0.190
AL-420	0.036	-0.380
AL-421	0.030	-0.710
AL-422	0.028	-1.340
AL-423	14.849	-0.683
AL-424	0.019	-0.350
AL-425	0.032	0.250
AL-426	0.042	-0.410
AL-427	0.031	0.700
AL-428	0.035	0.520
AL-429	0.040	-0.960
Al-430	0.035	-1.930

Arroyo Lapa South Fossil Wood Nitrogen Data

Sample	N/mg	$\delta^{15}N$
AL-W-1	0.019	-2.280
AL-W-2	0.018	-6.380
AL-W-2	2.963	14.901
AL-W-2	0.003	-6.580
AL-W-3	0.003	-34.660
AL-W-3	0.010	-3.460
AL-W-4	0.008	-14.220
AL-W-4	0.008	-10.310
AL-W-5	0.015	-9.100
AL-W-6	0.007	-21.400
AL-W-6	3.098	-6.992
AL-W-7	0.008	-1.090
AL-W-7	0.008	-21.120
AL-W-8	0.007	-9.710
AL-W-8	0.007	-19.970
AL-W-9	0.008	-12.850
AL-W-9	0.009	-10.090
AL-W-9-2	0.006	-10.400

Sample	N/mg	$\delta^{15}N$
AL-W-11	0.012	-12.930
AL-W-11	0.005	-8.830
AL-W-13	0.004	-14.510
AL-W-13	0.000	-26.590
AL-W-14	0.004	-32.080
AL-W-15	0.004	-23.510
AL-W-15	0.009	-13.210
AL-200W	1.471	41.215
AL-202W	2.992	-9.232
AL-204W	9.908	-6.484
AL-206W	1.312	43.776
AL-212W	1.114	-15.338
AL-235W	1.746	-10.248
AL-235W	1.848	-6.525
AL-238W	0.801	-14.859
AL-244W	2.539	4.511
AL-246W	0.970	173.709
AL-258W	1.574	-23.702
AL-263W	7.946	4.192
AL-264W	4.183	-13.597
AL-264W	11.837	2.874
AL-265W	8.482	-2.689
AL-265W	12.503	35.429
AL-266W	10.107	1.736
AL-266W	2.078	-35.665
AL-268W	5.835	-4.160
AL-270W	4.560	9.189
AL-271W	8.266	-0.096
AL-271W	6.179	2.544
AL-272W	2.470	-18.093
AL-284W	1.861	-1636.037
AL-296W	9.724	-0.838
AL-296W	1.530	-16.314
AL-297W	6.764	5.242
AL-322W	2.003	-4.727
AL-324W	0.980	-40.450
AL-329W	7.087	-3.061
AL-330W	1.226	-33.480
AL-333W	3.237	-46.564
AL-334W	2.405	81.050
AL-335W	1.668	34.259
AL-336W	4.624	-1.137
AL-336W	4.805	5.544
AL-336W	3.161	13.407
AL-363W	5.026	4.488
AL-371W	18.483	-1.154
AL-399W	2.333	5.718
AL-404W	6.627	2.089
AL-406W	10.979	-4.174
AL-408W	7.445	-0.627

B23. Raw Nitrogen Data: Arroyo Serrucho

Sample	N/mg	$\delta^{15}N$
AS-1	5.922	-4.408
AS-1	8.115	-5.703
AS-2	19.598	-3.798
AS-2	16.968	-1.033
AS-4	20.214	-2.980
AS-5RR	0.017	-2.580
AS-5Rr	0.023	-1.310
AS-5	13.107	-6.474
AS-5	19.079	-2.256
AS-5	7.346	2.708
AS-6	19.507	-3.493
AS-8	12.396	-6.070
AS-8	11.794	-12.534
AS-8	22.561	-1.959
AS-9	16.434	-2.413
AS-9	18.129	-3.433
AS-10	19.276	-0.173
AS-10	19.156	-4.137
AS-11	15.470	-4.880
AS-11	23.782	-1.519
AS-13Rr	0.027	-1.850
AS-13	14.192	-1.431
AS-13	19.150	1.303
AS-16	12.747	-6.670
AS-16	8.373	-0.488
AS-17	22.624	2.420
AS-18	5.375	-14.813
AS-18	11.220	4.821
AS-20A	0.017	-2.730
AS-22	0.000	0.000
AS-23	22.122	-5.122
AS-24	18.885	-4.764
AS-25	18.725	-10.107
AS-25	14.136	-5.275
AS-28	0.018	-1.710
AS-30A	0.014	-4.220
AS-30B	0.016	-3.050
AS-30C	0.017	-5.030
AS-33	15.711	-4.262
AS-33	8.476	0.873
AS-35	8.519	-5.930
AS-37	21.091	-0.381
AS-38	21.731	-2.459
AS-40	10.881	-0.733
AS-40	11.777	-10.500
AS-41	13.080	-1.021
AS-41-2	20.984	-0.796
AS-43	26.701	-0.612
AS-46	8.098	-10.509
AS-47	21.231	-1.397
AS-47	22.655	-2.612

Sample	N/mg	$\delta^{15}N$
AS-50A	0.012	-5.130
AS-53	23.133	-4.104
AS-54	12.128	-7.326
AS-54	12.979	-1.003
AS-55	25.898	-2.348
AS-55	24.211	-4.203
AS-56	7.548	-2.597
AS-57	0.016	-3.560
AS-57	12.693	-5.038
AS-58	12.219	-0.361
AS-58R	7.113	-1.691
AS-59	16.872	0.827
AS-59	7.998	-1.609
AS-61	20.179	-1.094
AS-62	13.211	-3.377
AS-65	5.749	-6.740
AS-65	23.439	0.896
AS-66	4.394	-3.356
AS-66	7.944	-6.642
AS-100	17.328	-8.955
AS-101	5.753	-8.387
AS-101RR	0.021	-0.810
AS-102	6.094	-3.228
AS-102RR	0.017	-3.570
AS-103	5.878	0.676
AS-103RR	0.011	-2.600
AS-104	14.495	-6.601
AS-105	4.783	6.308
AS-105Rr	0.010	-3.790
AS-106	9.239	-6.224
AS-106Rr	0.042	-0.520
AS-106Rr	0.038	-0.250
AS-106Rr	0.028	-1.500
AS-106	22.373	-0.783
AS-106	6.883	3.219
AS107RR	0.027	-2.640
AS-107	9.943	-4.802
AS-108	15.011	-9.521
AS-109	8.638	-3.207
AS-110	10.057	-2.708
AS-111Rr	0.025	-0.560
AS-111	12.841	33.518
AS-112	7.920	21.435
AS-113	10.414	1.386
AS-114RR	0.018	-1.220
AS-114	7.723	0.027
AS-115	0.021	-2.380
AS-116	9.268	1.537
AS-117RR	0.025	-0.450
AS-117	8.035	4.049
AS-119	5.751	-2.418
AS-119Rr	0.012	-0.380

Arroyo Serrucho Fossil Wood Nitrogen Data

Sample	N/mg	$\delta^{15}N$
AS-W1	0.007	-2.410
AS-W4	0.005	-3.120
AS-W5	0.003	-21.040
AS-W7	0.006	-3.650
AS-W8	0.003	-27.490
AS-W9	0.002	-6.580

B24. Raw Nitrogen Data: Chacay Melehue

Sample	N/mg	$\delta^{15}N$
CM-107	0.008	-2.47
CM-109	0.005	-1.52
CM-113	0.007	-10.36
CM-113	0.003	-9.15
CM-117	0.005	-5.87
CM-133	0.02	-5.96
CM-137	0.009	-7.08
CM-140	0.007	-5.54
CM-144	0.013	1.13
CM-155	0.015	-4.24
CM-159	0.012	2.31
CM-162	0.006	1.29
CM-165	0.032	-3.05
CM-172	0.011	-2.08
CM-176	0.014	-3.1
CM-179	0.019	-0.08
CM-184	0.035	-2.55
CM-188	0.016	-3.37
CM-198	0.015	-2.29
CM-202	0.021	-3.11
CM-205	0.044	-0.8
CM-205	0.017	-1.42
CM-207	0.026	-1.12
CM-212	0.012	-4.79
CM-36	0.013	-4.89
CM-39	0.011	-0.78
CM-39R	0.037	-0.43
CM-45	0.011	-2.81
CM-65	0.017	-0.1
CM-68	0.007	11.05
CM-74	0.006	-1.42
CM-79	0.012	-4.45
CM-87	0.01	-6.91
CM-92	0.015	0.51
CM-93	0.006	1.31
CM-94	0.024	-2.46
CM-95B	0.025	-1.98
CM-97	0.014	-2.34
CM-99	0.029	-1.03
CM-107	0.012	-0.86
CM-111	0.007	0.95
CM-113	0.005	-4.83
CM-115	0.004	-27.48
CM-123	0.002	-13.08
CM-133	0.015	-2.7
CM-148	0.015	-9.33
CM-151	0.011	8.13
CM-165	0.013	-2.03
CM-169	0	0
CM-172	0.019	-0.21
CM-184	0.015	-4.32
CM-225	3.110	5.377

Sample	N/mg	$\delta^{15}N$
CM-31	0.01	-7.9
CM-39	0.002	-48.17
CM-39	0.017	-7.04
CM-42	0.028	2.84
CM-58	0.021	-3.69
CM-68	0.009	-7.49
CM-71	0.009	5.4
CM-89	0.01	-13.59
CM-224	27.967	-5.120
CM-90	13.219	-2.380

TB25. Comparison of Carbon data for Alanine Standard from 2008 to 2011 (AN= Alanine)

Name	Weight/Vol	C (Sam)	$\delta^{13}C$ (Sam)	TOC
ALANINE	0.78	0.315	-26.910	2.475
ALANINE	0.75	0.303	-26.910	2.475
ALANINE	0.82	0.331	-26.910	2.475
ALANINE	0.86	0.347	-26.910	2.475
AN-3	0.87	0.353	-26.758	2.466
AN-5	0.71	0.320	-26.823	2.219
AN-7	0.74	0.293	-26.832	2.529
AN-8	0.7	0.270	-27.402	2.592
AN-1	0.6	0.272	-27.010	2.206
AN-10	0.7	0.326	-26.870	2.147
AN-3	0.6	0.275	-26.840	2.182
AN-5	0.7	0.334	-27.410	2.096
AN-7	0.6	0.25	-26.900	2.400
AN-9	0.7	0.258	-27.020	2.713
AN-1	0.6	0.272	-27.010	2.206
AN-10	0.7	0.326	-26.870	2.147
AN-3	0.6	0.275	-26.840	2.182
AN-5	0.7	0.334	-27.410	2.096
AN-7	0.6	0.25	-26.900	2.400
AN-9	0.7	0.258	-27.020	2.713
AL	2.4	0.89	-27.660	2.697
AN1	0.3	0.09	-27.510	3.333
AN3	0.3	0.13	-27.600	2.308
AN5	0.2	0.07	-26.760	2.857
AN6	0.1	0.1	-26.980	1.000
AN7	0.1	0.08	-26.640	1.250
AN11	0.4	0.18	-26.950	2.222
AN9	0.2	0.07	-27.020	2.857
AN12	0.5	0.11	-27.010	4.545
AN-1	0.6	0.233	-26.820	2.575
AN-3	0.6	0.259	-26.710	2.317
AN-5	0.6	0.259	-26.940	2.317
AN-7	0.7	0.253	-26.830	2.767
AN-8	0.7	0.288	-26.750	2.431
AN-3	0.8	0.291	-26.780	2.749
AN-5	0.8	0.313	-26.880	2.556
AN-7	0.8	0.341	-26.900	2.346
AN-8	0.8	0.325	-26.840	2.462
AN-1	0.8	0.421	-26.780	1.900
AN-3	0.8	0.232	-26.740	3.448
AN-5	0.8	0.3	-26.700	2.667
AN-6	0.8	0.319	-26.940	2.508
AN-1	1.1	0.381	-26.700	2.887
AN-5	0.7	0.309	-26.940	2.265
AN-6	0.7	0.25	-27.030	2.800
AN-3	0.7	0.254	-26.750	2.756
AN-1	0.7	0.301	-27.190	2.326
AN-10	0.6	0.223	-27.060	2.691
AN-11	0.6	0.209	-26.990	2.871
AN-3	0.6	0.229	-27.040	2.620
AN-5	0.7	0.277	-26.750	2.527

Name	Weight/Vol	C (Sam)	$\delta^{13}C$ (Sam)	TOC
AN-7	0.7	0.307	-26.910	2.280
AN-9	0.6	0.211	-26.890	2.844
AN-3	0.6	0.234	-27.030	2.564
AN-5	0.5	0.213	-26.930	2.347
AN-7	0.5	0.23	-26.700	2.174
AN-8	0.7	0.269	-26.720	2.602
AN-1	0.5	0.197	-26.890	2.538
AN-11	0.8	0.183	-26.890	4.372
AN-3	0.6	0.239	-26.970	2.510
AN-5	0.5	0.22	-27.110	2.273
AN-7	0.7	0.294	-27.110	2.381
AN-9	0.7	0.272	-26.810	2.574
ALANINE	0.69	0.279	-26.910	2.475
ALANINE	0.84	0.339	-26.910	2.475
ALANINE	0.71	0.287	-26.910	2.475
ALANINE	0.83	0.335	-26.910	2.475
AN-1	0.86	0.325	-26.928	2.649
AN-3	0.68	0.274	-26.439	2.483
AN-5	0.67	0.269	-26.249	2.486
AN-7	0.86	0.322	-26.853	2.667
AN-8	0.85	0.362	-26.841	2.351
ALANINE	0.3332	0.135	-26.910	2.475
ALANINE	0.2807	0.113	-26.910	2.475
ALANINE	0.3136	0.127	-26.910	2.475
ALANINE	0.3218	0.130	-26.910	2.475
std 3	0.2922	0.118	-27.962	2.468
std 5	0.3098	0.118	-27.125	2.629
std 7	0.3242	0.129	-26.479	2.506
std 8	0.3236	0.127	-28.075	2.538
test	0.3	0.121	-27.321	2.489
		Average	-26.948	2.516
		Maximum	-26.640	4.545
		Minimum	-27.660	1.000
		Std Dev	0.216	0.512